CONTRIBUTIONS OF THE 3' *HOX* GENES, *HOXA1*, *HOXB1*, AND *HOXB2*, TO PATTERNING OF THE AXIAL SKELETON DURING DEVELOPMENT

BY

C2008
Rachel R. Buckley

B.S. Biology, University of Kansas, 2002

Submitted to the graduate degree program in Anatomy and Cell Biology and the Graduate Faculty of the University of Kansas in partial fulfillment of the requirements for the degree of Doctor of Philosophy

_____
Chairperson Robb E. Krumlauf, Ph.D.

_____
Kenneth R. Peterson, Ph.D.

_____
Brenda J. Rongish, Ph.D.

_____
Paul A. Trainor, Ph.D.

_____
Douglas E. Wright, Ph.D.

Date Defended May 23, 2008

The dissertation committee for Rachel R. Buckley certifies that this is the approved version of the following dissertation:

CONTRIBUTIONS OF THE 3' *HOX* GENES, *HOXA1*, *HOXB1*, AND *HOXB2*, TO PATTERNING OF THE AXIAL SKELETON DURING DEVELOPMENT

Committee:

_____

Chairperson Robb E. Krumlauf, Ph.D.

_____

Kenneth R. Peterson, Ph.D.

_____

Brenda J. Rongish, Ph.D.

_____

Paul A. Trainor, Ph.D.

_____

Douglas E. Wright, Ph.D.

Date Approved: May 23, 2008

Abstract

Hoxb1-null mice exhibit early patterning defects in the hindbrain, including the failure of rhombomere 4 to maintain its unique identity (Studer et al., 1996). As a result, the facial muscles are not innervated, and these embryos (98%) die soon after birth, unable to suckle. *Hoxb1* expression, however, is not limited to the developing hindbrain. During early somitogenesis, *Hoxb1* expression in the paraxial mesoderm extends anteriorly into the region that will give rise to the cervical somites (Murphy and Hill, 1991). Although skeletal phenotypes have been reported in other *Hox* mutants, no skeletal phenotypes have been described in the *Hoxb1* loss-of-function mutant line. To investigate whether Hoxb1, as well as related proteins Hoxa1 and Hoxb2, are involved in vertebral development, we use Alizarin Red/Alcian Blue staining to characterize the skeletons of 18.5dpc *Hoxa1*, *Hoxb1*, and *Hoxb2* loss-of-function single and double mutant embryos. Our analysis reveals that the loss of Hoxb1 and Hoxb2 function leads to multiple homeotic transformations along the vertebral column. In the cervical region, the following single segment anterior transformations are observed: C2→C1, C6→C5, and C7→C6. At the cervicothoracic vertebral transition, *Hoxb1* mutants exhibit T1→C7 anteriorizations. In both *Hoxb1* and *Hoxb2* mutants, T2→T1 transformations are present. The dosages of both *HoxB* genes seem to be important, since the homeotic transformations significantly increase in penetrance in *Hoxb1*/*Hoxb2* *trans*-heterozygotes, compared to single

heterozygotes. Through the use of transgenic mouse strains, we were also able to reproduce all of the above transformations upon addition of extra copies of *HoxB* genes. This approach also allowed us to characterize an effect of anterior *HoxB* genes on occipital bone development. Interestingly, the defects observed in these loss-of-function mutants and transgenic mice occur at the boundaries between morphologically distinct vertebral domains. In conclusion, these data show that the anterior *HoxB* genes, particularly, *Hoxb1* and *Hoxb2*, play a critical role in patterning the paraxial mesoderm that will give rise to the axial skeleton.

Acknowledgements

The research presented here was performed in the laboratory of Dr. Robb Krumlauf at the Stowers Institute for Medical Research. I would like to thank my mentor Robb for providing me with an excellent learning environment and guidance as I made my way through coursework and experiments. I also owe a great deal of gratitude to all of my labmates, past and present, who have each contributed to my scientific learning. Additionally, special thanks go to Youngwook Ahn and Christof Nolte for sharing with me their transgenic mouse lines. Many of my labmates provided thoughtful discussions about the various sections of this dissertation; some of them (referenced in the following) even offered “inspiration” during the writing of the acknowledgements page:

"Dr. Erica Perryn is the coolest person in the whole wide world, and, without her help, this dissertation would only be 2 pages long. I am indebted to her forever and, in fact, will be giving her my firstborn child as a thank you for all her help."

"Scientifically speaking, I was a lost puppy until I encountered the brilliance of Dr. Nolte, whose extraordinarily high level of scientific acuity left me awestruck. Without his patience, guidance, and gentle demeanor, I would have been irrecoverably lost in the scientific quagmire that stretched before me. If I had additional time, I would spend it under his tutelage increasing my learning in every aspect of life and science, which, until now, I had taken for granted."

"I was under a lot of pressure during the process of writing my dissertation, and I don't mean from the obvious sources. Certain of my colleagues forced me, and

I mean that literally, to acknowledge their negligible help, as if it were meaningful in some way. There is only one person who actually deserves my profound thanks, and that is the phenomenal Dr. Tara Alexander. She is extraordinary in every way: brilliant, noble, thoughtful, and creative. I could go on listing her attributes, but it would take 293 pages to even begin to describe her infinite supply of positive qualities. Instead, I will just say that, without Dr. Alexander, my dissertation and my life would be meaningless. It is only through her magnanimous support that I have been able to make anything out of my life. So, Dr. Alexander, thank you from the bottom of my heart for everything, and I mean everything."

I also would like to thank my dissertation committee (Dr. Robb Krumlauf, Dr. Ken Peterson, Dr. Brenda Rongish, Dr. Paul Trainor, and Dr. Doug Wright) for their invaluable input and discussions regarding these experiments and results. Thank you for encouraging me to keep the bigger picture always in mind.

On a more personal note, I am eternally indebted to my family for the love and support they have given me throughout this entire process. To my brother Bobby Chennault: thank you for always being interested in what I do, and I love you for taking the time to figure it all out. To my “mom” and “dad” (Becky and Chuck Buckley): thank you for seeing me through the last four years and always being in my corner. Lastly, but certainly never least, to my husband and best friend Dave Buckley: thanks for being my sounding board and “partner in crime” as we made our ways through graduate school together. More than that, thank you for making our house feel like a home; I love you.

Table of contents

List of figures

Chapter 1. Introduction

Chapter 2. Materials and Methods

Chapter 3. The role of *Hoxb1* during the development of the axial vertebrae

Appendix D. Whole-mount *in situ* hybridization studies with *HoxB* genes in *Hoxb1* and *Hoxb2* mutant embryos

List of Tables

Chapter 1. Introduction

Appendix C. Tables of skeletal phenotypes identified in *Hox* individual and compound mutants and increased gene dosage transgenic mice

Abbreviations

aaa	anterior arch of the atlas
AbdA	*Abdominal-A*
AbdB	*Abdominal-B*
Antp	*Antennapedia*
A/P	anterior/posterior
AT	anterior tuberculum
AVE	anterior visceral endoderm
ba	branchial arch
BAC	bacterial artificial chromosome
BBR	Behringer's Blocking Reagent
BCIP	5-bromo-4-chloro-indoyl-phosphatase
BOB	basioccipital bone
bp	base pair
BSA	bovine serum albumin
C	cervical vertebra
Ca	caudal vertebra
Ca^{2+}	calcium
cDNA	complimentary deoxyribonucleic acid
CMV	cytomegalovirus promoter
CO_2	carbon dioxide
Cranial nerve V	trigeminal nerve

Cranial nerve VII	facial nerve
Cranial nerve IX	glossopharyngeal nerve
Cranial nerve XI	accessory nerve
C-terminal	carboxy terminal
dATP	deoxyadenosine 5’ triphosphate
dCTP	deoxycytidine 5’ triphosphate
dGTP	deoxyguanosine 5’ triphosphate
dTTP	deoxythymidine 5’ triphosphate
ddH_2O	double distilled water
DEPC	diethylpyrocarbonate
Dfd	*Deformed*
DIG	digoxigenin
DMF	dimethyl formamide
DNA	deoxyribonucleic acid
dpc	days post conception
DR2	direct repeat, 2bp spacing
DR5	direct repeat, 5bp spacing
DTT	dithiothreitol
EGTA	ethylene glycol tetraacetic acid
EOB	exoccipital bone
EtOH	ethanol
exd	*extradenticle*

FGF	fibroblast growth factor
g	gram
HCl	hydrochloric acid
HOM-C	homeotic complex
IP	interparietal bone
$K_3Fe(CN)_6$	potassium ferricyanide
$K_4Fe(CN)_63H_2O$	potassium ferrocyanide
kb	kilobase
KOH	potassium hydroxide
L	lumbar vertebra
lab	*labial*
M	Molar
MeOH	methanol
mg	milligram
µg	microgram
µl	microliter
µm	micrometer
ml	milliliter
$MgCl_2$	magnesium chloride
mm	millimeter
mM	milliMolar
mRNA	messenger ribonucleic acid

ms	microseconds
NaOH	sodium hydroxide
N/A	not applicable
NaCl	sodium chloride
NBT	nitroblue tetrazolium
Neo	*neomycin* selectable marker
ng	nanogram
$(NH_4)_2SO_4$	ammonium sulfate
NP40	Nonidet P40
P	postnatal day
pb	*proboscipedia*
PBS	phosphate buffered saline
PCR	polymerase chain reaction
PFA	paraformaldehyde
Pro K	proteinase K
PSM	presomitic mesoderm
pv	prevertebra
r	rhombomere
RA	Retinoic Acid
RAR	Retinoid A Receptor

RARE	Retinoic Acid Response Element
RE	restriction enzyme
RNA	ribonucleic acid
RT-PCR	reverse transcriptase polymerase chain reaction
RXR	Retinoid X Receptor
S	sacral vertebra
SCJ	sternocostal junction
Scr	*Sex combs reduced*
SDS	sodium dodecyl sulfate
SOB	supraoccipital bone
SSC	saline sodium citrate
T	thoracic vertebra
TAE	Tris-Acetate-EDTA buffer
Tg	transgenic
Tris	2-amino-2 (hydroxymethyl)-1,3-propanediol
tRNA	transfer ribonucleic acid
Ubx	*Ultrabithorax*
UTR	untranslated region
UV	ultraviolet
V	volts
VA	vertebrarterial canal
WT	wild-type

Chapter 1

Introduction

1.1 Segmental patterning of the vertebrate embryonic body plan

During vertebrate development, the process of morphological segmentation along the embryo's axes generates a series of repeated anatomical units that contribute to the overall body plan. Functionally, segmentation allows body region specification, which can be easily visualized during head and trunk development. Within the head region, subdivision of the neural tube into individual segments creates morphologically-distinct areas of the brain that each carry out specific functions during brain formation and patterning. Similarly, segmentation of the presomitic mesoderm within the trunk generates paired blocks of paraxial mesoderm from which the reiterated skeleton and muscles of the adult body arise. Thus, segmentation during embryonic development is crucial for building the body plan upon which segmented structures in the adult organism are founded. The following section will focus on the important developmental processes preceding segmentation, as well as factors that are critical to the segmental patterning of the vertebrate body plan.

1.1.1 Establishing the three germ layers

Following implantation of the embryo, extensive cell rearrangement movements, known as gastrulation, occur in the blastula via cell migration. The purpose of gastrulation is to establish the three germ layers: the outer layer, ectoderm, which contributes to the epidermis and nervous system; the inner layer, endoderm,

which gives rise to the lining of the digestive tract and its associated organs; the middle layer, mesoderm, which generates the remaining organs (heart, kidney, gonads), connective tissues (bone, cartilage, tendons, muscles, blood vessels), and blood cells. Once these three germ layers are established, the process of organogenesis begins, by which cells interact and rearrange themselves into tissues and organs.

In the chick, after the outer cell mass of the blastula has invaded the endometrium during implantation, the inner cell mass undergoes reorganization and divides into two layers: the epiblast and the hypoblast. The hypoblast covers the blastocoel and contributes to the development of extraembryonic tissues, including the yolk sac.

The epiblast will give rise to the embryo itself, as it further divides into the amnion layer and the embryonic epiblast. The structure of the early mouse embryo is unique, because it initially forms as an egg cylinder with the epiblast located interiorly and the visceral endoderm on the outside, unlike other mammalian embryos. Cells of the inner cell mass undergo epithelialization and arrange collectively into an embryonic disk, which becomes thickened at the presumptive caudal end of the embryo. Once this thickening has occurred, an anterior expansion of cells initiates primitive streak formation. Thus, gastrulation begins in the mouse blastula at about 6.5 days post conception (dpc) with the formation of the primitive streak. As gastrulation continues into the late primitive-streak stage, the streak extends distally to the tip of the egg cylinder, marking the anterior-posterior (A/P)

axis of the embryo. At the anterior end of the primitive streak lies the node: an organizing structure in the mouse that is functionally similar to the dorsal blastopore lip in amphibians and Henson's node in birds since it is responsible for organizing and patterning the A/P axis of the embryo. A specified extraembryonic tissue known as the anterior visceral endoderm (AVE) is also required for the orientation of the A/P axis and the specific patterning of the adjacent anterior embryonic tissues (Beddington and Robertson, 1999). However, signaling molecules, such as Chordin and Noggin, from the node are necessary to help maintain the anterior patterning activity of the AVE, suggesting that the node and AVE act cooperatively to pattern the embryonic axis (Bachiller et al., 2000). As the primitive streak extends posteriorly, epiblast cells are recruited for ingression into the blastocoel. Within the primitive streak, epiblast cells undergo an epithelial to mesenchymal transition and migrate between the epiblast and the visceral endoderm. In the early-primitive-streak embryo, the first cells to migrate through the primitive streak are precursors of the extraembryonic mesoderm. As gastrulation proceeds and the primitive streak extends into the vicinity of the embryonic mesoderm and definitive endoderm precursors, these epiblast cells migrate into the blastocoel. The cells of the embryonic mesoderm will give rise to the heart and cranial mesenchyme precursors, while the endodermal cells will contribute to the foregut. The cells that will give rise to the neuroectoderm and surface ectoderm remain in the epiblast layer and are displaced proximally. Cells continue migrating through the primitive streak, and their location along the streak determines their mesodermal fate. This means that the most anterior region at

the node gives rise to the axial mesoderm (including the notochord and prechordal plate), the paraxial mesoderm originates from the streak's perinodal segment, lateral mesoderm comes from the mid-segment, and from the posterior-most region of the primitive streak arises the extraembryonic mesoderm.

At the completion of gastrulation, the three germ layers of the mouse embryo are essentially positioned in a reverse orientation, with the ectoderm on the inner aspect of the embryo and the mesoderm and endoderm on the outside. This configuration is a result of the egg cylinder structure in which the mouse embryo initially develops. Since the primary purpose of gastrulation is to correctly position the germ layers for subsequent morphogenesis, the mouse embryo must undergo a turning or rotational process that takes place between 8.5 and 9.25dpc in order to assume the proper conformation of the vertebrate embryo (Figure 1 A-D).

1.1.2 Segmentation of the murine paraxial mesoderm

Around 8.0dpc in mouse development, the unsegmented presomitic mesoderm (PSM) that lies in bilateral rods alongside the notochord undergoes segmentation, as cells bud off from the anterior end of the PSM and form a symmetrical pair of spherical epithelial blocks of cells (Figure 1A-D). This process of segmentation along the anterior-posterior axis, known as somitogenesis, generates repeated somites that will later differentiate into dorsal connective tissues, including bone, cartilage, muscle, and dermis. In the mouse, a new pair of somites is formed every 120 minutes until about 14.0dpc when 65 pairs of somites extend from the prospective occipital region to the posterior tip of the embryo.

Figure 1. Early mouse embryo development

(A) – (D) Scanning electron micrographs of mouse embryos during early somitogenesis stages. (A) An 8.0dpc embryo prior to turning with 1-7 pairs of somites; (B) A slightly older, still unturned, embryo with 6-8 somite pairs; (C) The process of embryo turning by 8.5dpc; (D) A completely turned 9.0dpc embryo with 15-18 pairs of somites.

(E) Schematic representation of a transverse section through the differentiated somite as cell migration from this structure begins (Adapted from Gilbert 2003).

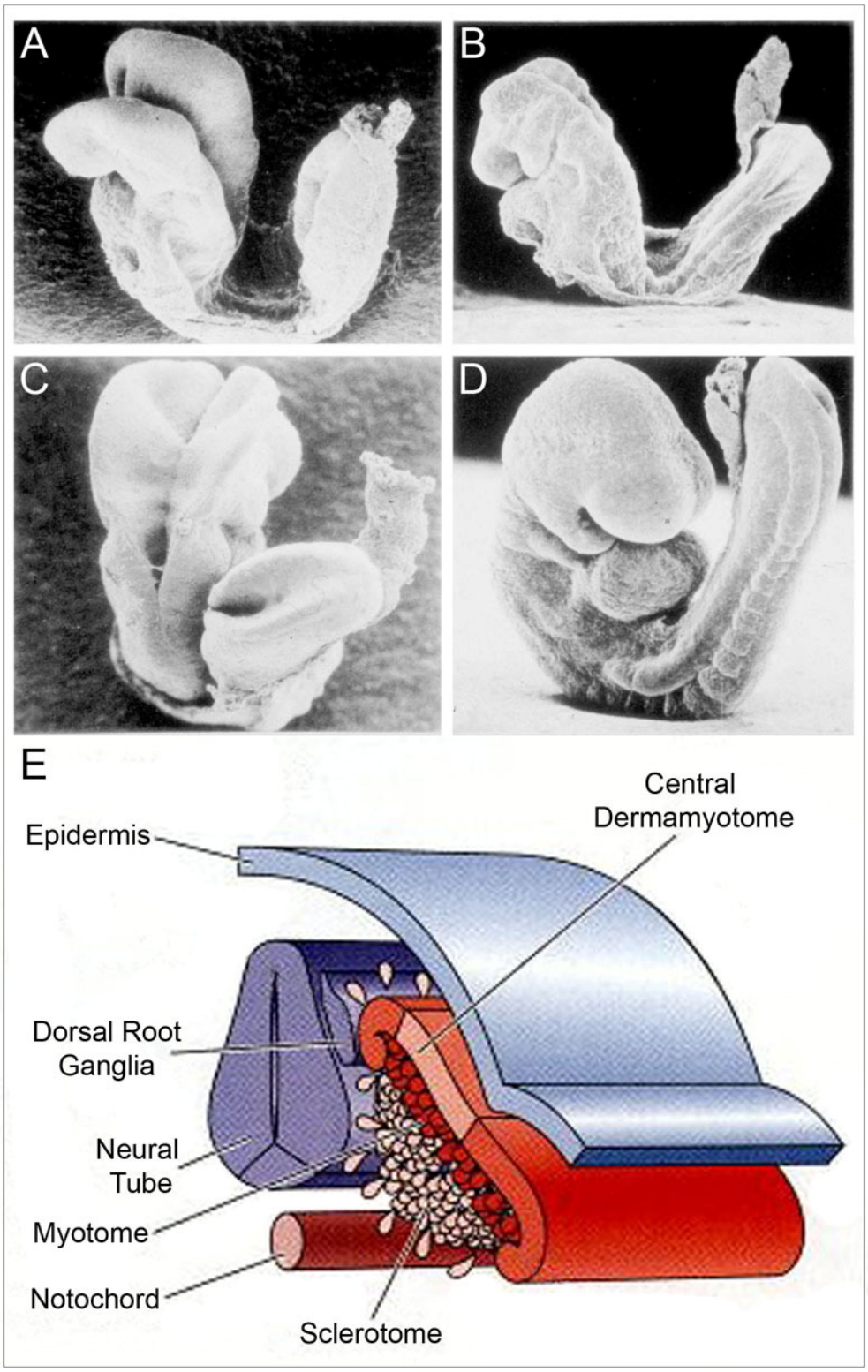
A
B
C
D
E
Central
Dermamyotome
Epidermis
Dorsal Root
Ganglia
Neural
Tube
Myotome
Notochord
Sclerotome

Each somite matures into sclerotome and dermamyotome compartments (Figure 1E). The fate of different somitic compartments depends upon their location along the dorsoventral and mediolateral axes. For instance, from the dorsal portion of the somite (dermamyotome) emerges dermis and skeletal muscles, while the ventral sclerotome gives rise to the bone, cartilage, and tendons. With respect to the mediolateral axis, the cells of the medial portion of the somite generate the muscles of the back, and cells from the lateral region form the limbs and muscles of the body wall. The sclerotome is formed from the ventromedial portion of the somite. These cells undergo an epithelial-to-mesenchymal transition and migrate toward the notochord. The first 5 somites will contribute to the occipital bones of the skull, and the more caudal somites will give rise to the vertebrae and thoracic ribs (Figure 2). The precursors of the axial vertebrae (prevertebrae) arise during the process of somite resegmentation, in which the sclerotome of the caudal half of one somite fuses with the sclerotome from the rostral half of the next adjacent somite. The unique characteristics of each vertebra will be summarized in Chapter 3. The sternum to which the ribs attach ventrally is derived from the lateral plate mesoderm.

The muscle precursors of the epaxial and hypaxial myotomes are located in the dorsomedial and ventrolateral lips of the dermamyotome, respectively. The epaxial myotome generates the deep muscles of the back, while the hypaxial myotome gives rise to the intercostal muscles and the ventral body wall. The muscle precursors from various A/P axis levels of the ventrolateral dermamyotome migrate to form the tongue, diaphragm, and limb muscles. Once myotome differentiation is

Figure 2. Somites give rise to vertebrae

Schematic representation of epithelialized somites. Somite pairs are depicted in colored boxes on each side of the neural tube (white box). Individual somites are grouped into occipital (red, 1-4), cervical (blue, 5-11), thoracic (yellow, 12-24), lumbar (green, 25-30), sacral (lavender, 31-34), and caudal (orange, 35+) regions. Pictured below the schematic is an 18.5dpc wild-type CD1 mouse skeleton (forelimbs removed) with the corresponding axial regions labeled as colored boxes (as above) along the length of the A/P axis.

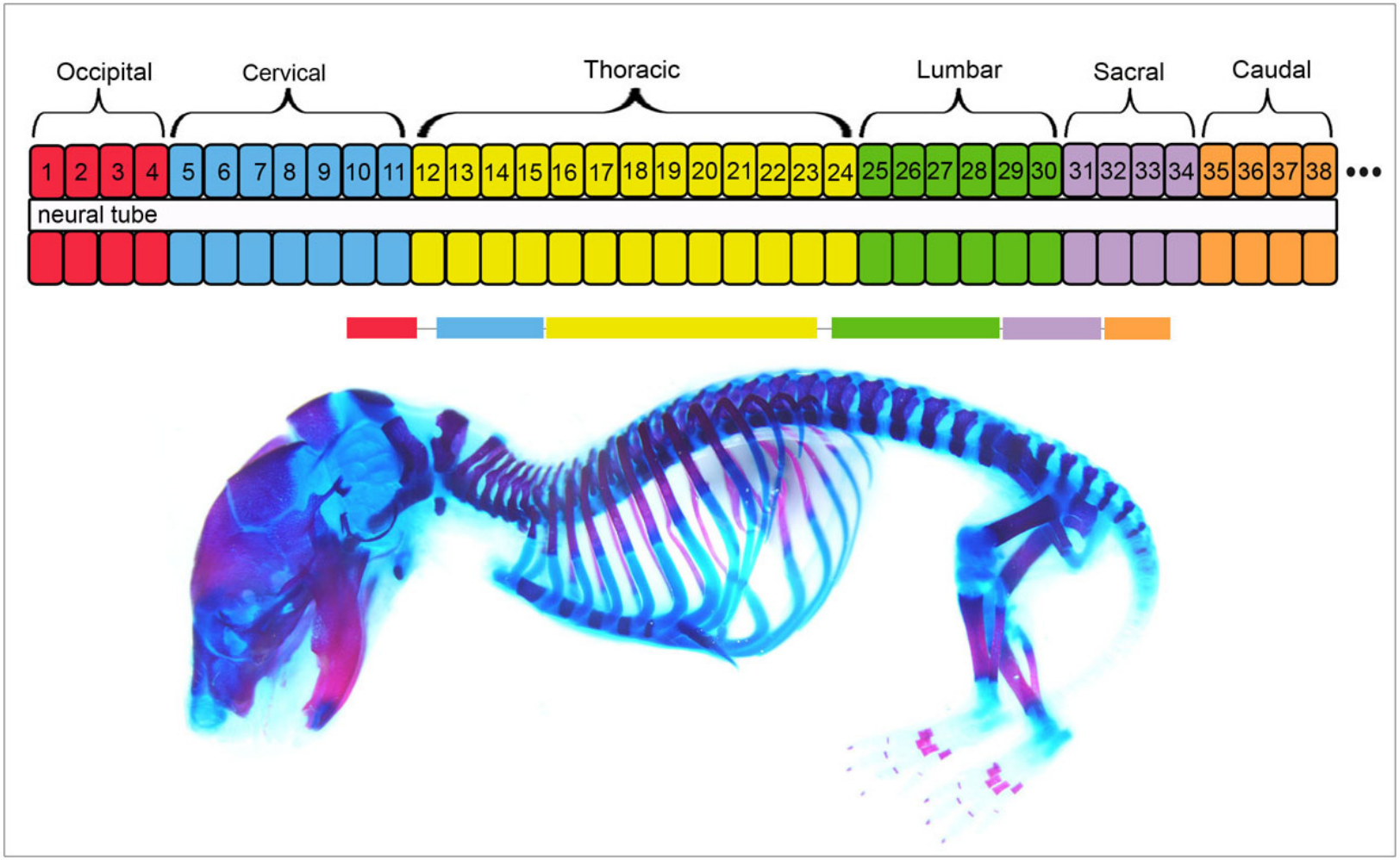
Occipital
Cervical
Thoracic
Lumbar
Sacral
Caudal
1 2 3 4 5 6 7 8 9 10 11 12 13 14 15 16 17 18 19 20 21 22 23 24 25 26 27 28 29 30 31 32 33 34 35 36 37 38
neural tube

complete, the remaining dermotomal cells differentiate into mesenchyme and mix with the lateral mesoderm to form the dermis and subcutaneous tissue.

1.1.3 Segmentation of the murine hindbrain

The central nervous system develops from three subdivisions within the neural tube: the forebrain (prosencephalon), the midbrain (mesencephalon), and the hindbrain (rhombencephalon). This three-vesicle stage of brain development is transient, as the forebrain further subdivides into the telencephalon and diencephalon; the hindbrain subdivides into the metencephalon and myelencephalon. In early development, the presumptive hindbrain is transiently divided into seven individual segments, termed rhombomeres, which will give rise to the adult hindbrain structures: the cerebellum, pons, and medulla oblongata (Figure 3A). This segmented pattern of the hindbrain specifies the origins of the cranial nerves, giving each rhombomere a different developmental fate. The two-segment periodicity of the hindbrain creates a functional organization of the rhombomeres with respect to the cranial ganglia, branchiomotor nerves, and neural crest cells that emerge from each segment (Figure 3B). For example, ganglia from rhombomere 2 (r2) contribute to the fifth (trigeminal) cranial nerve, r4 ganglia form the seventh (facial) and eighth (vestibuloacoustic) nerves, and r6 ganglia form the ninth (glossopharyngeal) nerve. Neural crest cells also use these segmented streams adjacent to rhombomeres 2, 4, and 6 to migrate ventrolaterally from the hindbrain into the first, second, and third branchial arches, respectively. Kulesa *et al*. showed that the regions lateral to r3 and r5 contained no neural crest cells. Instead, the neural crest originating from these

Figure 3. Segmentation of the mouse hindbrain

(A) Scanning electron micrograph of the neural tube's interior surface at the level of the hindbrain in an 8.5dpc mouse embryo. The individual segments, or rhombomeres, are labeled r1-r7.

(B) Schematic representation of the sensory and motor components that are derived from the hindbrain. To illustrate both functions, the motor components are shown on the right and the sensory components on the left. The Vth (trigeminal), VIIth (Facial), IXth (Glossopharyngeal) cranial motor nerves are comprised of neurons from r2/r3, r4/r5, and r6/7, and they exit the neural tube to innervate the first, second, and third branchial arches, respectively. The sensory ganglia associated with rhombomeres 2, 4, 6/7 are shown.

r = rhombomere; g = sensory ganglion; ov = otic vesicle; m = motor nerve; b = branchial arch.

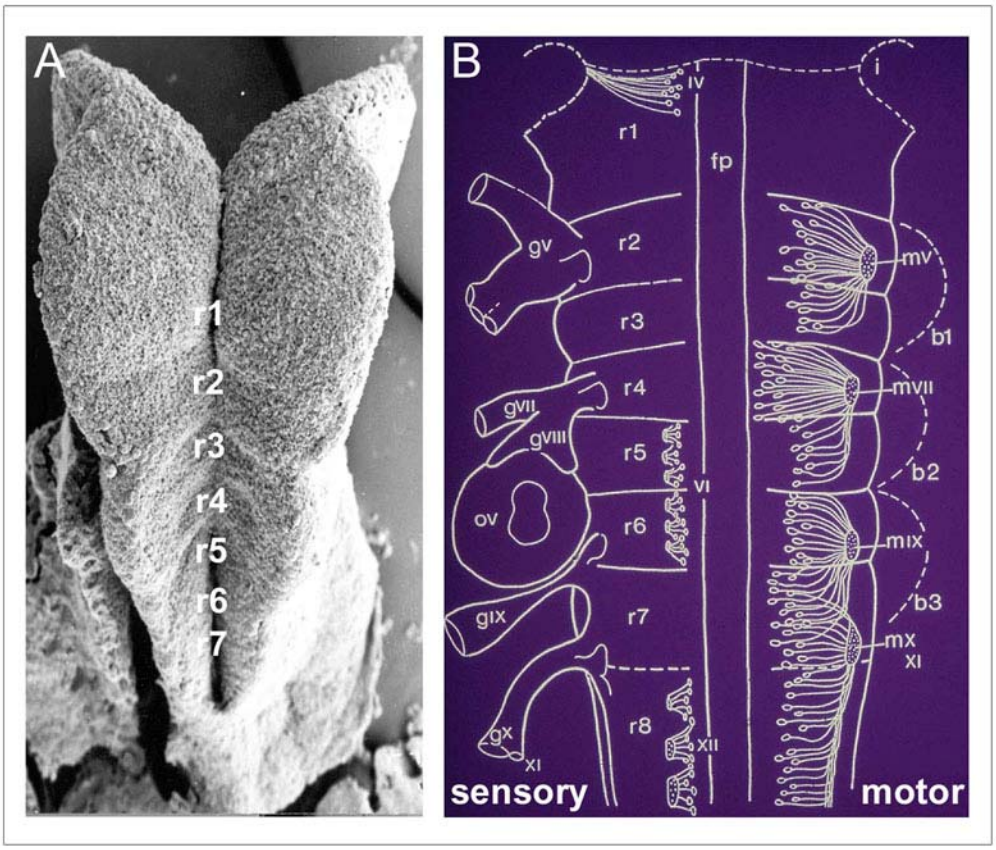
A
r1
r2
r3
r4
r5
r6
r7
B
IV
r1
fp
gV
r2
r3
r4
gVII
gVIII
r5
VI
ov
r6
gIX
r7
r8
gX
XI
XII
sensory
i
mV
b1
mVII
b2
mIX
b3
mX
XI
motor

rhombomeres migrated rostrally and caudally to adjoin neural crest streams exiting from r2, r4, and r6 (Kulesa and Fraser, 1998). Within the head region, cranial neural crest dorsolateral migration from the neural tube through the branchial arches contributes significantly to craniofacial development, generating the skeletal muscle, bone, and cartilage of the face. As a result of its immense developmental potential in forming cranial, as well as trunk, vagal, and cardiac tissues, the neural crest is often referred to as the fourth germ layer.

Each rhombomere has unique molecular and cellular properties correlated with specific domains of gene expression. In order to establish a unique rhombomere identity, the developing hindbrain must restrict cell mingling to maintain organized patterns of gene expression. This means that while cells within a single rhombomere may intermingle freely, they must not be allowed to mix with the cells of adjacent rhombomeres. Several signaling molecules and pathways are involved in maintaining such strict rhombomeric boundaries. The Eph/ephrin signaling pathway and the *Hox* gene transcription factors are responsible for generating the hindbrain compartments and the identity of each segment. Other transcription factors, such as kreisler and Krox20, contribute to the specification of the rhombomeres (Figure 4).

The *kreisler* (*kr*) gene has an important role in early hindbrain segmentation. It encodes a Maf/basic leucine zipper (b-ZIP) protein (krml1), whose expression is limited to rhombomere (r) 5 and r6 (Cordes and Barsh, 1994). In the *kreisler* mutant mouse, r5 is missing, but r6 is still present, indicating that kreisler is important for the formation of r5 (Manzanares et al., 1999b).

Figure 4. Gene expression profiles in the mouse hindbrain

The seven rhombomeres are alternately-colored to distinguish each segment, with the anterior-most rhombomere (r1) on the left side. The ventrally-located notochord is shown as a black rod under the hindbrain. The combination of *Hox* genes as well as other transcription factors, membrane proteins, secreted factors, and intracellular proteins give each rhombomere its specific identity. The darkly-shaded bars indicate strong gene expression, and the lightly-shaded bars indicate weak levels of expression.

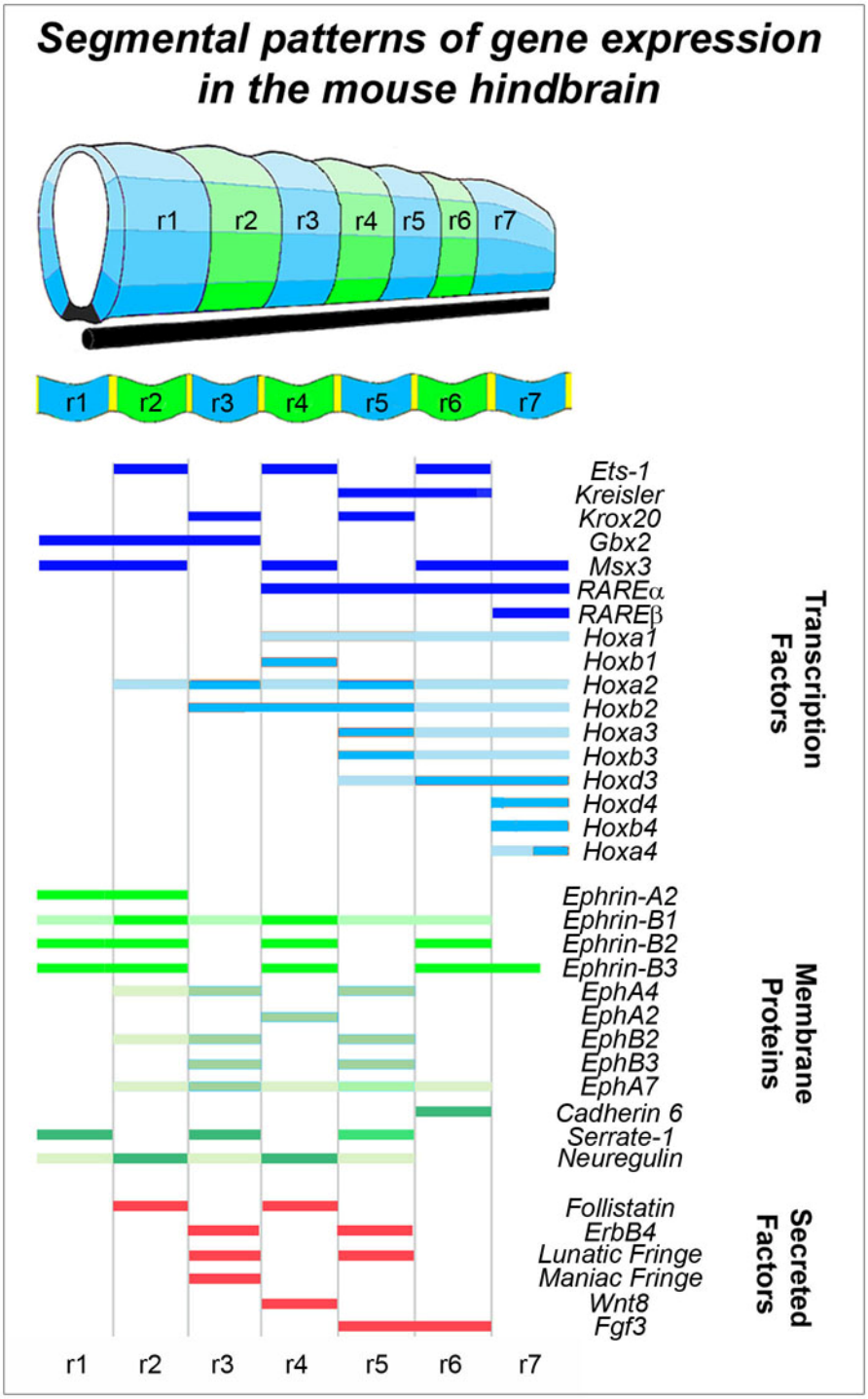
Segmental patterns of gene expression in the mouse hindbrain
r1
r2
r3
r4
r5
r6
r7
Ets-1
Kreisler
Krox20
Gbx2
Msx3
RAREα
RAREβ
Hoxa1
Hoxb1
Hoxa2
Hoxb2
Hoxa3
Hoxb3
Hoxd3
Hoxd4
Hoxb4
Hoxa4
Transcription Factors
Ephrin-A2
Ephrin-B1
Ephrin-B2
Ephrin-B3
EphA4
EphA2
EphB2
EphB3
EphA7
Cadherin 6
Serrate-1
Neuregulin
Membrane Proteins
Follistatin
ErbB4
Lunatic Fringe
Maniac Fringe
Wnt8
Fgf3
Secreted Factors

Kreisler may also be a direct regulator of *Krox20*, which is a zinc finger transcription factor that is expressed in r3 and r5. When *kreisler* is ectopically expressed in transgenic mice, *Krox20* expression is prolonged in r3 (Theil et al., 2002). *Krox20* also plays a critical role in specifying rhombomere identity; conserved r3/r5 enhancers for both *Hoxa2* and *Hoxb2* contain high-affinity *Krox20* binding sites that are responsible for direct upregulation of both *Hox* group 2 genes by *Krox20* (Nonchev et al., 1996).

Kreisler and Krox20 cooperate to control the expression of target *Hox* genes in the developing hindbrain, particularly *Hoxb3*, thus playing a key cooperative role in maintaining segmental identity (Manzanares et al., 2002). *Krox20* further regulates Eph receptor expression that restricts cell mingling. The *EphA4* enhancer element that drives expression of the receptor in r3 and r5 contains eight Krox20 binding sites; mutations in these sites eliminate the activity of the enhancer, and overexpression of *Krox20* ectopically activates the *EphA4* enhancer (Theil et al., 1998). Later in development, these factors are also critical to the character of each segment, since they directly regulate the *Hox* genes that are expressed in a segment-restricted manner (Wilkinson, 2001). Prior to the formation of the rhombomeres, gene expression boundaries are diffuse in the hindbrain. The Eph receptors and their ephrin ligands in adjacent cells participate in bidirectional cell repulsion that sorts cells with the same identity into prospective rhombomeres (Xu et al., 1999).

1.2 *Hox* Genes

The *Hox* (or homeobox-containing) genes are a family of evolutionarily highly-conserved transcription factors that regulate anterior-posterior patterning along the axis of the developing embryo. They contain a homeobox that is 183 nucleotides in length; this encodes the homeodomain. This region functions as a DNA-binding motif and is typically located in exon 2 of the gene's coding sequence. The vertebrate *Hox* genes are related to the *Drosophila* homeotic gene complex (*HOM-C*) on chromosome 3 in the fly. There are 39 vertebrate *Hox* genes, and they are arranged into 4 separate chromosomal clusters (*HoxA* on chromosome 6, *HoxB* on chromosome 11, *HoxC* on chromosome 15, and *HoxD* on chromosome 2 in the mouse) that arose upon genome duplication. Each chromosomal cluster contains select members of each of the 13 paralogous groups (Figure 5). This organization also corresponds to the sequential manner by which they are activated from 3' to 5'. The most 3' mammalian *Hox* genes derive from the most 3' *Drosophila* HOM-C gene, *labial*, and are required for the formation of the more anterior structures of the body. Similarly, the most 5' mammalian *Hox* genes are related to the most 5' *Drosophila* HOM-C gene, *AbdB* (*Abdominal B*), and are required for the development of the posterior structures of the embryo. This feature of *Hox* temporal and spatial gene expression is referred to as colinearity. Furthermore, the expression domains of the *Hox* genes show rhombomeric-specific restriction in the hindbrain (Figure 3). Such expression patterns of the mouse *Hox* genes suggests a combinatorial code by which the actions of certain genes in concert specify a particular region along the A/P axis.

Figure 5. The four vertebrate *Hox* clusters

The *Hox* genes derive from the *Drosophila* HOM-C genes and are evolutionarily conserved from flies to human. There are 39 *Hox* genes in vertebrate species, and they are clustered on four separate chromosomes. The position of a gene within a cluster dictates its temporal and spatial expression in order to pattern the body axis: 3' *Hox* genes are expressed early and pattern anterior structures, and 5' *Hox* genes are expressed later in development and pattern posterior structures, a unique feature known as *Hox* colinearity. Additionally, *Hox* genes from different clusters form paralogous groups, based on their chromosomal position and temporal expression. In this schematic representation, genes within a paralogous group have the same-colored box. The previous *Hox* notations are listed below each gene (adapted from Henry 2000).

lab = labial; pb = proboscipedia; Dfd = deformed; Scr = sex combs reduced; Antp = antennapedia; Ubx = ultrabithorax; AbdA = abdominal-A; AbdB = abdominal-B.

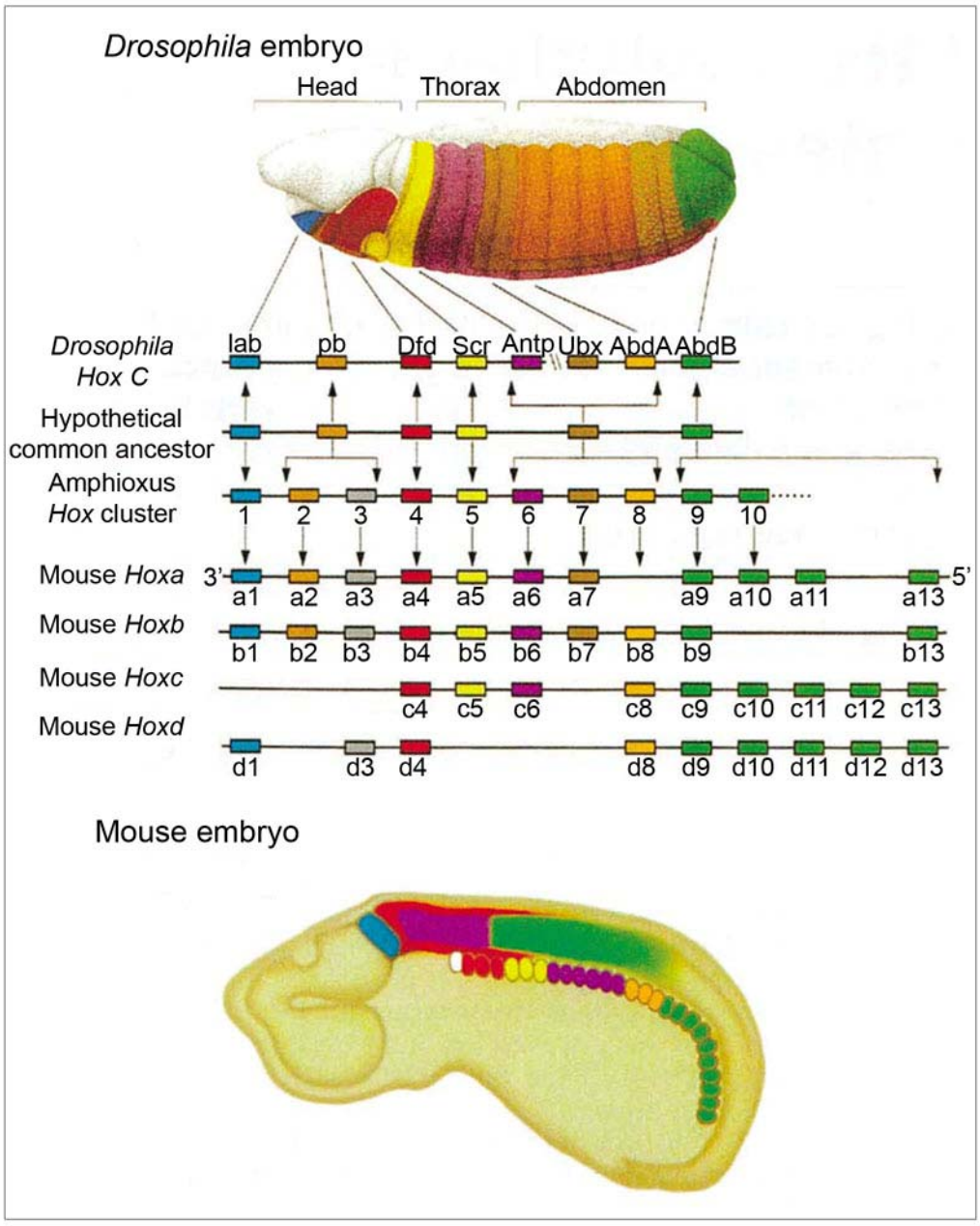
Drosophila embryo
Head
Thorax
Abdomen
Drosophila *Hox C*
lab
pb
Dfd
Scr
Antp
Ubx
AbdA
AbdB
Hypothetical common ancestor
Amphioxus *Hox* cluster
1 2 3 4 5 6 7 8 9 10
Mouse *Hoxa*
3'
5'
a1 a2 a3 a4 a5 a6 a7 a9 a10 a11 a13
Mouse *Hoxb*
b1 b2 b3 b4 b5 b6 b7 b8 b9 b13
Mouse *Hoxc*
c4 c5 c6 c8 c9 c10 c11 c12 c13
Mouse *Hoxd*
d1 d3 d4 d8 d9 d10 d11 d12 d13
Mouse embryo

Expression of paralogous groups tends to align near specific rhombomeres, providing segmental identity along the embryo's A/P axis (Lumsden and Krumlauf, 1996).

Previous studies have shown that retinoids influence the spatial expression patterns of the *Hox* genes. Severe developmental deformities have been observed in vertebrate embryos that received systemic treatments of retinoic acid, including reductions in the sizes of the forebrain, midbrain, and hindbrain regions, dependent on the time of retinoic acid exposure (Morriss-Kay et al., 1991). The Retinoid A and Retinoid X receptors (nuclear receptors RAR and RXR) mediate the actions of retinoic acid. These receptors function as heterodimers which form a sequence-specific DNA binding complex to direct target gene activation through a Retinoic Acid Responsive Element (RARE) (Dilworth et al., 1999). Those *Hox* genes located in the 3' region of the chromosomal cluster (thus, having early expression in the anterior regions of the embryo) display a much earlier response to retinoic acid than those genes located in the 5' region whose expression comes on later during development in posterior regions (Simeone et al., 1991). A wide variety of functional studies have shown that these genes regulate regional identity in a number of diverse tissues (for review, see (Maconochie et al., 1996)). The region of particular interest to the lab is the hindbrain and how the *Hox* genes are involved in patterning this structure.

1.2.1 The Role of *Hox* Genes in Mesoderm Development

The various roles of *Hox* genes in the developing embryo have been ascertained through the analysis of individual loss-of-function *Hox* mutants.

Phenotypes observed in these mutants often affect more than just the axial skeleton. For example, *Hoxa11* mutants show malformations of both the forelimb and hindlimb (Small and Potter, 1993); the second spinal ganglion undergoes degeneration and takes on an abnormal morphology in *Hoxb8* mutants (van den Akker et al., 1999). However, since this dissertation focuses on the impact of 3' *Hox* genes on vertebral development, this portion of the chapter will primarily address the expression of *Hox* genes in the presomitic and somitic mesoderm that patterns the vertebrae and the ability of *Hox* mutations (single, double, triple, and whole-cluster) in all four chromosomal clusters to generate homeotic transformations within the axial skeleton. The following review of *Hox* mutants will show that mutations within this family of transcription factors largely affect the transitions between distinct vertebral regions, which can be divided into cervical, upper thoracic (T1-T7), lower thoracic (T8-T13), lumbar, sacral, and caudal sections. Figure 6 has been included as a reference for wild-type axial skeleton anatomy. Additionally, this chapter will address the effects of different gene targeting strategies within *Hox* clusters on skeletal development. Overall, the *Hox* genes appear to be more important for giving individual vertebrae their distinct morphological features, instead of determining the total number of vertebrae. Figure 7 and Table 1 illustrate the reported anterior limits of expression only for those *Hox* genes expressed in vertebral precursors (presomitic mesoderm, somites, or prevertebrae), in addition to the presence of axial skeleton phenotypes observed in individual *Hox* mutants.

Figure 6. Wild-type anatomy of the axial skeleton

Dissected skeletons of 18.5dpc wild-type CD1 embryos, prepared by a Alizarin Red/Alcian blue double staining method.

(A) Dorsal view of the ossification centers that give rise to the occipital bone: Supraoccipital bone (SOB) is positioned anteriorly, paired Exoccipital bones (EOB) are positioned laterally, and the Basioccipital bone (BOB) is positioned posteriorly.

(B) Lateral view of the seven cervical vertebrae: C1 contains a ventral anterior arch of the atlas (aaa); C1-C7 vertebral bodies are located ventrally (left), and neural arches are located dorsally (right).

(C) Lateral view of the thirteen thoracic vertebrae and their associated ribs: T1-T7 contain “true” ribs; rib pairs from T8-T13 are “floating” ribs; the last two pairs (T12-T13) are “false” ribs. Thoracic vertebral bodies are located dorsally (right), and ribs project ventrally (left).

(D) Ventral view of the sternum: sternum ossification is inhibited where rib pairs from T1-T7 (R1-R7) form sternocostal junctions, resulting in an anterior manubrium (M), four separate sternebrae (S1-S4), and a posterior xiphoid process (X).

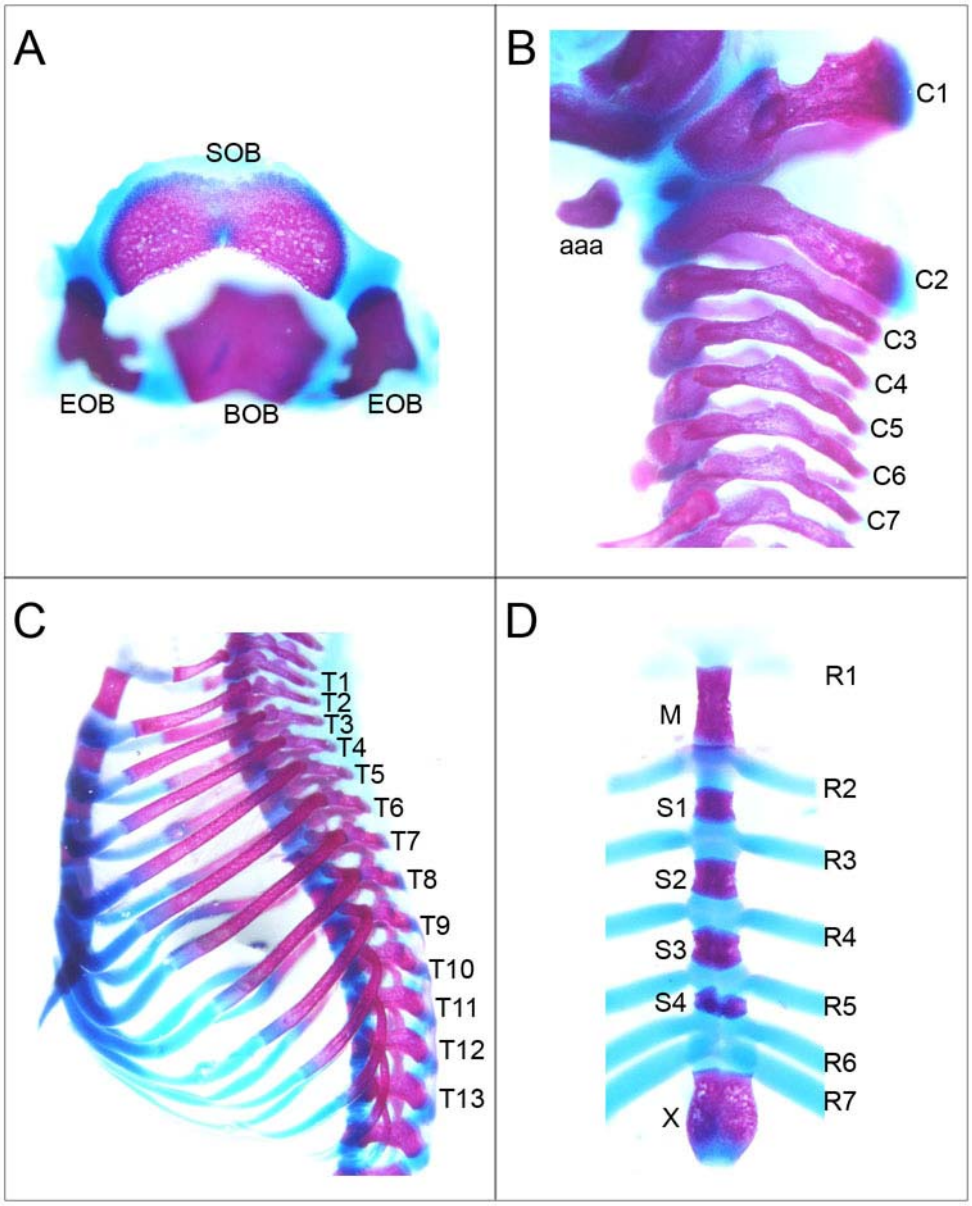
A
SOB
EOB
BOB
EOB
B
C1
aaa
C2
C3
C4
C5
C6
C7
C
T1
T2
T3
T4
T5
T6
T7
T8
T9
T10
T11
T12
T13
D
R1
M
R2
S1
R3
S2
R4
S3
R5
S4
R6
R7
X

Figure 7. *Hox* genes pattern vertebral precursors

Schematic representation of *Hox* gene expression in developing vertebrae. Individual vertebral precursors (prevertebrae, pv) are grouped into cervical (pv1-7), thoracic (pv8-20), lumbar (pv21-26), sacral (pv27-30), and caudal (pv31+) regions. The most anterior limit of expression that has been reported for each paralogous group is shown.

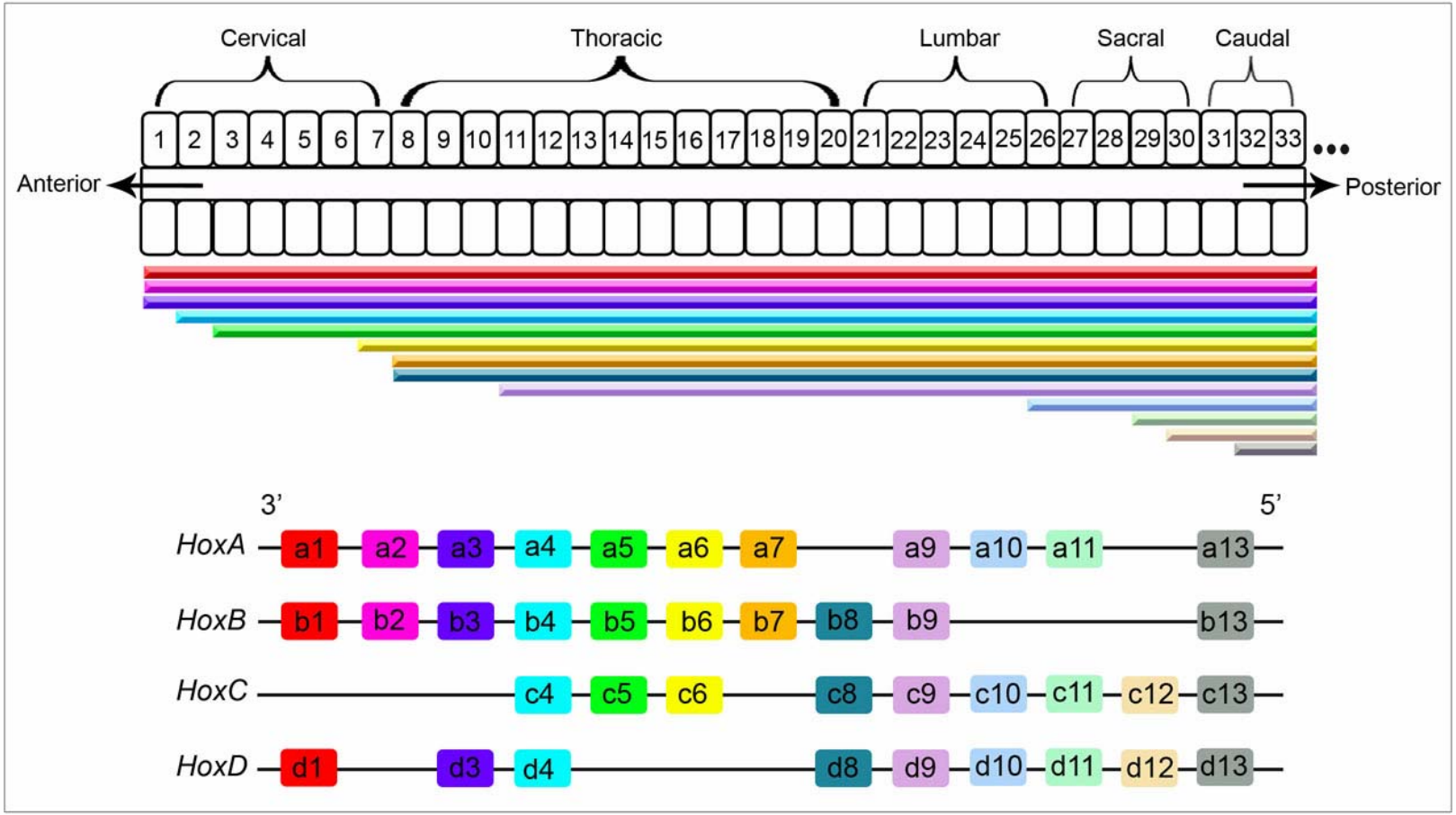
Cervical
Thoracic
Lumbar
Sacral
Caudal
1 2 3 4 5 6 7 8 9 10 11 12 13 14 15 16 17 18 19 20 21 22 23 24 25 26 27 28 29 30 31 32 33
Anterior
Posterior
3'
5'
HoxA a1 a2 a3 a4 a5 a6 a7 a9 a10 a11 a13
HoxB b1 b2 b3 b4 b5 b6 b7 b8 b9 b13
HoxC c4 c5 c6 c8 c9 c10 c11 c12 c13
HoxD d1 d3 d4 d8 d9 d10 d11 d12 d13

Table 1. *Hox* gene expression in vertebral precursors and published skeletal phenotypes

The *Hox* genes for whom expression domains in vertebral precursors and associated phenotypes in the axial skeleton have been established are listed here.

*not applicable

**not reported

Listed in parentheses are the references for each gene's expression boundary and mutant phenotypes: 1:Dupé (1997); 2: Barrow (1996); 3: Manzanares (1999); 4: Akasaka (1996); 5: Condie (1993); 6: Burke (1995); 7: Gaunt (1989); 8: Geada (1992); 9: Coré (1997); 10: Vogels (1990); 11: Deschamps (1993); 12: Tiret (1993); 13: Chen (1997); 14: Kessel (1992); 15: Peterson (1994); 16: Izpisua-Belmonte (1991); 17: Lufkin (1991); 18: Chisaka (1992); 19: Gendron-Maguire (1993); 20: Rijli (1993); 21: Chisaka (1991); 22: Manley (1997); 23: Horan (1994); 24: Kostic (1994); 25: Ramirez-Solis (1993); 26: Manley (2001); 27: Saegusa (1996); 28: Boulet (1996); 29: Horan (1995); 30: Jeannotte (1993); 31: Rancourt (1995); 32: Garcia-Gasca (2000); 33: Chen (1998); 34: van den Akker (1999); 35: Medina-Martinez (2003); 36: Le Mouellic (1992); 37: van den Akker (2001); 38: Chen (1997); 39: Suemori (1995); 40: Fromental-Ramain (1996); 41: Rijli (1995); 42: Carpenter (1997); 43: Small (1993); 44: Favier (1995); 45: Davis (1994).

Hox Gene	Somite boundary	Prevertebra boundary	Axial skeleton phenotype?
Hoxa1	PSM (1)	n/a*	no (17, 18)
Hoxb1	PSM (2)	n/a*	n/r**
Hoxa2	n/r**	n/r**	no (19, 20)
Hoxb2	PSM (2)	n/a*	yes (2)
Hoxa3	4 (3)	Occipital (3)	no (21)
Hoxb3	n/r**	C1 (4)	yes (22)
Hoxd3	4 (5)	Occipital (5)	yes (5)
Hoxa4	7 (6, 7)	C2 (6, 7)	yes (23, 24)
Hoxb4	6 (6)	C1; C2 (4, 7)	yes (25, 26)
Hoxc4	7 (6)	C2; C4 (6, 8)	yes (27, 28)
Hoxd4	n/r**	C2 (4, 7)	yes (29)
Hoxa5	n/r**	C3 (4)	yes (30)
Hoxb5	n/r**	C2 (4)	yes (31)
Hoxc5	10 (6)	C5; C7 (4, 6)	n/r**
Hoxa6	n/r**	T1 (9)	yes (24)
Hoxb6	n/r**	C7 (4)	yes (31)
Hoxc6	12 (6)	C7; T1 (4, 6)	yes (32)
Hoxa7	n/r**	T3 (4)	no (33)
Hoxb7	15 (6)	T3; C6 (6, 10)	yes (33)
Hoxb8	Amb. (6)	Amb.; C7; T1 (4, 6, 11)	yes (34, 35)
Hoxc8	17 (6)	T1; T5 (4, 6, 12)	yes (36)
Hoxd8	18 (6)	T6 (6)	yes (37)
Hoxa9	23 (6)	T11 (6)	yes (38)
Hoxb9	Amb. (6)	Amb.; C3 (6, 13)	yes (38)
Hoxc9	23 (6)	T11 (6)	yes (39)
Hoxd9	29 (6)	L4 (6)	yes (40)
Hoxa10	n/r**	T13 (14)	yes (41)
Hoxc10	n/r**	n/r**	n/r**
Hoxd10	31 (6)	L6 (6)	yes (42)
Hoxa11	n/a*	n/r**	yes (43)
Hoxc11	n/a*	L2 (15)	n/r**
Hoxd11	34 (6)	L4; S3 (6, 16)	yes (44, 45)

1.2.2 Targeted mutations of individual *Hox* genes within each cluster

HoxA cluster single mutants

Hoxa1 mutants

Even though *Hoxa1* transcripts are detected in the presomitic mesoderm at early neurulation stages (Dupé et al., 1997), the loss of Hoxa1 function affects mainly branchial arch derivatives. Previous studies aimed at eliminating Hoxa1 protein function in the mouse have used two separate targeting events that generate differing phenotypes (Chisaka et al., 1992; Lufkin et al., 1991). Lufkin *et al*. deleted the region surrounding the start site for *Hoxa1* transcription, including the proximal promoter, the transcription start site, the translation initiation site, and the first 88 amino acids. The *neomycin* resistance gene was inserted into this region, followed by several stop codons. The phenotypes resulting from this targeting event ranged from inner ear defects to alterations in the bones of the developing cranium. Specifically, the cochlear duct and semicircular canals are missing. Minor modifications to the interparietal bone (IP) occurred, such that its lateral edges were more acutely defined in *Hoxa1*$^{-/-}$ 18.5dpc embryos. The exoccipital bone (EOB) appeared to be compressed, and the characteristic concave lateral border was absent from the basioccipital bone (BOB). They observed neither branchial arch nor vertebral malformations; spinal nerves and ganglia appeared normal. In contrast, Chisaka *et al*. disrupted Hoxa1 by inserting the *neomycin* cassette into the homeobox domain. Defects observed in the resulting *Hoxa1*$^{-/-}$ newborn mice were found in the middle and external ear. Mutants lacked middle ear ossicles, and the auricle and external

acoustic meatus of the external ear were malformed. They did, however, observe defects in the cochlea and vestibule (inner ear compartments), similar to Lufkin *et al*. Due to the lack of middle and external ear defects in the previous report, Chisaka *et al*. propose that the differences in phenotypes may be due to a difference in gene targeting strategies.

***Hoxa2* mutants**

Two separate groups have reported on the targeted deletion of *Hoxa2* (Gendron-Maguire et al., 1993; Rijli et al., 1993). The first targeting allele was generated upon deletion of the 3' end of exon 1 (159bp), the entire intron, the splice acceptor site, and the 5' end of exon 2 (33bp); a *neomycin* selection cassette was inserted to replace the deleted region (Gendron-Maguire et al., 1993). In order to create the second targeted allele, the 5' untranslated region (UTR), translational initiation site, and the first 72 amino acids of the Hoxa2 protein were deleted; the *neomycin* selection cassette replaced the deleted region (Rijli et al., 1993). In each case *Hoxa2* mutants mice display homeotic transformations, such that the skeletal elements derived from the second branchial arch are absent. Instead, they are replaced by first branchial arch-derived elements. Specifically, Reichert's cartilaginous primordium is absent, resulting in the loss of the lesser horn of the hyoid bone, the stapes, and the styloid cartilaginous anlage. Consequently, a duplication of the skeletal elements from the first branchial arch produces a duplication middle ear, including two symmetrical mallei and tympanic bones. These mice also lack the pinna of the external ear and exhibit wide clefts in the secondary palate. Finally, both

groups noticed alterations in the shape, as well as the lateral and rostral borders, of the BOB, which is derived from the occipital region of the somitic mesoderm, not branchial arch neural crest. This is interesting, since there are no reports to date that demonstrate *Hoxa2* mRNA expression in the occipital somite precursors.

***Hoxa3* mutants**

Chisaka and Capecchi disrupted *Hoxa3* expression by inserting a *neomycin* selection cassette into the homeodomain (Chisaka and Capecchi, 1991). *Hoxa3* homozygous mutant mice fail to survive past the first 12 hours following birth. Defects observed in these neonates center around the neck and upper thoracic region. In particular, mutants lack thymus and parathyroid tissues and have reduced thyroid and submaxillary structures. They also exhibit several cardiac and arterial defects. The clavicle is displaced more anteriorly at the level of the axis (C2), instead of at the WT level (C4). The larynx and trachea are displaced dorsally, closer to the vertebrae. Cartilages of the cricoid and thyroid are shorter and thicker, and the lesser horn of the hyoid is missing. Facial defects observed in *Hoxa3* homozygotes are due to the shortening of the mandible and maxilla, as well as an alteration in the squamosal bone's zygomatic process, which contributes to the zygomatic arch. Even though the anterior limit of *Hoxa3* in vertebral precursors lies at the level of the 4th occipital somite (Manzanares et al., 1999a), no defects have been reported in the axial skeletons of these mice. However, the contribution of *Hoxa3* to axial skeleton development will be addressed in the context of combined *Hoxb3* and *Hoxd3* mutations later in this chapter.

***Hoxa4* mutants**

The mutations described thus far have proven lethal for homozygous animals during the perinatal period. *Hoxa4* homozygotes, however, survive to adulthood and are fertile (Horan et al., 1994). *Hoxa4* was mutated upon insertion of the *neomycin* cassette into the first helix of the homeobox domain in the opposite orientation to *Hoxa4* transcription. Skeletal phenotypes observed in the resulting *Hoxa4* homozygotes were variable in penetrance and expressivity. Forty-eight percent of neonates developed ribs on C7, while a smaller number displayed sternal defects, ranging from sternebrae fusions to crankshaft sternums. Interestingly, when Horan *et al*. overexpressed *Hoxa4*, they found that the C7 rib phenotype was suppressed. Five of the seven homozygotes that survived to adulthood possessed the dorsal process characteristic of C2 on both C2 and C3. Kostic and Capecchi also similarly disrupted *Hoxa4*, except they targeted a *neomycin* cassette into the third helix of the homeodomain, eliminating the DNA-binding portion of Hoxa4 protein (Kostic and Capecchi, 1994). The resulting homozygous mice were viable and fertile. While this group did not observe C7 ribs anlagen (presumably a posterior transformation of C7 to T1), they did report a similar anterior transformation of C3 into C2 with respect to the dorsal process only in all homozygotes analyzed. Additionally, C2 and C4 appeared normal, although alterations in C4 may be difficult to observe since the morphology of C4 closely resembles that of C3. Although *Hoxa4* transcripts are detected weakly at the border between the C1 and C2 prevertebrae (pv1 and pv2), a strong level of expression extends up to the level of pv2/pv3. The transformations

within these mutants, particularly, the C2/C3 malformations, correspond almost precisely with the *Hoxa4* anterior boundary of expression (Gaunt et al., 1989).

***Hoxa5* mutants**

The anterior limit of *Hoxa5* in the prevertebrae was found to lie at the level of C3 (Akasaka et al., 1996). To investigate the importance of *Hoxa5* expression in prevertebrae, the *neomycin* gene was introduced into the third helix of the *Hoxa5* homebox sequence, eliminating the DNA-binding ability of Hoxa5 protein (Jeannotte et al., 1993). Fifty percent of mutants possessing two targeted alleles died during the perinatal period due to a general failure to thrive. The skeletal defects seen in homozygous neonates and adults were classified as both anterior and posterior homeotic transformations in the cervical and thoracic regions. A posterior transformation of C7 to T1 could be seen in 73% of *Hoxa5* homozygous perinatal animals, such that one or both sides of C7 contained extensive ribs. One-third of these ribs fused ventrally with ribs from T1 prior to the contact of T1 ribs to the sternum. However, some C7 ribs did form sternocostal junctions independent of the T1 ribs. The ribs sometimes observed on the seventh cervical vertebrae of *Hox5* heterozygotes were smaller and rarely extensive. Over 90% of *Hoxa5* homozygous adults and perinatal animals were found to be missing the anterior tuberculi (AT) of C6, resulting in a sixth cervical vertebrae that resembles C3 through C5. This anterior transformation did not interfere with the entry of the vertebral artery into the ventral canals of C6. The above transformations gave these animals a vertebral distribution of C6/T14/L6, indicating that the seventh cervical vertebra is instead

classified as a thoracic vertebra. Furthermore, 19% of homozygous embryos showed a pair of ribs on L1, indicating a second anterior transformation of the first lumbar vertebra into a thoracic vertebra. This resulted in some animals with 15 pairs of ribs instead of the normal 13 pairs. Finally, the sternal morphology of *Hoxa5* homozygotes is significantly altered in a small number of mutants. Fission of the two manubrium sterni results in an extra sternebrae in 9% of the mutants. The fourth sternebra may be fused to the third sternebra and is reduced in size. A "crankshaft" sternal appearance in these mutants results from the asymmetric attachment of ribs to different points of the sternum, causing ossification of the sternal bands to be inhibited in an asymmetric manner along the anterior-posterior axis of the sternum. Finally, the xiphoid process often contains fissures that are more significant than those sometimes found in wild-type or *Hoxa5* heterozygous animals.

***Hoxa6* mutants**

The first helix of the Hoxa6 homeodomain was disrupted upon *neomycin* gene targeting (Kostic and Capecchi, 1994). Mutant animals with two targeted alleles survive to adulthood and are fertile with no outward abnormalities. The transformations observed in these homozygotes are relatively mild. The ribs found on C7 in 43% of the mutants are more fully developed than those rarely found on C7 in wild-type animals. Sometimes these mutant ribs fused with T1 ribs, and other times they formed independent sternocostal junctions. This phenotype represents a partial posterior transformation of C7 into T1, since the remaining characteristics of C7 were normal. C6 was never found to be transformed. Similarly, the ribs

extending from T1 and T2 appeared normal. However, the processus spinous (a dorsal spinal process characteristic of WT T2) was sometimes found on T1, yet absent from T2. The authors further note that this process can occasionally be found on both T1 and T2 in wild-type animals. Additionally, 2 of 29 *Hoxa6* homozygous animals displayed the crankshaft sternal morphology. These phenotypes centered at the cervicothoracic vertebral boundary strongly correlate to the anterior boundary of *Hoxa6* gene expression at the level of pv8, the precursor to T1 (Coré et al., 1997).

***Hoxa7* mutants**

When the *Hoxa7* gene locus was mutated by inserting the *neomycin* gene into the homeodomain, homozygous animals were viable and fertile (Chen et al., 1998). All heterozygous (n=29) and homozygous (n=16) mutants appeared outwardly normal with no skeletal defects. *Hoxa7* transcripts can be visualized in the prevertebrae up to an anterior limit at T3 (Akasaka et al., 1996). However, unlike previous *Hox* genes with defined expression boundaries in the somitic mesoderm and corresponding skeletal defects, no malformations are seen in *Hoxa7* single mutants. Nevertheless, the ability of this gene to act synergistically with its co-paralogue *Hoxb7* to pattern the vertebrae will be discussed later in this chapter.

***Hoxa9* mutants**

Based solely on the anterior limit of *Hoxa9* expression in the prevertebrae at the level of pv18 (precursor of the 11th thoracic vertebra; (Burke et al., 1995)), one might predict vertebral homeosis to begin at the same level in *Hoxa9* loss-of-function mutants. However, previous *Hoxa9* mutant analysis supports the argument that the

limit of somitic expression does not dictate the vertebral level at which a *Hox* gene exerts its function. The *Hoxa9* gene was disrupted by the insertion of the *neomycin* gene into the homeodomain in the same direction as *Hoxa9* transcription (Fromental-Ramain et al., 1996). The mutation interrupted the third (recognition) helix of the homeodomain, eliminating the DNA-binding ability of the resulting Hoxa9 protein. Homozygous mice generated from this targeting event were viable and fertile; anterior transformations restricted to the lumbar region were dosage-dependent, since the penetrance and expressivity of the phenotypes increases as functional *Hoxa9* copies are removed. The first lumbar vertebra (L1) possessed a pair of ribs that were shorter than those on T13 and were oriented in a more posterior direction, indicating an L1 to T13 transformation. Additionally, the presence of ectopic accessory processes on L2 through L5 each resembled those normally associated with the immediately-anterior vertebra. The sixth lumbar vertebra was normal, as were the thoracic vertebrae. These findings suggest L5→L4→L3→L2→L1→T13 transformations within *Hoxa9* homozygous mice, which correlate nicely with the strong rostral limit of *Hoxa9* mRNA expression at pv20, or the thirteenth thoracic prevertebra.

***Hoxa10* mutants**

Similar phenotypes were noted when *Hoxa10* mutant mice were created. The *neomycin* selection cassette was inserted in the same orientation as *Hoxa10* transcription into the homeobox, interrupting the DNA-binding region. Homozygous mutants were viable with impaired fertility (Rijli et al., 1995). The same anterior

transformation of L1 to T13 was observed in *Hoxa10* homozygous adults, with partial anterior transformations in the remaining lumbar vertebrae. Unlike *Hoxa9* mutants, however, these mice also displayed defects in the sacral vertebrae. S1 and S2 were asymmetrically transformed in 10% of homozygotes, such that, on the right side of the animal, S1 articulated correctly with the right ilium bone; the left side of S1 possessed an L6-like transverse process. This shifted the articulation of the left ilium bone to the level of S2. Nine of 30 mutants had 6 rib pairs that fused to the sternum; mutant ribs were often shortened and resembled the next rib posterior. The tenth thoracic vertebra in wild-type animals represents a "transitional" vertebra, marking a change in the orientation of the dorsal process. On T3 through T9, this process points posteriorly, while from T11 to more caudal vertebrae, the process extends anteriorly. In *Hoxa10* mutants, the 10^{th} thoracic vertebra takes on features that are similar to T11. As a result, T9 becomes the transitional vertebra, as it possesses T10-like characteristics. *Hoxa10* heterozygotes display similar, although milder, phenotypes to those found in *Hoxa10* homozygotes. Interestingly, a majority of the phenotypes in *Hoxa10* mutants are observed in the thoracic-lumbar vertebral boundary. This position correlates to the strong rostral limit of *Hoxa10* gene expression in pv21, or the first lumbar prevertebra (Benson et al., 1995). However, it does not mean that *Hoxa10* is the only gene important for patterning this transition. The experiments investigating synergism between this gene and its co-paralogue *Hoxd10*, as well as the non-paralogous gene *Hoxd11*, will be discussed later in this chapter.

Hoxa11 mutants

Hoxa11 deletion was achieved upon ligation of a *neomycin* selection cassette into the 3' portion of the gene, disrupting the homeobox (Small and Potter, 1993). Mice that are homozygous for this mutation were found to have homeotic transformations in the lumbar region of the vertebral column. The thirteenth pair of ribs were absent from T13, indicating a T13→L1 posterior transformation. The authors note that this phenotype was also observed in *Hoxa11* heterozygotes, although, to a lesser extent: some rib portions of the thirteenth pair remained. T12 appeared normal, and there were no other posteriorizations. The lumbar region typically contains 6 vertebrae, with 5 being a wild-type variation. In some *Hoxa11* homozygotes, as many as 8 lumbar vertebrae were observed, including the transformation of the thirteenth thoracic vertebra into a lumbar vertebra. Finally, two homozygous mutants displayed defects in the fusion of ribs to the sternum. The second rib fused either in a more anterior position (with the first rib) or in a more posterior position, resulting in an abnormally segmented pattern of the sternum. The contribution of *Hoxa11* to the patterning of thoracic-lumbar vertebral transition will be discussed later in this chapter in the context of simultaneous *Hox* paralogous group 11 deletions.

HoxB cluster single mutants

Hoxb2 mutants

The expression profile of *Hoxb2* mRNA at 9.5dpc indicated a very diffuse pattern, with an anterior limit at r3 and extending to the PSM at the posterior end of

the embryo. Barrow and Capecchi disrupted *Hoxb2* by inserting the *neomycin* gene into the region encoding the protein's third (DNA-binding) helix of the homeodomain (Barrow and Capecchi, 1996). While the resulting heterozygous animals were outwardly normal and fertile, most homozygous mice died in two different groups within 3.5 weeks of birth. The first group (75%) died within the first 24 hours after birth, and the second group (13%) died around 21-25 days after birth. The presumed cause of death was an inability to suckle due to a noticeable facial paralysis. The most highly penetrant phenotype in homozygous animals was a split sternum that resulted in a severe split or a failure of the sternal bands in close proximity to fuse together. Although no heterozygous animals displayed sternal bifurcation, about 5% did have a crankshaft sternal morphology. An axial-to-atlas anterior transformation was observed in *Hoxb2* heterozygotes and homozygotes; affected mice showed a broadened neural arch and an ectopic anterior arch of the atlas. Interestingly, the orientation of the anterior arch present on C1 was altered, such that the arch was either parallel to C2 or tilted 45º, and the arches of homozygous mice were more severely affected than those in heterozygotes.

***Hoxb3* mutants**

The entire *Hoxb3* homeodomain was deleted and replaced by a *neomycin* selection cassette in order to generate *Hoxb3* mutant mice (Manley and Capecchi, 1997). The resulting homozygous mice were both viable and fertile with no defects in the various cartilages or bones of the throat and no transformations of cervical vertebrae. However, 2 of 18 animals displayed a defect in the formation of ventral

aspects of C1 and C2: an ossified fusion between the anterior arch of the atlas and the dens of the axis. Although there does not appear to be any overlap in the skeletal phenotypes of mice carrying mutations in *Hoxa3* and *Hoxb3*, there is evidence to suggest that simultaneous mutation of these two co-paralogues does result in more severe defects at a much higher degree of penetrance, since the expression profiles of both genes overlap at the level of pv1 (Akasaka et al., 1996; Manzanares et al., 1999a). These results will be described later in this chapter.

***Hoxb4* mutants**

Hoxb4 transcripts have been detected in somitic tissue corresponding to the prevertebrae (Gaunt et al., 1989). Low levels of *Hoxb4* mRNA are observed in pv1, but pv2 and more posterior prevertebrae express strong levels of this transcript. To investigate the function of *Hoxb4* expression in these tissues, two separate targeting alleles were generated, interrupting Hoxb4 function by taking advantage of traditional replacement and "hit and run" targeting protocols (Ramirez-Solis et al., 1993). The first allele contained two selectable markers that were inserted into the first exon of *Hoxb4*. Most of the resulting homozygous mice died either *in utero* or at birth. Homozygotes surviving until adulthood were found to be fertile. Those that died during the perinatal period had severe defects within the thoracic cavity, including a concave chest and herniations of the diaphragm. In addition, defects in the cervical and thoracic skeleton were observed. The neural arch of the axis was broadened like that of the atlas, and an ectopic anterior arch of the atlas was present on C2. Both the dens and the characteristic vertebral body of C2 were normal, suggesting a partial

anterior transformation of C2→C1. In rare cases, the neural arch of C3 was transformed to more closely resemble that of C2. A variety of sternal defects were observed, including defects in the fusion of paired sternal bands. Furthermore, this group showed that both the perinatal lethality and sternal defects were completely penetrant in both a 129SvEv inbred and 129SvEv-C57BL/6J hybrid backgrounds. The axial transformation, however, showed variable penetrance in the inbred background: only one of three homozygous newborns possessed an ectopic anterior arch of the atlas on C2. From these results, the authors conclude that genetic background contributes only partially to phenotypic variability. To evaluate the effects of disrupting exon 2, a second mutant allele was generated by introducing a premature stop codon into the region of the homeodomain that encodes the helix that confers DNA-binding specificity. Homozygous mice from this mutant line did not demonstrate the same perinatal lethality observed in the previous line. Instead, most animals survived until adulthood and were able to successfully breed. These mice had no diaphragm hernias or sternal defects. However, the axial transformation was still present. An ectopic anterior arch of the atlas could be found on 20% of these *Hoxb4* homozygotes, and 50% showed a broadened (C1-like) neural arch, with one animal having a partially duplicated C2 neural arch.

To further test the effect of the presence of a selectable marker in the targeted locus, a second group generated *Hoxb4* mutant alleles in which the selectable marker was either present, reversed in orientation, or removed (Manley et al., 2001). The first allele was constructed by insertion of the *neomycin* selection cassette into the

first exon of the *Hoxb4* locus (*Hoxb4*^{PolII}), much like the first allele created by Ramirez-Solis *et al*, except that only one selectable marker was used to interrupt the exon. Most of the mice homozygous for this allele die at birth. Although they show increased body curvature, no vertebral column defects were observed that could account for this. The axial-to-atlas homeotic transformation and complete sternal bifurcation (89%) seen by Ramirez-Solis *et al* were similarly observed in *Hoxb4*$^{PolII-/-}$ P0 pups. A second targeted allele was generated in which the transcriptional orientation of the *neomycin* cassette was reversed but still retained in the first exon flanked by LoxP sites (*Hoxb4*^{nl}). Newborn pups that contained this allele in a homozygous condition had similar body wall defects but at a much lower frequency (41%), suggesting that the orientation of the selectable marker carries dramatic effects for sternal development. Finally, in order to assess the developmental effect of removing the *neomycin* cassette, fertilized eggs generated by intercrossing *Hoxb4*$^{nl+/-}$ mice were collected and injected with a *cre*-expression vector to facilitate cre-mediated deletion of the *neomycin* cassette (*Hoxb4*^{loxP}). The removal of the *neomycin* cassette in *Hoxb4*$^{loxP-/-}$ neonates completely eliminates the split sternum defect. Taken together, the results from the studies on *Hoxb2* and *Hoxb4* mutations (Barrow and Capecchi, 1996; Manley et al., 2001; Ramirez-Solis et al., 1993) demonstrate that both of these genes play roles and may act cooperatively in the development of the sternum. The authors tested also whether the effects of the *Hoxb2* or *Hoxb4* mutations acted in *cis* or *trans* to disrupt each other and/or neighboring *HoxB* genes through immunohistochemistry and *in situ* hybridization. The first experiment to test

this hypothesis used a *Hoxb1*$^{+/-}$;*Hoxb2*$^{+/-}$ transheterozygous embryo at 9.5dpc. They speculated that if the *Hoxb2 neomycin* insertion acted in *cis*, then no protein would be produced from the *Hoxb1* gene locus. If it resulted in a *trans*-effect, then the wild-type Hoxb2 protein encoded on one allele would be capable of driving expression from the wild-type *Hoxb1* locus located on the other allele. A Hoxb1-specific antibody was used in whole-mount immunohistochemistry; no staining was observed in rhombomere 4, suggesting that the *neomycin* insertion has a *cis*-effect on neighboring genes. Furthermore, *Hoxb4 in situ* expression analysis was carried out in a *Hoxb2* mutant background on 12.5dpc hemisected embryos. The data show that no *Hoxb4* transcripts can be detected in the ventral body wall of a *Hoxb2* homozygote. These two results, taken together with the *Hoxb4* targeted deletion analysis, led to the conclusion that insertion of a selectable marker into either the *Hoxb2* or *Hoxb4* locus impacts the ability of both genes to pattern the ventral body wall. Additionally, all strains examined (*Hoxb2*$^{-}$, *Hoxb4*^{PolII}, *Hoxb4*^{nl}, and *Hoxb4*^{loxP}) retained the axial-to-atlas homeotic transformations, suggesting that this transformation is due to mutations in either *Hoxb2* or *Hoxb4* and not the presence of the selectable marker. Since both co-paralogous genes *Hoxa4* and *Hoxb4* have been found to play important roles in the patterning of the cervical vertebrae, studies that investigate the ability of these two genes to act synergistically will be discussed later in this chapter.

Hoxb5 and _Hoxb6_ mutants

Rancourt *et al*. investigated the genetic interaction between *Hoxb5* and *Hoxb6* by analyzing the newborn skeletons of single *Hoxb5* and *Hoxb6* homozygotes, as well

as *Hoxb5*/*Hoxb6* *trans*-heterozygotes (Rancourt et al., 1995). Each gene was individually targeted by the insertion of a *neomycin* selection cassette into the first coding exon of an allele capturing either 8.9kb (*Hoxb5*) or 10.1kb (*Hoxb6*) of the endogenous locus. *Hoxb5* homozygotes showed an anterior shift of the shoulder girdle by 1-2 cervical vertebrae. The scapula's rostral edge lines up with C5 in wild-type mice; *Hoxb5* homozygotes showed alignment of the scapula with either C3 or C4. *Hoxb6* homozygotes demonstrated defects in the formation of the first two pairs of ribs. T1 ribs were either absent or shortened with no sternal attachments. T2 ribs were bifurcated, forming two sternocostal junctions: one at the wild-type T1 position (immediately anterior to the manubrium) and a second at its expected position (immediately posterior to the manubrium). This phenotype was described as a "T2 bifurcation" and was found in 50% of *Hoxb6*$^{-/-}$ animals. Rib phenotypes associated with T2 bifurcation included T1 rib shortening, a ventral T1 rib only, a gap between the dorsal and ventral T1 rib, and a fusion between T1 and T2 ribs. Additionally, several phenotypes were shared between *Hoxb5*$^{-/-}$ and *Hoxb6*$^{-/--}$ mutants. C6→C5 transformations were characterized by the absence of anterior tuberculi on the ventral side of C6, and C7→C6 transformations were characterized by the presence of ectopic anterior tuberculi and vertebral foramen on C7. Both homeotic transformations were identified in 34% and 54% of *Hoxb5* homozygotes, respectively; *Hoxb6* homozygotes contained both of these transformations, each with a 28% frequency. Finally, partial T1→C7 transformations were the most predominant phenotype, characterized by the absence of rib heads (caput costae) on

T1, occurring in 66% of *Hoxb5*$^{-/-}$ mice and 64% of *Hoxb6*$^{-/-}$ mice. Because the phenotypes of individual *Hoxb5* and *Hoxb6* homozygotes overlap significantly, the authors postulated that there may be a synergistic reaction between these two genes in specifying the cervicothoracic skeleton, even though the boundary of *Hoxb5* expression extends more anteriorly (pv2) than does the *Hoxb6* expression limit (pv7; (Akasaka et al., 1996)). The phenotypes resulting from the generation of *Hoxb5*/*Hoxb6 trans*-heterozygotes will be discussed later in this chapter.

***Hoxb7* mutants**

The most anterior prevertebra to receive patterning information from *Hoxb7* has been reported as anterior as C6 and as posterior as T3, leading to speculation about the level at which this gene may affect homeosis of the vertebral column (Burke et al., 1995; Vogels et al., 1990). Chen *et al*. described skeletal phenotypes in mice with *Hoxb7* targeted mutations. A replacement vector was used to insert a *neomycin* selection cassette into the *Hoxb7* homeodomain, resulting in a premature stop and disruption of the protein (Chen et al., 1998). *Hoxb7* homozygous mice targeted in this way were viable, and both sexes were fertile. Abnormal rib patterning was identified in 3 of 36 (12%) *Hoxb7*$^{-/-}$ adult mice. Two mice possessed T1/T2 rib fusions, and the T1 ribs of the third affected homozygote were reduced to anlagen. Interestingly, two independent groups have identified pv10, the precursor for the third thoracic vertebra, as the anterior-most prevertebra expressing *Hoxa7* and *Hoxb7* (Akasaka et al., 1996; Burke et al., 1995), suggesting that both genes may be important for specifying anterior thoracic vertebrae, even though *Hoxa7* loss-of-

function mutants possess no skeletal defects (Chen et al., 1998). The skeletal phenotypes of mice with mutations in both *Hoxb7* and its co-paralogue *Hoxa7* will be discussed later in this chapter.

***Hoxb8* mutants**

Previous studies have established an expression profile for *Hoxb8* in the segmented paraxial mesoderm; these results identify pv7 (C7 precursor) as the anterior-most expressing prevertebra at 12.5dpc (Deschamps and Wijgerde, 1993). This suggests that *Hoxb8* may play an important role in patterning C7 and the cervicothoracic vertebral boundary. To better understand this role, *Hoxb8* mutants were generated, revealing homeotic transformations similar to those observed in other *HoxB* mutants. The *Hoxb8* gene locus was mutated using a "hit and run" strategy, by which two codons in the homeodomain's highly conserved hexapeptide motif were altered ($Hoxb8^{hp}$; (Medina-Martinez and Ramirez-Solis, 2003)). This mutation did not affect the stability of Hoxb8 protein; instead, it altered the ability of Hoxb8 protein to specifically perform its DNA binding function. Both $Hoxb8^{hp+/-}$ and $Hoxb8^{hp-/-}$ neonates demonstrated homeotic transformations of the thoracic skeleton, including the absence of T1 ribs, fusion between T1 and T2 ribs, and the joining of T2 ribs at the expected T1 rib sternocostal junction. Rarely, T1 and T2 ribs were found fused to those of T3, and T8 ribs formed ectopic junctions with the sternum. Both of these observations occurred independent of the T1/T2 rib fusions, which were labeled by the authors as T2→T1 anterior transformations. Since more than twice the percentage of $Hoxb8^{hp-/-}$ animals (47% compared to 18% in $Hoxb8^{hp+/-}$ mice) was

affected overall, the authors conclude that changes in gene dosage alter the penetrance of these thoracic transformations.

A second group investigated the loss of Hoxb8 protein function using a different genetic approach to disrupt the *Hoxb8* locus (van den Akker et al., 1999). They used a replacement-type targeting vector to directionally insert a *lacZpoly*A fragment and a *neomycin* cassette (flanked by *loxP* sites) into the first exon of *Hoxb8*. This construct was used to generate two mouse lines: one that contained the floxed *neomycin* cassette (*Hoxb8lacZneo*$^{+}$) and one in which the *neomycin* cassette was removed upon CMV-*Cre* excision (*Hoxb8lacZneo*$^{-}$). Both mutant strains produced viable homozygous adults, but their fertility was not addressed. A thoracic vertebral malformation was found to be fully penetrant in *Hoxb8*$^{-/-}$*lacZNeo*$^{+}$ mice. In these mutants, the ribs of T1 were either significantly reduced or fused to those of T2, resulting in 3 sternal bands (instead of 4) and 6 pairs of ribs with sternocostal junctions (instead of 7). *Hoxb8*$^{+/-}$*lacZNeo*$^{+}$ mice were also affected. Thirty-eight percent of these heterozygotes showed abnormal rib sternocostal junctions, including an inversion of the wild-type T1 and T2 junctions and shifts in the points of contact between the ribs of T1 through T5 with the sternum. Both of these phenotypes were only observed unilaterally. Similar phenotypes were observed in the *Hoxb8lacZNeo*$^{-}$ mutant strain but with much less penetrance and severity (6% in *Hoxb8*$^{+/-}$*lacZNeo*$^{-}$ mice; 33% in *Hoxb8*$^{-/-}$*lacZNeo*$^{-}$ mice).

The results from these two groups show that altering the first exon (van den Akker et al., 1999) or the second exon (Medina-Martinez and Ramirez-Solis, 2003) of

Hoxb8 causes anterior transformations of the first two thoracic vertebrae. Although these phenotypes are exaggerated in the presence of the *neomycin* cassette, they still persist in the absence of the selectable marker.

***Hoxb9* mutants**

At 9.5dpc, mouse embryos variably express *Hoxb9* transcripts up to a rostral boundary between somites 7 and 8, which will undergo resegmentation to give rise to pv3, the precursor to the third cervical vertebra (Chen and Capecchi, 1997). *Hoxb9* mRNA is detected at low levels in the anterior somites, but strongly in the more posterior somites. The rostral boundary of expression may suggest that the role of *Hoxb9* may extend rostrally to pattern cervical vertebrae. However, stronger levels of expression in the posterior somites argue that *Hoxb9* may perform an important function in more caudal regions of the embryo. A knock-out strategy was devised to distinguish between these two possibilities. The *Hoxb9* gene locus was targeted for mutation by the insertion of the *neomycin* cassette into the homeodomain through a replacement vector. Although $Hoxb9^{-/-}$ adults were viable and fertile with no outward abnormalities, defects in the thoracic skeleton were observed. Fusions between T1 and T2 ribs were observed in 83% of homozygotes, with the majority of these transformations found bilaterally. Independent of the T2→T1 transformations, articulations of T8 ribs with the sternum were observed in 54% of homozygotes (n = 24), 7% of heterozygotes (n = 27), and 0 wild-type animals (n = 11). These results support the argument that gene expression profiles alone are not reliable for predicting the functional output of each gene. Since co-paralogous genes *Hoxa9* and

Hoxb9 affect the patterning of the thoracic vertebrae, their combined functions were assessed through the analysis of *Hoxa9*/*Hoxb9* double mutants and will be discussed later in this chapter.

Within *HoxB* single mutants, sternal defects were only observed in *Hoxb2*- and *Hoxb4*-null mice. This suggests that there is a functional genetic boundary between *Hoxb4* and *Hoxb5* with respect to sternal patterning. Since there have been no reports of skeletal defects in *Hoxb1* mutants, it is still unclear whether *Hoxb2* is the most anterior *HoxB* gene to affect the development of the sternum. Mutations within several of the *HoxB* genes produce similar anterior homeotic transformations. Taken with the results of nonallelic noncomplementation gathered from *Hoxb5*/*Hoxb6* double mutant analysis, this suggests that there is a degree of overlap or redundancy among neighboring genes in this cluster, even though these genes exist in non-paralogous groups. The effects of a *HoxB* cluster deletion of *Hoxb1* through *Hoxb9* address this issue and will be discussed later in this chapter.

HoxC cluster single mutants

Hoxc4 mutants

As the *HoxC* chromosomal cluster does not contain paralogous members of groups 1, 2, or 3, *Hoxc4* is the most 3' gene located in the cluster. Unlike its co-paralogous genes *Hoxa4*, *Hoxb4*, and *Hoxd4*, the rostral limit of *Hoxc4* expression in prevertebrae is located more posteriorly. At 12.5dpc, its expression is weak in pv4 but strong in pv5-pv7 (Geada et al., 1992), suggesting that the role of *Hoxc4* may not entirely overlap with that of its co-paralogues, with respect to the anterior cervical

skeleton. Two groups have individually created nonfunctional alleles to investigate the effects of targeted *Hoxc4* mutagenesis. Both groups used nearly identical strategies by deleting a significant portion of the *Hoxc4* homeodomain and inserting the *neomycin* resistance gene in its place by a replacement-type targeting vector. However, there are slight differences in the phenotypes observed by these two groups, and the reason may lie in the genetic backgrounds used to propagate each mutant line. The first group injected cells from their positively-targeted clones into C57bl/6 blastocysts and bred the resultant chimeras into a non-agouti A/J strain (Saegusa et al., 1996). The second group injected positive cell lines into 129s6/SVEV blastocysts and crossed their chimeras into the C57bl/6 strain (Boulet and Capecchi, 1996). The *Hoxc4*-null mice generated by Saegusa *et al*. were viable and fertile as adults. Although C1 through C6 appeared normal, partial C7→T1 transformations were observed: rib anlagen were present in both heterozygotes and homozygotes, 27% and 84%, respectively. Some wild-type mice may have a poorly developed T2 spinous process, but it is never prominent on T3. Mutants were found to have T3→T2 anterior transformations, complete with a more developed dorsal spinous process on T3 ($Hoxc4^{+/-}$: 7%; $Hoxc4^{-/-}$: 47%). T8 ribs with sternocostal junctions were observed either unilaterally or bilaterally and only in homozygotes (5/19 or 26%); an additional or fifth sternal band was found in two of these 5 mice. Finally, $Hoxc4^{+/-}$ (33%) and $Hoxc4^{-/-}$ (63%) animals displayed fissures in the sternum's xiphoid process. In contrast to the previous group's mutants, the *Hoxc4*-null mice generated by Boulet and Capecchi often die 1-2 days after birth. The few that survive until adulthood are

smaller than normal but retain their fertility. Similar T3→T2→T1 anterior transformations were observed in newborn and adult *Hoxc4*$^{-/-}$ mice. However, the cervical vertebrae and T1 were normal. Defects in the thoracic ribs included: 1. a fully-penetrant decrease in the length of T2 and T3 ribs compared to wild-type ribs, and 2. T8 rib sternocostal junctions, either unilateral or bilateral, in 85% of *Hoxc4*$^{-/-}$ and 8% of *Hoxc4*$^{+/-}$ mice. Additionally, the homozygotes occasionally possessed a coordinating 5th sternal band. In wild-type mice, T10 is known as the transitional vertebra, since it represents the most anterior thoracic vertebra to show a lumbar-type articulation between the pre- and postzygapophyses. In *Hoxc4* homozygous adults, T10 retains thoracic-type morphology, suggesting an anterior T10→T9 transformation. Instead, T11 is this mutant's transitional vertebra (T11→T10). The distinction is much more difficult in *Hoxc4* heterozygotes, as the transformations are much weaker. In these animals, T10 has an intermediate morphology, and T11 is occasionally the transitional vertebra. Taken together, the results from these two groups reveal that *Hoxc4* plays a significant role in patterning thoracic skeletal elements. However, slight variations in the phenotypes of each groups' mutants may be due to differences in genetic background.

***Hoxc6* mutants**

A *Hoxc6* loss-of-function allele was generated upon inserting the *neomycin* resistance marker into the homeodomain in the second exon by a targeting vector (Garcia-Gasca and Spyropoulos, 2000). A T2→T1 homeotic transformation, or articulation of the second pair of ribs with the first pair, was observed in 60% of

Hoxc6 homozygotes. The translocation of the wild-type T2 spinous process onto T3 and/or the deletion of this process from T2 constitute a T3→T2 transformation; this transition was found at an even greater penetrance: 90% in *Hoxc6*$^{-/-}$ and 70% in *Hoxc6*$^{+/-}$ animals. Additionally, sternal phenotypes were observed in both heterozygotes and homozygotes, including deletion of a sternal band, variation in sternebrae length, and shortening of the manubrium. Thus, all of the phenotypes observed in *Hoxc6* mutants are contained within the upper thoracic skeleton and sternum, corresponding to the reported anterior level of *Hoxc6* expression at pv7/8, or the C7 and T1 precursors (Akasaka et al., 1996; Burke et al., 1995).

***Hoxc8* mutants**

The *Hoxc8* anterior limit of mRNA expression at pv8 (Tiret et al., 1993) suggests that this gene may play a critical role in patterning T1 and the cervicothoracic boundary. However, this function could not be verified in *Hoxc8* mutants. The *Hoxc8* gene locus was targeted upon insertion of the E. coli *lacZ* gene by homologous recombination (Le Mouellic et al., 1992). The majority of skeletal phenotypes observed impacted the thoracic-lumbar vertebral boundary. For instance, 100% of *Hoxc8*$^{-/-}$ animals possessed a fully developed pair of ribs on L1, representing an anterior L1→T13 transformation; occasionally, this transformation was observed in wild-type and *Hoxc8*$^{+/-}$ animals but at a much lower frequency. The overall numbers of thoracic and lumbar vertebrae did not differ from wild-type though. An additional or fifth sternebra was observed between the articulations of T6 and T7 ribs in 79% of homozygotes, and 64% of the homozygous animals had ectopic T8 rib

sternocostal junctions. In cases where the T8 ribs did not symmetrically contact the sternum, a bifurcation of the xiphoid process resulted. The above phenotypes were also detected in *Hoxc8*$^{+/-}$ animals, but with variable degrees of penetrance. The T12→T11 transformation, however, was specific to homozygotes. In these animals, the cartilaginous portion of the ribs extending from T12 (at birth) was equal in length to that found on T11 ribs. The authors argue that since the ossified portion of newborn T12 ribs is usually twice the length of the cartilaginous portion, this defect in the mutant T12 ribs represents a T12→T11 anterior transformation. Since no transformations were observed anterior to T6 or posterior to L2, the authors conclude that *Hoxc8* plays a very specific role in the patterning of the posterior thoracic skeleton. Co-paralogous gene *Hoxb8* is expressed strongly from pv7 and more posteriorly, and it acts to help pattern the anterior thoracic vertebrae (Deschamps and Wijgerde, 1993; Medina-Martinez and Ramirez-Solis, 2003). However, evidence from recent studies (discussed later in this chapter) suggests that, although *Hoxb8* and *Hoxc8* single mutants do not generate phenotypes in the same vertebrae, these two genes may still function cooperatively to specify both anterior and posterior thoracic elements.

***Hoxc9* mutants**

The last gene of the *HoxC* cluster to demonstrate skeletal phenotypes upon mutation is *Hoxc9*. Although pv18 (T11 precursor) was identified as the most anterior vertebra to express *Hoxc9* transcripts (Burke et al., 1995), *Hoxc9* loss-of-function mutants possess homeotic transformations in the vertebrae anterior to this

level of expression. A replacement-type vector was used to remove a 5kb portion of the *Hoxc9* locus, including the coding exons, and insert the *neomycin* selection cassette in its place (Suemori et al., 1995). Homozygous animals generated in this way possessed anteriorly-transformed thoracic vertebrae. The majority of homeotic transformations follow a one-segment rule, such that a posterior vertebra is transformed to resemble the vertebra found immediately anterior to it. However, T10 through T13 in *Hoxc9* mutants were all transformed to a T9 morphology, based on the increase in the size of the transverse process. As stated before, the wild-type T10 vertebra represents a transitional vertebra. Since T10 through T13 of homozygous mutants were transformed to T9, the transitional vertebra phenotype was now contained on L1. Despite this change in vertebral identity, the L1 ribs more closely resembled those of the wild-type T13, not T10. No further transformations were observed in the remaining posterior vertebrae. The sternum and its associated rib contacts were severely affected in homozygous mutants. Abnormal fusion of the 4^{th} sternebra to the xiphoid process was observed at 100% penetrance, and 85% of the mutants had severe bends or fusions between adjacent ribs. The eighth, and sometimes ninth, pairs of ribs formed ectopic sternocostal junctions (62% and 38%, respectively). Finally, the distal tips of the floating ribs (T12 and T13) were transformed to resemble those of the anterior attached ribs; instead of being flat, as in wild-type mice, these ends were sharp. The effect of the *Hoxc9* mutation appears to be dependent on gene dosage, since *Hoxc9*$^{+/-}$ mice shared some similar transformations, but at a reduced level of penetrance. T11 represented the transitional

vertebra, and although heterozygotes had a normal sternal morphology, 50% of the T8 rib pairs formed ectopic sternocostal junctions (SCJ).

Thus far, targeted mutagenesis of four of the nine genes located within the *HoxC* chromosomal cluster results in anterior homeotic transformations of the thoracic skeleton. Interestingly, these transformations can be found at the boundaries between morphologically-distinct vertebrae (i.e. at the cervicothoracic and thoracic-lumbar transitions). This suggests a very important role for *HoxC* genes in regulating these transitional vertebral boundaries.

HoxD **cluster single mutants**

Hoxd3 **mutants**

A *neomycin* selection cassette was inserted into the *Hoxd3* homeobox at nucleotide 82, creating a targeting vector to disrupt the homeodomain's second helix and, ultimately creating a nonfunctional Hoxd3 protein (Condie and Capecchi, 1993). Most of the homozygotes generated in this way died within the first 5 days of birth; however, the authors noted four *Hoxd3*$^{-/-}$ mice that survived through adulthood and were fertile. Unlike the phenotypes reported in animals with homozygous mutations of the paralogous genes *Hoxa3* and *Hoxb3* (Chisaka and Capecchi, 1991; Manley and Capecchi, 1997), *Hoxd3*$^{-/-}$ mice have much more severe defects of the upper cervical vertebrae. First, a fully penetrant anterior transformation was observed as the anterior arch of the atlas (aaa) fused to the BOB. This effectively remodeled the craniocervical joint, such that the skulls of homozygous mutants rest on C2 instead of C1. Additional alterations in C1 morphology included narrowing of the neural arch

and lateral masses, absence of cartilaginous foramina from the lateral masses, and fusion of the lateral masses with the exoccipital bones. These changes in C1 were found at varying degrees of penetrance within *Hoxd3* homozygotes, but they clearly reflect an anteriorization of C1 into an occipital bone identity. Consequently, the C2 vertebrae of these mutants possessed several C1-like characteristics. Both the dens and superior articular surfaces were absent from mutant C2 vertebrae, axial neural arches were thickened similar to C1, and the cartilaginous foramina that were absent from C1 lateral masses were found on C2. Occasionally, additional ossified bone material was found between the neural arches of C1 and C2. Together, these alterations in C2 morphology point to a partial C2→C1 anterior transformation.

Interestingly, those *Hoxd3* homozygotes that survived past the neonatal stage and into adulthood still retained the same phenotypes as neonates that died after birth. The authors present two theories to explain the early postnatal lethality. First, the remodeling of C1 and C2 that occurred in homozygotes could severely compromise the lateral stability of the craniocervical joint, leading to accidental internal decapitation as the mothers attempted to move the pups. However, this option does not explain how the four homozygous mutants with transformed C1 and C2 (and presumed compromised craniocervical joint stability) survived into adulthood. Thus, the authors offer another explanation that may or may not occur in conjunction with the previous theory. The restructuring of the atlas and axis also affects the pathways that protect and control the entry/exit of arteries from the vertebral column. Abnormal entry points are suggested to result in restriction of the arteries during head

and neck movement. Consistent with this hypothesis, the authors found that the vertebral arteries of two homozygous mice found dead at birth were abnormally narrow.

The final skeletal phenotype observed in homozygous mutants was a crankshaft sternum, generated by the asymmetrical joining of rib pairs to the sternum. Interestingly, a partial fusion of the anterior arch of the atlas was observed in 15% of *Hoxd3*$^{+/-}$ mice, representing an intermediate C1→Occipital Bone transformation. C2 retained its dens and was untransformed in *Hoxd3* heterozygotes. All of these mutant phenotypes correspond with the anterior limit of *Hoxd3* expression in the occipital somites (Condie and Capecchi, 1993), further implicating an important role for *Hoxd3* in modeling the craniocervical joint. The ability of *Hoxd3* to act synergistically with co-paralogues *Hoxa3* and *Hoxb3* will be addressed later in this chapter.

***Hoxd4* mutants**

Hoxd4 transcripts share the same expression profile as *Hoxb4* transcripts in the prevertebrae: weak in pv1, but strong in pv2 and more posterior cervical prevertebrae (Gaunt et al., 1989). In order to understand the role of *Hoxd4* transcripts in this region, a *Hoxd4* knock-out mouse strain was created. A targeting vector containing the *neomycin* cassette in the region of the *Hoxd4* exon 2, which encodes the homeodomain's third helix, was used to replace the endogenous *Hoxd4* locus via homologous recombination, disrupting the specific DNA binding function of Hoxd4 protein (Horan et al., 1995a). *Hoxd4* heterozygotes and homozygotes were both

viable and fertile as adults. Complete and incomplete C2→C1 anterior transformations were observed in *Hoxd4* heterozygous and homozygous animals. Partial C2→C1 transformations were observed in $Hoxd4^{+/-}$ (10%) and $Hoxd4^{-/-}$ (33%) mutants with an ectopic anterior arch on C2. A small number of heterozygotes and homozygotes had a decreased dens on C2, even though the vertebral body of the axis remained untransformed. A more complete transformation was observed in 25% of *Hoxd4* homozygotes, whose axial lateral articular surfaces had been remodeled to more closely resemble those of C1. Additionally, these mice possessed incomplete lateral foramina (a C1-type feature) on C2. An occasional fusion of the anterior arch of the atlas with the BOB was seen in these animals, similar to *Hoxd3* homozygotes. Defects in the dorsal neural arches of C1, C2, and C3 were highly penetrant: 83% of heterozygotes and 93% of homozygotes. These malformations included fusions between the arches, as well as both widening and splitting of individual arches. The fourth, fifth, and sixth cervical vertebrae appeared normal, but extensive rib anlagen were observed in $Hoxd4^{+/-}$ (17%) and $Hoxd4^{-/-}$ (33%) mice.

Interestingly, the *Hoxd4* mutant phenotypes were similar to those observed in mice that were mutant for the co-paralogous gene, *Hoxb4*, with respect to the first two cervical vertebrae. Unlike *Hoxc4* mutants, however, no thoracic transformations were observed in the *Hoxd4* mutants. These two observations suggest: 1. a cooperative role for *Hoxb4* and *Hoxd4* in patterning the anterior cervical skeleton, and 2. non-overlapping functions for *Hoxc4* and *Hoxd4*, since their roles appear to be specific to patterning the thoracic and cervical skeleton, respectively. The ability of

Hoxd4 to act in a cooperative manner with co-paralogues *Hoxa4* and *Hoxb4* to pattern the axial skeleton will be addressed later in this chapter.

***Hoxd8* mutants**

The *Hoxd8* gene locus was targeted by the insertion of the *neomycin* gene into the second exon through a replacement-type vector, disrupting the homeodomain (van den Akker et al., 2001). Mutant mice generated by this strategy were found to be both viable and fertile as heterozygous and homozygous adults. The anterior limit of *Hoxd8* gene expression has been mapped independently by two groups to the level of pv13 (T6 precursor; (Burke et al., 1995) and pv18 (T11 precursor; (Izpisua-Belmonte et al., 1990)), suggesting that this gene may play a role in patterning posterior thoracic vertebrae. However, defects in the axial skeleton of these mutants were minor and showed a low degree of penetrance. A T8 rib sternocostal junction and a small L1 rib were observed unilaterally in *Hoxd8* heterozygotes (18% and 6%, respectively). *Hoxd8* homozygotes were even less affected by this mutation. A unilateral ectopic junction between a T8 rib and the sternum was seen in only 9% of homozygotes.

Such a minor impact on the thoracic vertebrae suggests that *Hoxd8* does not play a significant role in patterning this region of the axial skeleton. However, since these phenotypes do overlap with those observed in mice carrying mutations in co-paralogous genes *Hoxb8* and *Hoxc8* , investigations into the functional redundancy among these three genes have been performed using both double and triple mutants. These results will be reviewed later in this chapter.

***Hoxd9* mutants**

A replacement-type vector was used to specifically target the *neomycin* selection cassette into the region of the second exon of *Hoxd9* that encodes the first helix of the homeodomain, disrupting the DNA-binding specificity of Hoxd9 protein (Fromental-Ramain et al., 1996). Homozygous *Hoxd9* mutants were viable and fertile. However, they contained vertebral transformations in the lumbar and sacral regions. Although L1 and L6 morphology was normal, one-segment anterior transformations were observed at the level of L2 through L5 (L5→L4→L3→L2) in 85% of homozygotes. Unilateral transformations of L3 through L5 were observed in the remaining 15%. Partial anteriorizations of L3-L5 were also observed in 50% of *Hoxd9* heterozygotes. The sacral vertebrae underwent similar anterior transformations. Partial S2→S1 transformations occurred in 30% of the homozygotes; in these cases, both S1 and S2 contained bilateral extensions of the ilium's articular surface (this feature is unique to wild-type S1). The fusion that occurs between wild-type S2 and S3 was instead found between S3 and S4 in 95% of *Hoxd9*$^{-/-}$ adults, suggesting an anteriorization of the S4 vertebra. These fusions were also found in 40% of *Hoxd9* heterozygotes. Finally, S4 morphological characteristics (fusion of the transverse processes and vertebral body with those of the immediately-anterior neighbor) were seen on the first caudal vertebra (Ca1) in 30% of homozygotes (Ca1→S4). Similar to mice lacking functional copies of the co-paralogous gene *Hoxa9*, *Hoxd9* mutants display anterior homeotic transformations affecting a majority of the lumbar vertebrae. Interestingly, L6 is never transformed in

either of these single mutants. Also, transformations of the sacral and caudal vertebrae are unique to *Hoxd9* mutants, since no *Hoxa9* mutants have been identified with defects in these regions. Even though the strong anterior boundary of *Hoxd9* gene expression (pv23, 3rd lumbar prevertebra; (Duboule and Dollé, 1989)) is located more posterior than the *Hoxa9* boundary in the eleventh thoracic prevertebra (pv18; (Burke et al., 1995)), it is possible that the functions of both genes overlap in patterning the lumbar vertebrae but not more posterior vertebrae. The skeletal phenotypes of *Hoxa9*/*Hoxd9* double mutants will be discussed later in this chapter.

***Hoxd10* mutants**

The *neomycin* cassette was targeted into the second exon of the *Hoxd10* gene locus, disrupting the second helix of the protein's homeodomain. This targeted construct then replaced the endogenous locus via homologous recombination to generate *Hoxd10* mutant mice (Carpenter et al., 1997). *Hoxd10* homozygous adults were viable. Although the females were fertile, $Hoxd10^{-/-}$ males showed decreased fertility. Since hindlimb defects are prevalent and are shown to affect gait and adduction in these mutants, the authors suggest that this impairs the ability of the males to mount the females for copulation, leading to male infertility. In addition to disrupted hindlimb development, *Hoxd10* mutants display anterior transformations of the sacral vertebrae. Wild-type animals possess three sacral vertebrae whose transverse processes fuse to each other (S1-S3); the transverse process of S4 remains unfused. In half of the homozygous mutants observed, 50% had four or five fused sacral vertebrae, suggesting that more posterior vertebrae are transformed into a more

anterior morphology. This phenotype was even observed in two heterozygous mutants that demonstrated unilateral fusions of S1-S4. Similarly, the shapes of the transverse processes of these vertebrae were altered to resemble that of more anterior sacral vertebrae. In wild-type animals, a "wing-shaped" transverse process can be found only on S1 and S2. The processes of S3 and S4 are different: they are club-shaped and project anteriorly. Most of the *Hoxd10* homozygotes analyzed possessed 3 or 4 transverse processes resembled the S1/S2 "wing-shaped" morphology. Finally, in wild-type animals, S1 is the only vertebrae to articulate with the pelvis; in *Hoxd10* homozygotes, both the S1 and S2 vertebrae formed such articulations, suggesting an S2→S1 transformation. The authors note that this transformation specifically sets the stage for the rest of the more posterior sacral and anterior caudal vertebrae to take on anterior phenotypes. The sacral anterior transformations shown here affect both the morphological and functional characteristics of each vertebra. Interestingly, sacral vertebrae phenotypes observed in *Hoxd10* mutants are shared by both the co-paralogous *Hoxa10* and non-paralogous *Hoxd9* mutants. The expression profiles of these three genes overlap strongly in the posterior prevertebrae (Benson et al., 1995; Dollé and Duboule, 1989; Duboule and Dollé, 1989). The redundancy in function among group 10 paralogous genes, as well as the cooperative functions of these two *HoxD* cluster neighbors, will be addressed later in this chapter.

***Hoxd11* mutants**

The expression profile of *Hoxd11* in the posterior portion of the embryo suggests that this gene may function in patterning the caudal vertebrae. *Hoxd11*

transcripts are detected at the level of pv24, or the fourth lumbar prevertebra (Izpisua-Belmonte et al., 1990). *Hoxd11* mutant alleles were generated by two independent groups to assess the effects of this gene on the development of the axial skeleton. Similar targeting strategies were used, in that the mutant vector containing a *neomycin* selection cassette replaced either a portion of the *Hoxd11* genomic region. The difference between the two targeted alleles was the placement of the *neomycin* cassette within the locus. For the first allele, the selection cassette was inserted into exon 2 at the site encoding the first helix of the homeodomain's DNA-binding motif (Davis and Capecchi, 1994). In the second allele, the *neomycin* gene replaced a deleted region of the *Hoxd11* locus containing the 3' end of the intron, the splice donor site, and the same 5' end of the homeobox corresponding to the homeodomain's first α-helix (Favier et al., 1995). Interestingly, the resulting phenotypes of *Hoxd11* mutants targeted by either of these strategies were identical. Although *Hoxd11* homozygous mice are viable as adults, female mice were fertile, but male mice exhibited either infertility or reduced fertility. In either case, the origin of the infertility remains unknown. Anterior homeotic transformations affected the region of the sacral vertebrae with variable expressivity. A wild-type animal possesses 6 lumbar, 4 sacral, and a variable number of caudal vertebrae. Both groups report a duplicated or additional lumbar vertebra (L7). The next four vertebrae possess the characteristic sacral appearance (S5). Davis and Capecchi report an additional sacral vertebra in 25% of their homozygous mutants, adding that they never observe mutants with additional lumbar and sacral vertebrae (i.e., L7:S5).

Another common observation is the presence of an asymmetric intermediate vertebra that possesses a lumbar-like transverse process on one side and a first sacral-like transverse process on the other side. These transformations cause the ilium articulation to occur at a vertebra located one segment posterior to the wild-type articulation point. Both groups conclude that an anterior homeosis of the sacral and first caudal vertebrae likely explains the transformations observed in these mutants, instead of a hypothesis supporting a supernumerary lumbar vertebra. The anterior sacral phenotypes observed in *Hoxd11* mutants are shared with mice carrying a mutation in the non-paralogous *Hoxa10* gene. Interestingly, co-paralogous *Hoxa11* mutants contain no transformations within the sacral vertebrae. However, recent data suggest that the absence of any *Hox11* function (i.e., through *Hoxa11*/*Hoxc11*/*Hoxd11* triple homozygous mutants) severely impacts the development of sacral vertebrae. The relationships between *Hoxd11* and non-paralogous and co-paralogous *Hox* genes will be discussed later in this chapter.

1.2.3 Double and triple *Hox* mutants

The expression profiles of *Hox* genes within a paralogous group often overlap in the somitic and pre-somitic mesoderm, and analysis of single *Hox* mutants shows that several incompletely penetrant skeletal phenotypes are shared within these groups. Thus, it is reasonable to expect that simultaneous mutations of paralogous genes may demonstrate an additive effect with respect to phenotype severity and penetrance. Additionally, neighboring non-paralogous genes may also act synergistically to specify a specific region of the axial skeleton. For these reasons,

several groups have investigated the degree of *Hox* gene redundancy in patterning the vertebrae through the use of *Hox* double and triple knock-out mutant mice.

Hox Paralogous Group 3 double mutants

Hoxa3/*Hoxb3* double mutants

Identical targeting strategies were used to create individual mutations in each of the *Hoxa3* and *Hoxb3* gene loci, as previously described (Chisaka and Capecchi, 1991; Manley and Capecchi, 1997). The *Hoxa3* mutation did not produce defects in the mesodermally-derived axial skeleton. *Hoxb3* mutants, however, were observed with a fusion of the C1 anterior arch to the C2 dens. These two individual mutants shared no common phenotypes, but subsequent studies indicate that they act synergistically to pattern the cervical vertebrae (Manley and Capecchi, 1997). Heterozygous mice for each mutant strain were intercrossed to generate compound heterozygotes (i.e., $Hoxa3^{+/-}/Hoxb3^{+/-}$). Skeletal phenotypes at low penetrance were observed in the compound heterozygotes, even though single heterozygotes were completely normal. For instance, defects of the aaa (fusion to the dens/split in two or deletion/fusion to the BOB) were observed in 23% of $Hoxa3^{+/-}/Hoxb3^{+/-}$ newborns. One compound heterozygote was found to be missing the lateral foramina from C1. Both of these defects suggest partial transformations of the first cervical vertebra to either an occipital or C2 fate. To further investigate the synergistic effects of these genes, compound heterozygotes were crossed, producing the following mutants: $Hoxa3^{+/-}/Hoxb3^{-/-}$, $Hoxa3^{-/-}/Hoxb3^{+/-}$, and $Hoxa3^{-/-}/Hoxb3^{-/-}$. Not surprisingly, then, more novel phenotypes were generated with increased levels of penetrance as

functional copies of each gene were removed. Both *Hoxa3*$^{+/-}$/*Hoxb3*$^{-/-}$ and *Hoxa3*$^{-/-}$/*Hoxb3*$^{+/-}$ newborns demonstrated an increase in the *Hoxb3*$^{-/-}$ phenotype, namely the fusion of the C1 aaa to the C2 dens. However, the removal of functional *Hoxb3* gene copies (*Hoxa3*$^{+/-}$/*Hoxb3*$^{-/-}$) results in unique phenotypes, including deletion of the aaa (8%), reduction in the C1 neural arch (23%), and remodeling of the C2 neural arch (8%). The C1 neural arch reduction was shared in common with *Hoxa3*$^{-/-}$/*Hoxb3*$^{+/-}$ (67%), and these mice carried unique transformations of their own: reduction in the size of the EOBs (58%), remodeling of the SOB (17%), fusion of C1 to the EOB by either its lateral masses or foramina (41%), deletion of the C1 lateral foramina (17%), and broadening of the C2 neural arch (17%). Finally, the complete removal of all *Hoxa3* and *Hoxb3* copies produced similar phenotypes, many of which were 100% penetrant. Interestingly, *Hoxa3*/*Hoxb3* double homozygous mutant phenotypes overlap with those of single *Hoxd3* mutants, particularly, the fusion of the aaa to the BOB and the reduction in the width of C1 and C2 neural arches. However, one phenotype (the reduction in the size of the EOB) is unique to the double mutants, suggesting that *Hoxd3* alone is not sufficient to completely specify these regions of the skull and anterior cervical vertebrae. All three *Hox3* paralogous group members seem to be required to fulfill this role; this concept will be addressed later in this chapter. These results clearly lend support to the idea that *Hox* genes act synergistically to specify vertebral identities, even when these roles are not implicated through single-mutant analysis.

Hoxa3/*Hoxd3* double mutants

It was previously shown that *Hoxa3* and *Hoxd3* single mutant phenotypes are not shared in common (Chisaka and Capecchi, 1991; Condie and Capecchi, 1993). Thus, Condie and Capecchi were surprised to find that these two genes function synergistically to specify the craniocervical junction (Condie and Capecchi, 1994). Since *Hoxd3*-null mutants possess an anterior transformation of C1 to an occipital bone identity, the authors expected to find this phenotype exaggerated in *Hoxa3*/*Hoxd3* double mutants. Instead, they found that C1 was completely eliminated in $Hoxa3^{-/-}/Hoxd3^{-/-}$ mice. To explain this phenomenon, they propose a model by which *Hox* genes differentially control the vertebral precursor cells' proliferative capacity.

Hoxb3/*Hoxd3* double mutants

The effects on skeletal development of *Hoxb3* and *Hoxd3* mutagenesis were previously described (Condie and Capecchi, 1993; Manley and Capecchi, 1997). Unlike single *Hoxa3* and *Hoxb3* mutants, *Hoxd3* homozygotes display a large number of malformations at the craniocervical junction. Even so, *Hoxb3* and *Hoxd3* heterozygotes were crossed to generate compound heterozygotes ($Hoxb3^{+/-}/Hoxd3^{+/-}$; (Manley and Capecchi, 1997)). Surprisingly, many of the same phenotypes observed in *Hoxd3* homozygotes were identified in the compound heterozygotes. To further investigate synergism between *Hoxb3* and *Hoxd3*, compound heterozygotes were mated in order to produce $Hoxb3^{-/-}/Hoxd3^{+/-}$, $Hoxb3^{+/-}/Hoxd3^{-/-}$, and $Hoxb3^{-/-}/Hoxd3^{-/-}$ mutants. Overall, the same mutant phenotypes were observed, but each phenotype

increased in penetrance as functional copies of each gene were removed. As with the *Hoxa3*/*Hoxd3* double homozygotes (Condie and Capecchi, 1994), it was surprising to find that, instead of exacerbating the C1 fusion to the EOB observed in *Hoxd3* single homozygotes, this vertebra was completely eliminated in all *Hoxb3*/*Hoxd3* double homozygotes. Consequently, the C2 neural arches in both *Hoxa3*/*Hoxd3* and *Hoxb3*/*Hoxd3* double homozygotes were remodeled to resemble the shape of the remaining cervical vertebrae (C3-C5). These two results suggest that all three genes are critical for ensuring that C1 and C2 vertebrae retain their unique characteristics. Overall the degree of synergistic interactions seems to be strongest between *Hoxb3* and *Hoxd3*, since these mutants produced the greatest number of malformations in the craniocervical region.

Hox Paralogous Group 4 double mutants

Hoxa4/*Hoxb4* double mutants

The phenotypes of mice with individual mutations in *Hoxa4*, *Hoxb4*, and *Hoxd4* have been previously described (Horan et al., 1995b; Horan et al., 1994; Ramirez-Solis et al., 1993). Since all three mutants contain transformations of some aspects of the anterior cervical vertebrae, compound mutants for these genes were generated to study the importance of synergism among *Hox* Group 4 paralogous members (Horan et al., 1995b).

Single *Hoxa4* and *Hoxb4* heterozygotes were crossed to create compound heterozygotes ($Hoxa4^{+/-}/Hoxb4^{+/-}$), which were further crossed to generate the remaining members of this allelic series ($Hoxa4^{+/-}/Hoxb4^{-/-}$; $Hoxa4^{-/-}/Hoxb4^{+/-}$;

Hoxa4$^{-/-}$/*Hoxb4*$^{-/-}$). Interestingly, the single homozygous phenotypes were not observed in these double mutants. Novel phenotypes in *Hoxa4*$^{-/-}$/*Hoxb4*$^{-/-}$ P0 pups were seen with variable penetrance instead. Seventy-eight percent of these mutants had a C2/C3 fusion at either the level of the neural arches or dorsal processes. Even more penetrant (100%) in this region was the loss of the lateral articular processes of C2 and C3. In rare cases, the rostral articular process of C4 was absent as well. The loss of articular processes may suggest a partial anterior shift in the identity of these vertebrae to resemble that of C1. Anterior C6→C5 and C7→C6 homeotic transformations occurred simultaneously with full penetrance in double homozygotes and were also found with variable penetrance in *Hoxa4*$^{+/-}$/*Hoxb4*$^{-/-}$ (2/3) and *Hoxa4*$^{-/-}$/*Hoxb4*$^{+/-}$ (20%).

***Hoxa4*/*Hoxd4* double mutants**

Similarly, no skeletal phenotypes are shared in common between *Hoxa4* and *Hoxd4* single mutants. However, *Hoxa4*/*Hoxd4* double mutants display novel phenotypes that increase in penetrance as functional copies of *Hoxa4* are removed from the *Hoxd4* mutant background. For example, a fusion between the neural arches of C2 and C3 increased from 6% in *Hoxa4*$^{+/-}$/*Hoxd4*$^{-/-}$ to 17% in *Hoxa4*$^{-/-}$/*Hoxd4*$^{-/-}$ mice. The loss of C2 and C3 articular processes increased from 33% in *Hoxa4*$^{+/-}$/*Hoxd4*$^{-/-}$ mutants to 56% in *Hoxa4*$^{-/-}$/*Hoxd4*$^{-/-}$ mice.

***Hoxb4*/*Hoxd4* double mutants**

Finally, the transformations of the anterior cervical skeleton observed in single *Hoxb4* and *Hoxd4* mutants are present at variable penetrance in *Hoxb4*/*Hoxd4*

double mutants, with increased levels seen as functional *Hoxb4* and *Hoxd4* copies are simultaneously removed. Additionally, novel phenotypes arise upon deletion of these genes. The aaa is fused to the posterior edge of the BOB (partial C1→Occipital bone). The partial C2→C1 transformation in single mutants becomes more penetrant and complete in double mutants, with an ectopic aaa and C1 lateral foramina observed on the mutant axis. Incomplete neural arches of C1-C3 are highly penetrant in double mutants, as are fusions of the C1 and C2 neural arches, loss of the C2 and C3 articular processes, and an ectopic aaa and dens on C3. Although C6→C5 and C7→C6 transformations persisted in these double mutants (i.e., translocation of AT from C6 to C7), they were less penetrant.

Hox Paralogous Group 7 double mutants

Hoxa7/*Hoxb7* double mutants

Homeotic transformations were found to be wholly-absent from *Hoxa7* mutants and only slightly penetrant in *Hoxb7* mutants (Chen et al., 1998). Nevertheless, *Hoxa7* and *Hoxb7* single heterozygotes were crossed to produce compound heterozygotes. These double mutants were further crossed, generating the following mutants: $Hoxa7^{+/-}/Hoxb7^{-/-}$, $Hoxa7^{-/-}/Hoxb7^{+/-}$, and $Hoxa7^{-/-}/Hoxb7^{-/-}$. All mutant strains were viable as adults. The compound heterozygotes contained no skeletal malformations, similar to *Hoxa7* single mutants. The penetrance of defects in the upper rib cage (T1/T2 rib fusions) increased as functional copies of both *Hoxa7* and *Hoxb7* were simultaneously removed: 45% of $Hoxa7^{+/-}/Hoxb7^{-/-}$; 9% of $Hoxa7^{-/-}/Hoxb7^{+/-}$; 71% of $Hoxa7^{-/-}/Hoxb7^{-/-}$. Even though the mutation in *Hoxa7* alone is not

capable of producing upper thoracic transformations, this gene still functions in patterning T1 and T2, since phenotypic penetrance increases as *Hoxa7* copies are removed in the *Hoxb7* mutant background. The authors argue that both genes may have overlapping functions.

Hox Paralogous Group 8 double mutants

Skeletal malformations were investigated using mutants generated through simultaneous mutations in *Hoxb8*, *Hoxc8*, and *Hoxd8* (van den Akker et al., 2001). Two of these three strains of mutant mice (*Hoxb8*$^{-/-}$/*Hoxc8*$^{-/-}$ and *Hoxb8*$^{-/-}$/*Hoxd8*$^{-/-}$) possessed T2→T1 transformations, as evident by either unilateral or bilateral T1/T2 rib fusions prior to the junction at the sternum. Only *Hoxb8*/*Hoxc8* and *Hoxc8*/*Hoxd8* double mutants had more posterior transformations, which included an extra sternebra between rib pairs 6 and 7, unilateral or bilateral L1 rib(s), and a complete shift of S1 to an L6 identity (S1→L6). Finally, two remaining phenotypes were unique to *Hoxc8*/*Hoxd8* double mutants: eight rib pairs joined at the sternum and the transitional vertebra was shifted to T12, instead of T10, as in wild-type animals. Overall, these results show a significant amount of phenotypes shared in common among *Hox8* single and double mutants, suggesting that this group of genes function in a larger context to pattern vertebrae ranging from the anterior thoracic to the sacral vertebrae.

Hox Paralogous Group 9 double mutants

Hoxa9/*Hoxb9* double mutants

The results from single *Hoxa9* and *Hoxb9* mutants suggest that these two genes pattern two separate regions of the vertebral column, since there is no overlap in their phenotypes (Chen and Capecchi, 1997; Fromental-Ramain et al., 1996). However, both genes are expressed in the prevertebrae that give rise to thoracic and lumbar vertebrae. In order to investigate a possible synergistic interaction between these two co-paralogous genes, individual *Hoxa9* and *Hoxb9* heterozygotes were bred to create compound *Hoxa9*/*Hoxb9* heterozygotes (Chen and Capecchi, 1997; Fromental-Ramain et al., 1996). Not surprisingly, the resulting mutants had no T2→T1 transformations, since this phenotype was absent from either single heterozygote. However, the authors report T8 rib sternocostal junctions (6%) and L1 ribs (38%) in $Hoxa9^{+/-}$/$Hoxb9^{+/-}$ mutants. The compound heterozygotes were further crossed in an attempt to exaggerate the effects of these genes on T1 and T2. The prevalence of T8 and L1 anteriorizations did increase as copies of *Hoxa9* and *Hoxb9* were simultaneously deleted. No T2 anteriorizations were observed in $Hoxa9^{-/-}$ /$Hoxb9^{+/-}$ mice, but as functional copies of *Hoxa9* were removed from the *Hoxb9*-null background, a corresponding increase in the penetrance of T2→T1 transformations occurred: 93% of $Hoxa9^{+/-}$/$Hoxb9^{-/-}$ and 100% of $Hoxa9^{-/-}$/$Hoxb9^{-/-}$ mutants. This result suggests that *Hoxa9* plays a role in T1/T2 patterning in conjunction with *Hoxb9*.

Hoxa9/*Hoxd9* double mutants

The lumbar vertebral phenotypes are shared in common between *Hoxa9* and *Hoxd9* individual mutants, so single heterozygotes were intercrossed to generate compound heterozygotes (Fromental-Ramain et al., 1996). Since both single heterozygotes displayed a subset of the phenotypes seen in individual homozygotes, it was not surprising that the *Hoxa9*$^{+/-}$/*Hoxd9*$^{+/-}$ mutants mimicked the *Hoxa9*$^{+/-}$ phenotype. To further investigate the effect of simultaneous deletion of these two group 9 paralogous genes, compound heterozygotes were crossed to generate *Hoxa9*$^{+/-}$/*Hoxd9*$^{-/-}$, *Hoxa9*$^{-/-}$/*Hoxd9*$^{+/-}$, and *Hoxa9*$^{-/-}$/*Hoxd9*$^{-/-}$ mutants. An initial anterior transformation of L1→T13 resulted in a posterior shift of the caudal vertebrae by a one-segment length. In these mutants, previously untransfomed vertebrae L6, S1, and S3 were now anteriorized. Finally, an S2→S1→L6 transformation produced a posterior shift in the vertebrae so that the ilium articulated ectopically at S2 instead of its wild-type position at S1. These phenotypes were exacerbated as copies of *Hoxa9* and *Hoxd9* were removed, resulting in fully penetrant phenotypes in *Hoxa9*/*Hoxd9* double homozygous mutants.

Hox Paralogous Group 10 double mutants

Hoxa10/*Hoxd10* double mutants

The rostral limits of both co-paralogous *Hoxa10* and *Hoxd10* genes map to pv21, or the first lumbar prevertebra (Benson et al., 1995; Dollé and Duboule, 1989). However, single mutations in either of these genes produce mice with very different vertebral transformations. The vertebrae at the transition between thoracic and

lumbar regions are affected in *Hoxa10* mutants (Rijli et al., 1995), while the *Hoxd10* mutation impacts the patterning of the sacral vertebrae (Carpenter et al., 1997). The *Hoxa10*/*Hoxd10* double homozygotes observed by Wahba *et al*. showed vertebral transformations that encompassed both lumbar and sacral regions (Wahba et al., 2001). An increase in the penetrance of the L1→T13 anteriorization (25% of double homozygotes) was observed over *Hoxa10* single homozygotes (11%). This transformation resulted in further anteriorizations of the remaining caudal vertebrae: the number of lumbar vertebrae was increased and the positional identity of sacral vertebrae was altered. Ultimately, this shifted the position of the pelvis with respect to the vertebral column more posteriorly. Each of these phenotypes was observed in mice with three mutant alleles ($Hoxa10^{+/-}/Hoxd10^{-/-}$ and $Hoxa10^{-/-}/Hoxd10^{+/-}$ mice) at lower levels of penetrance, suggesting that both genes act synergistically to pattern the lumbar and sacral vertebrae and their anterior and posterior boundaries.

Non-paralogous *Hox* gene double mutants

***Hoxa10*/*Hoxd11* double mutants**

Non-paralogous genes *Hoxa10* and *Hoxd11* share gene expression profiles in the lumbar vertebrae; the rostral limit of *Hoxa10* expression is at pv21, while the limit for *Hoxd11* is at pv24 (Benson et al., 1995; Izpisua-Belmonte et al., 1990). Similar to the comparison of phenotypes for *Hoxa10* to its co-paralogue *Hoxd10*, the phenotypes for *Hoxa10* and *Hoxd11* do not overlap. The thoracic-lumbar transition is altered in *Hoxa10* mutants, while sacral vertebrae are anteriorized in *Hoxd11* mutants (Carpenter et al., 1997; Rijli et al., 1995). Nevertheless, more severe and highly-

penetrant phenotypes were generated upon simultaneous mutation of both genes (Favier et al., 1996). Specifically, the *Hoxd11* homozygous phenotypes of the sacral vertebrae increased to full penetrance as copies of *Hoxa10* were deleted, as in *Hoxa10*$^{+/-}$/*Hoxd11*$^{-/-}$ mutants. Instead of affecting localized groups of vertebrae, mice with three or four deleted copies (*Hoxa10*$^{+/-}$/*Hoxd11*$^{-/-}$; *Hoxa10*$^{-/-}$/*Hoxd11*$^{+/-}$; *Hoxa10*$^{-/-}$/*Hoxd11*$^{-/-}$) displayed anteriorizations covering larger vertebral regions, spanning the entire length of the lumbar vertebrae and beyond. Just as in *Hoxa10*/*Hoxd10* double mutants, non-paralogous *Hoxa10*/*Hoxd11* double mutants combine the affected vertebral regions that are each singly affected by individual mutants.

***Hoxb5*/*Hoxb6* double mutants**

As previously reported, both *Hoxb5* and *Hoxb6* homozygotes were viable and fertile. This allowed the authors to initiate the following crosses to generate *trans*-heterozygotes, and single heterozygotes as controls, in an attempt to reveal a genetic interaction: *Hoxb5*$^{-/-}$x*Hoxb6*$^{+/-}$ and *Hoxb5*$^{+/-}$x*Hoxb6*$^{-/-}$ (Rancourt et al., 1995). Within the *trans*-heterozygous animals (*Hoxb5*$^{+/-}$;*Hoxb6*$^{+/-}$), the C6→C5 and C7→C6 homeotic transformations occurred at frequencies of 43% and 50%, respectively. The T1→C7 transformation was identified in 58% of the *trans*-heterozygotes, while the rib defects observed in *Hoxb6* homozygotes occurred at a much lower frequency in *trans*-heterozygotes (8%). Additionally, no skeletal phenotypes were found in either *Hoxb5* or *Hoxb6* single heterozygotes. Taken together, these results indicate that both *Hoxb5* and *Hoxb6* act cooperatively in patterning the lower cervical and upper thoracic skeletal elements (C6 through T2). Since the phenotypes are shared among

Hoxb5 and *Hoxb6* homozygotes and *trans*-heterozygotes and are not observed in single heterozygotes, the authors suggest that the individually-targeted mutations in both genes act as alleles of the same gene (nonallelic noncomplementation). Furthermore, they propose a gene dosage model to explain the development of these cervicothoracic phenotypes. Assuming that the Hoxb5 and Hoxb6 gene products function in similar and redundant roles, then a wild-type animal would contain four copies of the products necessary to pattern C6 through T2. In the case of single heterozygotes, three copies would be present and sufficient to produce wild-type vertebral structures, consistent with the absence of phenotypes in these animals. Both single homozygotes and *trans*-heterozygotes possess only two copies of the necessary products and, therefore, demonstrate the anterior homeotic transformations described above. This model and these results show that defects in skeletal patterning occur by decreasing the gene dosages of *Hoxb5* and *Hoxb6*.

***Hoxd9*/*Hoxd10* double mutants**

The last pair of non-homologous *Hox* genes to undergo simultaneous mutation is the neighboring pair *Hoxd9*/*Hoxd10*. As in single *Hoxd9* and *Hoxd10* mutants (Carpenter et al., 1997; Fromental-Ramain et al., 1996), the identities of sacral vertebrae were shifted anteriorly by one segment (de la Cruz et al., 1999). The initial transformation occurred with S2 that adopted an S1-like appearance (S1*), creating two sacral vertebrae with the morphology of wild-type S1. The remaining sacral and first caudal vertebrae also adopted the identity of the vertebrae located immediately anterior, constituting an overall Ca1→S4→S3→S2→S1 transition. In these mutants,

four sacral vertebrae were found fused together, unlike wild-type animals, in which three sacral vertebrae fuse. Finally, no lumbar defects were observed in *Hoxd9*/*Hoxd10* double homozygotes, even though these vertebrae had undergone significant one-segment anterior transformations in *Hoxd9* single mutants.

Hox Paralogous Group 4 triple mutants

Hoxa4/*Hoxb4*/*Hoxd4* triple mutants

The simultaneous deletion of all *Hoxa4*, *Hoxb4*, and *Hoxd4* functional copies through a series of compound mutant matings generated triple homozygous mice (*Hoxa4*$^{-/-}$/*Hoxb4*$^{-/-}$/*Hoxd4*$^{-/-}$; (Horan et al., 1995b)). The phenotypes observed in double mutants (Horan et al., 1995b) were shared in common with the triple mutants. However, additional transformations occurred that expanded beyond the anterior limits of *Hoxa4, Hoxb4,* or *Hoxd4* rostral expression boundaries (Gaunt et al., 1989; Geada et al., 1992). Both partial and complete transformations of C2 through C5 into a C1 identity were observed in *Hoxa4*$^{-/-}$/*Hoxb4*$^{-/-}$/*Hoxd4*$^{-/-}$ P0 pups, including the presence of ectopic aaa (C2-C5) and lateral foramina (C2-C4), which are morphological characteristics unique to wild-type C1. The C6→C5 transformation (absence of AT on C6) was 100% penetrant, but the corresponding C7→C6 transformation was variable. Two of three triple homozygotes had very small unilateral AT on C7, suggesting a partial C7→C6 transformation. The remaining triple homozygote had no AT at all. The authors speculate that this may represent either a C7→C5 transformation or a complete lack of C7 transformation. They do not report on the absence or presence of vertebral foramen on C7. The presence of these

canals ectopically on C7 would help to identify a C7→C5 transformation. Overall, these results clearly show that the increase in the number of transformed vertebrae depends heavily on the relative dosage of each gene present. Furthermore, vertebrae that lie beyond the anterior limits of *Hox* paralogous group 4 expression were increasingly transformed in *Hoxa4*/*Hoxb4*/*Hoxd4* triple homozygous mutants; thus, the removal of functional copies of *Hoxa4*, *Hoxb4*, and *Hoxd4* may disrupt unknown *trans*-regulatory interactions among these genes that are necessary to establish each gene's distinct anterior boundary of expression.

Hox Paralogous Group 8 triple mutants

Hoxb8/*Hoxc8*/*Hoxd8* triple mutants

Since the combined double *Hoxb8*/*Hoxc8*, *Hoxb8*/*Hoxd8*, and *Hoxc8*/*Hoxd8* mutants produced such similar phenotypes, it is very likely that redundancy in this paralogous group has developed in order to ensure the proper specification of the vertebrae affected in each of these mutant strains. Thus, it is not surprising that the triple $Hoxb8^{-/-}$/$Hoxc8^{-/-}$/$Hoxd8^{-/-}$ mutant possesses the full complement of phenotypes found in the double mutants: bilateral T1/T2 rib fusions, ectopic sternal band between the 6th and 7th rib pairs, bilateral L1 rib anlagen, T12 as the transitional vertebra (T12→T10), and an S1→L6 anterior transformation (van den Akker et al., 2001).

Hox Paralogous Group 10 and Group 11 triple mutants

The effects of loss of function of each of the following genes has been previously described through the use of mutant targeting alleles containing insertions of the *neomycin* selectable marker: *Hoxa10*, *Hoxd10*, *Hoxa11*, and *Hoxd11*

(Carpenter et al., 1997; Davis and Capecchi, 1994; Rijli et al., 1995; Small and Potter, 1993). Mutations in *Hoxc10* and *Hoxc11* have not yielded skeletal defects; this does not, however, preclude a functional role for these *HoxC* genes in a more global context. To generate mutants with simultaneous loss of each of the Group 10 or Group 11 *Hox* genes, triple heterozygotes were generated by conventional genetic crosses (Wellik and Capecchi, 2003).

***Hoxa10*/*Hoxc10*/*Hoxd10* triple mutants**

The mating of male and female triple *Hox10* heterozygotes produced mutant 18.5dpc embryos lacking all functional copies of *Hoxa10*, *Hoxc10*, and *Hoxd10*. These mice completely lack lumbar vertebrae. Instead, the vertebrae in the lumbar region have been fully transformed to a thoracic identity, complete with the characteristic thoracic morphology and rib pairs on each transformed vertebra extending from T13. These ectopic rib formations are carried through to the transformed sacral region. The sacral vertebrae are only partially transformed, since their rib formations fuse laterally, as the "wing-shaped" lateral processes would on wild-type sacral vertebrae. Because of these sacral fusions, the pelvis and hindlimbs are able to articulate as they would normally.

***Hoxa11*/*Hoxc11*/*Hoxd11* triple mutants**

The same mating scheme was followed to produce triple *Hoxa11*/*Hoxc11*/*Hoxd11* homozygous mutants. The overall phenotype in these mice was distinct from the *Hox10* triple homozygotes. These mutants had normal lumbar vertebrae, but the sacral and first seven caudal vertebrae were completely transformed

into a lumbar morphology. Surprisingly, these pelvis and hindlimbs in these mutants also associate normally with the vertebral column, despite the absence of sacral vertebrae.

Taken together, these results indicate that *Hox10* paralogues are critical to pattern the lumbar region, and *Hox11* paralogues pattern the sacral vertebrae. The authors speculate that shifts in *Hox10* and *Hox11* gene expression in either a rostral or caudal manner changes the number and position of lumbar and sacral vertebrae, respectively. Additionally, neither group is involved in the proper articulation of the pelvis with the vertebral column, since it occurs in both sets of mutants as it would in wild-type mice. Combined with the individual mutant analyses, these studies clearly demonstrate the degree of functional redundancy among both *Hox10* and *Hox11* genes, as well as the ability of each group to globally pattern the posterior regions of the axial skeleton.

1.2.4 Large-scale *HoxB* cluster targeted mutation

Since homeotic transformations have been reported in mice containing single mutations in *Hoxb2* through *Hoxb9*, Medina-Martinez *et al.* questioned the overall contribution of the *HoxB* complex to skeletal malformations. A chromosomal engineering strategy was used to generate a large targeted deletion of *Hoxb1-Hoxb9* (*HoxBΔ1*; (Medina-Martinez et al., 2000)). Animals that contained only one copy each of *Hoxb1* through *Hoxb9* through this targeting strategy ($HoxB\Delta1^{+/-}$) were found to be similar to wild-type animals. This was surprising considering the gene dosage model used to explain the genetic interaction between *Hoxb5* and *Hoxb6* in *trans*-

heterozygotes with anterior cervicothoracic homeotic transformations (above). The *HoxBΔ1*$^{-/-}$ resulted in neonatal lethality, since none of these animals survived for more than 24 hours after birth. A series of anterior homeotic transformations were observed in the cervical and thoracic skeletal elements, similar to those observed in single *HoxB* homozygous mutants. C2→C1 transformations (increase in the C2 neural arch width and an ectopic anterior arch of the atlas) were observed in 12% of homozygotes. A C6→C5 and C7→C6 transformations occurred at 100% penetrance. The AT normally present on C6 were either absent or fused to ectopic C7 AT; in addition, C7 contained ectopic vertebrarterial (VA) canals. T1→C7 transformations were counted in animals whose T1 ribs were either completely absent or were shortened so that they no longer contacted the sternum. Often T1 ribs were found fused to those of T2. In these cases, T2 ribs made contacts with the sternum at the wild-type T1 rib position, representing an anterior transformation of T2→T1. The authors noted that T8 ribs occasionally resembled T7 ribs (T8→T7), since they formed ectopic junctions with the sternum, either unilaterally or bilaterally. Interestingly, all *HoxBΔ1*$^{-/-}$ animals observed displayed a bifurcated sternum, which further supports these previous conclusions: 1. multiple *HoxB* genes pattern the sternum, and 2. a mutation (via *neomycin* cassette insertion) of a single *HoxB* gene locus also affects the regulatory landscape of neighboring genes, leading to the disruption in sternal development (Barrow and Capecchi, 1996; Manley et al., 2001; Ramirez-Solis et al., 1993). Finally, the use of a large targeted deletion of *Hoxb1* through *Hoxb9* through chromosomal engineering allowed the authors to address the

impact of *HoxB* gene loss-of-function without the use of a resistance marker. Since they observed no posterior transformations in the *HoxBΔ1* mutants, they conclude that these types of transformations found in previous *Hox* mutants represent a gain-of-function in genes targeted by insertion of a selection cassette into the locus (Horan et al., 1994; Jeannotte et al., 1993; Kostic and Capecchi, 1994).

1.3 *Hoxb1* Expression, Gene Regulation, and Mutations

The mouse homeobox-containing gene *Hoxb1* belongs to the *Hox* paralogous group 1 and is located at the most 3' position on the *HoxB* chromosomal cluster. Early in development, *Hoxb1* exhibits a dynamic expression pattern (Frohman et al., 1990). Before neurulation, at 7.5dpc, *Hoxb1* expression is first detected in the gastrulating embryo. It is established in the neuroectoderm, the primitive streak, and the newly formed mesoderm, rostral to the node. At neurulation, the neural plate also expresses *Hoxb1*, specifically in the region of the mesoderm; it is not observed in the more anterior neuroectoderm that will become the midbrain and forebrain. At the early somite stage (8.5dpc), *Hoxb1* mRNA expression consists of two domains: the prospective r4 in the hindbrain and the posterior half of the embryo, including the posterior neural tube, PSM, and the gut. By the end of neurulation, rhombomere boundaries disappear, and *Hoxb1* expression is restricted to r4 and the remaining PSM (Figure 8; (Murphy and Hill, 1991)).

Figure 8. *Cis*-regulatory elements direct modular *Hoxb1* expression

(A) Rhombomere-specific modules in the 5' regulatory region control *Hoxb1* expression in the hindbrain through repression (r3/r5) or activation (r4). An unpublished long-range repressor element has also been identified in this region. Tissue-specific neural, mesodermal, and foregut enhancers are found in the 3' region.

(B) – (E) Time-course of *Hoxb1* gene expression. (B) *lacZ* expression in the posterior half of a 7.5dpc embryo; (C) – (E) *Hoxb1 in situ* hybridization signal observed in r4 and presomitic mesoderm at 8.5dpc (C), 9.0dpc (D), and 9.5dpc (E).

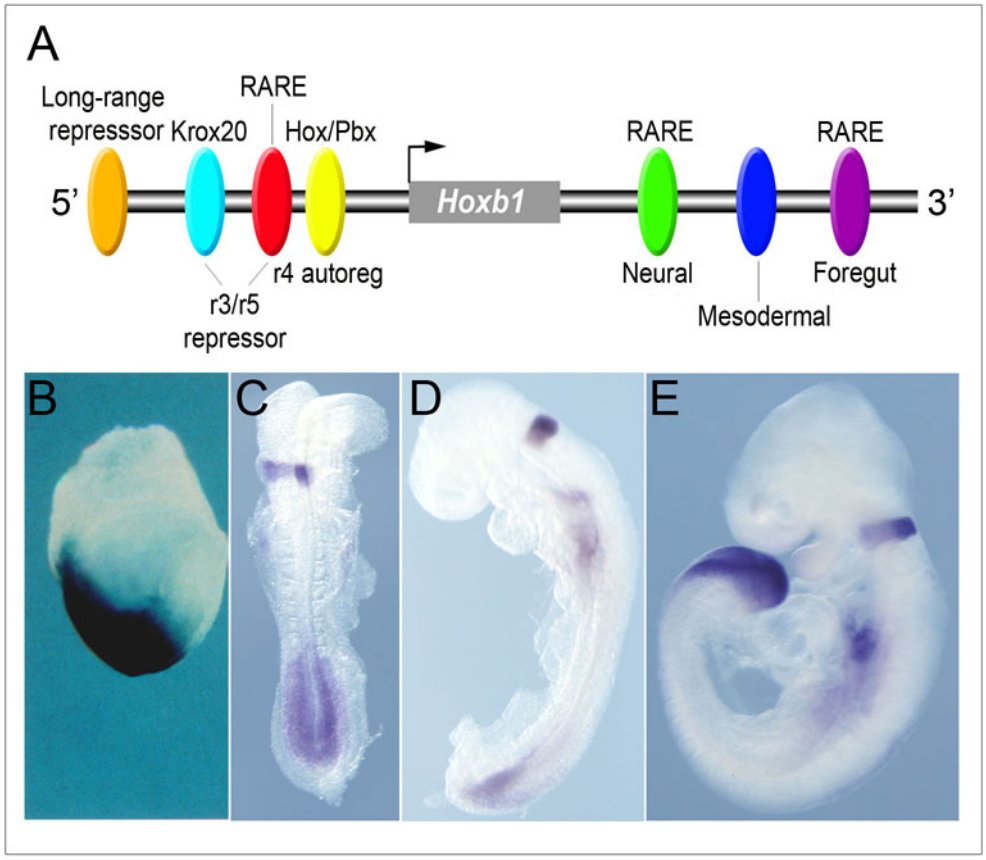
A
Long-range
represssor
Krox20
RARE
Hox/Pbx
5'
Hoxb1
RARE
RARE
3'
r4 autoreg
r3/r5
repressor
Neural
Mesodermal
Foregut
B
C
D
E

Several regulatory elements have been identified both upstream and downstream of the *Hoxb1* coding sequence that direct the appropriate expression from this gene locus (Marshall et al., 1994; Pöpperl et al., 1995; Studer et al., 1998; Studer et al., 1994). Positive regulation of *Hoxb1* in r4, which is necessary for specifying the r4 identity, involves direct autoregulation mediated by a 5' r4 enhancer; this regulation depends upon interactions between Hoxb1 and Pbx proteins. The vertebrate *Pbx* gene is homologous to the *Drosophila* gene *extradenticle* (*exd*); exd proteins bind DNA cooperatively with the HOM-C proteins (Pöpperl et al., 1995). Hoxa1 is also known to interact with Pbx and SOX/OCT proteins to mediate the *Hoxb1* retinoic acid expression through the same r4 enhancer (Figure 8; (Di Rocco et al., 2001; Studer et al., 1998)). In fact, switching this *Hoxb1* auto-regulatory element into the *Hoxa1* promoter enabled newly-regulated Hoxa1 protein to perform the functions of both Hoxa1 and Hoxb1, with respect to r4 patterning, even in the context of a *Hoxb1* loss-of-function mutation (Tvrdik and Capecchi, 2006).

A conserved 5' RARE limits the broad *Hoxb1* expression domain generated by the r4 enhancer by repressing *Hoxb1* transcription in r3 and r5, restricting expression solely to the r4 (Studer et al., 1994). Thus retinoids, and their nuclear receptors, are required to define a segment-restricted region of *Hoxb1* expression late during hindbrain development.

These 5' elements are responsible for mediating the auto-, para-, and cross-regulatory mechanisms that affect *Hoxb1* expression. Several groups investigating the 3' control region of the mouse *Hoxb1* locus have identified enhancer elements located

within this region. Marshall *et al*. reported the presence of two tissue-specific enhancers that together are responsible for establishing the early *Hoxb1* expression in the mesoderm and neuroectoderm, as well as mediating the early response to retinoic acid. The neural enhancer contains a DR2 RARE (retinoic acid response element with 2bp between direct repeats of a consensus sequence) that mediates the retinoic acid response (Marshall et al., 1994). A second RARE (DR5 RARE) was identified more 3' of the neural RARE, mediating the *Hoxb1* response to retinoic acid in foregut tissues (Huang et al., 1998; Langston et al., 1997). Finally, as part of its role in specifying the r4 identity, Hoxb1 is shown to cooperatively bind with Pbx at a bipartite Hox/Pbx site of the r4 enhancer located in the 5' region of the *Hoxb2* locus. This direct cross-regulatory mechanism functions to restrict *Hoxb2* to an r4 domain (Maconochie et al., 1997). In addition, recent work in the Krumlauf lab has shown that *Hoxa2* is directly regulated by Hoxb1 in r4 (Tümpel et al., 2007). It is through these enhancer elements that the auto-, para-, and cross-regulatory interactions of *Hoxb1* and the appropriate expression of *Hoxb1*, *Hoxb2*, and *Hoxa2* are established and maintained in r4 of the developing hindbrain (Figure 9; (Melton et al., 2004)).

To date, investigations into the developmental role of *Hoxb1* have been limited to the developing hindbrain. In order to better understand this role, several targeted mutagenesis strategies have been employed. A loss-of-function allele was generated by inserting a *lacZ*/*neomycin* cassette into the first exon of the *Hoxb1* gene locus and introducing a frameshift mutation in the homeobox (Studer et al., 1996). Mice targeted by this approach exhibit 98% lethality within 24 hours of birth. It was

Figure 9. The genetic regulatory network that patterns rhombomere 4 gene expression

Schematic representation of the network of regulatory interactions that initiate (left) and maintain (right) *Hoxb1* expression in r4 of the hindbrain. For initiation, retinoids and *Hoxa1* (blue arrows) provide input via the 5' regulatory region of the *Hoxb1* locus. To maintain *Hoxb1* expression in r4, Hoxb1 feeds back on itself through an autoregulatory element (green arrow); *Hoxb2* (a downstream Hoxb1 target) gene product interacts with cofactors (Prep/Meis/Pbx; thick black arrow) to further drive *Hoxb1* r4 expression. *Hoxb1*, *Hoxb2*, and *Hoxa2* (a downstream Hoxb1 target (thick black arrow) which regulates its own expression in r4 (orange arrow)) gene products further specify r4 identity through r4 target genes (thin black arrows).

Adapted from (Tümpel et al., 2007).

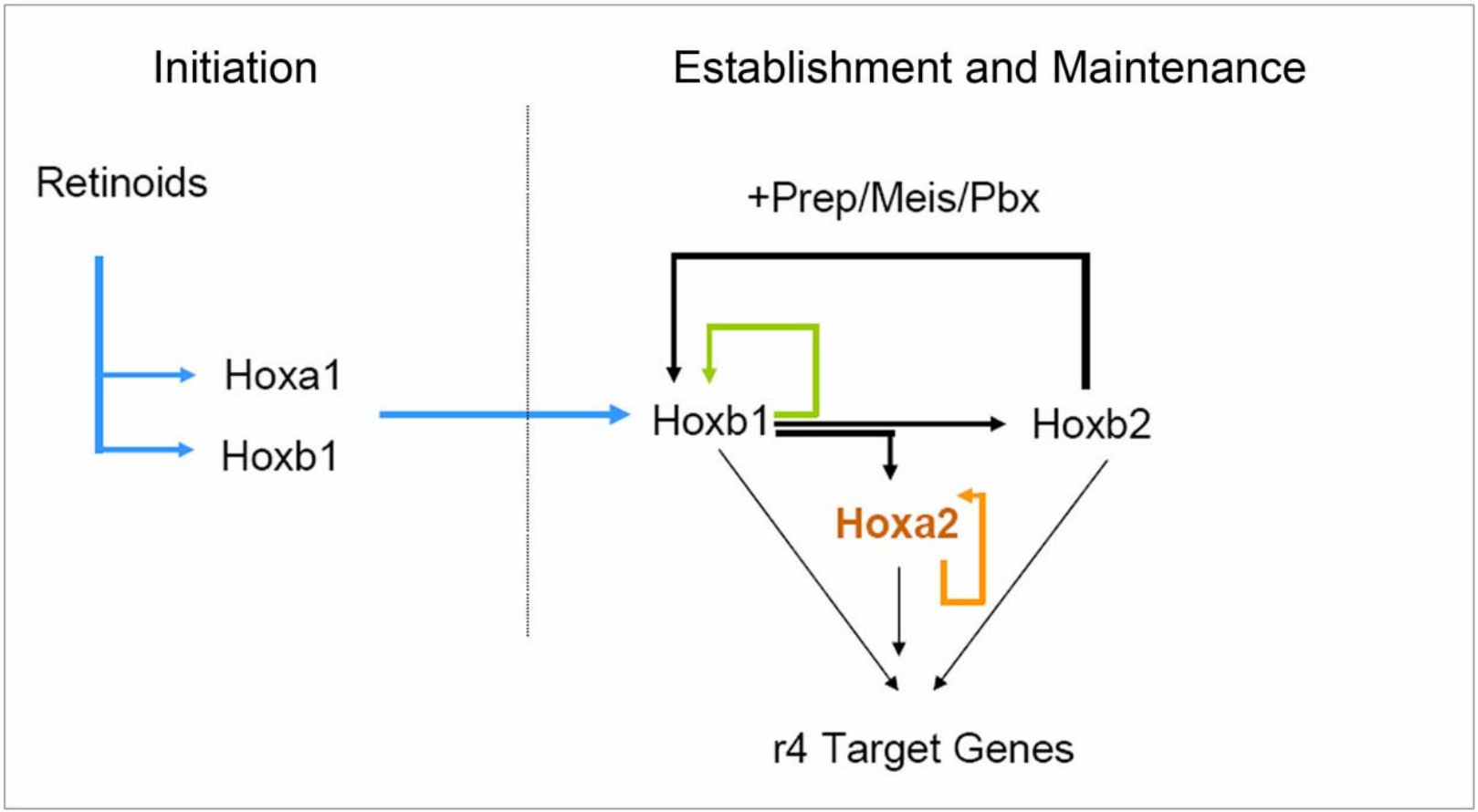
Initiation
Establishment and Maintenance
Retinoids
+Prep/Meis/Pbx
Hoxa1
Hoxb1
Hoxb1
Hoxb2
Hoxa2
r4 Target Genes

determined through mutant analysis that *Hoxb1* plays a role in maintaining the identity of r4, since mice lacking this gene display altered r4 segment identity and abnormal migration of facial branchiomotor and contralateral vestibuloacoustic efferent neurons. A second group generated a *Hoxb1* mutant allele by disrupting both exons: 12bp were inserted into exon 1, and the *neomycin* cassette was targeted into exon 2 (Goddard et al., 1996). Interestingly, these mice did not display the significant perinatal lethality seen by the previous group. However, the loss of the facial nerve's somatic motor component indicated, as in the previous mutant, that these motor neurons were incorrectly specified due to homozygous loss of Hoxb1 function. Thus the common defect in these two mutants is not the organization of r4 or its neural crest derivatives; instead, the identity of neurons specified in r4 is severely affected.

As stated above, previous work has shown that Hoxa1 acts through a 5' enhancer element to initiate early *Hoxb1* gene expression. However, it was not previously clear whether this was the only *Hoxa1* input into *Hoxb1* regulation. To better understand the relationship between these two genes in patterning the early hindbrain, several targeting strategies have been performed to generate simultaneous loss of both Hoxa1 and Hoxb1 function. Studer *et al*., analyzed the effects of point mutations in the 3' neural RARE enhancer alone, as well as in the context of *Hoxa1*- and *Hoxb1*-null conditions (Studer et al., 1998). In the homozygous $Hoxb1^{3'RARE}$ mutant, *Hoxb1* transcripts are detected at much lower levels than wild-type in the neuroectoderm of 7.5dpc embryos. However, there was no difference between mutants and wild-type with respect to the later *Hoxb1* expression in r4, suggesting

one of two things: 1. the 3' RARE is specifically involved in the early regulation of *Hoxb1* in the neuroectoderm and not later r4 expression, or 2. some other mechanism compensates for r4 expression in the absence of this 3' RARE. Since the *Hoxa1* locus also contains a 3' RARE (Langston and Gudas, 1992), Studer *et al*. investigated the possibility that the *Hoxa1* and *Hoxb1* 3' RAREs may act together to regulate *Hoxb1* r4 expression, supporting the latter explanation above. The analysis of *Hoxb1* mRNA expression in double RARE mutants showed a decrease in r4 transcripts, but to varying degrees. Only a portion of the 8.5-9.5dpc embryos showed *Hoxb1* down-regulation in r4. Nevertheless, the decrease suggests that both RAREs participate in the establishment of *Hoxb1* hindbrain expression through auto- and para-regulation. This synergistic interaction between *Hoxa1* and *Hoxb1* was further confirmed through analysis of $Hoxa1^{-/-}/Hoxb1^{3'RARE}$ and $Hoxa1^{-/-}/Hoxb1^{-/-}$ double mutants.

The above mutant lines (*Hoxa1*-null, *Hoxb1*-null, and $Hoxb1^{3'RARE}$) were also used to assess the degree of synergism between these two genes with respect to hindbrain patterning, as well as the second branchial arch and its derivatives (Gavalas et al., 1998). Overall, patterning defects were observed in combined mutants within the r4-r6 hindbrain region, giving rise to defects in cranial nerves VII through XI. Additionally, the second branchial arch (ba2) was involuted by 10.5dpc; consequently, ba2 skeletal derivatives (inner, middle, and external ear structures) were variably absent or reduced in size. A similar selective loss of ba2 derivatives was also observed by Rossel and Capecchi, despite the fact that the selectable *neomycin* cassette was removed in their *Hoxa1* and *Hoxb1* targeted alleles.

Finally, synergistic interactions among *Hoxa1*, *Hoxb1*, and *Hoxb2* in regulating neuronal differentiation and motor neuron migration were indicated by the observation that defects in the specification of neuronal subpopulations were present in all three single mutant lines (Gavalas et al., 2003). *Hoxb1* mutant neurons derived from r4 were switched from an r4 to an r2 fate. The *Hoxa1* mutant phenotype resulted in a partial respecification of r4 neurons, since *Hoxb1* function was still present, although reduced. *Hoxb2* mutant r4 neurons possessed a defect in the migratory pathway, such that a reduced number of facial branchiomotor neurons migrated caudally; instead, a second group displayed trigeminal motor neuron migratory behaviors. Taken together, the failure of each mutant to correctly specify the migratory motor neurons of the facial nerve indicates that both *Hoxa1* and *Hoxb2* are required to facilitate the role of *Hoxb1* in hindbrain neuronal patterning.

Until now, investigations into the regulation and functions of *Hox* genes, including *Hoxb1*, have been focused primarily in the neuroectoderm. Even though *Hoxb1* transcripts have been detected in tissues other than the hindbrain, there have been no reports describing the effects of *Hoxb1* gene expression in mesodermally-derived tissues.

1.4 Aim of the project

Interestingly, the more posterior *Hox* genes have received more attention with respect to their roles in patterning the axial skeleton than have anterior *Hox* genes. This project aims to establish the effect of the expression of *Hoxb1* and its co-paralogue *Hoxa1* in precursors of mesodermally-derived tissues, specifically, the

axial skeleton, through the use of individual and compound mutant mouse strains. Although the contribution of *Hoxb2* to axial skeleton development has been reported (Barrow and Capecchi, 1996), this project will attempt to more fully-describe the effects of loss of Hoxb2 function singly and in combination with the *Hoxb1* mutation. The above approaches will allow us to assess the impacts of decreases in each gene's dosage. Through the use of plasmid and Bacterial Artificial Chromosome (BAC) transgenics, we will investigate potential gain-of-function effects by increasing *Hoxb1* gene dosage. We hypothesize that the latter approach will permit a greater perturbation of skeletal development, as, theoretically, we will be adding back through transgenesis more copies of *Hoxb1* than we could ever remove via traditional targeted gene knockout strategies (i.e. 2 endogenous copies).

Chapter 2

Materials and Methods

2.1 Genotyping embryo yolk sacs

Yolk sacs were individually harvested in ice-cold PBS upon careful dissection of each embryo from its decidua in the mother's uterine horn and collection into a 1.7ml Eppendorf tube. Forceps were briefly rinsed in water between embryo dissections to prevent contamination. To isolate DNA for genotyping by PCR, yolk sacs (8.5-18.5dpc) were heated to 95ºC for 10 minutes in 50mM NaOH. The following PCR setup was performed to genotype each yolk sac with respect to the appropriate gene(s) of interest:

Component	Volume	Final Concentration
2X PCR Reddy Mix	10µl	1X
Oligonucleotides	2µl/each	0.1µg/µl
DNA template	1µl	~100-250ng
ddH_2O	up to 20µl	N/A

The 2X PCR Reddy Mix is a commercially-available product that contains: 0.625 units of ThermoPrime *Taq* DNA Polymerase, 75mM Tris-HCl (pH 8.8 at 25ºC), 20mM $(NH_4)_2SO_4$, 1.5mM $MgCl_2$, 0.01% (v/v) Tween-20, and 0.2mM each of dATP, dCTP, dGTP, and dTTP. The following cycling conditions were performed to amplify the expected PCR products:

Step	Temperature	Time
1. Initial denature step	94ºC	3 minutes
2. Dentaure	94ºC	1 minute
3. Anneal	55ºC	1 minute
4. Extend	72ºC	2 minutes
5. Final Extension	72ºC	10 minutes

The denaturing, annealing, and extension steps (2-4) were repeated 30 times prior to the final extension. PCR products were loaded into individual wells cast into a 1% Agarose gel, and gel electrophoresis in 1X TAE was performed at 125V. Agarose gels were post-stained with Ethidium Bromide for 15 minutes prior to visualization/imaging of PCR products under UV light.

2.1.1 PCR primer sequences for genotyping *Hox* loss-of-function mutant and *HoxB* transgenic mice

***Hoxa1* mutation**

Primer Name	Sequence
A1S	5'-GCCATTGGCTGGTAGAGTCACGTGT-3'
A1AS	5'-CATGGGAGTCGAGAGGTTTCCAGAG-3'
A1NeoS	5'-GATGGAAGCCGGTCTTGTCGATCAG-3'

The A1S and A1AS primers will amplify the wild-type 570bp product, and A1NeoS and A1AS primers will amplify the mutant 700bp product.

***Hoxb1* mutation**

Primer Name	Sequence
2.9P2	5’-AGCTTCAGCTCTGTGACATACTGCCG-3’
2.9P5	5’-GAATAATACTGAGAAGGCCCATAGCTGG-3’
BG3C	5’-TAGATGGGCGCATCGTAACCGTGCAT-3’

The 2.9P2 and 2.9P5 primers will amplify the wild-type 372bp product, and BG3C and 2.9P5 primers will amplify the mutant 465bp product.

***Hoxb2* mutation**

Primer Name	Sequence
B2for	5’-CCGCGAAATTGCTCCATTGCATA-3’
B2KO2	5’-TGGCGGCGGTGACCGCAGAGCAG-3’
B2KO3	5’-CCTCAGGAAGATCGCACTCCAG-3’

The B2for and B2KO2 primers will amplify the wild-type 370bp product, and B2for and B2KO3 will amplify the mutant 525bp product.

***Hoxa1* and *Hoxb1* mutations**

As above, the A1S/A1NeoS/A1AS and 2.9P2/BG3C/2.9P5 primer sets will produce genotype information to determine *Hoxa1* and *Hoxb1* mutant zygosity status.

***Hoxb1* and *Hoxb2* mutations**

As above, the 2.9P2/BG3C/2.9P5 and B2for/B2KO2/B2KO3 primer sets will produce genotype information to determine *Hoxb1* and *Hoxb2* mutant zygosity status.

***Hoxb1* and *HoxB* cluster deletion mutations**

Transnetyx, Inc., a Tennessee-based genotyping company, received yolk sac samples from embryos derived from matings between the *Hoxb1* and *HoxB* mutant lines. The official Transnetyx website, www.transnetyx.com, describes their protocol:

"Our proprietary automated system prepares the samples, isolates the DNA, matches the DNA in duplicate with a custom designed assay and finally reads and formats the results with 99.973% accuracy."

***Hoxb1-Hoxb5* transgene**

Primer Name	Sequence
CDN Tn-3	5'-AATGAATAACTGTCAGGTAGGGAGCC-3'
CDN Tn-4	5'-TATGTTCTCTAAGGGTAGTGTCCCG-3'

Together, these primers will amplify a 365bp product from the *Hoxb1-Hoxb5* transgene, if present.

***Hoxb1* mutation and *Hoxb1-Hoxb5* transgene**

As above, the 2.9P2/BG3C/2.9P5 and CDNTn-3/Tn-4 primer sets will produce genotype information to determine *Hoxb1* mutant zygosity and *Hoxb1-Hoxb5* transgenic status.

***Hoxb1-Hoxb9* transgene**

Primer Name	Sequence
Hoxb5-5'	5'- ACGAAGTACAGTGCATCGCT-3'
EGFPsr	5'- TCAGGGTCAGCTTGCCGTAG-3'

Together, these primers will amplify a 375bp product from the *Hoxb5-eGFP* transgene.

***Hoxb1* transgene**

Primer Name	Sequence
CDN-286	5'-AGCTCGGATCCACTAGTAACG-3'
CDN-288	5'- ATAGGTCCCTCTAGTTCTTTG-3'

Together, these primers will amplify a 309bp product that contains a region from the vector backbone and a region from the 5' end of the *Hoxb1* capture cassette used to generate the transgene.

2.2 Skeletal preparations

Mouse embryos (18.5dpc) within the harvested uterine horn were submersed in ice-cold PBS for at least one hour to induce hypothermia, resulting in death. Neonatal pups (P0) were anesthetized by up to 50 minutes of either CO_2 or isofluorane gas inhalation and then submersed in ice-cold PBS to induce euthanasia. Animals were then transferred to ice-cold 95% EtOH for 1 hour, rocking. After 1 hour, fresh 95% EtOH was applied, and the bodies were stored at 4ºC. The skin, viscera, connective tissue, and muscle were carefully removed. The skeletons were

then stained with a combined Alizarin Red S/Alcian Blue 8 GX staining solution overnight, rocking at room temperature:

5ml of 0.4% Alcian Blue 8 GX in 70% EtOH

5ml of Glacial Acetic Acid

70ml of 95% EtOH

20ml ddH_2O

1ml of 0.5% Alizarin Red S in ddH_2O

Final Volume = 100ml

The next day, the skeletons were rinsed briefly in water and any remaining tissues were dissolved upon the addition of 2% KOH for 6 hours. Skeletons were then rinsed in 0.25% KOH for 30 minutes and further processed through a graded glycerol series: 20% glycerol/0.25% KOH for 1 hour, 33% glycerol/0.25% KOH for 1 hour, and 50% glycerol/0.25% KOH overnight, rocking at room temperature. The next day, a fresh solution of 50% glycerol/0.25% KOH was applied for further clearing and storage.

2.3 Whole mount *in situ* hybridization of mouse embryos

2.3.1 Solutions

PBT: 1x PBS plus 1% Tween.

Sheep serum: Inactivate by heating to 70ºC for 30 minutes, store in aliquots at -20ºC.

NTMT: 100mM NaCl, 100mM Tris-HCl pH 9.5, 50mM $MgCl_2$, 1% Tween-20, 2mM (0.5mg/ml) Levamisole.

200x NBT: 50mg/ml NBT in 70% DMF.

200x BCIP: 25mg/ml BCIP in water.

MABT: 100mM Maleic acid, 150mM NaCl, 0.1% Tween-20. Add water to desired volume.

20x SSC: 175.3g NaCl, 88.2g Sodium Citrate, 800ml water. Adjust pH to 7.0, bring volume to 1L and autoclave.

10% SDS: DEPC-treat 400ml water and autoclave. Add 50g SDS and heat to 68ºC while stirring. Adjust pH to 7.2 with HCl. Adjust volume to 500ml with DEPC-water.

Blocking solution: 10% sheep serum/1% BBR (Behringer's Blocking Reagent)/PBT

2.3.2 *In situ* probe design and synthesis

Constructs containing *Hoxb1*, *Hoxb2*, and *Hoxb4* cDNA's were obtained from Krumlauf lab stocks for use in cDNA probe synthesis. The following linearization reaction was performed:

10µg template DNA

2µl Restriction Enzyme

7µl RE buffer

0.7µl BSA, if necessary

add ddH_2O to a total volume of 70µl

Each linearization reaction was incubated at 37ºC for 2 hours, and an additional 2µl of restriction enzyme was added, followed by a second 2 hour incubation at 37ºC. To synthesis antisense probes from each of the linearized constructs, the following synthesis reaction was performed:

10µl DEPC-treated ddH_2O

4µl Transcription buffer

2µl DTT

2µl DIG nucleotide mixture

2µl Linearized plasmid

0.5µl RNasin Ribonuclease inhibitor

2µl RNA Polymerase

Each synthesis reaction was incubated at 37ºC for 2 hours, spiked with another 2µl of RNA Polymerase, and then incubated another 2 hours. For antisense *Hoxb1* probe synthesis, the #1299 construct (Figure 10A) was linearized with EcoRI and transcribed with T3 RNA Polymerase. For antisense *Hoxb2* probe synthesis, the #865 construct (Figure 10B) was linearized with EcoRI and transcribed with T7 RNA Polymerase. For antisense *Hoxb4* probe synthesis, the #650 construct (Figure 10C) was linearized with BglII and transcribed with T3 RNA Polymerase. To check for probe synthesis, a small aliquot of each probe was run on a 1% Agarose gel. Once adequate synthesis was confirmed, each probe was treated with DNaseI for 30 minutes at 37ºC to digest any contaminating DNA. Following DNaseI treatment, synthesized probes were purified through the commercially-available NucAway Spin Columns to further remove contamination. At this point, the probes were ready for use in hybridization reactions or were stored at -20ºC for future use.

Figure 10. *Hoxb1*, *Hoxb2*, and *Hoxb4* constructs for *in situ* hybridization probe synthesis

(A) About 900bp of mouse *Hoxb1* cDNA was cloned into pBluescriptKS, restoring the BamHI and eliminating the EcoRV restriction enzyme (RE) sites. The cDNA region cloned includes the initiation codon downstream of EcoRI, HindIII, and NcoI sites. To generate an antisense probe, this construct was cut with EcoRI and synthesized with T3 RNA Polymerase.

(B) Roughly 3kb of mouse *Hoxb2* cDNA was cloned into pBluescriptKS, retaining the EcoRI and NotI RE sites. To generate antisense probe, this construct was cut with EcoRI and synthesized with T7 RNA Polymerase.

(C) A 1.3kb fragment of mouse *Hoxb4* cDNA was cloned into the EcoRI site of pBluescriptKS. This fragment also contains an internal BglII RE site, which can be used to linearize the construct prior to synthesis with T3 RNA Polymerase to generate an antisense probe.

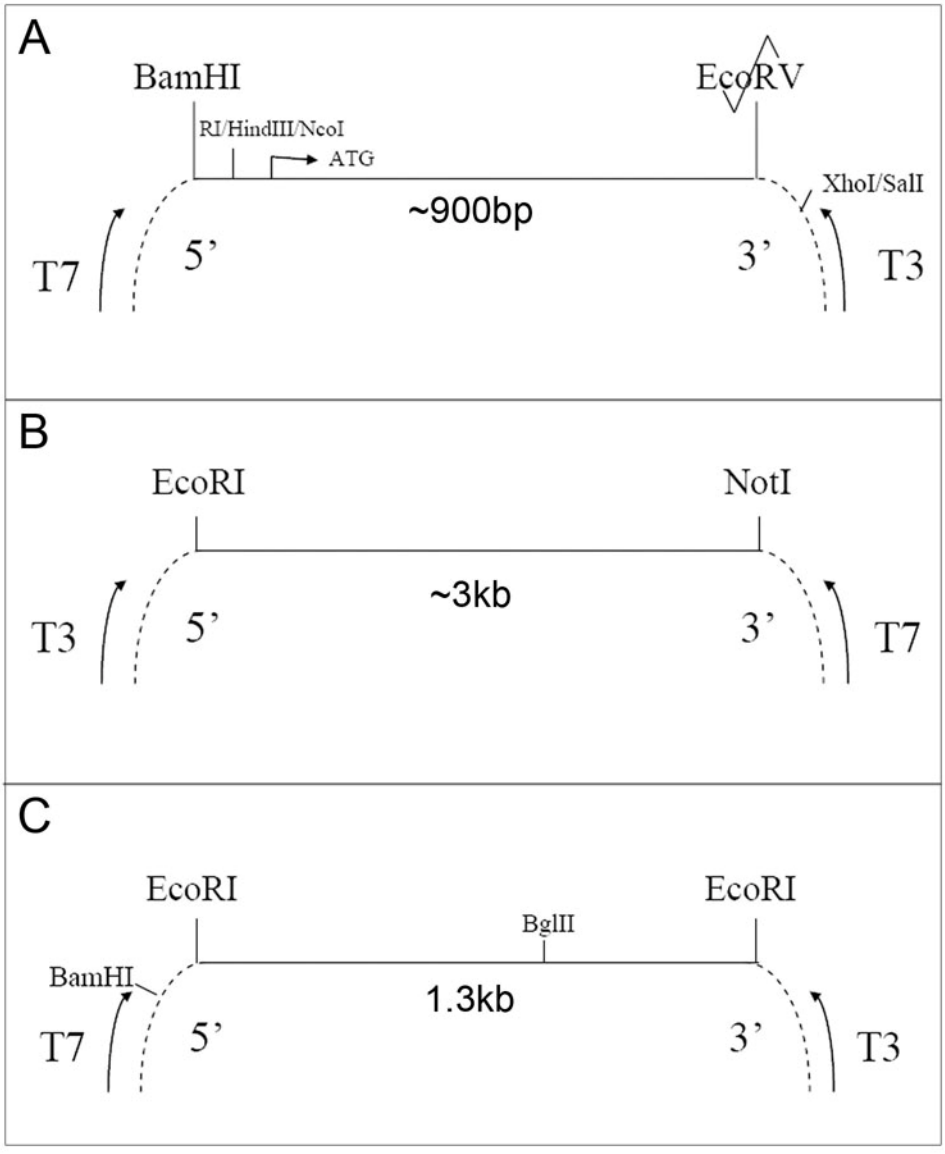
A
BamHI
EcoRV
RI/HindIII/NcoI
ATG
XhoI/SalI
~900bp
T7
5'
3'
T3
B
EcoRI
NotI
~3kb
T3
5'
3'
T7
C
EcoRI
EcoRI
BglII
BamHI
1.3kb
T7
5'
3'
T3

2.3.3 *In situ* hybridizations

Embryos were dissected in PBS and openings were introduced by forceps into the forebrain, hindbrain, and neural tube to allow probe penetration. They were then fixed overnight in 4%PFA/PBS at 4ºC on a nutator. The next day, embryos were washed twice (15 minutes each) in 100% MeOH at room temperature on a nutator and stored until further use at -20ºC. Embryos were then rehydrated through the following MeOH/PBT series: 75% MeOH/PBT for 5 minutes, 50% MeOH/PBT for 5 minutes, 25% MeOH/PBT for 5 minutes, followed by two more washes with PBT, each 5 minutes. Proteinase K (Pro K) treatments were performed according to the following schedule: 6 minutes for 8.5dpc, 10 minutes for 9.5dpc, 15 minutes for 10.5dpc, and 17 minutes for 11.5dpc. A 10 minute wash in 2mg/ml glycine made fresh with PBT and 2 more 5 minute washes in PBT followed Pro K treatment. Embryos were postfixed in 4%PFA/0.2% glutaraldehyde in PBT for 20 minutes at room temperature. Two more PBT washes followed, each 5 minutes. Embryos were equilibrated into hybridization solution with a 10 minute wash in 1:1 mixture of hybridization solution/PBT and a 10 minute wash in hybridization solution:

50% formamide

5X SSC pH 4.5

1% SDS

50µg/ml yeast tRNA

50µg/ml heparin

Then they underwent prehybridization for at least 1 hour in a 70ºC hybridization oven. Hybridization was performed by adding 1µg/ml of DIG-labeled RNA probe to the embryos in prehybridization mix and incubating in a 70ºC hybridization oven overnight twice. Following hybridization of the probe, embryos were washed in prehybridization buffer for 5 minutes at 70ºC, a ½ volume of 5X SSC, pH 4.5 was added and washed over the embryos for 5 minutes, also at 70ºC. These washes were repeated twice more with the same volume of 2X SSC. They were then washed three times for 30 minutes each in 50% formamide, 5X SSC pH 4.5, 1% SDS at 70ºC. An additional three washes for 30 minutes each were performed with 50% formamide, 2X SSC, pH 4.5 at 65ºC. At room temperature, the following washes were performed: MABT rinse, then two 10 minute MABT washes, two 30 minute MABT washes, two 10 minute PBS washes, one 5 minute PBT wash. The embryos underwent blocking with 10% sheep or goat serum/1%BBR/PBT for 1 ½ hour at room temperature. The primary antibody (antiDig) was diluted 1:2000 in blocking solution and applied overnight at 4ºC, nutating. The next day, embryos were rinsed in 0.1% BSA in PBT and then washed 5 times in 0.1% BSA in PBT for 45 minutes each. Two 30 minute PBT washes preceded three 15 minute washes with freshly-prepared NTMT. The color reaction was initiated upon application of 3.5µl/ml each of NBT and BCIP in NTMT. This part of the protocol was performed in the dark and proceeded until the desired amount of staining had been reached. Once the desired color reaction had been achieved, embryos were processed through the following washes: NTMT for 10 minutes at room temperature, 3 x 15 minute PBT washes at

room temperature, and postfix in 4% PFA/0.1% Glutaraldehyde overnight at 4ºC, nutating. The next day, embryos were washed three times in PBT and then dehydrated through a graded MeOH in PBT series: 25%, 50%, 75%, and 100% MeOH. Once fully dehydrated, embryos were stored at -20ºC. Prior to imaging, embryos were rehydrated through the reverse MeOH in PBT series.

2.4 Slide-mounted *in situ* hybridizations

Sagittal sections (7μm-thick) were cut through paraffin-embedded intact mouse embryo heads to reveal the anatomy of the sagittal suture and for use in slide-mounted *in situ* hybridizations with probes designed against specific osteogenic markers, specifically, *Bmp2*, *Bmp4*, *Cbfa1*/*Runx2*, *Dlx5*, *Msx1*, *Msx2*, and *Spp1*. Constructs containing cDNA from each of the above genes were obtained as generous gifts from the labs of Dr. Linheng Li (SIMR; *Bmp2* and *Bmp4*), Dr. Gerard Karsenty (Baylor College of Medicine; *Cbfa1*/*Runx2*), Dr. John Rubenstein (UCSF; *Dlx5*), Dr. Robert Hill (Western General Hospital; *Msx1*), Dr. Robert Maxson (USC; *Msx2*), and Dr. Brigid Hogan (Duke Medical Center; *Spp1*). Vector maps for these constructs may be found in Figures 11 and 12. To linearize each construct and synthesize probes for *in situ* hybridization, the following restriction enzymes and RNA Polymerases were used: *Bmp2* with EcoRI and T3, *Bmp4* with KpnI and T3, *Cbfa1*/*Runx2* with EcoRI and T7, *Dlx5* with HindIII and T7, *Msx1* with SacI and T7, *Msx2* with EcoRI and T7, and *Spp1* with EcoRI and SP6. Sectioning through mouse heads and standard *in situ* hybridization protocols were performed by the Histology Core Facility at the Stowers Institute for Medical Research.

Figure 11. *Bmp2*, *Bmp4*, *Cbfa1*/*Runx2*, and *Dlx5* constructs for *in situ* hybridization probe synthesis

(A) ~1kb of mouse *Bmp2* cDNA was cloned into the BamHI site of pBluescriptSK(-), retaining SacI and EcoRI RE sites. To generate an antisense probe, this construct was linearized with EcoRI and transcribed with T3 RNA Polymerase.

(B) 1.6kb of mouse *Bmp4* cDNA was cloned into the EcoRI site of pBluescriptSK(-), retaining SacI and KpnI RE sites. KpnI was used to linearize the construct, and T3 RNA Polymerase was used to transcribe antisense probe.

(C) 270bp of mouse *Cbfa1*/*Runx2* sequence, including the 5'UTR and first 15 residues of coding sequence, was cloned into the SmaI site of pBluescriptKS(-). EcoRI and XbaI sites were retained. To generate antisense probe, the construct was linearized with EcoRI and transcribed with T7 Polymerase.

(D) The complete *Dlx5* coding sequence, without UTRs, was cloned into pBluescriptKS, retaining HindIII and XbaI RE sites. To generate antisense probe, the construct was linearized with HindIII and transcribed with T7 Polymerase.

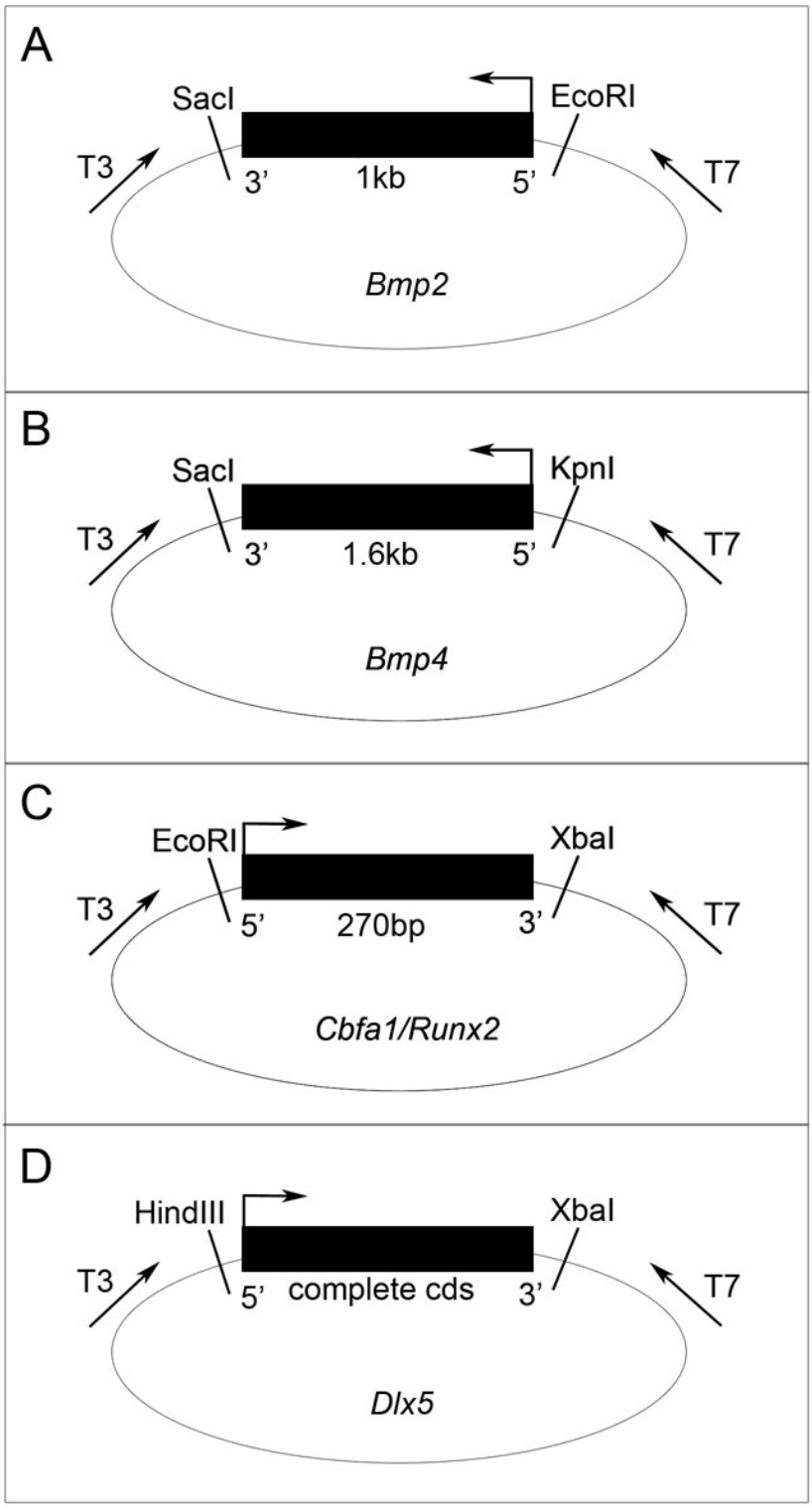
A
SacI
EcoRI
T3
3'
1kb
5'
T7
Bmp2
B
SacI
KpnI
T3
3'
1.6kb
5'
T7
Bmp4
C
EcoRI
XbaI
T3
5'
270bp
3'
T7
Cbfa1/Runx2
D
HindIII
XbaI
T3
5'
complete cds
3'
T7
Dlx5

Figure 12. *Msx1*, *Msx2*, and *Spp1* constructs for *in situ* hybridization probe synthesis

(A) ~900bp of mouse *Msx1* cDNA was cloned into the multiple cloning site of pBluescriptSK(-), retaining SacI and EcoRI RE sites. To generate an antisense probe, this construct was linearized with SacI and transcribed with T7 RNA Polymerase.

(B) Exon 1 of mouse *Msx2* cDNA was cloned into the EcoRI and SalI sites via PCR of WMVΦ2, retaining both RE sites. EcoRI was used to linearize the construct, and T7 RNA Polymerase was used to transcribe antisense probe.

(C) ~1kb of mouse *Spp1* cDNA was cloned into the HindIII site of pGEM-1, retaining an EcoRI site. To generate antisense probe, the construct was linearized with EcoRI and transcribed with SP6 Polymerase.

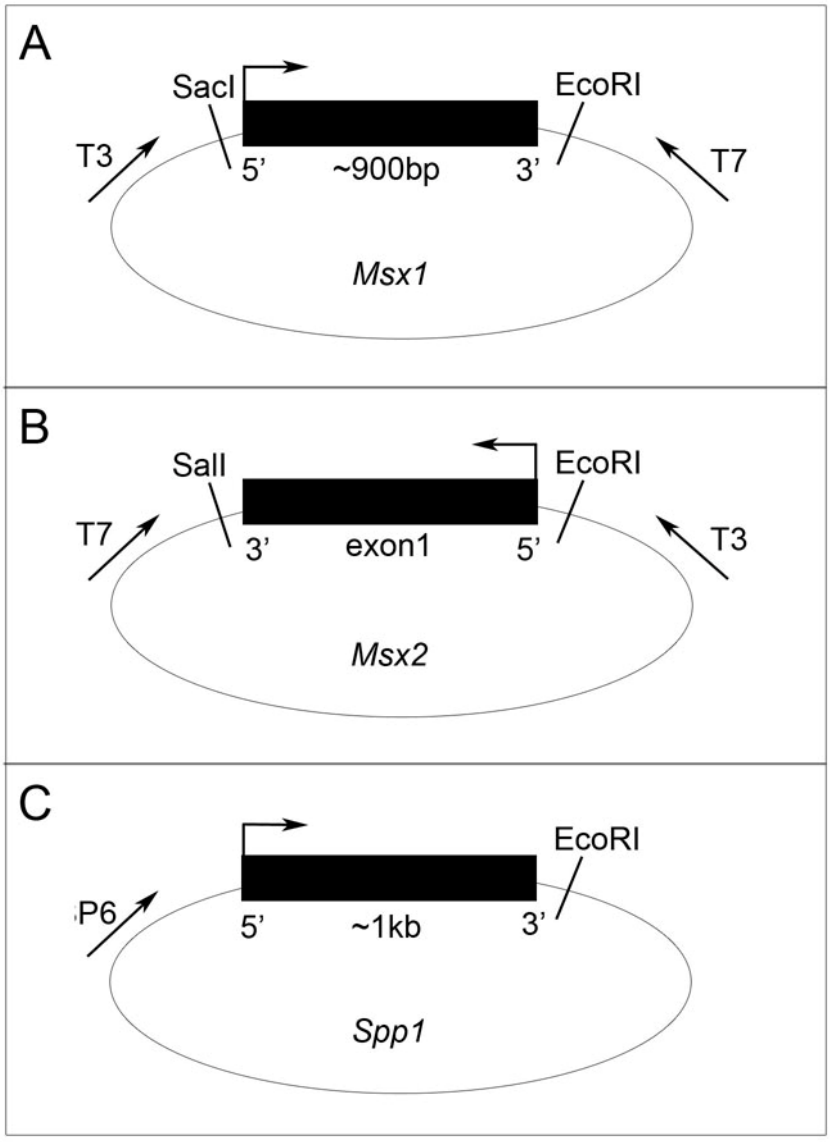
A
SacI
EcoRI
T3
T7
5'
~900bp
3'
Msx1
B
SalI
EcoRI
T7
T3
3'
exon1
5'
Msx2
C
EcoRI
P6
5'
~1kb
3'
Spp1

2.5 von Kossa staining

As an assay for calvarial bone development, von Kossa staining was performed on 7μm-thick sagittal paraffin-embedded sections through the sagittal suture, to detect Ca^{2+} deposits in the parietal bones. Sectioning and von Kossa staining was performed on these sections by the Histology Core Facility at the Stowers Institute for Medical Research using the following protocol. Paraffin sections were deparaffinized and hydrated in distilled water before being placed in a 5% silver nitrate solution and exposed to bright sunlight for 10-20 minutes. Once the calcium salts had generated the desired color (brown-black), the reaction was stopped. The slide-mounted sections were then rinsed with distilled water and placed into a 5% sodium thiosulfate solution for 2-3 minutes. Next, they were rinsed with distilled water and counterstained in nuclear fast-red for 5 minutes. After another rinse with distilled water, the sections underwent dehydration and clearing steps that involved two changes of 95% alcohol, absolute alcohol, and xylene. They were then mounted with a synthetic resin at the end of the procedure.

2.6 *In ovo* electroporations

Eggs containing chicken embryos were incubated at 37ºC until reaching 6-10 somites stages (Hamburger Hamilton stages 8-10). The eggshells were wiped with Ethanol prior to opening to prevent bacterial contamination, clear tape placed over the top, and 3-4ml of albumin were withdrawn from each egg. An oval-shaped window was cut into the top of the eggshell, exposing the underlying chicken embryo. India ink was injected underneath the Area Pellucida, allowing easier visualization of the

developing somites in order to accurately stage the embryos by somite number. For neural tube injections, if necessary, the closed neural tube was perforated once at the level of the hindbrain (where DNA injection will occur) and again at the forebrain to allow the DNA to completely fill this portion of the neural tube. The DNA construct(s) mixed with Fast Green dye for visualization were then injected into the neural tube at the level of the hindbrain by mouth pipet, filling the neural lumen up to the forebrain. Electrodes were immersed in Hank's buffered solution prior to electroporation, and the positive and negative leads were positioned on either side of the embryo parallel to the anteroposterior axis at the level of the developing head, 4mm apart, making contact with the blastoderm. Five pulses of 20V, each 50ms in length were applied. The injected DNA was thus transferred to the side of the positive electrode and incorporated solely into the hindbrain on the same side. The electrodes were then cleaned by rinsing and brushing in Hank's buffered solution before the next use. A second piece of clear tape was applied over the oval window, and the embryos were cultured *in ovo* for 24 hours before being harvested for gene expression analysis by *LacZ*- or *GFP*-reporter expression. Embryos were carefully dissected away from all of the surrounding membranes prior to reporter analysis. Those embryos co-electroporated with *GFP*-containing reporters were imaged immediately following dissection, since the *GFP* signal decreases significantly over time.

2.7 Staining method for β-galactosidase assay using X-gal

2.7.1 Solutions

Fixative: All made in PBS : 1% Formaldehyde, 0.2% Glutaraldehyde, 2mM $MgCl_2$, 5mM EGTA, and 0.02% Nonidet P40 (NP40). Store at 4ºC.

Stain Solution: 5mM $K_3Fe(CN)_6$, 5mM $K_4Fe(CN)_63H_2O$, 2mM $MgCl_2$, 0.01% Sodium deoxycholate, and 0.02% NP40. Store in the dark at 4ºC.

Stock substrate: 40mg/ml Xgal dissolved in dimethyl formamide (DMF). Store in the dark at 4ºC.

Working stain solution: Add 1ml of X-gal stock to 39ml of stain solution. Store in the dark at 4ºC.

2.7.2 Method

Chicken embryos that had undergone *in ovo* electroporations with various *LacZ*-containing constructs were harvested after a 24-hour culture at 37ºC, and all surrounding membranes were carefully removed. Embryos were washed in PBS at room temperature and fixed in cold fixative for 30-90 minutes at 4ºC, depending on the stage. Then the embryos were washed three times in wash solution (20 minutes each) at room temperature. The wash solution was replaced with working stain solution, and the embryos remained in this solution in the dark for up to 36 hours. Once the staining was complete, the embryos were thoroughly rinsed in PBS and stored in PBS/0.01% Sodium azide at 4ºC.

Chapter 3

The role of *Hoxb1* during the development of the axial vertebrae

3.1 Formation of the skeleton

The bones of the vertebrate skeleton are derived from mesenchyme that arises from one of two sources: 1. mesoderm, leading to the bone formation in the limbs, trunk, and part of the head, or 2. neural crest cells, resulting in bone formation in the face and branchial arch region. These skeletal elements become components of either the axial or appendicular skeleton. The axial skeleton includes the bones of the head, vertebral column, and the ribs, while the appendicular skeleton is comprised of the bones of the limbs as well as the limb girdles. Osteogenesis occurs by one of two major pathways: intramembranous or endochondral ossification. Intramembranous ossification proceeds directly from mesenchymal cell condensations to form bone. This type of bone formation primarily gives rise to many of the flat bones of the skull. Neural crest-derived mesenchymal cells condense near or around blood vessels and differentiate into osteoblasts, which secrete an osteoid matrix rich in Type I Collagen and proteoglycans. Those osteoblasts that become embedded in this matrix are called osteocytes. In order for osteocytes to maintain communication with each other and to obtain oxygen and other nutrients from the capillaries, they form a network of cellular processes (trabeculae). As calcification proceeds, trabeculae interconnect to form a spongy meshwork. The cells surrounding the developing bone spicules form the periosteum, becoming osteoblasts that continue to secrete bone matrix and increase the size of the compact bone. During the process of endochondral ossification, the

mesenchyme initially forms a cartilaginous model that is replaced later in development by bone. This type of bone formation contributes to much of the growth of the vertebral skeleton that is derived from segmented blocks of mesodermal tissue known as somites.

3.2 Vertebral development

During somite development, ventromedial epithelial cells transform into a mesenchymal population of cells called the sclerotome. Those cells in the cranial portion of the somite are loosely packed, while those in the caudal part are more condensed. Prior to the formation of prevertebrae and during a process known as somitic resegmentation, cells from the posterior half of one somite mix with those from the anterior half of the next caudal somite to form a condensation of precartilaginous mesenchyme that makes up the primordium of the vertebral body. The paired lateral sclerotome condensations migrate out dorsally and laterally to form the precartilaginous primordia of the neural arches and, where appropriate, the ribs. Both sets of prechondrogenic cell populations then differentiate into chondroblasts, are activated, and begin to proliferate. This increase in cell number leads to growth of the developing cartilage. During the next stage (chondrocyte maturation), the cells stop dividing and start secreting a cartilaginous matrix. In early chondrogenesis, the chondroblasts are associated with high amounts of hyaluronic acid, which promotes the migration and proliferation of these cells, and small amounts of Type I Collagen. Those cells that become trapped in the matrix are called chondrocytes. A change in both the composition and amount of extracellular matrix present signals the transition

from the second stage to the third stage: chondrocyte hypertrophy. At this stage, cells switch from producing Type I Collagen to a cartilage-specific Type X Collagen, a marker of chondrogenic maturation. During this period of growth of the cartilage model, the perichondrium (a mesenchymal cell condensation surrounding the developing cartilage) begins producing osteoprogenitors. The newly-formed osteoprogenitors begin to produce an osteoid matrix around the cartilage model. The cartilage cells then secrete alkaline phosphatase, and the cartilaginous matrix undergoes calcification. This calcified matrix inhibits nutrient diffusion throughout the model, contributing to chondrocyte death. As the matrix breaks down, osteoprogenitors from the periosteum invade and contact the calcified matrix, initiating their differentiation into osteoblasts. The matrix is then removed and replaced by osteoid deposits. Developing bony spicules are further remodeled by osteocytes, which are multinucleated cells that specialize in localized bone removal.

The mouse axial skeleton is divided into morphologically-distinct regions, consisting of cervical, thoracic, lumbar, sacral, and caudal segments. The developmental programs specifying each segment are established early in the presomitic mesoderm and are maintained in the resegmented somites that give rise to prevertebral precursors. It is worth noting here that the first four somites that arise from the PSM do not contribute to the axial skeleton through the formation of prevertebral segments. These occipital somites give rise to the three mesenchymal condensations (basioccipital, exoccipital, and supraoccipital) that will undergo intramembranous ossification to form the occipital bone in the adult mouse skull.

The remaining somites (cervical, thoracic, lumbar, etc.) undergo resegmentation into prevertebrae, each of which will contribute to a single vertebra.

Among vertebrate species, the numbers of vertebrae contained within each of these regions vary greatly. Within the mouse, the arrangement of vertebrae follows this vertebral formula: seven cervical, thirteen thoracic, six lumbar, four sacral, and a variable number of caudal segments (C7/T13/L6/S4). Each region can be readily identified by characteristics unique to the vertebral bodies. Additionally, individual vertebrae often contain skeletal elements that set them apart from others found within the same morphologically-distinct region. However, all vertebrae contain a body and a neural arch that encompasses the vertebral foramen. Each neural arch contains a pedicle, two lateral processes that fuse to form the spinous process, and two transverse processes. To facilitate articulation with adjacent vertebrae, the neural arch possesses both superior and inferior articular processes. Since the present study mainly addresses homeotic transformations within the cervical and thoracic vertebrae, the following section will provide a detailed description of the skeletal elements contained within these regions.

Seven cervical vertebrae form the support of the neck. Generally, the cervical vertebrae differ from remaining vertebrae by their small bodies and small, bifid spinous processes; the exception is the seventh cervical vertebra, whose spinous process is long and non-bifid. The atlas (cervical vertebrae 1, C1) articulates with the skull, specifically, the occipital bone, at the atlantoccipital joint, allowing nodding and lateral flexion movements to occur. C1 anatomy reveals several unique

characteristics that distinguish this vertebra from the rest of the cervical vertebrae. C1 is ring-shaped, has no body or spinous process, and has a short anterior arch and long posterior arch. The anterior arch of the atlas (aaa) is ventrally-located and articulates with the dens of the axis to form a pivot-type synovial joint, allowing skull rotation at the atlantoaxial joint. C1 is the widest cervical vertebrae with two lateral masses that give rise to the superior and inferior articular facets. The superior articular facet is elongated and faces inward and upward to support the occipital condyles on each side, forming an ellipsoid-type of synovial joint that allows vertical movement of the skull. The inferior facet is flatter and more circular, facing downward and inward to articulate with C2 articular surfaces. The neural arch of C1 is broad and continues to widen dorsally. The transverse processes of C1 contain foramen transversarium (or vertebrarterial (VA) canals) through which the vertebral artery ascends upward and laterally before turning medially and posteriorly to pass behind the superior articular lateral process. This artery usually enters at the level of C6; however, it has been found to enter at the 7^{th} or 5^{th} cervical vertebrae, a variation that is not necessarily bilateral. The axis (C2) contains a ventral bony protrusion (dens or odontoid process) that extends cranially, on which the posterior aspect of the aaa articulates and allows lateral rotation of the skull about the neck. The aaa surrounds the dens ventrally, and the transverse ligament of C1 surrounds the dorsal aspect of the dens. The body of C2 contains a large upward- and outward-facing facet that articulates with the inferior surface of the C1 lateral mass. Similarly, the inferior surface of the C2 lateral mass contains a facet that articulates with the

superior articular process of C3. The neural arch of C2 is also broadened, but not to the extent of that of C1, representing an intermediate width between the neural arches of C1 and the remaining cervical vertebrae. C3 through C5 are nearly identical, which makes identifying defects within these vertebrae very difficult. They each contain VA canals on the ventral part of the vertebral body. C6 also contains VA canals, as well as unique ventrally-located anterior tuberculi. C7 is the last cervical vertebrae and represents the start of the cervicothoracic junction: a transitional region at which the spinal canal decreases to the size of the thoracic spine. This transition can be easily appreciated upon observation of the cross-sectional area of the cervical spinal canal: this area is largest at the level of C2 and smallest at C7. Similarly, aspects of C7 begin to resemble those of the thoracic vertebrae. For example, C7 typically lacks VA canals, although, rarely, VA canals can be present on C7. The inferior articular process of C7 forms a facet joint with T1 that shows greater resemblance to those of the thoracic region than the cervical region. Although rare, the costal component of the large C7 transverse process may develop into a cervical rib.

The thirteen thoracic vertebrae each contain a pair of ventrolateral-projecting ribs that form as extensions of each vertebra's transverse process. The first seven pairs form sternocostal junctions with a ventromedially-located sternum. T1 rib pairs join immediately anterior to the manubrium. T2 ribs meet the sternum between the manubrium and the first sternal band. Another prominent feature of T2 is its dorsal spinous process, which helps to distinguish this vertebra from the remaining thoracic

vertebrae. T3, T4, and T5 rib pairs form junctions with the sternum immediately posterior to the first, second, and third sternebrae, respectively. The ribs from T6 and T7 join the sternum together between the fourth sternebra and the xiphoid process. Rib pairs derived from T8 through T13 represent "false ribs," since they do not connect to the sternum. Instead, T8-T11 ribs form cartilaginous connections to the ribs immediately anterior to each of them. T12 and T13 ribs are also termed "floating ribs" as they form no connections to the adjacent rib pairs. Interestingly, these elements of the thoracic skeleton (vertebrae plus ribs and sternum) arise from different embryologic origins. The vertebrae and ribs are derived from somitic mesoderm, while the sternum is derived from lateral plate mesoderm. Due to the fact that the sternum and ribs are derived from different embryological origins, the developmental program of each is initially independently controlled.

Beginning at 12dpc in the mouse, stage I of sternal development is initiated as condensations of the lateral plate mesoderm appear posterior to the clavicle and anterior to the developing T1 ribs (reviewed in (Ramirez-Solis et al., 1993)). By stage II, or 13dpc, these chondrogenic condensations have begun to differentiate into procartilage and elongate both caudally and ventromedially. The paired condensations are then joined at the end of stage II. Half a day later, stage III is achieved as the ribs contact the developing sternum. Stage IV of sternal development begins with fusion across the midline of the paired procartilaginous condensations at their anterior ends. Once fusion between these condensations has occurred, the procartilage then differentiates into cartilage at the point of fusion. In this way,

differentiation of the sternal precursors into cartilage proceeds through the remaining stages of development in a rostral-to-caudal manner. Ossification of the cartilage is inhibited where the ribs contact the sternal rudiments, such that ossified sternebrae are separated by cartilaginous sternocostal junctions formed by joining the costal cartilages of the ribs to the sternum. Once formed, the sternum contains an anterior manubrium, four sternebrae or sternal bands, and a posterior xiphoid process.

3.3 Skeletal phenotypes resulting from loss-of-function studies within targeted individual *Hox* mutants

3.3.1 Wild-type skeletal variations

Previous work in the Krumlauf lab generated data suggesting that variations in wild-type skeletal development are due to differences in genetic background (see Appendix). Briefly, the degree to which individual calvaria of 18.5dpc mice had undergone ossification varied greatly among 129s6/SVEV, CD1, CBA, C57bl/6, and F1 (CBA;C57bl/10) wild-type strains. The parietal bones of 129s6/SVEV mice showed the least amount of ossification, while these same bones in CD1 mice had the most ossification, resulting in skulls that appeared the most similar to what is expected in wild-type skulls by 18.5dpc. Since all of our mutant lines were initially propagated in the purebred 129s6/SVEV background strain, this observation led us to focus our current study on mice maintained in a mixed 129s6/SVEV;CD1 background in an attempt to generate skeletons that most-closely recapitulated the CD1 developmental program.

To further investigate the hypothesis that genetic background plays a role in skeletal development, we observed several strains of wild-type mice for natural vertebral variations at 18.5dpc. The anatomy of wild-type mouse skeletons was described in the previous section. The majority of animals follow the typical 7 cervical, 13 thoracic, 6 lumbar, 4 sacral axial vertebrae formula (7C, 13T, 6L, 4S) with a variable number of caudal segments. However, a number of variations can be found in the individual vertebrae of wild-type animals. The following is a description of the wild-type variations discovered in 142 mice among several purebred and mixed genetic backgrounds, including 129s6/SVEV; CD1, 129s6/SVEV, CBA, CD1, C57bl/6, and F1 (C57bl/10; CBA). A table containing the numbers of variations observed in all backgrounds, along with their relative frequencies, can be found in the Appendix.

The anterior-most variation was found at the craniocervical junction. One of 30 CD1 embryos was found with a fusion of the aaa to the BOB. This variation occurred with a frequency of <1% within the entire wild-type population. Changes in C2 morphology have been characterized as either narrowing or splitting of the dorsal aspect of the neural arch. Six of 81 129s6/SVEV;CD1 mice (7%) and 4 of 30 CD1 mice (13%) possessed this axis variation; all cases were unilateral, affecting a total of 10 mice (7%). The unilateral absence of a C3 VA canal occurred in one of 8 mice (13%) within the C57bl/6 population, representing <1% of the total wild-type population. Another common variation is the presence of rib anlagen on C7 (Figure 13), which range from small (nearly pin-point) to large (extensive) and may be found

Figure 13. Ectopic C7 rib anlagen in various wild-type backgrounds

(A) Seventh cervical vertebra as it is present in the majority of wild-type animals (129s6/SvEv;CD1, 129s6/SvEv, CD1, F1 (CBA x C57bl/10), CBA, and C57bl/6), without cervical rib heads.

(B) C7 with bilateral rib anlagen (asterisks) observed in the same wild-type strains.

(C) Graph depicting the frequency of unilateral or bilateral C7 rib anlagen in 129s6/SvEv;CD1 (n=81), 129s6/SvEv (n=6), CD1 (n=30), F1 (n=9), CBA (n=8), and C57bl/6 (n=8) backgrounds.

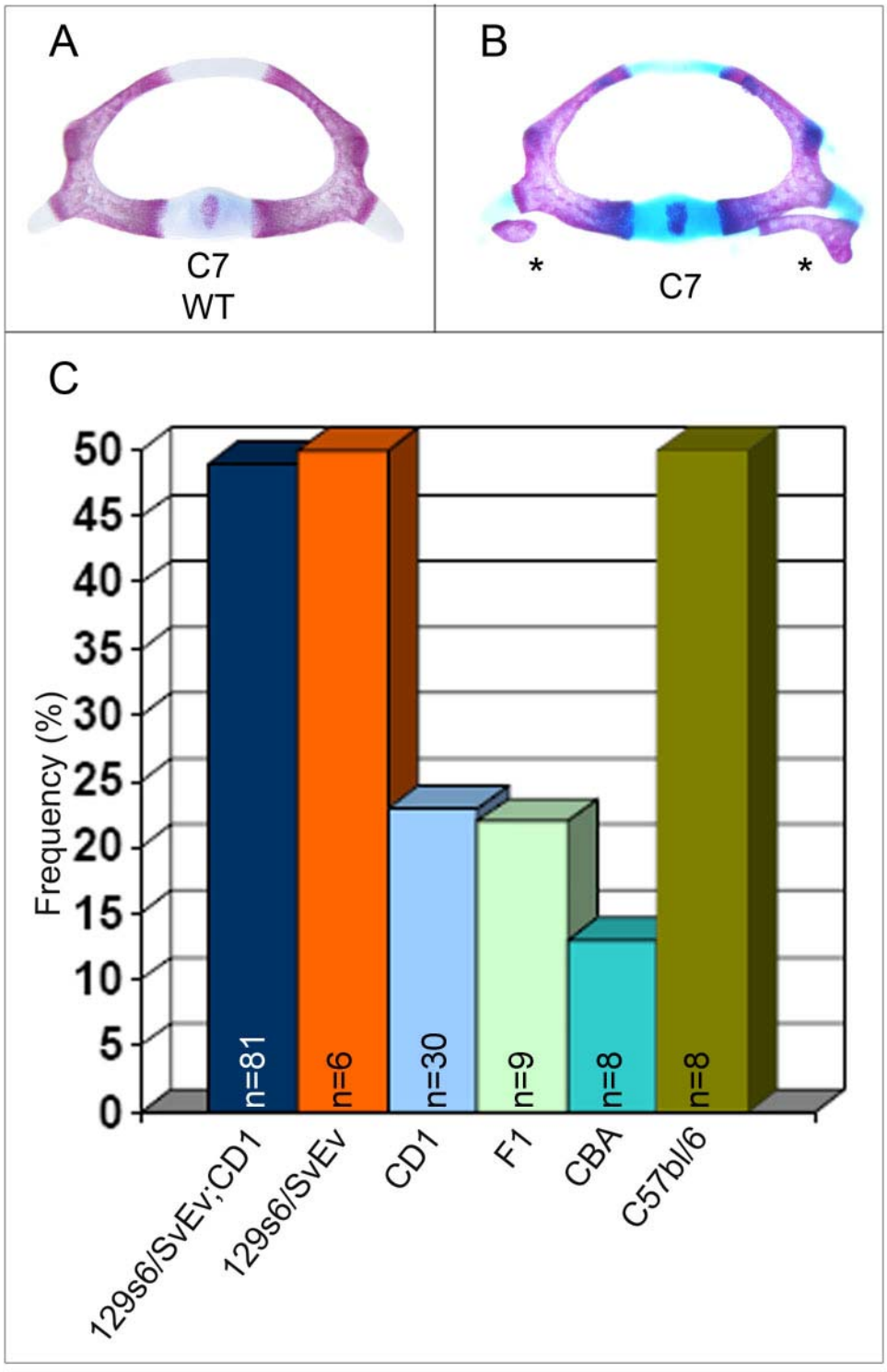
A
C7
WT
B
*
C7
*
C
Frequency (%)
50
45
40
35
30
25
20
15
10
5
0
n=81
n=6
n=30
n=9
n=8
n=8
129s6/SvEv;CD1
129s6/SvEv
CD1
F1
CBA
C57bl/6

within the total population unilaterally (21%), bilaterally (19%), or unilaterally fused to T1 ribs (<1%). This variation was present within all genetic backgrounds observed. A single T1 rib was observed fused to C7 rib anlagen unilaterally in 1 of 30 129s6/SvEv;CD1 mice, representing less than 1% of the total wild-type population. The ribs emanating from T8 normally form cartilaginous connections to the ribs immediately anterior (those of T7). Within the 129s6/SVEV;CD1 (15%), CD1 (40%), and F1 (11%) populations, unilateral or bilateral articulations of T8 ribs were found at the sternum posterior to the 7th set of thoracic ribs and anterior to the xiphoid process, resulting in 8 SCJs, instead of 7. Interestingly, only two CD1 mice were found to have an extra sternal band as a result, affecting 1% of the total population. Finally, ribs on the first lumbar vertebra (L1) were found either unilaterally or bilaterally only within the 129s6/SVEV;CD1 (12%) and CD1 (40%) backgrounds. Since these observations represent variations within wild-type populations, it was not surprising that similar alterations were seen in *Hox* mutant skeletons in the following study. The comparison of wild-type variability among 129s6/SvEv;CD1, CD1, and *Hox* mutants maintained in a 129s6/SvEv;CD1 mixed genetic background will be addressed later in this chapter.

3.3.2 Analysis of skeletal defects in single *Hox* mutants

The majority of phenotypes described in these studies represent anterior homeotic transformations of vertebrae, such that individual vertebrae take on characteristics of the vertebra immediately anterior. Interestingly, posterior homeotic transformations, in which vertebrae assume a more posterior identity, were rarely

observed in this study. The following description details the observations used to identify these homeotic transformations.

As previously stated, the aaa is characteristic of C1. Thus, the ectopic presence of this element on C2, with or without widening of the C2 neural arch, represents a C2→C1 anterior homeotic transformation. Since C6 possesses a unique characteristic (ventrally-located AT), a C6→C5 transformation is defined by the absence of these tuberculi on C6; instead, C6 takes on the appearance of C5. This is observed either unilaterally or bilaterally. A C7→C6 transformation often accompanies C6→C5 transformations. The wild-type C7 vertebra differs significantly from the rest of the cervical vertebrae. It lacks the ventral VA canals common to C3-C6, as well as the AT found on C6. In a C7→C6 transformation, one or both of these features are found either unilaterally or bilaterally. The presence of both ectopic AT and VA canals on C7 is called a complete transformation, while ectopic C7 VA canals alone represents a partial transformation. In rare instances, the C7→C6 transformation occurs independently of the C6→C5 transformation. In these cases, the AT present on C6 and C7 are found to be fused.

In the thoracic region, transformations of T1 and T2 are identified by a range of phenotypes. Rarely, T1 rib length is reduced; these ribs fail to connect to the sternum. Additionally, T2 ribs form their sternocostal junctions (SCJ) at the manubrium, which is the point of contact between wild-type T1 ribs and the sternum. Alternatively, the cartilaginous portions of the developing T1 and T2 ribs may fuse one or more times before making contact with the sternum. Taken together, these

three possibilities comprise the criteria for determining a T2→T1 transformation. Defects in the sternum included both a "crankshaft" appearance and partial or complete bifurcation. A "crankshaft" sternum is characterized by abnormal ossification of the sternal bands, such that one half of the sternal band fails to align with the other half. As a result, the costal cartilages insert into the sternum at different levels on each side. Sternal bifurcation may occur in the rostral or caudal portions of the sternum (partial) or extend along its entire length (complete).

The frequency of variations observed in wild-type populations was also recorded for each *Hox* mutant line. The majority of these variations were previously identified as *Hox* mutant phenotypes in previous studies (Studer et al., 1998). This work will show that, within *Hoxa1*, *Hoxb1*, and *Hoxb2* single and compound mutants, many of these vertebral variations do not occur with significantly increased frequencies compared to wild-type animals. Thus, they do not represent *Hoxa1*, *Hoxb1*, or *Hoxb2* mutant homeotic transformations. However, where appropriate, a statistically significant increase in phenotypic penetrance is noted. Phenotypes that were unique to each mutant strain will be presented alone, while those that were observed in multiple mutant strains will be shown together.

***Hoxa1* mutants**

Since *Hoxa1* lies upstream of *Hoxb1* in a regulatory network patterning the hindbrain (Lufkin et al., 1991), we decided to investigate whether the same interaction between these two genes operates in the paraxial mesoderm to pattern the axial skeleton by comparing *Hoxa1* and *Hoxb1* mutant phenotypes. For this reason,

Figure 14. *Hoxa1* mutant skeletal analysis

(A) Schematic representations of the endogenous and targeted *Hoxa1* alleles. The *neomycin* selectable marker replaced a 5' portion of the locus containing the promoter, transcriptional start site, translational initiation site, and the first 88 amino acids. A stop codon at the end of the *neomycin* cassette prevented further transcription of the *Hoxa1* transcript.

(B) Fifth cervical vertebra in wild-type 129s6/SvEv;CD1 mice at 18.5dpc.

(C) The presence of a unilateral ectopic anterior tuberculum on the left side (asterisk) of a $Hoxa1^{+/-}$ mutant's C5 vertebra.

(D) Sixth cervical vertebra in wild-type 129s6/SvEv;CD1 mice with its unique bilateral anterior tuberculi.

(E) Graph depicting the frequency of the C5→C6 transformation in *Hoxa1* heterozygotes (not statistically significant).

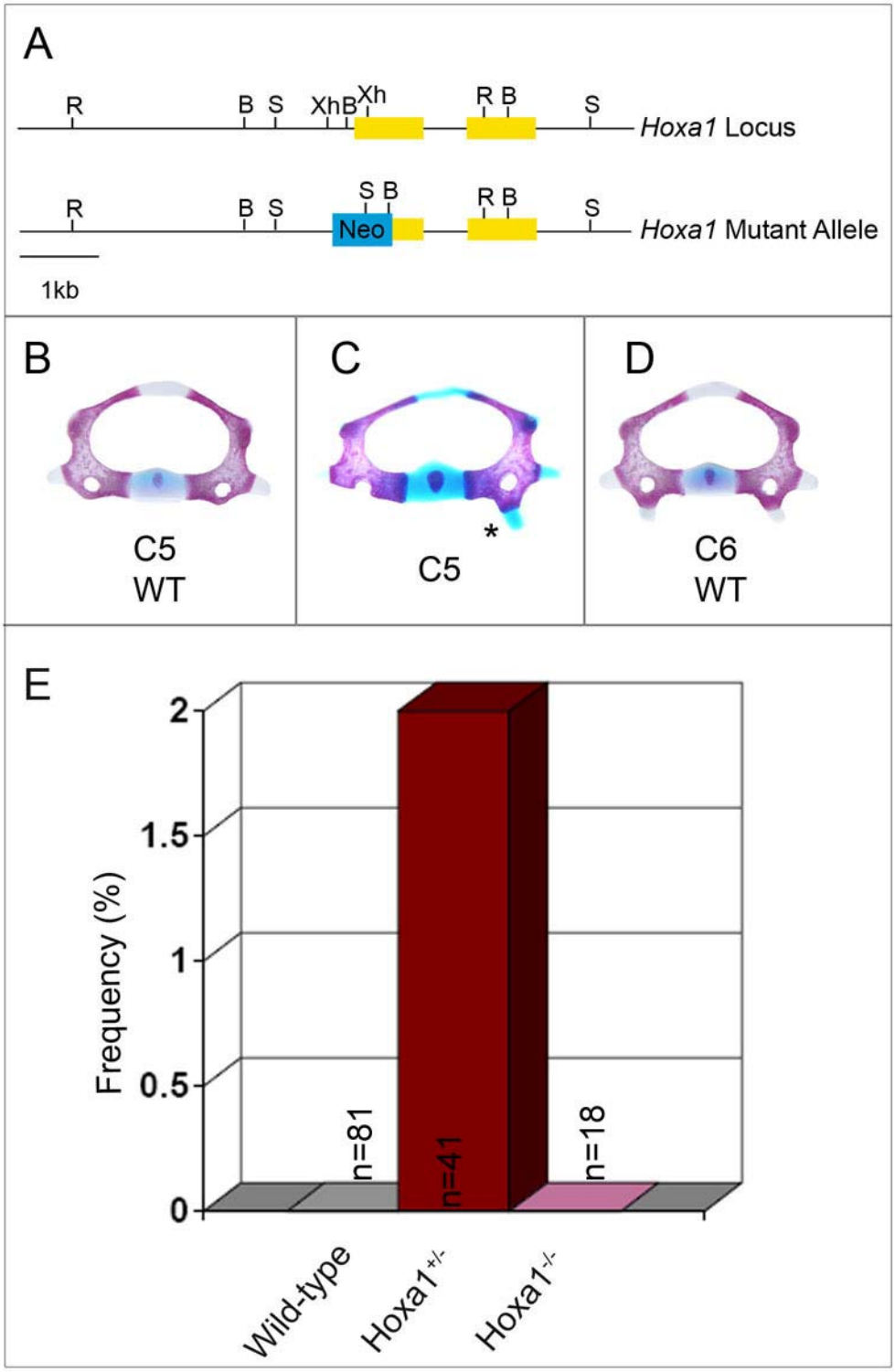
A
R
B S
XhB
Xh
R B
S
Hoxa1 Locus
R
B S
S B
Neo
R B
S
Hoxa1 Mutant Allele
1kb
B
C5
WT
C
C5
*
D
C6
WT
E
Frequency (%)
2
1.5
1
0.5
0
n=81
n=41
n=18
Wild-type
Hoxa1+/-
Hoxa1-/-

skeletal preparations were performed on *Hoxa1* heterozygous (n = 41) and homozygous (n = 18) embryos at 18.5dpc and analyzed for homeotic transformations. The *Hoxa1* mutant line came from Lufkin *et al*., in which the upstream region including the proximal promoter, transcriptional start site, translation initiation site, and the first 88 amino acids were replaced upon insertion of the *neomycin* gene into this region followed by a stop codon (Figure 14A; (Chisaka et al., 1992; Lufkin et al., 1991)). A table containing the numbers of variations observed in all mutants, along with their relative frequencies, can be found in Appendix C.

The majority of phenotypes identified in both *Hoxa1* heterozygotes and homozygotes represent variations that occur in wild-type populations. The exceptions are unilateral C5→C6 (Figure 14B) and C6→C5 (Figure 17) transformations found in one heterozygous embryo (2%). However, this phenotype was not found to be statistically significant. These two homeotic transformations, although rare, were previously unreported (Murphy and Hill, 1991).

***Hoxb1* mutants**

Previous studies in our lab of the *Hoxb1* mutant line (MB3A) have demonstrated clear phenotypes of the axial skeleton, including homeotic transformations of the cervical vertebrae and sternal defects (unpublished data). Since *Hoxb1* mRNA transcripts are readily detected in the PSM that gives rise to the somite-derived vertebrae (Studer et al., 1996), it is likely that these defects are a result of changes in *Hoxb1* gene expression in the PSM. The present study aims to further characterize these mutant phenotypes.

Two independent mutations were targeted via homologous recombination into the *Hoxb1* gene locus to eliminate Hoxb1 protein function (Barrow and Capecchi, 1996). The first replacement allele contained a *LacZ* gene and *neomycin* selectable marker (*LacZ*/*neo* fusion) inserted in-frame into the first exon, and the second allele had a frameshift mutation at the *SstI* site in the homeobox. Both constructs were targeted into AB2.2 embryonic stem cells, and positive clones were injected into C57Bl/6 blastocysts. The resulting mutants were crossed into a 129/Sv background strain and analyzed in a mixed 129/Sv and C57Bl/6 genetic background. Ninety-eight percent of *Hoxb1* homozygous mutants targeted with either the *LacZ*/*neo* fusion or the homeobox frameshift mutation died within 24 hours of birth. As stated previously, loss of Hoxb1 function by these targeting methods alters the migrating motor neurons of the facial (VIIth) nerve. The facial muscles of these mice are inappropriately innervated, and the cause of death is likely due to an inability to suckle after birth. Following these experiments, mutants containing the *LacZ*/*neo* fusion were used to propagate a *Hoxb1* mutant line maintained in a purebred 129s6/SvEv genetic background (Figure 15A). However, due to decreased fecundity, low progeny number, and observations of developmental delay (see Appendix B), this line was bred into the CD1 background to facilitate homozygous mutant analysis. The following section is a description of the skeletal phenotypes characterized in *Hoxb1* mutant mice that were maintained in a mixed 129s6/SvEv and CD1 genetic background.

Figure 15. *Hoxb1* and *Hoxb2* targeting strategies

(A) and (B) Schematic representations of the endogenous and targeted *Hoxb1* and *Hoxb2* alleles. A *LacZ*/*neomycin* fusion was inserted in-frame into the first coding exon of *Hoxb1* (A) and *Hoxb2* (B), resulting in non-functional transcripts for each gene.

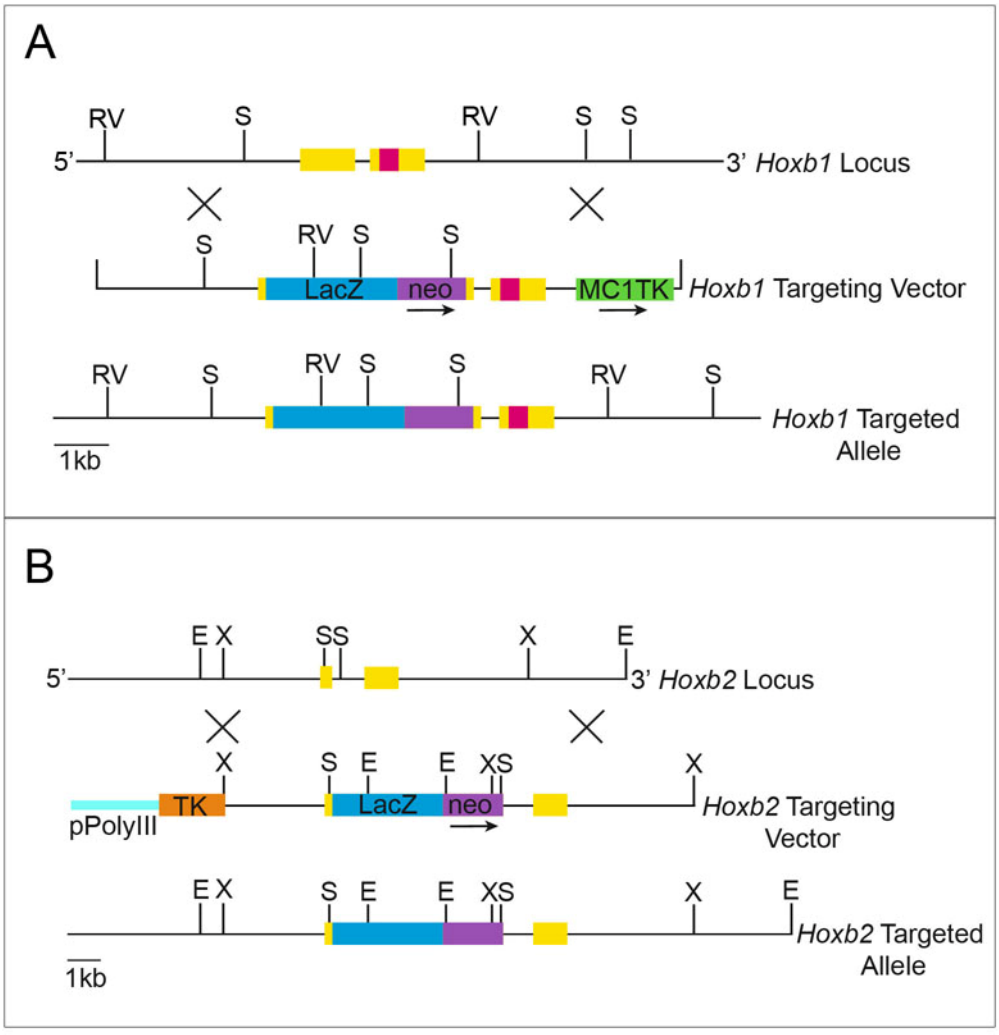
A
RV
S
RV
S
S
5'
3' Hoxb1 Locus
S
RV
S
S
LacZ
neo
MC1TK
Hoxb1 Targeting Vector
RV
S
RV
S
S
RV
S
Hoxb1 Targeted Allele
1kb
B
E
X
S
S
X
E
5'
3' Hoxb2 Locus
X
S
E
E
X
S
X
TK
pPolyIII
LacZ
neo
Hoxb2 Targeting Vector
E
X
S
E
E
X
S
X
E
Hoxb2 Targeted Allele
1kb

Within the cervical vertebrae, both *Hoxb1* heterozygotes and homozygotes possess the following anterior homeotic transformations with various degrees of penetrance: C2→C1, C6→C5, and C7→C6. The C2→C1 transition is evident by the presence of an ectopic aaa on the ventral side of C2 (Figure 16). Occasionally, the C2 dorsal neural arch is expanded in width to resemble that of C1. Although the C2→C1 transformation was found in both *Hoxb1* heterozygotes and homozygotes, the penetrance was significantly increased only in $Hoxb1^{-/-}$ mice ($Hoxb1^{+/-}$: 3%; $Hoxb1^{-/-}$: 24%). The AT present ventrally on wild-type C6 are often absent from *Hoxb1* mutants, with homozygotes being more severely affected than heterozygotes ($Hoxb1^{+/-}$: 6%; $Hoxb1^{-/-}$: 59%; Figure 17). In these cases, the tuberculi are instead found on C7, along with VA canals, indicating a full homeotic transition of C7 into C6 ($Hoxb1^{+/-}$: 6%; $Hoxb1^{-/-}$: 69%; Figure 18). Rarely, AT were observed on both C6 and C7 and were found to be fused, representing an additional aspect of the C7→C6 anterior transformation. Though a single $Hoxb1^{+/-}$ mouse (1%) demonstrated this phenotype, a statistically significant increase over wild-type animals was only observed in $Hoxb1^{-/-}$ mice (14%).

Skeletal defects were also observed in the anterior thoracic ribs. Specifically, T1 ribs were present in some animals only as primordial structures ($Hoxb1^{+/-}$: 1%; $Hoxb1^{-/-}$: 14%), suggesting a partial anteriorization of T1 to a C7 identity (Figure 19). As a result of T1→C7 transformations, some mice possessed ectopic T2 rib SCJs present at the wild-type T1 rib SCJ, the manubrium ($Hoxb1^{+/-}$: 1%; $Hoxb1^{-/-}$: 7%). Alternatively, the ribs extending from T1 and T2 could be found fused one or more

Figure 16. Anterior transformation of C2 into a C1-like identity in *Hox* loss-of-function mutants

(A) Wild-type C1 and C2 vertebrae in the 129s6/SvEv;CD1 genetic background at 18.5dpc. An anterior arch of the atlas is present on the ventral aspect of C1.

(B) C2→C1 homeosis: the presence of an ectopic C1-like anterior arch on the ventral aspect of C2 (asterisk).

(C) Graph depicting the frequency of the C2→C1 transformation in loss-of-function mutants: *Hoxb1*$^{+/-}$, *Hoxb2*$^{+/-}$, *Hoxb2*$^{-/-}$, and *Hoxb1*$^{+/-}$;*Hoxb2*$^{+/-}$ phenotypes are not statistically significant; *Hoxb1*$^{-/-}$ phenotypes do represent a statistically significant increase with respect to wild-type (asterisk) and *Hoxb1*$^{+/-}$ mutants (double asterisk).

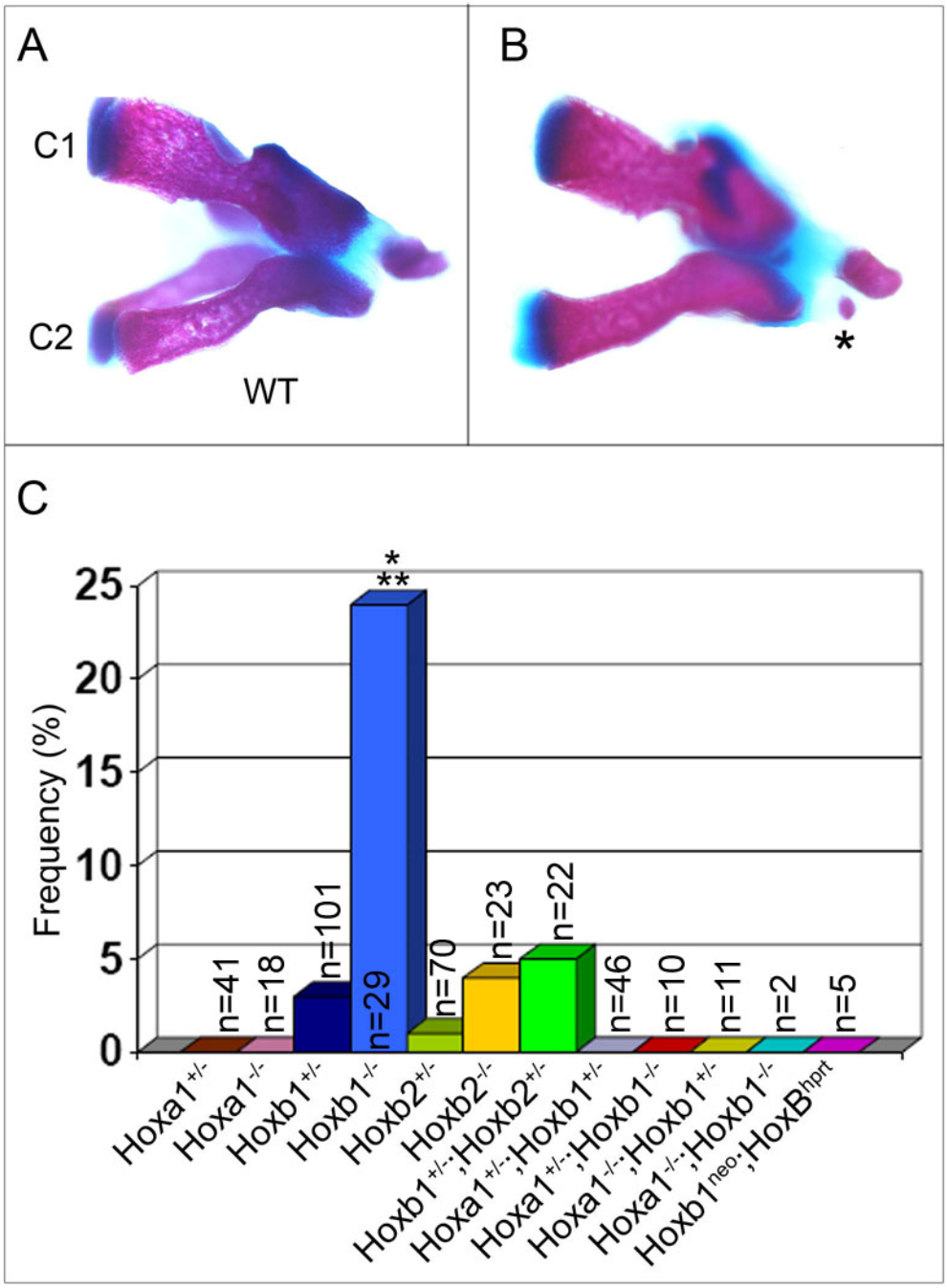
A
C1
C2
WT
B
*
C
Frequency (%)
25
20
15
10
5
0
n=41
n=18
n=101
n=29
n=70
n=23
n=22
n=46
n=10
n=11
n=2
n=5
*
**
Hoxa1+/-
Hoxa1-/-
Hoxb1+/-
Hoxb1-/-
Hoxb2+/-
Hoxb2-/-
Hoxb1+/-;Hoxb2+/-
Hoxa1+/-;Hoxb1+/-
Hoxa1+/-;Hoxb1-/-
Hoxa1-/-;Hoxb1+/-
Hoxa1-/-;Hoxb1-/-
Hoxb1neo;HoxBhprt

Figure 17. Anterior transformation of C6 into a C5-like identity in *Hox* loss-of-function mutants

(A) Wild-type C5 vertebra in the 129s6/SvEv;CD1 genetic background at 18.5dpc.

(B) Wild-type C6 vertebra with its unique ventrally-located bilateral anterior tuberucli.

(C) The bilateral absence of anterior tuberculi (asterisks) from C6 in *Hox* mutants.

(D) Graph depicting the frequency of the C6→C5 transformation in loss-of-function mutants: *Hoxa1*$^{+/-}$, *Hoxa1*$^{-/-}$;*Hoxb1*$^{+/-}$, and *Hoxb1*^{neo};*HoxB*^{hprt} mutant phenotypes are not statistically significant; *Hoxb1*$^{+/-}$ (statistically significant with respect to wild-type, asterisk), *Hoxb1*$^{-/-}$ (statistically significant with respect to wild-type (asterisk) and *Hoxb1*$^{+/-}$ mutants (double asterisk)), *Hoxb2*$^{+/-}$ (statistically significant with respect to wild-type, asterisk), *Hoxb2*$^{-/-}$ (statistically significant with respect to wild-type (asterisk) and *Hoxb2*$^{+/-}$ (double asterisk)), *Hoxb1*$^{+/-}$;*Hoxb2*$^{+/-}$ (statistically significant with respect to wild-type (asterisk) and *Hoxb1*$^{+/-}$ and *Hoxb2*$^{+/-}$ mutants (double asterisk)), *Hoxa1*$^{+/-}$;*Hoxb1*$^{-/-}$ (statistically significant with respect to wild-type (asterisk) and *Hoxa1*$^{+/-}$ mutants (double asterisk)), *Hoxa1*$^{-/-}$;*Hoxb1*$^{-/-}$ (statistically significant with respect to wild-type, asterisk).

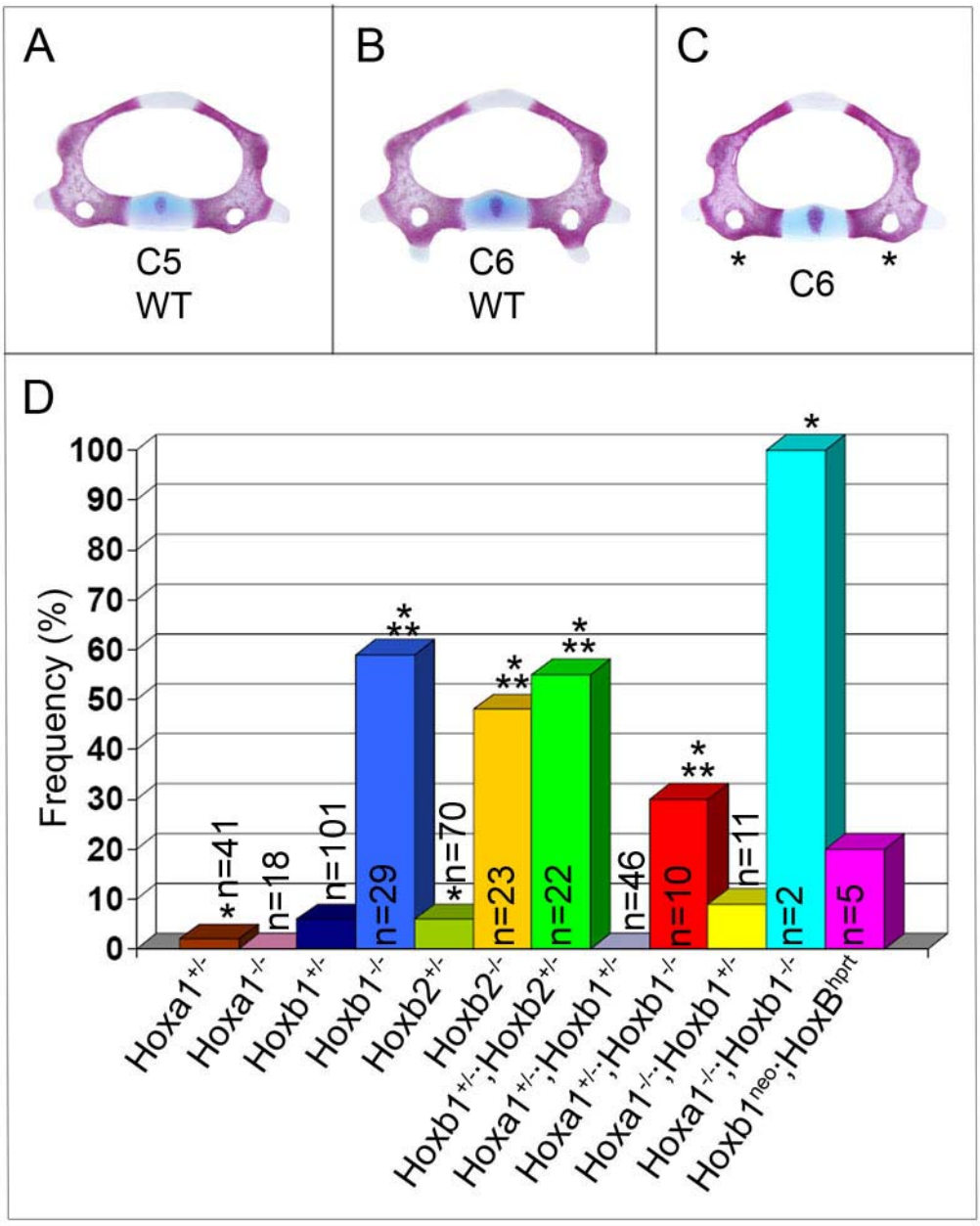
A
C5
WT
B
C6
WT
C
*
C6
*
D
Frequency (%)
100
90
80
70
60
50
40
30
20
10
0
*n=41
n=18
n=101
n=29
*n=70
n=23
n=22
n=46
n=10
n=11
n=2
n=5
Hoxa1+/-
Hoxa1-/-
Hoxb1+/-
Hoxb1-/-
Hoxb2+/-
Hoxb2-/-
Hoxb1+/-;Hoxb2+/-
Hoxa1+/-;Hoxb1+/-
Hoxa1+/-;Hoxb1-/-
Hoxa1-/-;Hoxb1+/-
Hoxa1-/-;Hoxb1-/-
Hoxb1neo;HoxBhprt

Figure 18. Anterior transformation of C7 into a C6-like identity in *Hox* loss-of-function mutants

(A) Wild-type C6 vertebra in the 129s6/SvEv;CD1 genetic background at 18.5dpc. C6 contains both vertebrarterial canals and bilateral anterior tuberculi.

(B) Wild-type C7 vertebra lacks both anterior tuberculi and vertebrarterial canals.

(C) The bilateral presence of anterior tuberculi (asterisks) and vertebrarterial canals (arrows) on C7 in *Hox* mutants.

(D) Graph depicting the frequency of the C7→C6 transformation in loss-of-function mutants: $Hoxb1^{+/-}$, $Hoxa1^{-/-}$;$Hoxb1^{+/-}$, and $Hoxb1^{neo}$;$HoxB^{hprt}$ mutant phenotypes are not statistically significant; $Hoxb1^{-/-}$ (statistically significant with respect to wild-type (asterisk) and $Hoxb1^{+/-}$ mutants (double asterisk)), $Hoxb2^{+/-}$ (statistically significant with respect to wild-type, asterisk), $Hoxb2^{-/-}$ (statistically significant with respect to wild-type (asterisk) and $Hoxb2^{+/-}$ (double asterisk)), $Hoxb1^{+/-}$;$Hoxb2^{+/-}$ (statistically significant with respect to wild-type (asterisk) and $Hoxb1^{+/-}$ and $Hoxb2^{+/-}$ mutants (double asterisk)), $Hoxa1^{+/-}$;$Hoxb1^{-/-}$ (statistically significant with respect to wild-type (asterisk) and $Hoxa1^{+/-}$ mutants (double asterisk)), $Hoxa1^{-/-}$;$Hoxb1^{-/-}$ (statistically significant with respect to wild-type (asterisk) and $Hoxa1^{-/-}$ mutants (double asterisk)).

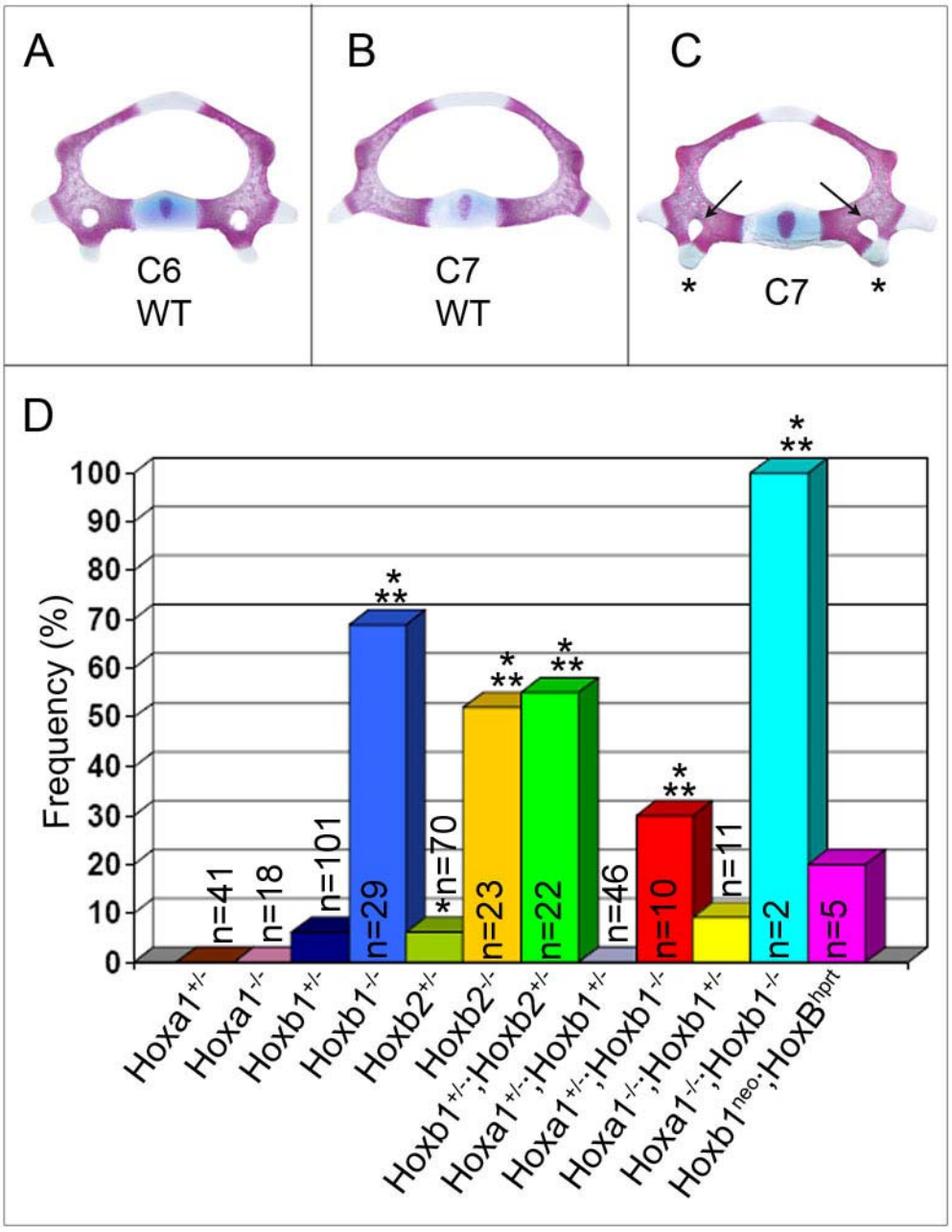
A
C6
WT
B
C7
WT
C
*
C7
*
D
Frequency (%)
100
90
80
70
60
50
40
30
20
10
0
n=41
n=18
n=101
n=29
*n=70
n=23
n=22
n=46
n=10
n=11
n=2
n=5
Hoxa1+/-
Hoxa1-/-
Hoxb1+/-
Hoxb1-/-
Hoxb2+/-
Hoxb2-/-
Hoxb1+/-;Hoxb2+/-
Hoxa1+/-;Hoxb1+/-
Hoxa1+/-;Hoxb1-/-
Hoxa1-/-;Hoxb1+/-
Hoxa1-/-;Hoxb1-/-
Hoxb1neo;HoxBhprt

Figure 19. Anterior transformation of T1 into a C7-like identity in *Hox* loss-of-function mutants

(A) The C7 vertebra in the 129s6/SvEv;CD1 genetic background at 18.5dpc lacks cervical ribs in the majority of wild-type mice.

(B) Wild-type T1 vertebra with the first pair of ventrally-projecting thoracic ribs.

(C) The bilateral shortening of mutant T1 ribs (asterisks) such that no contact is made with the sternum.

(D) Graph depicting the frequency of the T1→C7 transformation in loss-of-function mutants: *Hoxb1*$^{+/-}$ and *Hoxb1*$^{+/-}$;*Hoxb2*$^{+/-}$ mutant phenotypes are not statistically significant; *Hoxb1*$^{-/-}$ (statistically significant with respect to wild-type (asterisk) and *Hoxb1*$^{+/-}$ mutants (double asterisk)).

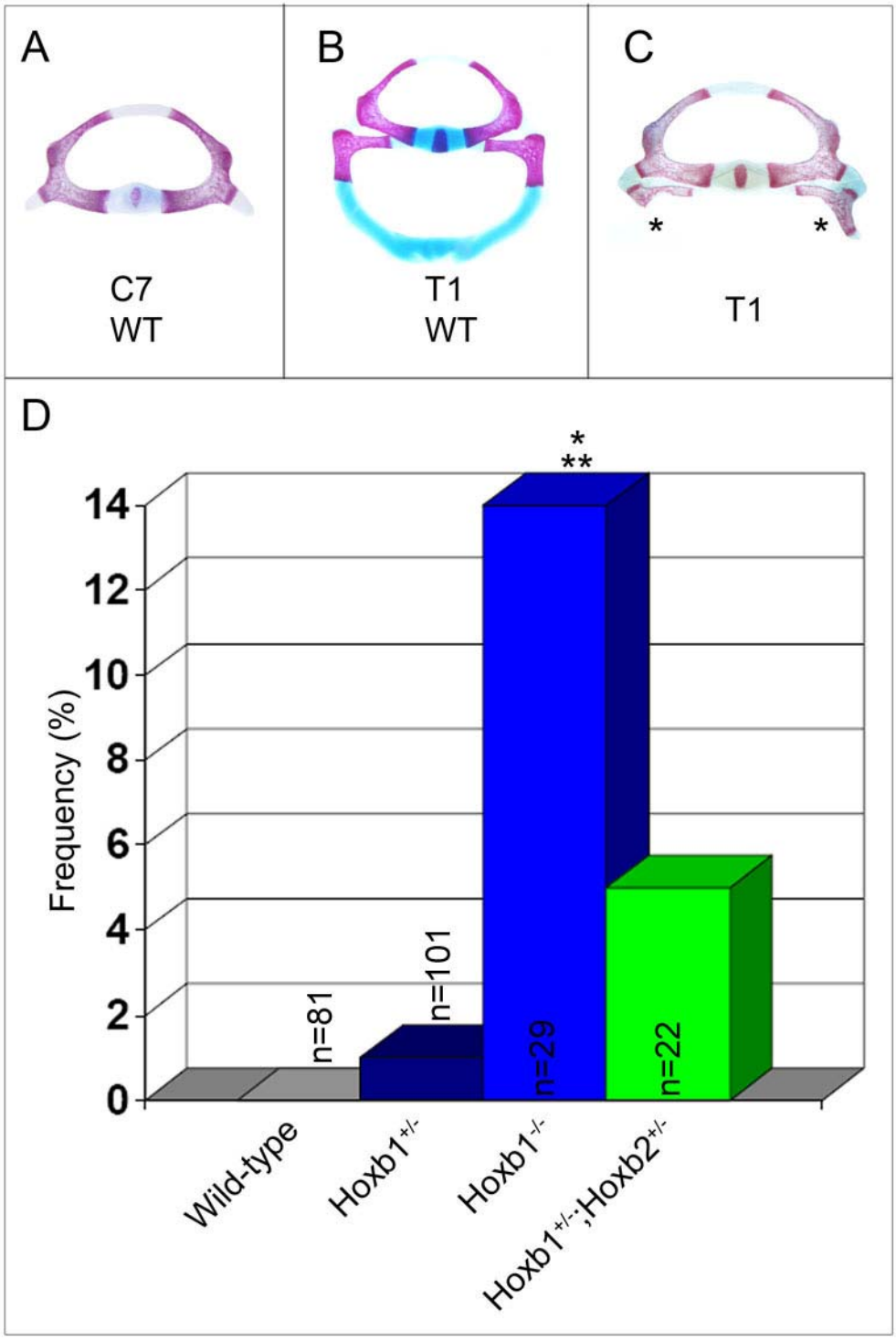
A
C7
WT
B
T1
WT
C
*
*
T1
D
*
**
14
12
10
8
6
4
2
0
Frequency (%)
n=81
n=101
n=29
n=22
Wild-type
Hoxb1+/-
Hoxb1-/-
Hoxb1+/-;Hoxb2+/-

times prior to forming an SCJ (*Hoxb1*$^{+/-}$: 7%; *Hoxb1*$^{-/-}$: 55%). These rib fusions may persist up to the point of contact with the SCJ, resulting in a more anterior junction for the T2 rib, or the ribs may separate and form two separate junctions at the appropriate locations. Taken together, these phenotypes describe an anterior T2→T1 transformation (Figure 20), which was observed with significantly higher incidences in both heterozygous (8%) and homozygous (62%) *Hoxb1* mutants.

Finally, sternal defects were present in the form of either reduced numbers of sternal bands (3 instead of 4) or sternum bifurcation (partial or complete). With respect to the reduction in sternebrae number, only *Hoxb1* homozygotes were affected (7%). However, the prevalence of this phenotype over wild-type animals was not found to be statistically significant. The sternum bifurcation, however, was present in only *Hoxb1* homozygotes (34%) and was observed with significantly increased frequency over wild-type mice (Figure 21).

Interestingly, all of the *Hoxb1* homozygous phenotypes that were observed at significant frequencies over wild-type were also shown to occur with significantly increased frequency over heterozygous mice, suggesting a gene dosage effect, such that, as functional copies of *Hoxb1* are eliminated, phenotypic penetrance increases.

Figure 20. Anterior transformation of T2 into a T1-like identity in *Hox* loss-of-function mutants

(A) Wild-type T1 and T2 vertebrae at 18.5dpc. T1 rib pairs join at the anterior-most portion of the sternum, the manubrium; T2 rib pairs join immediately posterior to the manubrium.

(B) T1 and T2 costal cartilages fuse one or more times prior to joining the sternum (asterisk). Additionally, T2 ribs form an ectopic sternocostal junction at the manubrium (arrow head). The *Hox* mutants may demonstrate one or both of these defects that characterize the T2→T1 transformation.

(C) Graph depicting the frequency of the T2→T1 transformation in loss-of-function mutants: $Hoxa1^{+/-}$;$Hoxb1^{+/-}$ and $Hoxb1^{neo}$;$HoxB^{hprt}$ mutant phenotypes are not significant; $Hoxb1^{+/-}$ (statistically significant with respect to wild-type (asterisk), $Hoxb1^{-/-}$ (statistically significant with respect to wild-type (asterisk) and $Hoxb1^{+/-}$ mutants (double asterisk)), $Hoxb2^{-/-}$ (statistically significant with respect to wild-type (asterisk) and $Hoxb2^{+/-}$ (double asterisk)), $Hoxb1^{+/-}$;$Hoxb2^{+/-}$ (statistically significant with respect to wild-type (asterisk) and $Hoxb1^{+/-}$ and $Hoxb2^{+/-}$ mutants (double asterisk)), $Hoxa1^{+/-}$;$Hoxb1^{-/-}$ (statistically significant with respect to wild-type (asterisk) and $Hoxa1^{+/-}$ mutants (double asterisk)), $Hoxa1^{-/-}$;$Hoxb1^{-/-}$ (statistically significant with respect to wild-type (asterisk) and $Hoxa1^{-/-}$ mutants (double asterisk)).

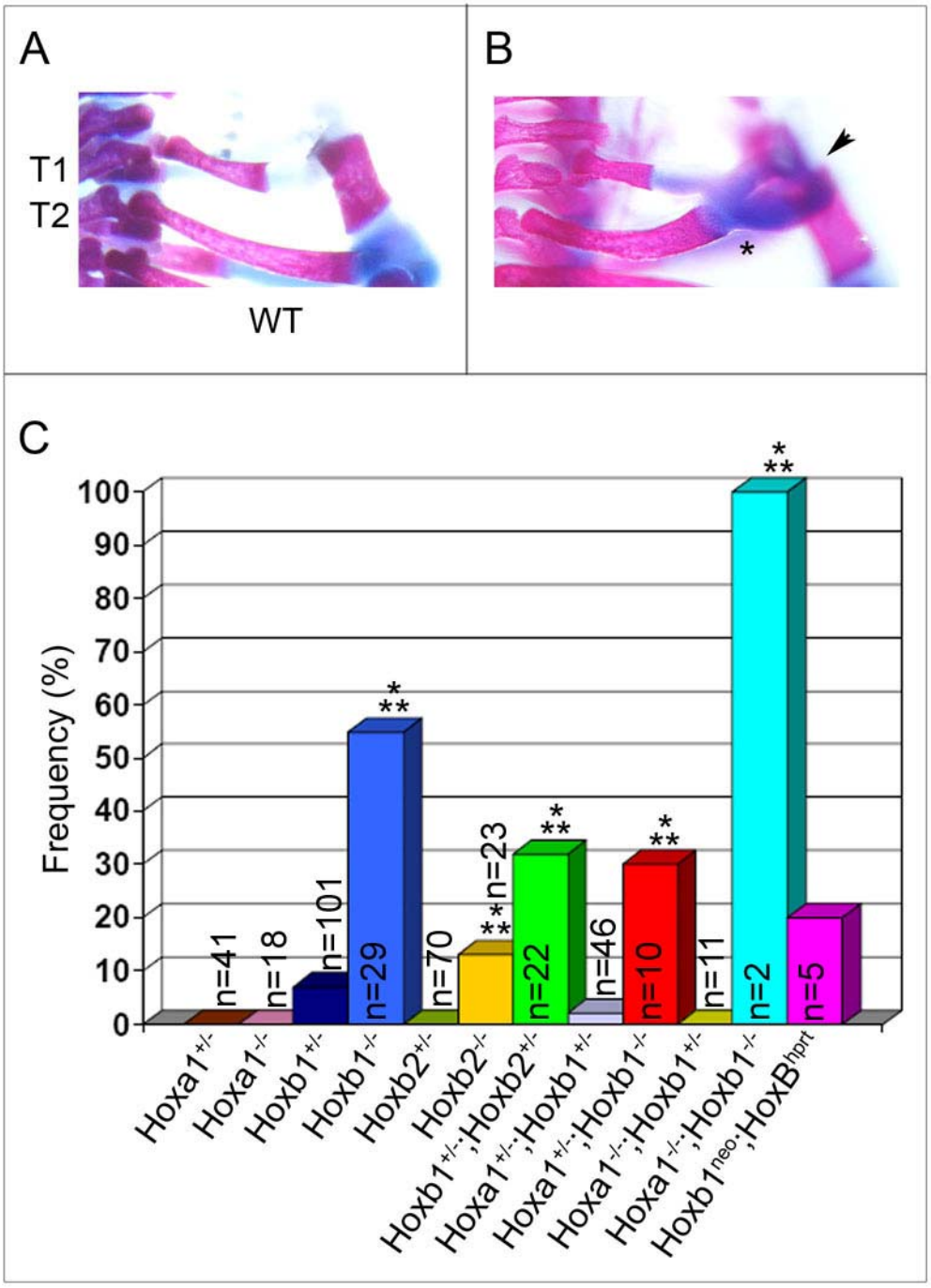
A
T1
T2
WT
B
*
C
Frequency (%)
100
90
80
70
60
50
40
30
20
10
0
n=41
n=18
n=101
n=29
n=70
n=23
n=22
n=46
n=10
n=11
n=2
n=5
*
**
Hoxa1+/-
Hoxa1-/-
Hoxb1+/-
Hoxb1-/-
Hoxb2+/-
Hoxb2-/-
Hoxb1+/-;Hoxb2+/-
Hoxa1+/-;Hoxb1+/-
Hoxa1+/-;Hoxb1-/-
Hoxa1-/-;Hoxb1+/-
Hoxa1-/-;Hoxb1-/-
Hoxb1neo;HoxBhprt

Figure 21. Bifurcation of the sternum in *Hox* loss-of-function mutants

(A) Wild-type sternum with rib pairs labeled R1-R7 in the 129s6/SvEv;CD1 genetic background at 18.5dpc.

(B) Complete sternal bifurcation from the anterior manubrium to the posterior xiphoid process in *Hox* mutants. Sternal bifurcation was scored as either partial or complete, depending on the mutant line.

(C) Graph depicting the frequency of the sternum bifurcation phenotype in loss-of-function mutants: the $Hoxa1^{+/-}$;$Hoxb1^{+/-}$ phenotype is not statistically significant; $Hoxb1^{-/-}$ (statistically significant with respect to wild-type (asterisk) and $Hoxb1^{+/-}$ mutants (double asterisk)), $Hoxb2^{-/-}$ (statistically significant with respect to wild-type (asterisk) and $Hoxb2^{+/-}$ (double asterisk)), $Hoxb1^{+/-}$;$Hoxb2^{+/-}$ (statistically significant with respect to wild-type (asterisk) and $Hoxb1^{+/-}$ and $Hoxb2^{+/-}$ mutants (double asterisk)), $Hoxa1^{+/-}$;$Hoxb1^{-/-}$ (statistically significant with respect to wild-type (asterisk) and $Hoxa1^{+/-}$ mutants (double asterisk)), $Hoxa1^{-/-}$;$Hoxb1^{-/-}$ (statistically significant with respect to wild-type (asterisk), $Hoxb1^{neo}$;$HoxB^{hprt}$ (statistically significant with respect to wild-type asterisk).

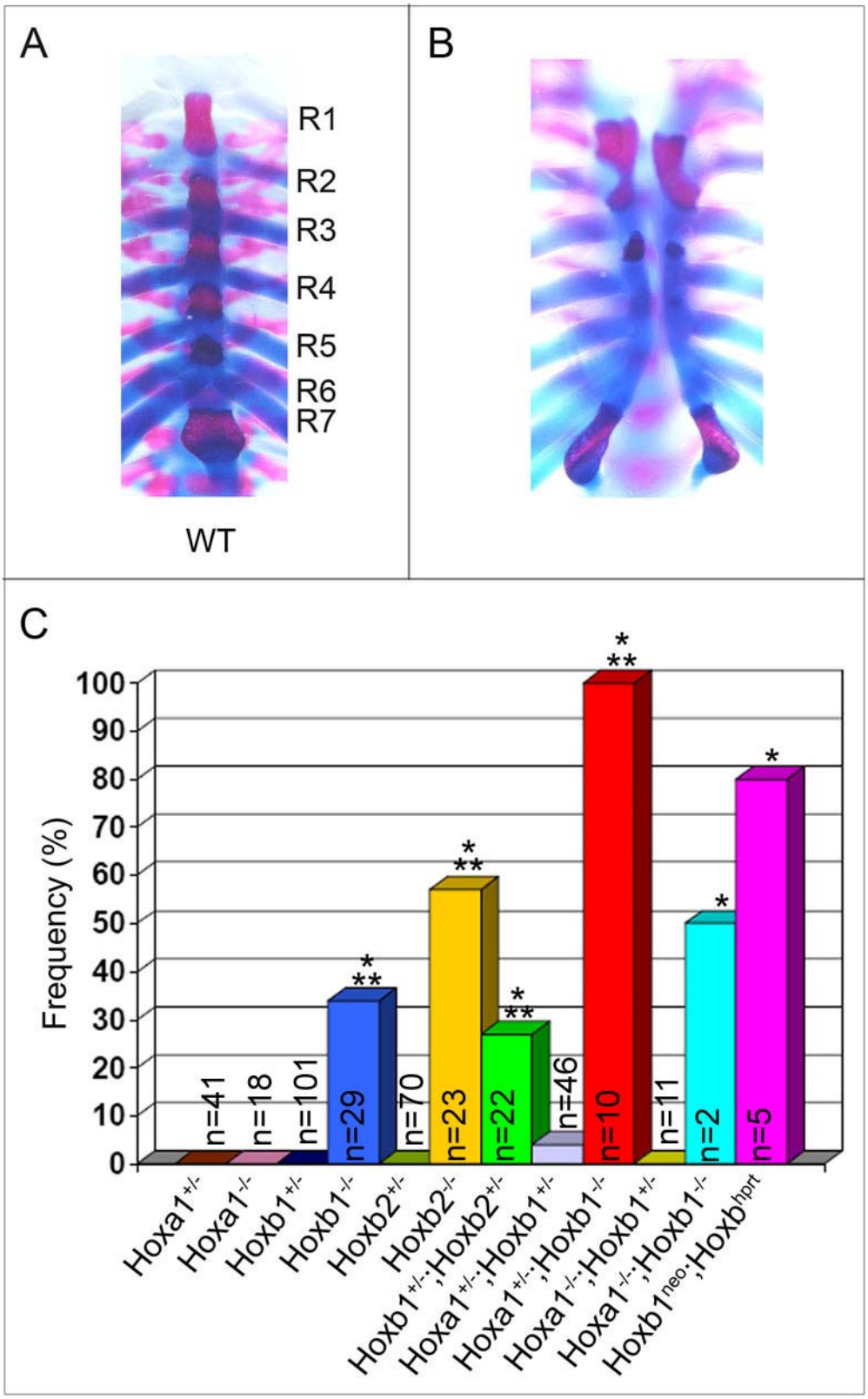
A
R1
R2
R3
R4
R5
R6
R7
WT
B
C
Frequency (%)
100
90
80
70
60
50
40
30
20
10
0
n=41
n=18
n=101
n=29
n=70
n=23
n=22
n=46
n=10
n=11
n=2
n=5
*
**
Hoxa1+/-
Hoxa1-/-
Hoxb1+/-
Hoxb1-/-
Hoxb2+/-
Hoxb2-/-
Hoxb1+/-;Hoxb2+/-
Hoxa1+/-;Hoxb1+/-
Hoxa1+/-;Hoxb1-/-
Hoxa1-/-;Hoxb1+/-
Hoxa1-/-;Hoxb1-/-
Hoxb1neo;Hoxbhprt

***Hoxb2* mutants**

Homeotic transformations of the anterior cervical vertebrae C1 and C2 were previously reported, along with sternal malformations, in *Hoxb2* heterozygous and homozygous mice targeted by insertion of a *neomycin* selection cassette into the homeodomain of exon 2 (Gavalas et al., 1998; Goddard et al., 1996; Studer et al., 1998; Studer et al., 1996). In order to better understand the role of *Hoxb2* in patterning the axial skeleton in mutant mice targeted with a *LacZ*/*neomycin* insertion into exon 1 (Figure 15B), we prepared and analyzed heterozygous and homozygous mutant skeletons at 18.5dpc in a mixed 129s6/SvEv; CD1 genetic background. Similar to the previous report, C2→C1 anterior transformations were observed in our *Hoxb2* mutants (Figure 16). However, the levels of penetrance for both heterozygotes and homozygotes were low (*Hoxb2*$^{+/-}$: 1%; *Hoxb2*$^{-/-}$: 4%) and were not significantly increased over wild-type mice. Sternal bifurcations were present in *Hoxb2*$^{-/-}$ mice (57%), but were completely absent from heterozygous mice (Figure 21). Interestingly, several novel phenotypes were identified within this mutant line, all of which are shared with *Hoxb1* mutants. An anterior transformation of C6→C5 was observed in *Hoxb2* mutants at significantly increased levels over wild-type (*Hoxb2*$^{+/-}$: 6%; *Hoxb2*$^{-/-}$: 48%; Figure 17). As in *Hoxb1* mutants, the C7→C6 transformation (Figure 18) was linked to the C6→C5 transformation, since these two phenotypes were identified in the same skeletal preparations. The fusion of C6 and ectopic C7 AT was even observed in a single *Hoxb2* homozygote (4%) as an additional aspect of the C7→C6 transformation. The penetrance of this portion of the phenotype, however, was not found to be significantly increased over wild-type mice. Finally,

statistically significant T2→T1 anteriorizations were seen only in homozygotes (13%) that had either fusions between T1 and T2 ribs or an ectopic T2 rib SCJ at the manubrium (Figure 20). As was observed for *Hoxb1*, the effect of *Hoxb2* on patterning the axial skeleton appears to be directly related to gene dosage.

3.3.3 Analysis of skeletal defects in double *Hox* mutants

Hoxa1/*Hoxb1* double mutants

As previously stated, several key experiments have shown that synergistic interactions between *Hoxa1* and *Hoxb1* are responsible for early hindbrain and branchial arch patterning, ultimately determining the fate of motorneurons migrating from r4 (Dupé et al., 1997; Murphy and Hill, 1991). Since *Hox* paralogous group members are duplicate copies of an ancestral gene, they frequently share redundant functions. To better understand the relationship between these two genes in the paraxial mesoderm, we compared *Hoxa1* and *Hoxb1* single mutant vertebral phenotypes and observed *Hoxa1*/*Hoxb1* compound mutants for homeotic transformations of the axial skeleton.

Even though both *Hoxa1* and *Hoxb1* transcripts have been detected in the early PSM (Manley and Capecchi, 1997), only one skeletal phenotype was shared in common between *Hoxa1* and *Hoxb1* single mutants. The C6→C5 anterior transformation observed in 1 of 41 *Hoxa1* heterozygotes was seen with significantly increased penetrance in both *Hoxb1* heterozygotes and homozygotes. Nevertheless, novel phenotypes often arise in double *Hox* mutants, despite the fact that single mutant phenotypes do not overlap (e.g. *Hoxa3*/*Hoxb3* double mutants; (de la Cruz et

al., 1999; Horan et al., 1995b; Manley and Capecchi, 1997; van den Akker et al., 2001)). For this reason, we generated a series of *Hoxa1*/*Hoxb1* double mutants to investigate the effect of a progressive loss of both Hoxa1 and Hoxb1 function. *Hoxa1* heterozygotes were crossed with *Hoxb1* heterozygotes, producing *Hoxa1*/*Hoxb1* compound heterozygotes. *Hoxa1*$^{+/-}$;*Hoxb1*$^{+/-}$ mice were used to maintain the compound mutant line and were further intercrossed to create *Hoxa1*$^{+/-}$;*Hoxb1*$^{-/-}$, *Hoxa1*$^{-/-}$;*Hoxb1*$^{+/-}$, as well as *Hoxa1*$^{-/-}$;*Hoxb1*$^{-/-}$ 18.5dpc embryos for skeletal analysis.

***Hoxa1*/*Hoxb1* double heterozygotes**

None of the *Hoxa1*/*Hoxb1* double heterozygous phenotypes were present at significantly greater penetrance than single heterozygous phenotypes. However, three skeletal malformations that were not identified in our survey of wild-type variation were observed at a very low frequency in the double heterozygotes. A T2→T1 transformation was identified in 1 of 46 double heterozygotes whose T1 and T2 ribs were fused prior to joining the sternum (2%; Figure 20). Additionally, crankshaft and bifurcated sternums were present with frequencies of 2% and 4%, respectively (Figure 21).

***Hoxa1*$^{-/-}$/*Hoxb1*$^{+/-}$ and *Hoxa1*$^{+/-}$/*Hoxb1*$^{-/-}$ mutants**

As expected from single mutant analysis, *Hoxa1*$^{-/-}$;*Hoxb1*$^{+/-}$ embryos were less affected by the loss of three alleles than were *Hoxa1*$^{+/-}$;*Hoxb1*$^{-/-}$ embryos. One of the 11 *Hoxa1*$^{-/-}$;*Hoxb1*$^{+/-}$ mutant embryos analyzed (9%) was observed with coupled C6→C5 and C7→C6 anteriorizations (Figures 17 and 18, respectively). A greater number of transformations were observed in more *Hoxa1*$^{+/-}$;*Hoxb1*$^{-/-}$ mutants.

C6→C5, C7→C6, and T2→T1 transformations were all present in the same 30% of mutants (Figures 17, 18, and 20, respectively). While these three phenotypes were not present at statistically significant increased levels compared to *Hoxb1* homozygotes, their penetrance was significantly greater than that observed in *Hoxa1* heterozygotes. Finally, complete sternum bifurcations were completely penetrant in *Hoxa1*$^{+/-}$;*Hoxb1*$^{-/-}$ mutants at significantly higher frequencies than observed in either *Hoxa1*$^{+/-}$ or *Hoxb1*$^{-/-}$ single mutants (Figure 21). Thus, the *Hoxa1*$^{+/-}$;*Hoxb1*$^{-/-}$ double mutants appear to recapitulate the *Hoxb1* single mutant phenotypes. Although some of these phenotypes were significantly more penetrant than *Hoxa1* single mutant phenotypes, none of the previous double mutant phenotypes, with the exception of the sternum bifurcation, showed increased penetrance over single *Hoxb1* mutants.

***Hoxa1*/*Hoxb1* double homozygotes**

Only two *Hoxa1*/*Hoxb1* double homozygous embryos survived until 18.5dpc and were harvested for skeletal analysis. Interestingly, *Hoxa1*$^{-/-}$;*Hoxb1*$^{-/-}$ embryos possessed phenotypes not observed in either single mutant line (Figure 22). In one of these mutants, both EOBs were prematurely fused to the BOB, and the SOB was perforated twice. The C1 neural arch was bilaterally bifurcated in both double homozygotes. Transformations of the cervical and upper thoracic vertebrae were similar to those observed in *Hoxb1* single and *Hoxa1*/*Hoxb1* double mutants: C6→C5, C7→C6, and T2→T1 transformations were all completely penetrant

Figure 22. Skeletal phenotypes unique to *Hoxa1*/*Hoxb1* double homozygotes

(A) Wild-type occipital bone ossification centers are labeled: ventral basioccipital bone (BOB) and lateral exoccipital bones (EOB) at 18.5dpc.

(B) Ossification between the EOB's and BOB (arrows) in a double homozygous mutant.

(C) Wild-type supraoccipital portion of the developing occipital bone, located on the dorsal side of the embryo.

(D) Incomplete ossification of the supraoccipital bone resulting in two perforations (asterisks) located one either side of the midline.

(E) Wild-type C1 has a continuous wide and dorsally-projecting neural arch.

(F) Incomplete ossification or bifurcation of the atlas neural arch (arrow) is present bilaterally in this double homozygous mutant.

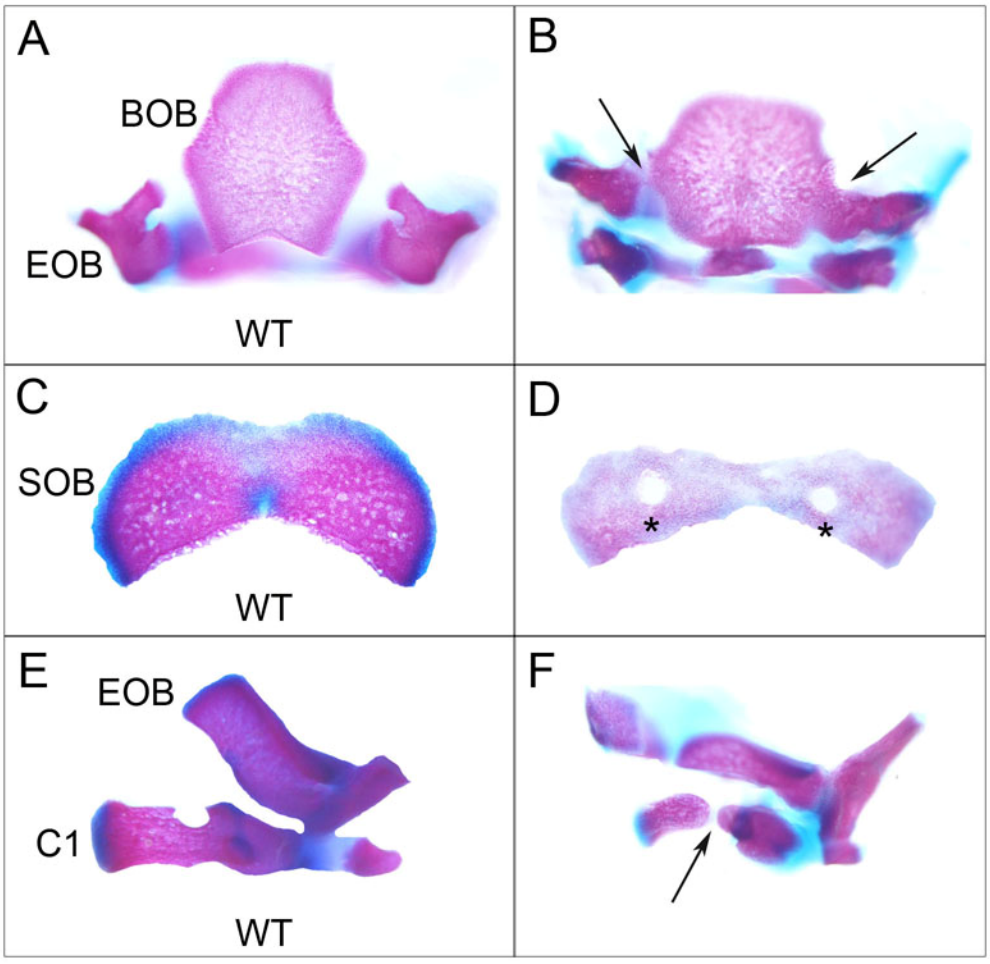
A
BOB
EOB
WT
B
C
SOB
WT
D
*
*
E
EOB
C1
WT
F

(Figures 17, 18, and 20, respectively). The penetrance of these homeotic anteriorizations were significantly increased over *Hoxa1*, but not *Hoxb1*, homozygotes. The final phenotype observed in these mutants was sternum bifurcation in one of the two double homozygous mutants, which was not statistically significant (Figure 21).

The small number of *Hoxa1*/*Hoxb1* double homozygous embryos somewhat limits the ability to speculate about the effects of gene dosage in a meaningful manner. However, the loss of three functional alleles of paralogous group 1 genes (*Hoxa1*$^{+/-}$;*Hoxb1*$^{-/-}$ and *Hoxa1*$^{-/-}$;*Hoxb1*$^{+/-}$) clearly demonstrates that *Hoxa1*/*Hoxb1* double mutant phenotypes are an extension of those phenotypes observed in *Hoxb1* single mutants. The simultaneous loss of Hoxa1 function in the context of the *Hoxb1* mutation does not increase phenotypic penetrance or introduce additional or more severe transformations. Of the two double homozygous embryos harvested for skeletal preparation, one was severely underdeveloped. Additionally, double homozygous 18.5dpc embryos were observed at a frequency much lower than would be expected by normal Mendelian ratios. Whereas 18 *Hoxa1*$^{-/-}$ and 29 *Hoxb1*$^{-/-}$ mutants were identified, only 2 *Hoxa1*$^{-/-}$;*Hoxb1*$^{-/-}$ mutants were observed. This strongly suggests that there is increased embryonic lethality associated with the double homozygous mutant condition. Interestingly, double homozygous mutants generated among other *Hox* co-paralogous groups do not share this embryonic lethality phenotype, as these mutants were obtained in previous studies at frequencies much closer to expected Mendelian ratios (Barrow and Capecchi, 1996). Thus,

reducing the number of functional paralogous group 1 genes seems to have a more severe effect on embryo survival than does eliminating the number of paralogues within other *Hox* paralogous groups.

***Hoxb1*/*Hoxb2* double mutants**

A number of studies have demonstrated an interaction between *Hoxb1* and *Hoxb2* in both the developing hindbrain and more caudal regions of the embryo. For example, a time-course of Hoxb1 immunohistochemical staining in *Hoxb2* homozygotes showed that, from 8.5-9.5dpc, Hoxb1 protein could no longer be detected in r4. Furthermore, staining was decreased in the caudal portion of the embryo, which included the lateral plate mesoderm, PSM, and primitive streak. This study also showed that Hoxb1 protein and *Hoxb2* transcripts can be visualized in overlapping regions of the hindbrain and in the mesoderm, although *Hoxb2* gene expression is much more diffuse (Maconochie et al., 1997). Subsequent reports demonstrated the direct regulation of *Hoxb2* expression by Hoxb1 through an r4 enhancer. One of these studies showed that the *Hoxb2* r4 enhancer contains bipartite Hox/Pbx and Prep/Meis binding motifs, and that Hoxb1 is capable of binding with cofactors and forming tetrameric complexes at these sites (Gavalas et al., 2003). In this way, the role of Hoxb1 in maintaining r4 identity is at least partially mediated through direct cross-regulation of *Hoxb2* expression. Finally, the functional importance of this interaction was demonstrated by the respecification of r4 motor neurons toward an r2 fate in both *Hoxb1* and *Hoxb2* single mutants (de la Cruz et al., 1999; Favier et al., 1996; Ramirez-Solis et al., 1993; Rancourt et al., 1995). Instead

of migrating and behaving as facial motor neurons, the transformed r4 neurons resembled those of the trigeminal nerve. The *Hoxb1* mutant transformation was more complete than the *Hoxb2* phenotype. Taken together with the previous data, these studies show that: 1) Hoxb1 directly regulates *Hoxb2* expression in the developing hindbrain; 2) Hoxb2 protein may act through a feedback mechanism to help maintain *Hoxb1* expression in both neural and mesodermal tissues; and 3) the roles of *Hoxb1* and *Hoxb2* in hindbrain patterning overlap during the specification of facial motor neurons. While the functional significance of the interaction between these two genes has been clearly indicated in the hindbrain, this relationship has not been explored in mesodermally-derived tissues. There is strong evidence in published literature suggesting that synergistic interactions between non-paralogous *Hox* genes are important for patterning the vertebral column (Medina-Martinez et al., 2000). The following section begins to address the functional redundancy between *Hoxb1* and *Hoxb2* in patterning the axial skeleton upon comparison of single mutant phenotypes and analysis of *Hoxb1*/*Hoxb2* trans-heterozygous phenotypes.

Unlike *Hoxa1* mutant skeletons, *Hoxb2* heterozygotes and homozygotes share many of the same phenotypes as *Hoxb1* mutants, including C2→C1 (Figure 16), C6→C5 (Figure 17), C7→C6 (Figure 18), and T2→T1 (Figure 20) transformations, as well as sternum bifurcations (Figure 21). Interestingly, no *Hoxb2* mutants possessed shortened T1 ribs or its associated phenotype: ectopic T2 SCJ at the manubrium. Thus the T2→T1 homeotic transformation in *Hoxb2* mutants is solely characterized by the fusion of T1 and T2 ribs. To investigate the possibility of

synergism between *Hoxb1* and *Hoxb2* during skeletal development, *Hoxb1* and *Hoxb2* single heterozygotes were intercrossed. The resulting trans-heterozygous progeny (*Hoxb1*$^{+/-}$;*Hoxb2*$^{+/-}$) were used to maintain the line and produce 18.5dpc embryos for skeletal analysis. Since the single heterozygotes often possessed homeotic transformations, it was not surprising that these same phenotypes were observed in trans-heterozygotes. One of 22 *Hoxb1*$^{+/-}$;*Hoxb2*$^{+/-}$ mutants had a partial C2→C1 transformation (Figure 16). As in the single heterozygotes, the penetrance of this phenotype was not significantly greater than wild-type mice. The remaining phenotypes (C6→C5, C7→C6, T2→T1, and sternum bifurcation) were observed at significantly increased levels over wild-type, *Hoxb1*, and *Hoxb2* heterozygous mice (Figures 17, 18, 20, and 21, respectively). The T2→T1 transformation in *trans*-heterozygotes was identical to that observed in *Hoxb1* heterozygotes; specifically, this transformation was characterized by T1/T2 rib fusions and T2 rib SCJs at the manubrium. A single T1 rib was shortened in one *Hoxb1*$^{+/-}$;*Hoxb2*$^{+/-}$ embryo, indicating a T1→C7 transformation (Figure 19). However, this phenotype was not significantly increased over wild-type animals. The bifurcated sternum phenotype was unexpected, since neither single heterozygous mutant possessed this defect. Taken together, these results indicate that *Hoxb1* and *Hoxb2* have an additive effect during the patterning of specific elements of the axial skeleton, since the penetrance of key homeotic transformations is increased over single mutant levels. Thus, a synergistic interaction between *Hoxb1* and *Hoxb2* likely plays an important role in

patterning the lateral plate and PSM that give rise to the sternum and vertebral column, respectively.

3.3.4 *Hoxb1* mutants in the context of the *HoxB* cluster deletion

As previously stated, the homozygous deletion of *Hoxb1* through *Hoxb9* (Davenne et al., 1999; Lufkin et al., 1991; Studer et al., 1996) resulted in several anterior homeotic transformations in cervical and upper thoracic vertebrae (C2→C1, C6→C5, C7→C6, T1→C7, T2→T1, and T8→T7), as well as a fully-penetrant, severe sternal defect. Of the cervical anteriorizations, the axis-to-atlas transformation was the least penetrant phenotype, occurring in 12% of homozygous mutants ($HoxB\Delta1^{-/-}$), compared to 100% penetrance of C6→C5 and C7→C6 transformations. Interestingly, the phenotypes of *Hoxb1* single homozygous mutants completely overlap with those of *HoxBΔ1* homozygotes. However, certain phenotypes in the whole-cluster deletion mutants demonstrate increased levels of penetrance over single *Hoxb1* mutants, suggesting that simultaneous mutations in other *HoxB* genes may be responsible for these defects. To test this hypothesis, we decided to introduce our *Hoxb1* mutation into the context of the *HoxBΔ1* deletion by mating *Hoxb1* heterozygotes to *HoxBΔ1* heterozygotes. Consequently, a proportion of the resulting mutant progeny would be expected to possess a single *Hoxb1* targeted allele ($Hoxb1^{neo}$) and a single *HoxBΔ1* deletion allele ($HoxB^{hprt}$). Such double mutants ($Hoxb1^{neo}/HoxB^{hprt}$) would lack any functional copies of *Hoxb1*, and gene dosage of *Hoxb2* through *Hoxb9* would be reduced by one-half. The above mating scheme produced five double mutants at 18.5dpc, whose genotypes were determined with

respect to the independent *Hoxb1* and *HoxBΔ1* targeting alleles. Their skeletons were prepared and stained for phenotypic analysis; resulting phenotypes were compared against 129s6/SvEv;CD1 mice, since both of these strains contribute to the above mutant's genetic background. Of these, only 1 out of the 5 was severely affected, containing 5 of the 8 vertebral transformations observed in the $Hoxb1^{-/-}$ embryos. This embryo possessed bilateral C6→C5, C7→C6, and T2→T1 anterior homeotic transformations (Figures 17, 18, and 20, respectively). Additionally, the sternum contained 3 instead of 4 sternebrae and was partially bifurcated. Sixty-percent of the $Hoxb1^{neo}/HoxB^{hprt}$ mutants demonstrated completely bifurcated sternums. Thus, these mutants presented sternal defects at a penetrance of 80% (Figure 21). Surprisingly, the last PCR-positive double mutant possessed no skeletal defects. Of all the phenotypes, sternal bifurcation was the only defect with a statistically-significant level of penetrance over wild-type animals.

3.3.5 Wild-type skeletal variations in *Hox* mutants

As stated previously, the patterning of the wild-type mouse skeleton follows the 7 cervical, 13 thoracic, 6 lumbar, 4 sacral (C7/T13/L6/S4) vertebral formula. In our study, the total number of vertebrae remained consistent, but morphological variation was observed in the skeletal elements located at the boundaries between morphologically-distinct vertebral regions. In these cases, transitional vertebrae displayed characteristics of the vertebra either immediately anterior or posterior to it. Several of these phenotypes have been previously classified as *Hox* mutant homeotic transformations. However, analysis of wild-type and *Hoxa1*, *Hoxb1*, *Hoxb2* single

and double mutants clearly shows that the variations in mutants do not occur with increased statistical significance over wild-type animals, with a few exceptions. Since the mutant analysis was carried out in the mixed 129s6/SvEv;CD1 genetic background, mutant versus wild-type comparisons were performed with respect to this background. However, there were two occasions in which the variations of interest were not present in the mixed wild-type strain, but were present in the CD1 strain. In these instances, CD1 mice were used as the basis for comparison. Where appropriate, this distinction is noted in the figure's graph. The following section describes skeletal variations in the context of *Hoxa1*, *Hoxb1*, and *Hoxb2* single and double mutants and addresses whether or not they occur at increased frequency relative to wild-type variation. The frequency of natural variation may be found in the same tables as *Hox* mutant phenotypes in Appendix A.

First, fusions of the aaa to the posterior aspect of the BOB occurred in *Hoxb1* single heterozygotes (2%) and homozygotes (7%), as well as one of the two *Hoxa1*/*Hoxb1* double homozygotes (50%; Figure 23). Although no wild-type mice in the mixed 129s6/SvEv;CD1 background possessed this variation, it was observed in one CD1 mouse (3%). Though statistically significant, penetrance in the *Hoxa1*/*Hoxb1* double homozygotes may decrease as more skeletons with this genotype are analyzed. The next variation observed was a splitting of the dorsal aspect of the neural arch of C2, either unilaterally or bilaterally (Figure 24). This phenomenon was present in a majority of the mutants analyzed: $Hoxa1^{+/-}$ (7%), $Hoxa1^{-/-}$ (22%), $Hoxb1^{+/-}$ (3%), $Hoxb1^{-/-}$ (3%), $Hoxb2^{+/-}$ (7%), $Hoxa1^{+/-}$;$Hoxb1^{+/-}$

Figure 23. Fusion of the anterior arch of the atlas to the basioccipital bone in wild-type and *Hox* loss-of-function mutant mice

(A) The ventrally-located basioccipital bone (BOB) and anterior arch of the atlas (aaa) are found as separate elements in a wild-type animal at 18.5dpc. The BOB displays a characteristic concave posterior border.

(B) Ossification between the BOB and aaa (arrow) in *Hox* loss-of-function mutants. As a result, the concave BOB border is eliminated.

(C) Graph depicting the frequency of BOB/aaa fusion in 129s6/SvEv;CD1 (n=81) and CD1 (n=30) wild-type mice. *Hoxb1*$^{+/-}$ and *Hoxb1*$^{-/-}$ phenotypes were not significant; a single *Hoxa1*$^{-/-}$;*Hoxb1*$^{-/-}$ mutant demonstrated this phenotype at a statistically-significant increase with respect to 129s6/SvEv;CD1 (asterisk) but not CD1 mice.

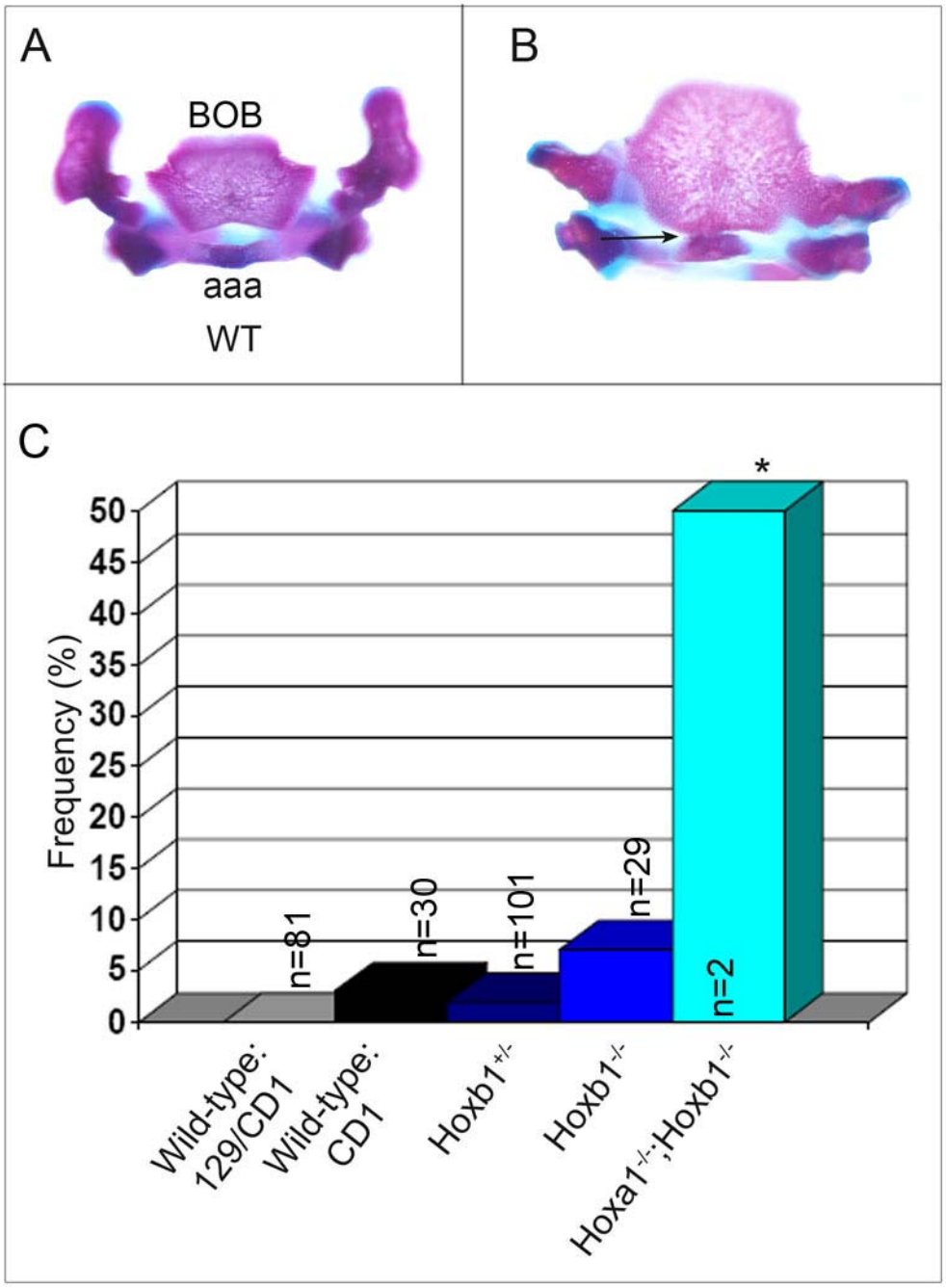
A
BOB
aaa
WT
B
C
Frequency (%)
50
45
40
35
30
25
20
15
10
5
0
n=81
n=30
n=101
n=29
n=2
*
Wild-type: 129/CD1
Wild-type: CD1
Hoxb1+/-
Hoxb1-/-
Hoxa1-/-;Hoxb1-/-

Figure 24. Bifurcation of the C2 neural arch in wild-type and *Hox* loss-of-function mutant mice

(A) The neural arches of C1 and C2 are shown, continuous from the ventral to the dorsal side in wild-type mice at 18.5dpc.

(B) C2 neural arch split (arrow) as seen from the dorsal side in *Hox* loss-of-function mutants.

(C) Graph depicting the frequency of BOB/aaa fusion in 129s6/SvEv;CD1 (n=81) wild-type mice and *Hox* mutants. *Hoxa1*$^{+/-}$, *Hoxa1*$^{-/-}$, *Hoxb1*$^{+/-}$, *Hoxb1*$^{-/-}$, *Hoxb2*$^{+/-}$, *Hoxa1*$^{+/-}$;*Hoxb1*$^{+/-}$, *Hoxa1*$^{+/-}$;*Hoxb1*$^{-/-}$, and *Hoxa1*$^{-/-}$;*Hoxb1*$^{-/-}$ mutant phenotypes were not statistically-significant.

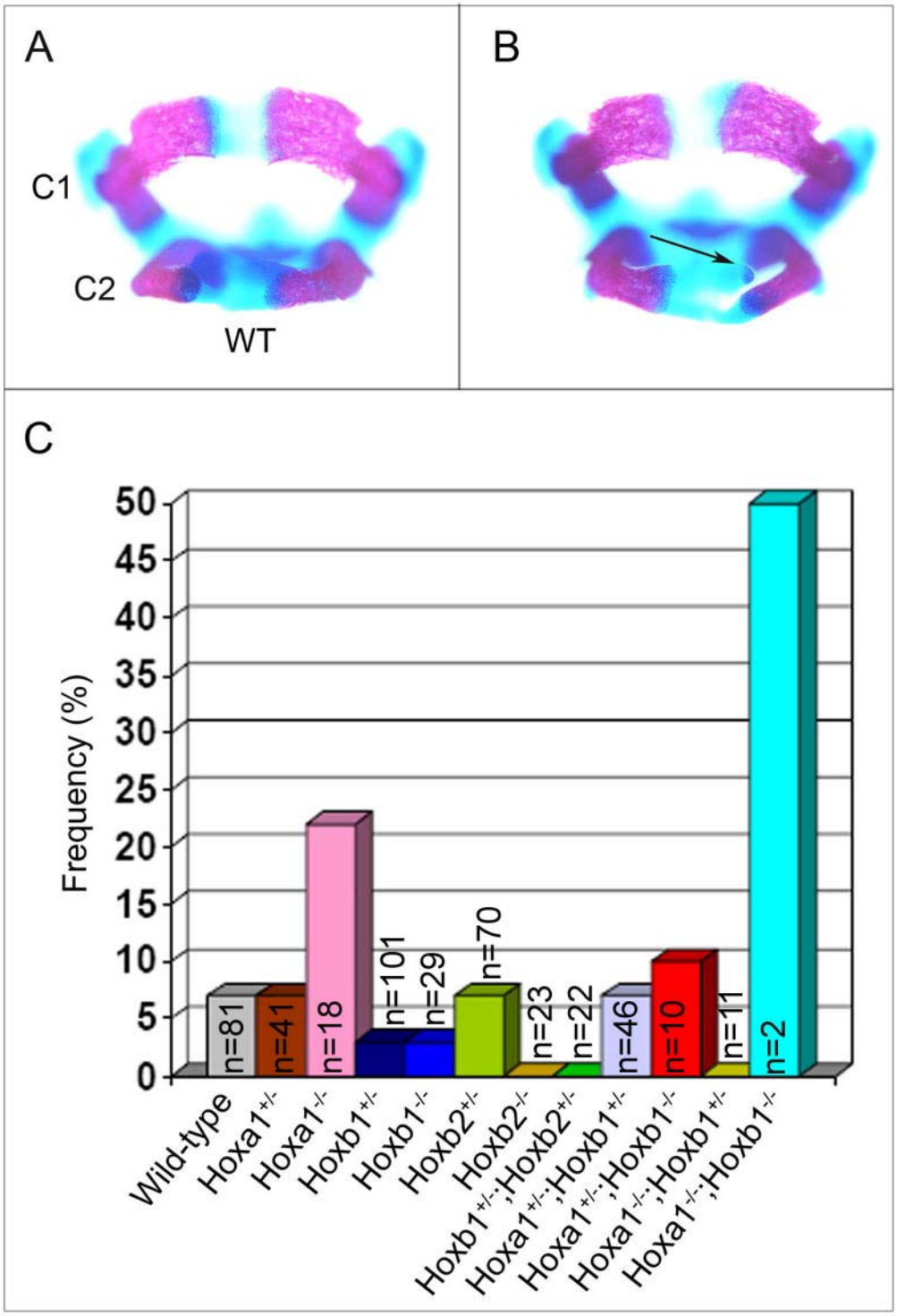
A
C1
C2
WT
B
C
Frequency (%)
50
45
40
35
30
25
20
15
10
5
0
n=81
n=41
n=18
n=101
n=29
n=70
n=23
n=22
n=46
n=10
n=11
n=2
Wild-type
Hoxa1+/-
Hoxa1-/-
Hoxb1+/-
Hoxb1-/-
Hoxb2+/-
Hoxb2-/-
Hoxb1+/-;Hoxb2+/-
Hoxa1+/-;Hoxb1+/-
Hoxa1+/-;Hoxb1-/-
Hoxa1-/-;Hoxb1+/-
Hoxa1-/-;Hoxb1-/-

(7%), *Hoxa1*$^{+/-}$;*Hoxb1*$^{-/-}$ (10%), and *Hoxa1*$^{-/-}$;*Hoxb1*$^{-/-}$ (50%). Additionally, 7% of 129s6/SvEv;CD1 mice demonstrated split C2 neural arches. None of the mutant variations were found to be present at statistically significant levels over wild-type mice. As previously indicated, rib anlagen are often present on C7, even though ribs are a characteristic typically confined to thoracic vertebrae. Compared to 129s6/SvEv;CD1 mice (49%), only one mutant (*Hoxa1*$^{+/-}$: 85%) demonstrated a significant increase in C7 rib penetrance (Figure 25). Although C7 ribs were identified in other *Hox* mutants (*Hoxa1*$^{-/-}$: 72%; *Hoxb1*$^{+/-}$: 10%; *Hoxb2*$^{+/-}$: 4%; *Hoxa1*$^{+/-}$;*Hoxb1*$^{+/-}$: 11%; *Hoxa1*$^{-/-}$;*Hoxb1*$^{+/-}$: 18%), none showed statistical significance. Fusions between C7 and T1 ribs were observed in a single *Hoxa1* heterozygote (2%) and a single 129s6/SvEv;CD1 mouse (1%; Figure 26). No statistical significance was found with respect to this variation in the *Hoxa1* mutant. The ribs extending from the eighth thoracic vertebra (T8) represent the first pair of non-attached ribs, meaning they do not contact the sternum. However, SCJs between the sternum and T8 ribs were observed in both wild-type and mutant mice either unilaterally or bilaterally immediately anterior to the xiphoid process (Figure 27). All loss-of-function mutants analyzed, except for *Hoxa1* heterozygotes, possessed T8 rib SCJs. The prevalence of this variation in both *Hoxa1*/*Hoxb1* homozygous mice was determined to be statistically significant with respect to wild-type, *Hoxa1*$^{-/-}$, and *Hoxb1*$^{-/-}$ mice. Again, the small double homozygous sample number may cause this phenotype to be over-represented in this class of embryos, making it difficult to determine whether this type of homeotic transformation is caused by a loss of both

Figure 25. The presence of C7 rib anlagen in wild-type and *Hox* loss-of-function mutant mice

(A) Seventh cervical vertebra as it is observed in wild-type 18.5dpc mice, specifically, the 129s6/SvEv;CD1 mixed genetic background.

(B) Representative C7 rib anlagen (asterisks), as that observed in wild-type and *Hox* loss-of-function mutants, present either unilaterally or bilaterally.

(C) Graph depicting the frequency of C7 rib anlagen in 129s6/SvEv;CD1 (n=81) wild-type mice and *Hox* mutants. *Hoxa1*$^{-/-}$, *Hoxb1*$^{+/-}$, *Hoxb2*$^{+/-}$, *Hoxa1*$^{+/-}$;*Hoxb1*$^{+/-}$, and *Hoxa1*$^{-/-}$;*Hoxb1*$^{+/-}$ mutant phenotypes were not statistically-significant; the *Hoxa1*$^{+/-}$ phenotype was statistically-significant with respect to wild-type mice.

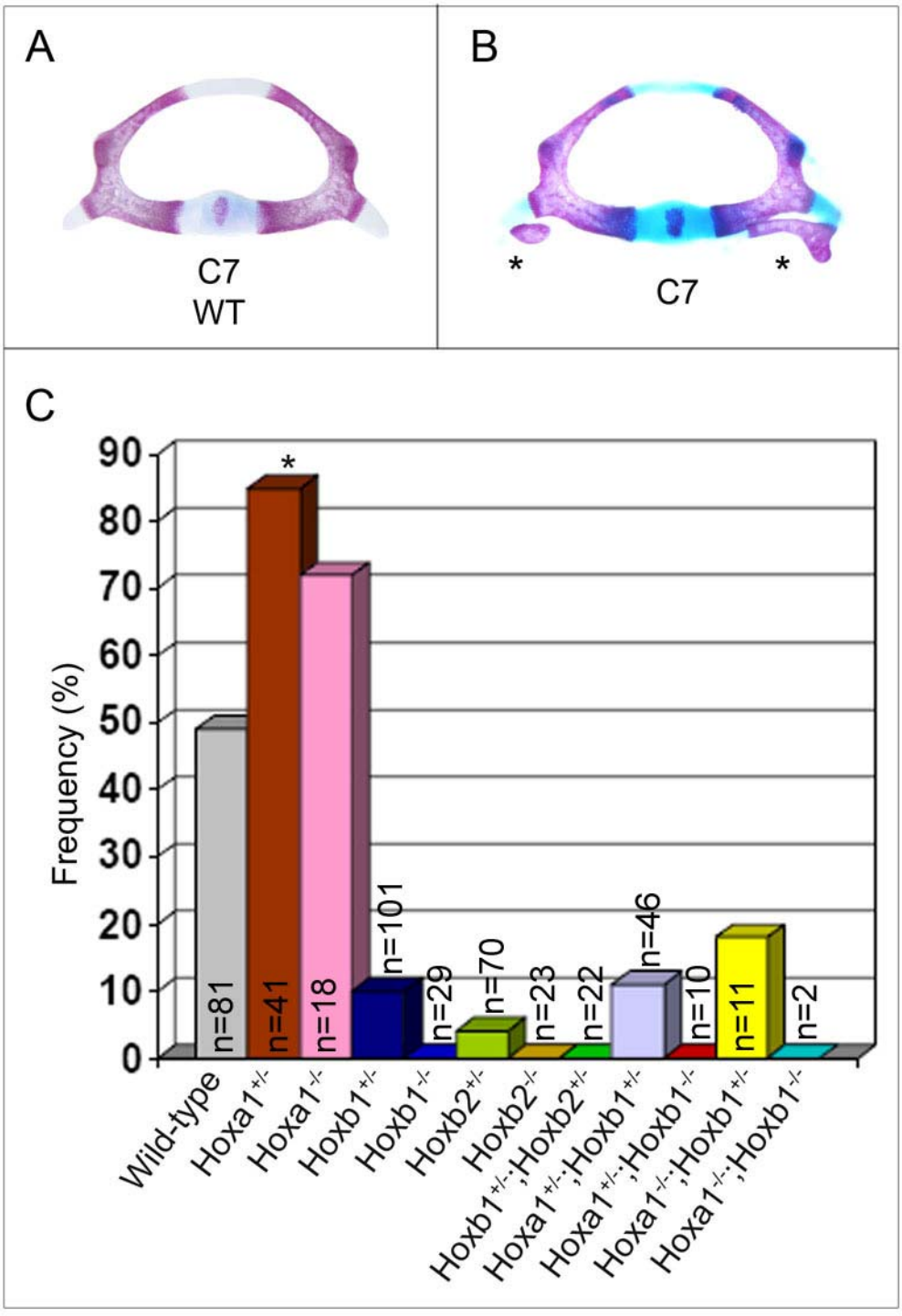
A
C7
WT
B
*
*
C7
C
Frequency (%)
90
80
70
60
50
40
30
20
10
0
*
n=81
n=41
n=18
n=101
n=29
n=70
n=23
n=22
n=46
n=10
n=11
n=2
Wild-type
Hoxa1+/-
Hoxa1-/-
Hoxb1+/-
Hoxb1-/-
Hoxb2+/-
Hoxb2-/-
Hoxb1+/-;Hoxb2+/-
Hoxa1+/-;Hoxb1+/-
Hoxa1+/-;Hoxb1-/-
Hoxa1-/-;Hoxb1+/-
Hoxa1-/-;Hoxb1-/-

Figure 26. Fusion between C7 and T1 ribs in wild-type and *Hoxa1* mutant mice

(A) Lateral view of the wild-type cervicothoracic vertebral transition at 18.5dpc. As in the majority of wild-type mice, ribs are absent from C7 but present on T1.

(B) Lateral view of a unilateral fusion of C7 rib anlage with a T1 rib (arrow), typical of that seen in wild-type (unilateral) and a *Hoxa1* loss-of-function mutant (bilateral).

(C) Graph depicting the frequency of C7/T1 rib fusion in 129s6/SvEv;CD1 (n=81) wild-type mice and a *Hoxa1* mutant. The $Hoxa1^{+/-}$ mutant phenotype was not statistically-significant.

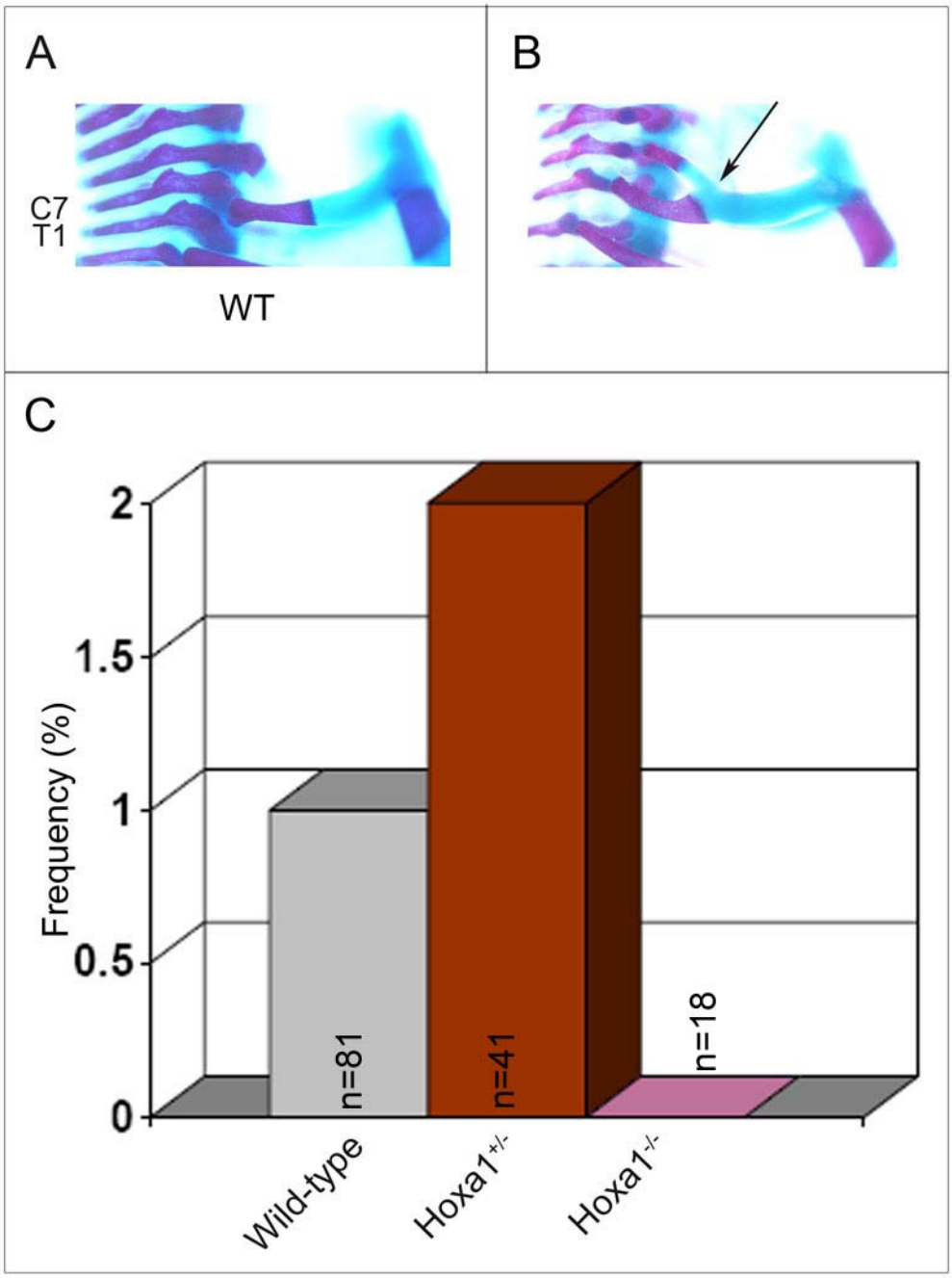
A
C7
T1
WT
B
C
Frequency (%)
2
1.5
1
0.5
0
n=81
n=41
n=18
Wild-type
Hoxa1+/-
Hoxa1-/-

Figure 27. Sternocostal junction of T8 ribs with the sternum in wild-type and *Hox* loss-of-function mutant mice

(A) Ventral view of the sternum with its associated thoracic rib (R1-R7) sternocostal junctions as it is observed in the majority of wild-type mice at 18.5dpc.

(B) Ventral view of the additional junction of T8 ribs with the sternum (asterisks), as observed in wild-type and *Hox* loss-of-function mutants. This variation was observed both unilaterally and bilaterally.

(C) Graph depicting the frequency of T8 rib sternocostal junctions in 129s6/SvEv;CD1 (n=81) wild-type mice and *Hox* mutants. *Hoxa1*$^{-/-}$, *Hoxb1*$^{+/-}$, *Hoxb1*$^{-/-}$, *Hoxb2*$^{+/-}$, *Hoxb2*$^{-/-}$, *Hoxb1*$^{+/-}$;*Hoxb2*$^{+/-}$, *Hoxa1*$^{+/-}$;*Hoxb1*$^{+/-}$, *Hoxa1*$^{+/-}$;*Hoxb1*$^{-/-}$, and *Hoxa1*$^{-/-}$;*Hoxb1*$^{+/-}$ C7/T1 rib fusions were not significant; this variation in both *Hoxa1*$^{-/-}$;*Hoxb1*$^{-/-}$ mutants was determined to be statistically-significant with respect to wild-type and *Hoxa1*$^{-/-}$ mutant mice.

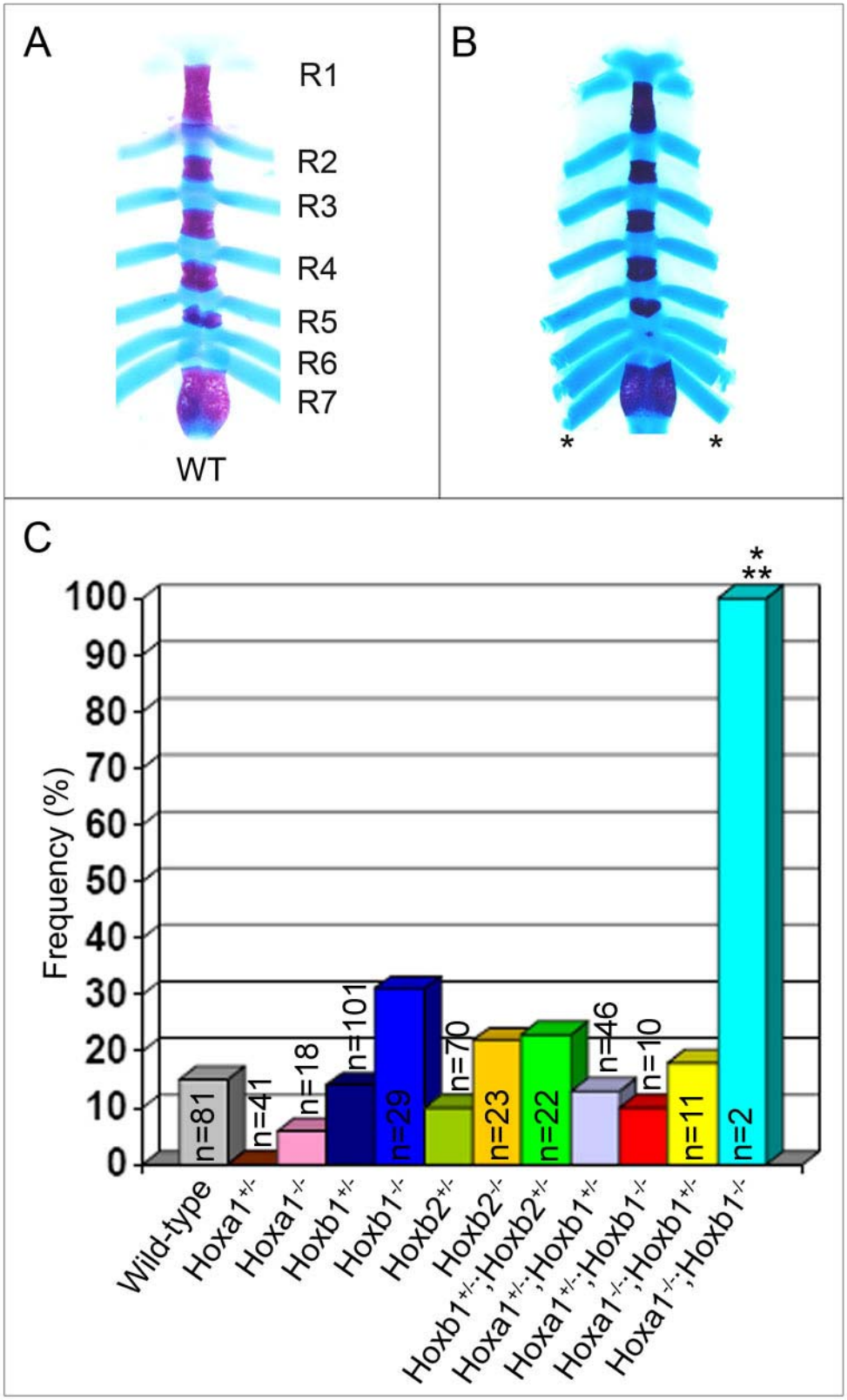
A
R1
R2
R3
R4
R5
R6
R7
WT
B
*
*
C
Frequency (%)
100
90
80
70
60
50
40
30
20
10
0
n=81
n=41
n=18
n=101
n=29
n=70
n=23
n=22
n=46
n=10
n=11
n=2
*
**
Wild-type
Hoxa1+/-
Hoxa1-/-
Hoxb1+/-
Hoxb1-/-
Hoxb2+/-
Hoxb2-/-
Hoxb1+/-;Hoxb2+/-
Hoxa1+/-;Hoxb1+/-
Hoxa1+/-;Hoxb1-/-
Hoxa1-/-;Hoxb1+/-
Hoxa1-/-;Hoxb1-/-

Hoxa1 and *Hoxb1* or is just the result of natural variation. As previously stated, the sternum typically contains four sternal bands between the manubrium and xiphoid process. Interestingly, the observation of T8 rib SCJs are often correlated with an additional (fifth) sternal band located between the SCJs of the sixth and seventh pairs of ribs in wild-type CD1 (7%), *Hoxb1*$^{+/-}$ (6%), *Hoxb2*$^{+/-}$ (6%), *Hoxb2*$^{-/-}$ (4%), and *Hoxa1*$^{+/-}$;*Hoxb1*$^{+/-}$ (2%) mice (Figure 28). This variation in any of the *Hox* mutants was not significantly increased over wild-type mice. Finally, L1 ribs were observed in 129s6/SvEv;CD1 (12%), *Hoxa1*$^{+/-}$ (2%), *Hoxb1*$^{+/-}$ (2%), *Hoxb2*$^{+/-}$ (7%), *Hoxb1*$^{+/-}$;*Hoxb2*$^{+/-}$ (5%), *Hoxa1*$^{+/-}$;*Hoxb1*$^{+/-}$ (2%) mice, but mutant variations were not significant with respect to wild-type animals (Figure 29). These results clearly support the hypothesis that variation in vertebral identity occurs naturally within transition regions separating morphologically-distinct vertebrae, specifically, the cervicothoracic and thoracic-lumbar regions. The overall observation that decreasing *Hox* gene dosage does not result in significantly-increased variations further suggests that, at least in *Hoxa1*, *Hoxb1*, and *Hoxb2* mutants, these variations within the axial skeleton are the result of natural variation and are not due to the loss of Hox gene function.

3.3.6 Neonatal Lethality observed in our *Hox* mutants

As previously reported, single *Hoxa1*, *Hoxb1*, and *Hoxb2* homozygotes exhibit perinatal lethality, dying within 24 hours of birth (Manley et al., 2001; Ramirez-Solis et al., 1993). Initially, this same observation was made for each of these mutant strains by our lab. However, over the course of our analysis of each of

Figure 28. Fifth sternal band present between the fourth sternebra and xiphoid process in wild-type and *Hox* loss-of-function mutants

(A) Ventral view of the sternum and its ossification centers as they are observed in the majority of wild-type mice at 18.5dpc: the anterior manubrium (M), four sternebrae (S1-S4), and the posterior xiphoid process (X). The first and second sternocostal junctions are separated by M; the second and third, by the first sternebra; the third and fourth, by the second sternebra; the fourth and fifth, by the third sternebra; the fifth and sixth, by the fourth sternebra. The sixth and seventh junctions separate the fourth sternebra and X.

(B) Ventral view of a fifth sternebra that separates the sixth and seventh sternocostal junctions (arrow) in wild-type and *Hox* loss-of-function mutants. As a result, the last sternebra and X are now separated by the seventh and eighth rib junctions.

(C) Graph depicting the frequency of T8 rib sternocostal junctions in 129s6/SvEv;CD1 (n=81) and CD1 (n=30) wild-type mice, as well as *Hox* mutants. This variation in $Hoxb1^{+/-}$, $Hoxb2^{+/-}$, $Hoxb2^{-/-}$, and $Hoxa1^{+/-}$;$Hoxb1^{+/-}$ mutants was not statistically-significant.

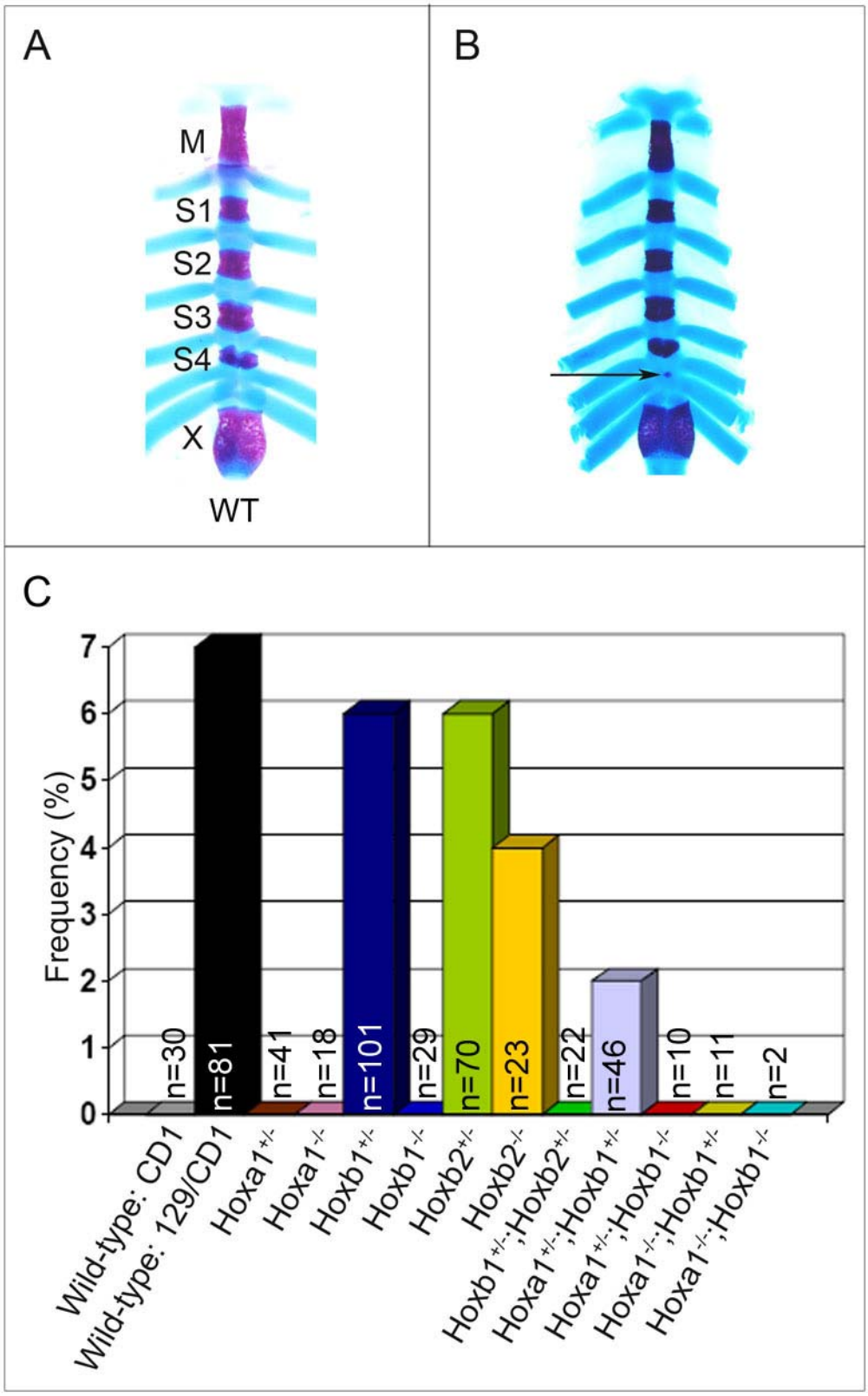
A
M
S1
S2
S3
S4
X
WT
B
C
Frequency (%)
0
1
2
3
4
5
6
7
n=30
n=81
n=41
n=18
n=101
n=29
n=70
n=23
n=22
n=46
n=10
n=11
n=2
Wild-type: CD1
Wild-type: 129/CD1
Hoxa1+/-
Hoxa1-/-
Hoxb1+/-
Hoxb1-/-
Hoxb2+/-
Hoxb2-/-
Hoxb1+/-;Hoxb2+/-
Hoxa1+/-;Hoxb1+/-
Hoxa1+/-;Hoxb1-/-
Hoxa1-/-;Hoxb1+/-
Hoxa1-/-;Hoxb1-/-

Figure 29. The presence of ribs on the first lumbar vertebra in wild-type and *Hox* loss-of-function mutants

(A) The first lumbar vertebra as it is observed in the majority of wild-type mice at 18.5dpc. L1 represents the first vertebra of the lumbar vertebral column and contains no ribs.

(B) L1 rib formations in wild-type and *Hox* mutants are present either unilaterally or bilaterally, as anlagen or fully-developed ribs.

(C) Graph depicting the frequency of T8 rib sternocostal junctions in wild-type (129s6/SvEv;CD1) and *Hox* mutant mice. These variations in $Hoxa1^{+/-}$, $Hoxb1^{+/-}$, $Hoxb2^{+/-}$, $Hoxb1^{+/-}$;$Hoxb2^{+/-}$, and $Hoxa1^{+/-}$;$Hoxb1^{+/-}$ mutants were not statistically-significant.

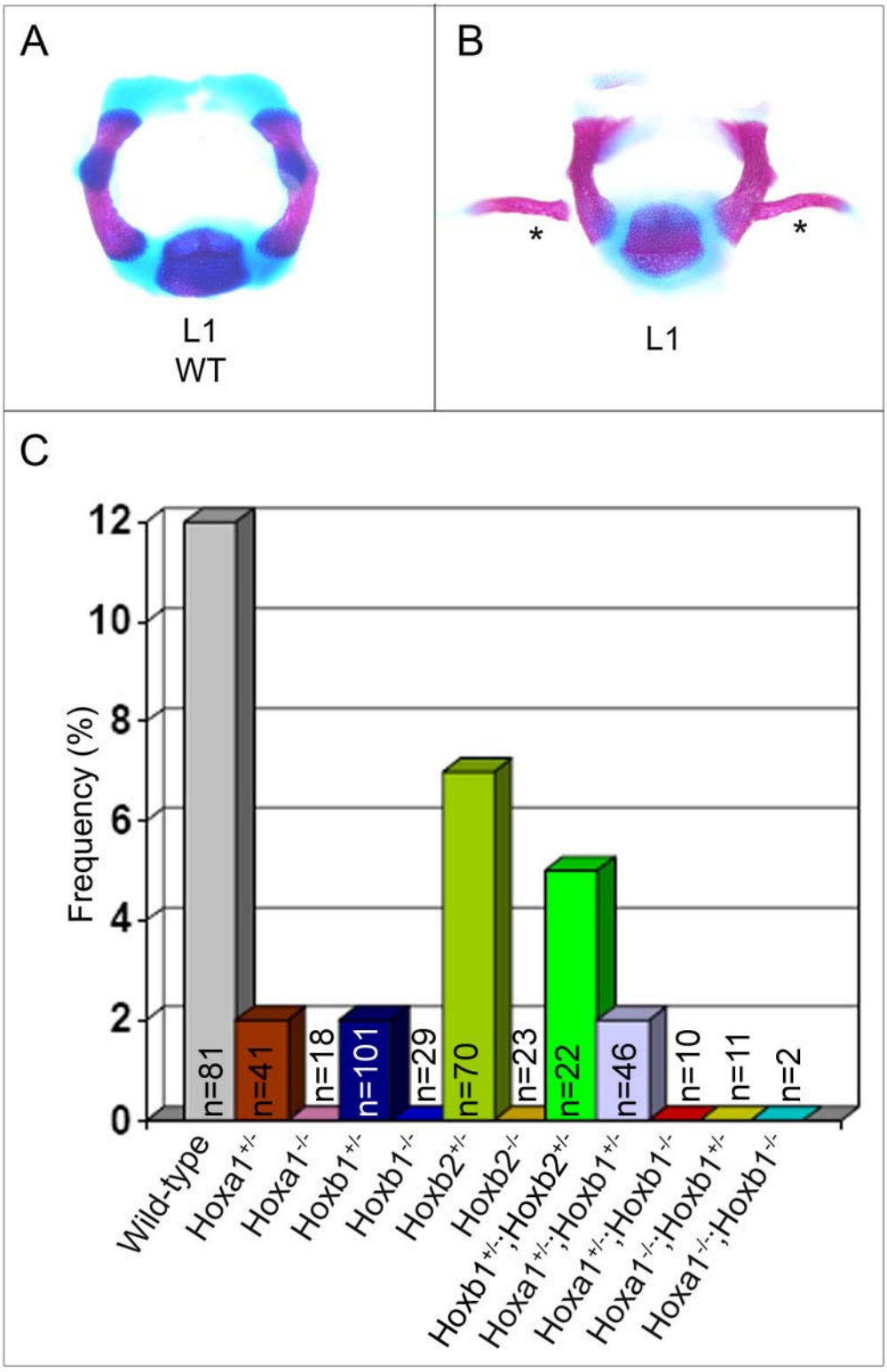
A
L1
WT
B
*
*
L1
C
Frequency (%)
0
2
4
6
8
10
12
n=81
n=41
n=18
n=101
n=29
n=70
n=23
n=22
n=46
n=10
n=11
n=2
Wild-type
Hoxa1+/-
Hoxa1-/-
Hoxb1+/-
Hoxb1-/-
Hoxb2+/-
Hoxb2-/-
Hoxb1+/-;Hoxb2+/-
Hoxa1+/-;Hoxb1+/-
Hoxa1+/-;Hoxb1-/-
Hoxa1-/-;Hoxb1+/-
Hoxa1-/-;Hoxb1-/-

these lines, we began to observe homozygous genotypes for all three mutants at weaning stages in both purebred 129s6/SvEv and mixed 129s6/SvEv;CD1 genetic backgrounds. The life spans of the homozygous mutants reach that observed for their heterozygous littermates. In the case of *Hoxa1* mutants, fertility of homozygous males did not seem to be affected, as they were able to successfully sire litters when paired with CD1 females. The fertility of *Hoxb1* or *Hoxb2* homozygous mutant adults was not tested. Interestingly, *Hoxa1* homozygous adults were observed in both purebred and mixed background strains. *Hoxb1* and *Hoxb2* individual homozygotes have been independently obtained through single heterozygote matings, as well as $Hoxb1^{+/-}$;$Hoxb2^{+/-}$ mutant intercrossings ($Hoxb1^{-/-}$;$Hoxb2^{+/+}$ and $Hoxb1^{+/+}$;$Hoxb2^{-/-}$ progeny) in the mixed 129s6/SvEv;CD1 strain. It is possible that one of the following two events may have occurred that would explain these observations. First, a modifier locus in another region of the genome could now be segregating with the targeted locus through subsequent inbreeding, potentially increasing the viability of progeny. The second explanation involves changes to the targeted allele. It was previously suggested that the *neomycin* cassette insertion into *HoxB* gene loci, particularly, in the gene's first exon, results in a gain-of-function effects on sternal development and ventral body wall closure (Manley et al., 2001; Manley and Capecchi, 1997; Ramirez-Solis et al., 1993; Rancourt et al., 1995), presumably by impacting the functions of neighboring *HoxB* genes. While not every skeletal phenotype observed in mice containing two targeted alleles is attributed to the *neomycin* insertion, it is possible that the neonatal lethality phenotype may also

represent a similar gain-of-function effect. Thus, a modification to the *neomycin* cassette could eliminate *cis*-acting effects on neighboring genes, rescuing the lethality phenotype. These two explanations are not mutually-exclusive, and both events may explain the observation of homozygous adults in each of the mutant lines. A similar phenomenon became apparent in $Hoxb1^{neo}/HoxB^{hprt}$ mutants that survived to weaning stages.

3.4 Identification of skeletal abnormalities in transgenic mice with increased *HoxB* gene dosage

Loss-of-function mutant analysis allowed us to investigate the phenotypic effect of decreasing a gene's dosage by as many as two copies. Alternatively, targeting strategies designed to increase gene dosage offer an advantage over loss-of-function mutations, since a greater number of copies can be added back than can be eliminated by the latter approach. Increasing gene dosage results in more protein being produced and, potentially, an even greater perturbation of the developmental program. Surprisingly, many of the resulting defects phenocopy those observed in loss-of-function mutants; few novel phenotypes were found. In either situation, this strategy provides an additional method by which the function of a gene may be determined. Christof Nolte and Youngwook Ahn, members of the Krumlauf lab, have generated genetic tools through BAC- and plasmid-transgenesis that produce extra copies of various *HoxB* gene combinations. The following section describes the effect of increased *HoxB* gene dosage on vertebral patterning.

3.4.1 Increasing *Hoxb1-Hoxb5* gene dosage (K411)

For this analysis, a 158kb BAC transgene was used, which contains a region of the *HoxB* locus spanning from the second exon of *Hoxb5* through *Hoxb1* plus 60kb downstream of the *HoxB* cluster; this BAC includes many known and putative regulatory elements. Tim Jinks inserted a *LacZ* reporter 53kb downstream of the *Hoxb1* coding region using a transposable element (Figure 30A). Christof Nolte used this transgene to generate transgenic mice in an F1 (CBA x C57bl/10) genetic background; skeletons were analyzed at 18.5dpc for skeletal defects and compared against F1 wild-type mice of the same age.

Three 18.5dpc embryos, identified by PCR genotyping, were found to possess the *Hoxb1-Hoxb5* transgene. One of these possessed four unique phenotypes. The remaining two embryos shared the same phenotype: absence of the fourth sternal band (3 sternal bands total), which was also observed in *Hoxb1* homozygotes (7%; not shown). Among the novel phenotypes were bilateral ectopic EOBs fused to the endogenous EOB (Figure 31), widening of the C1 neural arch (Figure 32), fusion of T1 and T2 neural arches dorsally (Figure 33), and, in one instance, a unilateral bifurcation of a T11 rib. The fusion of T1 and T2 neural arches represents a partial homeotic transformation of T2 towards a T1 identity. Additionally, two of these mice had rib anlagen present on C7, as in a percentage of wild-type animals (Figure 34). The small sample number makes it difficult to determine if these phenotypes are correlated with the presence of the transgene or are natural variations, as a statistically wild-type mice.

Figure 30. Transgenic targeting strategies to increase *HoxB* gene dosage

(A) Schematic representation of the 158kb BAC transgene containing endogenous *Hoxb1-Hoxb4* gene loci, the second coding exon of the *Hoxb5* locus, and 60kb of non-coding sequence downstream of the *Hoxb1* locus. A transposable element containing the *LacZ* reporter gene was inserted 53kb downstream of the end of the *Hoxb1* coding region.

(B) Schematic representation of the 138kb BAC transgene consisting of the *Hoxb1* through *Hoxb9* genes, including all of the known regulatory elements. The following reporter or epitope tags were inserted into the BAC: *mCherry* (*Hoxb9*, red), FLAG-tag (*Hoxb8*), *LacZ* (*Hoxb7*, blue), c-terminal Myc-tag (*Hoxb6*), and *eGFP* (*Hoxb5*, green). Fluorescent markers in *Hoxb5*, *Hoxb7*, and *Hoxb9* disrupt these loci, resulting in non-functional gene products. *Hoxb6* and *Hoxb8* loci presumably retained their functions. *Hoxb1-Hoxb4* were not altered.

(C) Schematic representation of the 20kb region of the endogenous *Hoxb1* gene locus captured to increase this gene's dosage. The transgene contains both coding exons (1 and 2) and all of the previously reported regulatory regions: r3/r5 repressor (green circle), r4 enhancer (yellow oval), neural enhancer (fuchsia oval), mesodermal enhancer (orange oval), and endodermal enhancer (turquoise oval).

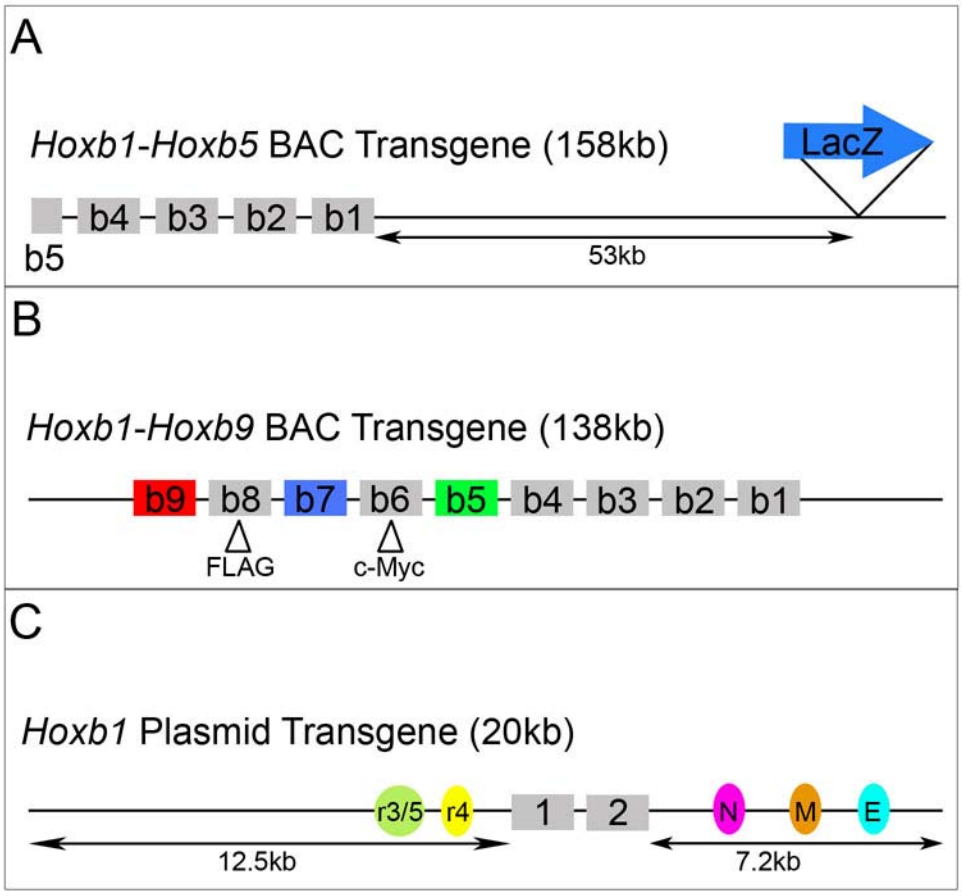
A
Hoxb1-Hoxb5 BAC Transgene (158kb)
LacZ
b4
b3
b2
b1
b5
53kb
B
Hoxb1-Hoxb9 BAC Transgene (138kb)
b9
b8
b7
b6
b5
b4
b3
b2
b1
FLAG
c-Myc
C
Hoxb1 Plasmid Transgene (20kb)
r3/5
r4
1
2
N
M
E
12.5kb
7.2kb

Figure 31. Ectopic exoccipital bone formation in transgenic mice with increased *HoxB* gene dosage

(A) Lateral view of the wild-type exoccipital bone (EOB) and first cervical vertebra (C1) at 18.5dpc.

(B) Presence of an underdeveloped ectopic EOB (asterisk) fused at its ventral aspect to the endogenous EOB located immediately anterior.

(C) An underdeveloped ectopic EOB (asterisk) that does not fuse anteriorly with the endogenous EOB or posteriorly with C1.

(D) A more developed ectopic EOB (asterisk), in which the dorsal aspect of this formation is fused to the dorsal portion of the C1 neural arch.

(E) Graph depicting the frequency of an ectopic EOB formation in transgenic mice with increased *HoxB* gene dosage: the *Hoxb1-Hoxb5* transgenic (Tg) phenotype was not significant; the *Hoxb1*$^{+/-}$;*Hoxb1-Hoxb5* Tg phenotype was statistically-significant with respect to the wild-type F1 population (asterisk).

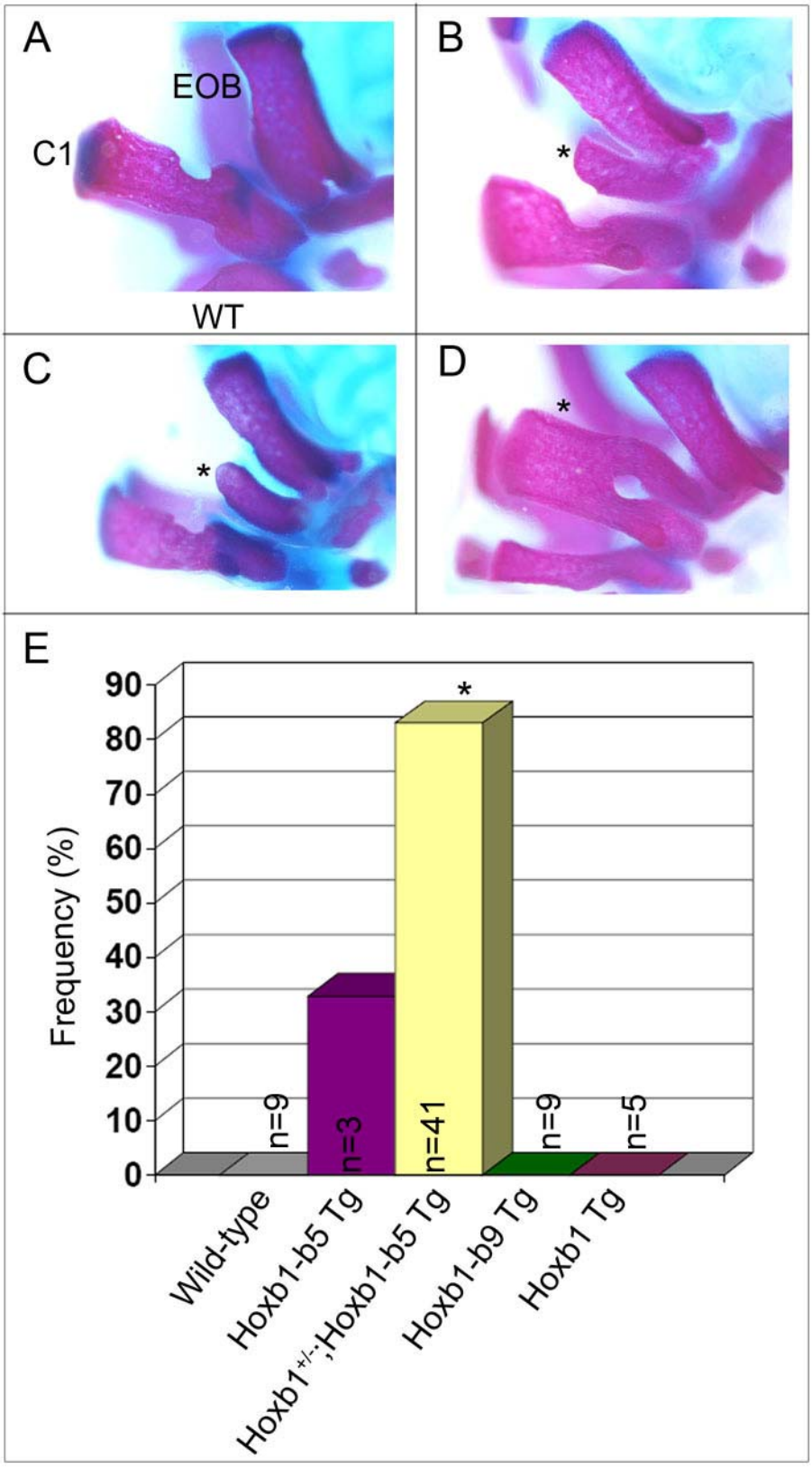
A
EOB
C1
WT
B
*
C
*
D
*
E
Frequency (%)
90
80
70
60
50
40
30
20
10
0
n=9
n=3
n=41
n=9
n=5
*
Wild-type
Hoxb1-b5 Tg
Hoxb1+/-;Hoxb1-b5 Tg
Hoxb1-b9 Tg
Hoxb1 Tg

Figure 32. Increased width of the dorsal aspect of the C1 neural arch in transgenic mice with increased *HoxB* gene dosage

(A) Lateral view of the wild-type exoccipital bone (EOB) and first cervical vertebra (C1) at 18.5dpc.

(B) The dorsal aspect of the C1 neural arch is markedly increased in width (asterisk), compared to the wild-type C1. Additionally, this embryo lacked an anterior arch of the atlas (arrow).

(C) Graph depicting the frequency of an increased C1 neural arch in transgenic mice with increased *HoxB* gene dosage: *Hoxb1-Hoxb5* transgenic (Tg) and *Hoxb1*$^{+/-}$;*Hoxb1-Hoxb5* Tg phenotypes were not significant.

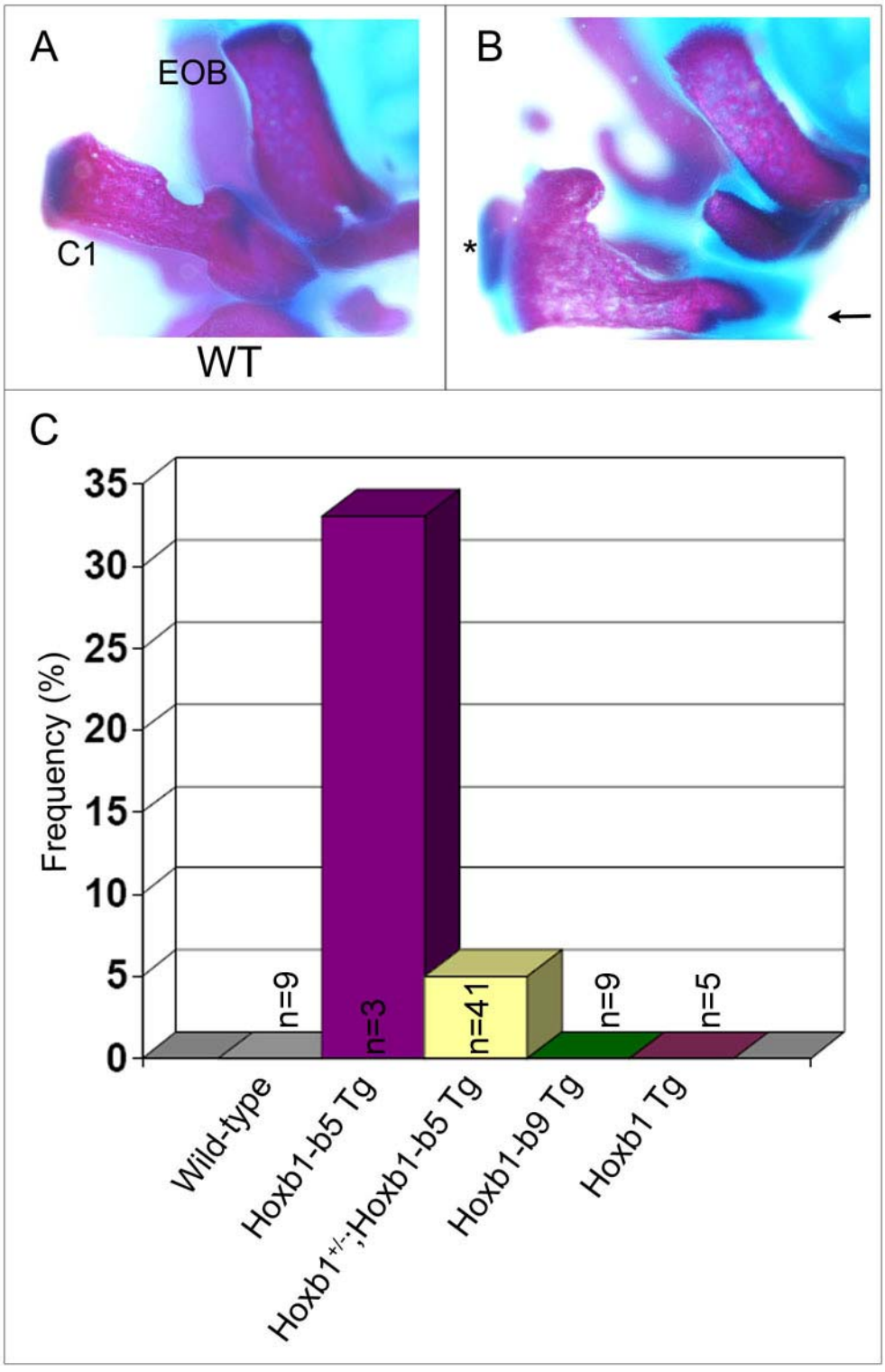
A
EOB
C1
WT
B
*
C
Frequency (%)
35
30
25
20
15
10
5
0
n=9
n=3
n=41
n=9
n=5
Wild-type
Hoxb1-b5 Tg
Hoxb1+/-;Hoxb1-b5 Tg
Hoxb1-b9 Tg
Hoxb1 Tg

Figure 33. Anterior transformation of T2 into a T1-like identity in transgenic mice with increased *HoxB* gene dosage

(A) Wild-type T1 and T2 vertebrae at 18.5dpc. T1 rib pairs join at the anterior-most portion of the sternum, the manubrium; T2 rib pairs join immediately posterior to the manubrium.

(B) Costal cartilages of T1 and T2 ribs fuse one or more times prior to joining the sternum (asterisk). Additionally, T2 ribs form an ectopic sternocostal junction at the manubrium (arrow). The *HoxB* transgenic mutants may demonstrate one or both of these defects that characterize the T2→T1 transformation.

(C) Fusion of the dorsal aspects of the T1 and T2 neural arches, representing an additional criterion for characterizing the T2→T1 transformation.

(D) Graph depicting the frequency of the T2→T1 transformation in transgenic mice with increased *HoxB* gene dosage: *Hoxb1-Hoxb5* transgenic (Tg) and *Hoxb1*$^{+/-}$;*Hoxb1-Hoxb5* Tg phenotypes were not significant; the *Hoxb1* Tg phenotype was statistically-significant with respect to wild-type (asterisk) and *Hoxb1*$^{+/-}$;*Hoxb1-Hoxb5* Tg mice (double asterisk).

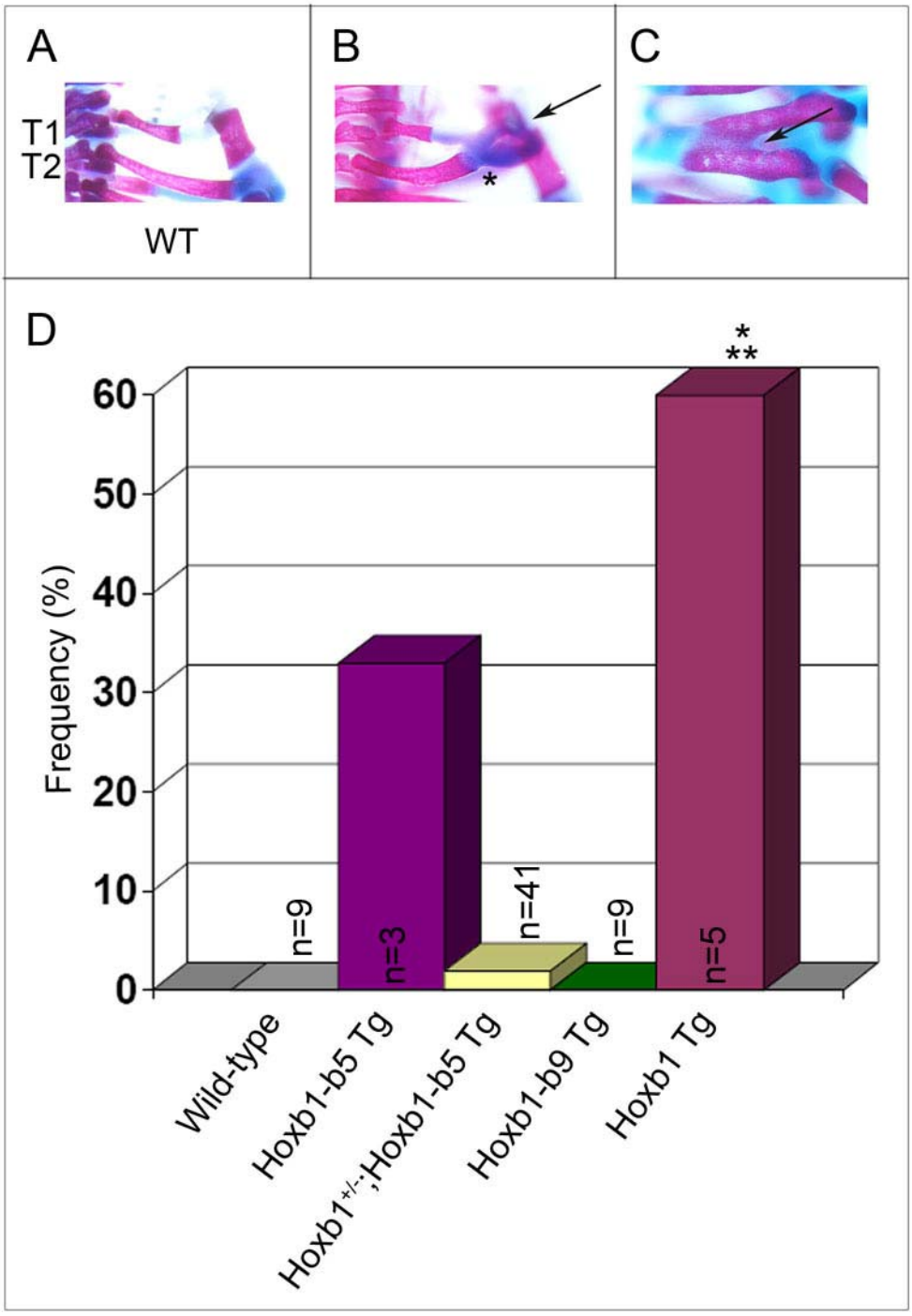
A
T1
T2
WT
B
*
C
D
*
**
60
50
40
30
20
10
0
Frequency (%)
n=9
n=3
n=41
n=9
n=5
Wild-type
Hoxb1-b5 Tg
Hoxb1+/-;Hoxb1-b5 Tg
Hoxb1-b9 Tg
Hoxb1 Tg

Figure 34. The presence of C7 rib anlage in wild-type and transgenic mice with increased *HoxB* gene dosage

(A) Seventh cervical vertebra as it is observed in wild-type 18.5dpc mice, without ribs heads extending from the transverse processes.

(B) Representative C7 rib anlagen (asterisks), as observed in some wild-type F1 mice and *HoxB* transgenic mutants, where it was present either unilaterally or bilaterally and as rib primordia or more developed cervical ribs.

(C) Graph depicting the frequency of C7 rib anlagen in wild-type F1 mice and transgenic mice with increased *HoxB* gene dosage: the *Hoxb1-Hoxb5* transgenic (Tg) phenotype was not significant; the *Hoxb1-Hoxb9* Tg phenotype was statistically-significant with respect to wild-type (asterisk).

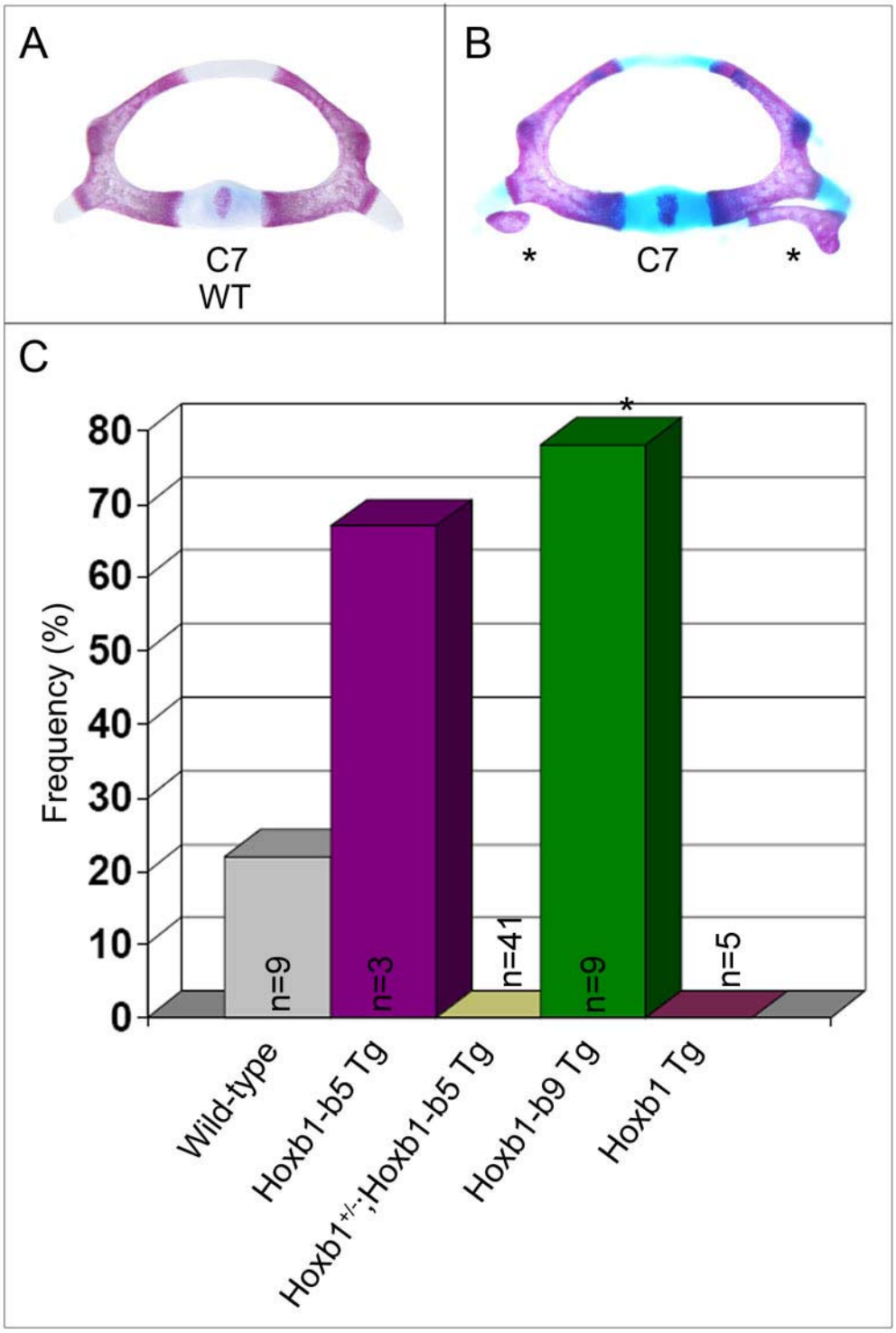
A
C7
WT
B
*
C7
*
C
Frequency (%)
80
70
60
50
40
30
20
10
0
n=9
n=3
n=41
n=9
n=5
*
Wild-type
Hoxb1-b5 Tg
Hoxb1+/-;Hoxb1-b5 Tg
Hoxb1-b9 Tg
Hoxb1 Tg

3.4.2 Increasing *Hoxb1-Hoxb5* gene dosage in the context of the *Hoxb1* mutation (KP1)

Next, we hypothesized that the previously described *Hoxb1* mutant phenotypes, including perinatal lethality, may be rescued by increasing the dosage of *Hoxb1* through the introduction of transgenes, specifically, the *Hoxb1-Hoxb5* transgene. To investigate this possibility, *Hoxb1* mutant mice were mated into the transgenic line that contained extra copies of *Hoxb1* through part of *Hoxb5*. The combination of genetic backgrounds in the resulting pups included 129s6/SvEv, CD1, CBA, and C57bl/10 strains. In order to be consistent in comparisons of all increased *HoxB* gene dosage mice, penetrance significance of phenotypes observed in these mutants was determined with respect to F1 (CBA x C57bl/10) wild-type mice.

Mutant mice were genotyped with respect to the *Hoxb1* mutant allele and the BAC transgene; those identified as *Hoxb1* heterozygotes that also contained the transgene ($Hoxb1^{+/-}$;Tg, aka KP1) were mated to maintain this new line as well as produce transgenic 18.5dpc embryos within the *Hoxb1* allelic series: $Hoxb1^{+/+}$; Tg, $Hoxb1^{+/-}$;Tg, and $Hoxb1^{-/-}$;Tg. Interestingly, an overwhelming majority of pups resulting from the above matings possessed the $Hoxb1^{+/-}$;Tg genotype. One $Hoxb1^{+/+}$;Tg embryo was produced, and no embryos were generated with the $Hoxb1^{-/-}$;Tg genotype. A total of 42 embryos were harvested in this line for skeletal analysis. The absence of *Hoxb1* homozygous transgenic mice in 18.5dpc embryo harvests suggested that the addition of the transgene fails to rescue neonatal lethality.

Hoxb1 heterozygous transgenic skeletons were able to recapitulate most of the skeletal defects observed in *Hoxb1-Hoxb5* transgenic animals, as well as some of the homeotic transformations seen in *Hoxb1* and *Hoxb2* single and double mutants. The presence of an ectopic EOB was observed at significantly increased penetrance over wild-type animals, occurring either unilaterally or bilaterally (Figure 31). Additionally, ectopic EOBs either fused anteriorly to the endogenous EOB, posteriorly to C1, or remained unfused. Occasionally, a thickening of the endogenous EOB was observed unilaterally or bilaterally. Two heterozygous transgenic embryos demonstrated an increase in the width of the C1 neural arch, but, as in *Hoxb1-Hoxb5* transgenic animals, this phenotype was not significantly penetrant (Figure 32). A partial C2→C1 transformation was present in two heterozygous transgenic animals, in which the dorsal aspects of C1 and C2 neural arches were fused; however, this phenotype was also not significantly penetrant (Figure 35). C6→C5 (Figure 36) and C7→C6 (Figure 37) transformations occurred in 12% and 7% of embryos, respectively, but these phenotypes were not significant with respect to wild-type mice. Thoracic transformations consisted of T1 rib shortening (T1→C7; Figure 38) and T2 rib bifurcation (Figure 33). Both instances affected only one mutant, each phenotype was present only unilaterally, and neither was statistically significant. The T2 rib bifurcation resulted in two sternocostal junctions: immediately anterior (ectopic) and posterior to the manubrium, indicating a partial T2→T1 anterior transformation. The presence of an ectopic EOB ossification center was the only highly penetrant phenotype observed in *Hoxb1*$^{+/-}$; Tg embryos. Interestingly, this was

Figure 35. Anterior transformation of C2 into a C1-like identity in transgenic mice with increased *HoxB* gene dosage

(A) Wild-type C1 and C2 vertebrae at 18.5dpc. An anterior arch of the atlas is present on the ventral aspect of C1.

(B) C2→C1 homeosis: the presence of an ectopic C1-like anterior arch on the ventral aspect of C2 (arrow) and fusion of the dorsal aspects of C1 and C2 neural arches (asterisk) characterize this transformation in *HoxB* transgenic mice.

(C) Graph depicting the frequency of C2→C1 transformation in transgenic mice with increased *HoxB* gene dosage: the *Hoxb1*$^{+/-}$;*Hoxb1-Hoxb5* Transgenic (Tg) phenotype was not significant; the *Hoxb1* Tg phenotype was statistically-significant with respect to wild-type (asterisk) and *Hoxb1*$^{+/-}$;*Hoxb1-Hoxb5* Tg mice (double asterisk).

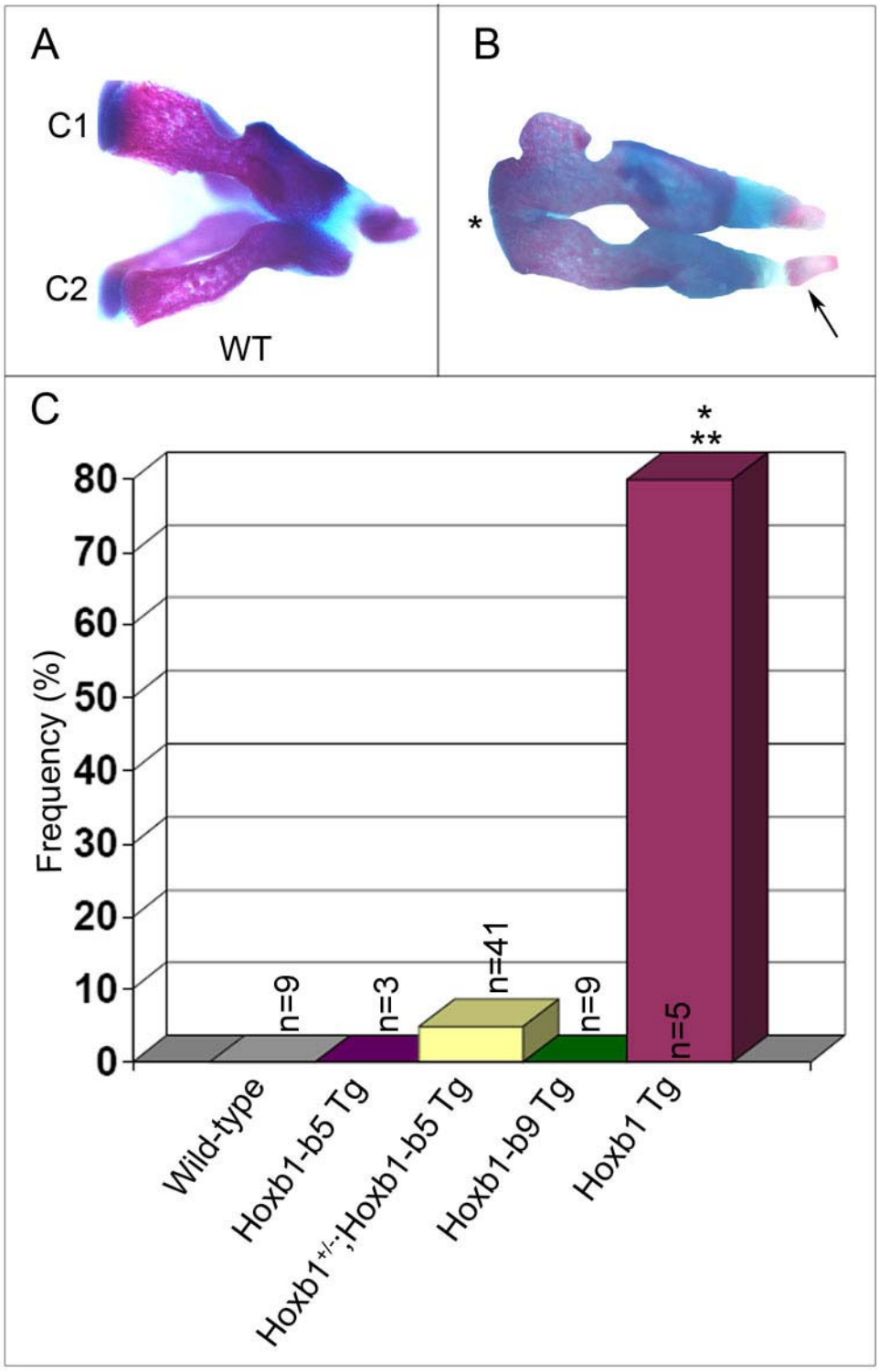
A
C1
C2
WT
B
*
C
*
**
80
70
60
50
40
30
20
10
0
Frequency (%)
n=9
n=3
n=41
n=9
n=5
Wild-type
Hoxb1-b5 Tg
Hoxb1+/-;Hoxb1-b5 Tg
Hoxb1-b9 Tg
Hoxb1 Tg

Figure 36. Anterior transformation of C6 into a C5-like identity in transgenic mice with increased *HoxB* gene dosage

(A) Wild-type C5 vertebra at 18.5dpc.

(B) Wild-type C6 vertebra with its unique ventrally-located bilateral anterior tuberculi.

(C) The bilateral absence of anterior tuberculi (asterisks) from C6 in *HoxB* transgenic mice.

(D) Graph depicting the frequency of C6→C5 transformation in transgenic mice with increased *HoxB* gene dosage: the *Hoxb1*$^{+/-}$;*Hoxb1-Hoxb5* Transgenic (Tg) phenotype was not significant; the *Hoxb1* Tg phenotype was statistically-significant with respect to wild-type (asterisk) and *Hoxb1*$^{+/-}$;*Hoxb1-Hoxb5* Tg mice (double asterisk).

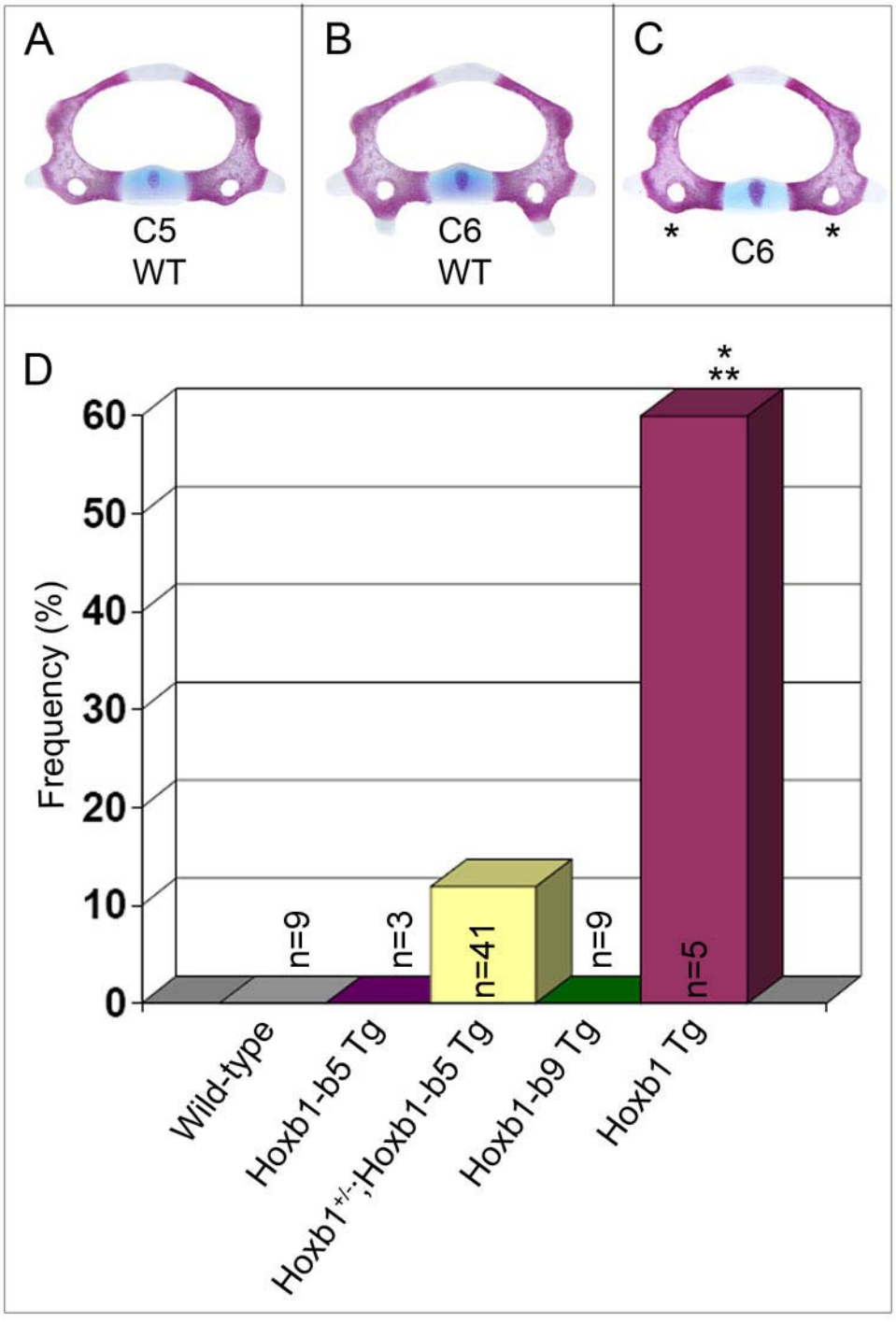
A
C5
WT
B
C6
WT
C
*
C6
*
D
Frequency (%)
60
50
40
30
20
10
0
*
**
n=9
n=3
n=41
n=9
n=5
Wild-type
Hoxb1-b5 Tg
Hoxb1+/-;Hoxb1-b5 Tg
Hoxb1-b9 Tg
Hoxb1 Tg

Figure 37. Anterior transformation of C7 into a C6-like identity in transgenic mice with increased *HoxB* gene dosage

(A) Wild-type C6 vertebra at 18.5dpc with vertebrarterial canals and bilateral anterior tuberculi.

(B) Wild-type C7 vertebra lacks both anterior tuberculi and vertebrarterial canals.

(C) The bilateral presence of anterior tuberculi (asterisks) and vertebrarterial canals (arrows) on C7 in *HoxB* transgenic mice.

(D) Graph depicting the frequency of C7→C6 transformation in transgenic mice with increased *HoxB* gene dosage: *Hoxb1*$^{+/-}$;*Hoxb1-Hoxb5* Transgenic (Tg), *Hoxb1-Hoxb9* Tg, and *Hoxb1* Tg phenotypes were not significant.

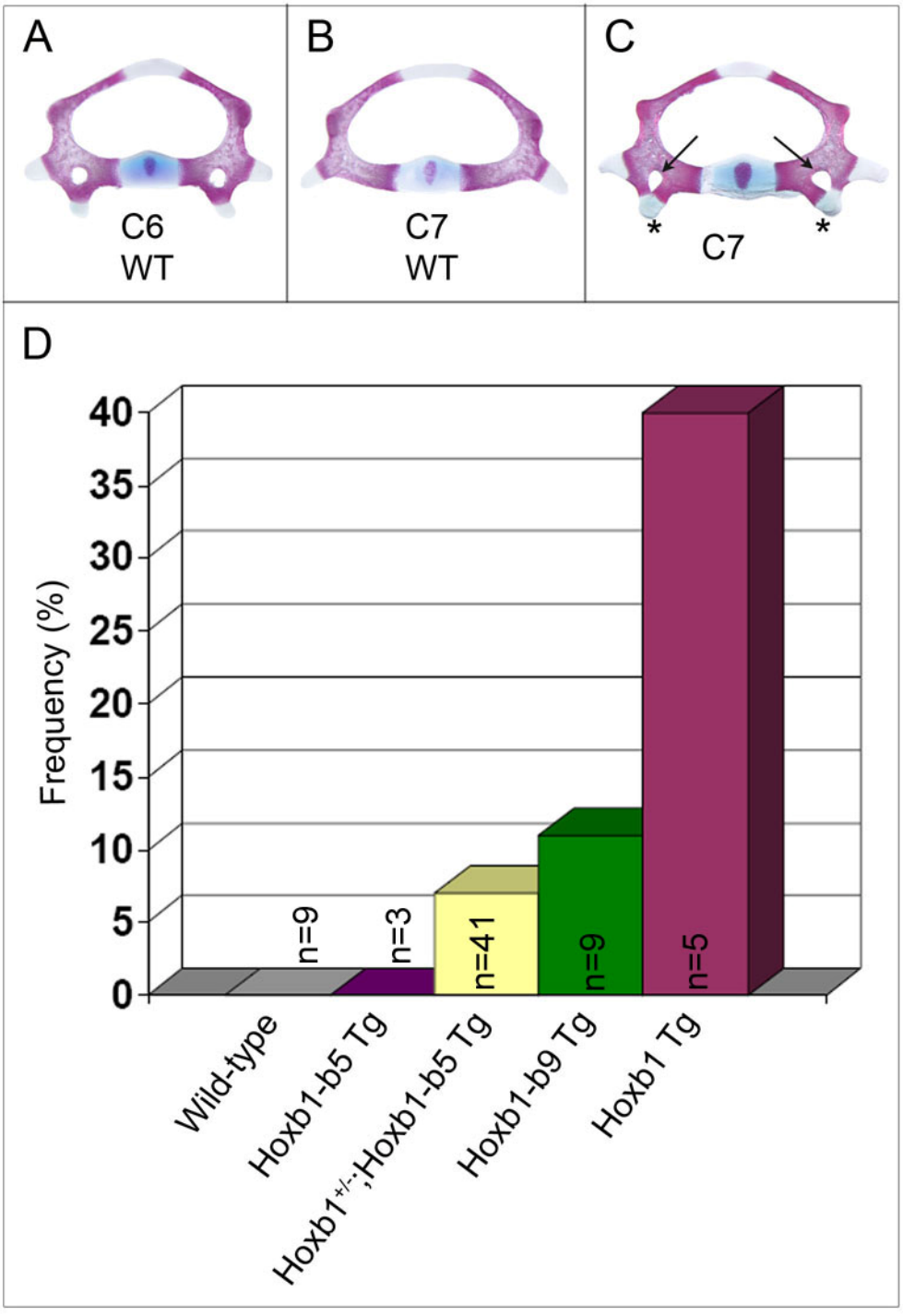
A
C6
WT
B
C7
WT
C
*
C7
*
D
Frequency (%)
40
35
30
25
20
15
10
5
0
n=9
n=3
n=41
n=9
n=5
Wild-type
Hoxb1-b5 Tg
Hoxb1+/-;Hoxb1-b5 Tg
Hoxb1-b9 Tg
Hoxb1 Tg

Figure 38. Anterior transformation of T1 into a C7-like identity in transgenic mice with increased *HoxB* gene dosage

(A) The C7 vertebra at 18.5dpc lacks cervical ribs in the majority of wild-type mice.

(B) Wild-type T1 vertebra with the first pair of ventrally-projecting thoracic ribs.

(C) The bilateral shortening of T1 ribs (asterisks) such that no contact is made with the sternum in *HoxB* transgenic mice.

(D) Graph depicting the frequency of T1→C7 transformation in transgenic mice with increased *HoxB* gene dosage: the *Hoxb1*$^{+/-}$;*Hoxb1-Hoxb5* Transgenic (Tg) phenotype was not significant; the *Hoxb1* Tg phenotype was statistically-significant with respect to wild-type F1 mice (asterisk).

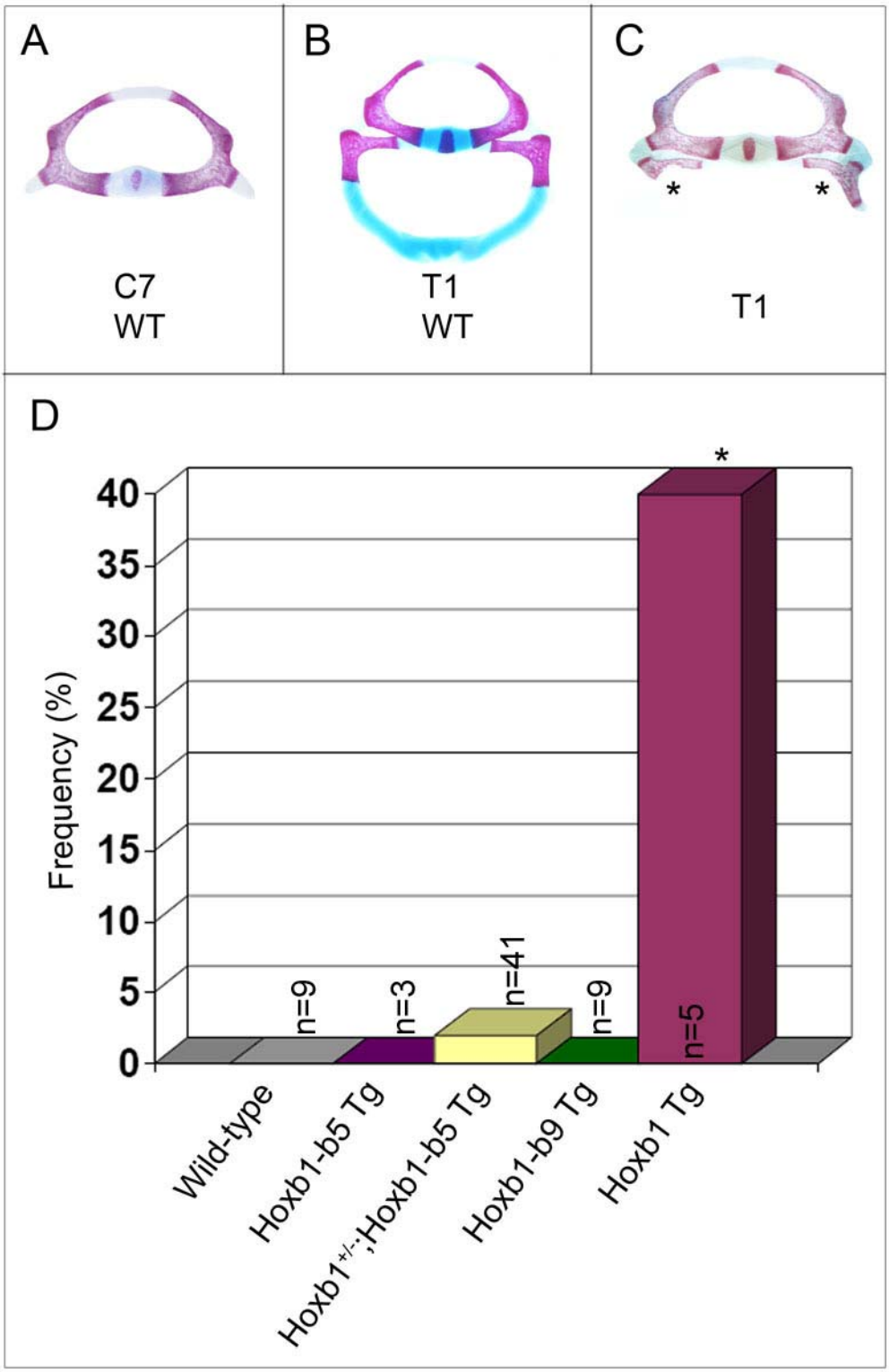
A
C7
WT
B
T1
WT
C
*
*
T1
D
Frequency (%)
40
35
30
25
20
15
10
5
0
n=9
n=3
n=41
n=9
n=5
*
Wild-type
Hoxb1-b5 Tg
Hoxb1+/-;Hoxb1-b5 Tg
Hoxb1-b9 Tg
Hoxb1 Tg

never observed in *Hoxb1* or *Hoxb2* single or compound mutants. Thus, this phenotype appears to be specific to the addition of increased copies of *Hoxb1* through partial *Hoxb5*, highlighting the importance of the complement of some of these genes in occipital bone development that is not appreciated through traditional loss-of-function studies involving *Hoxb2*, *Hoxb3*, *Hoxb4*, or *Hoxb5* mutations (Horan et al., 1995b).

3.4.3 Increasing *Hoxb1*-*Hoxb9* gene dosage (K828-47)

A 138kb BAC transgene containing *Hoxb1* through *Hoxb9* plus additional sequence on either side of the complex was used with the assumption that it would more completely recapitulate endogenous expression patterns, as compared to smaller transgenes. In order to monitor gene expression from this BAC, Youngwook Ahn inserted the reporters *eGFP*, *LacZ*, and *mCherry* in-frame into the coding regions of *Hoxb5*, *Hoxb7*, and *Hoxb9*, respectively. A stop codon at the end of each reporter ensures functional disruption of each of these genes. In contrast, *Hoxb6* and *Hoxb8* were labeled with c-terminal *Myc* and *FLAG* epitope tags, preserving their functionality. The remaining genes, *Hoxb1* through *Hoxb4*, were not altered (Figure 30B). Based on reporter gene expression analysis, this transgene seems to recapitulate endogenous *Hoxb5*, *Hoxb7*, and *Hoxb9* expression patterns. Thus, the remaining genes (*Hoxb1-Hoxb4*, *Hoxb6*, and *Hoxb8*) are also likely expressed normally. The resulting construct was used to generate a transgenic mouse line containing extra copies of *Hoxb1-Hoxb4*, *Hoxb6*, and *Hoxb8*, which was maintained in an F1 genetic background (CBA x C57bl/10). A single transgenic male was mated

to two F1 females, and embryos were harvested at 18.5dpc for skeletal analysis. Since these mice were generated in an F1 population, comparisons of all phenotypes to determine statistical significance was performed against stage-matched F1 embryos.

A total of 9 embryos were genotyped by PCR as transgenic positive mice. Unlike the previous transgenic mice, no defects were observed at the atlantoccipital joint or in the anterior cervical vertebrae. One embryo had rib anlagen present on C6 unilaterally (Figure 39). This same animal had a full transformation of C7→C6 on that same side. Partial unilateral C7→C6 transformations were observed in three transgenic embryos (Figure 37). Interestingly, C7 rib anlagen were present bilaterally in 78% of these mutants; the penetrance of this phenotype was found to be significantly increased over the observation of this variation in wild-type F1 animals (Figure 34). Two other wild-type variations (T8 rib sternocostal junctions and L1 ribs; Figures 40 and 41, respectively) were observed in transgenic skeletons, but they were not significantly increased over wild-type animals.

3.4.4 Increasing *Hoxb1* gene dosage (*Hoxb1*OE)

Because the penetrance of the majority of *Hoxb1* knock-out skeletal phenotypes is low, Christof Nolte in the lab devised a strategy for increasing the dosage of *Hoxb1* gene expression, and, in turn, Hoxb1 protein, in an attempt to further aggravate the defects in the axial skeleton. This strategy involved the generation of a plasmid-based transgene. The advantage of using a plasmid over a BAC is that plasmids are considerably smaller in size. Upon pronuclear

Figure 39. Partial anterior transformation of C6 into a T1-like identity in transgenic mice with increased *HoxB* gene dosage

(A) The wild-type C6 vertebra at 18.5dpc possesses both anterior tuberculi and vertebrarterial canals; cervical ribs are absent from this vertebra.

(B) The ectopic unilateral presence of rib primordium (asterisk) on the left side of the sixth cervical vertebra of a single *Hoxb1-Hoxb9* Tg embryo, suggesting a partial posterior C6→T1 transformation.

(C) Graph depicting the frequency of C6→T1 transformation in transgenic mice with increased *HoxB* gene dosage: the *Hoxb1-Hoxb9* Tg phenotype was not significant with respect to wild-type F1 mice.

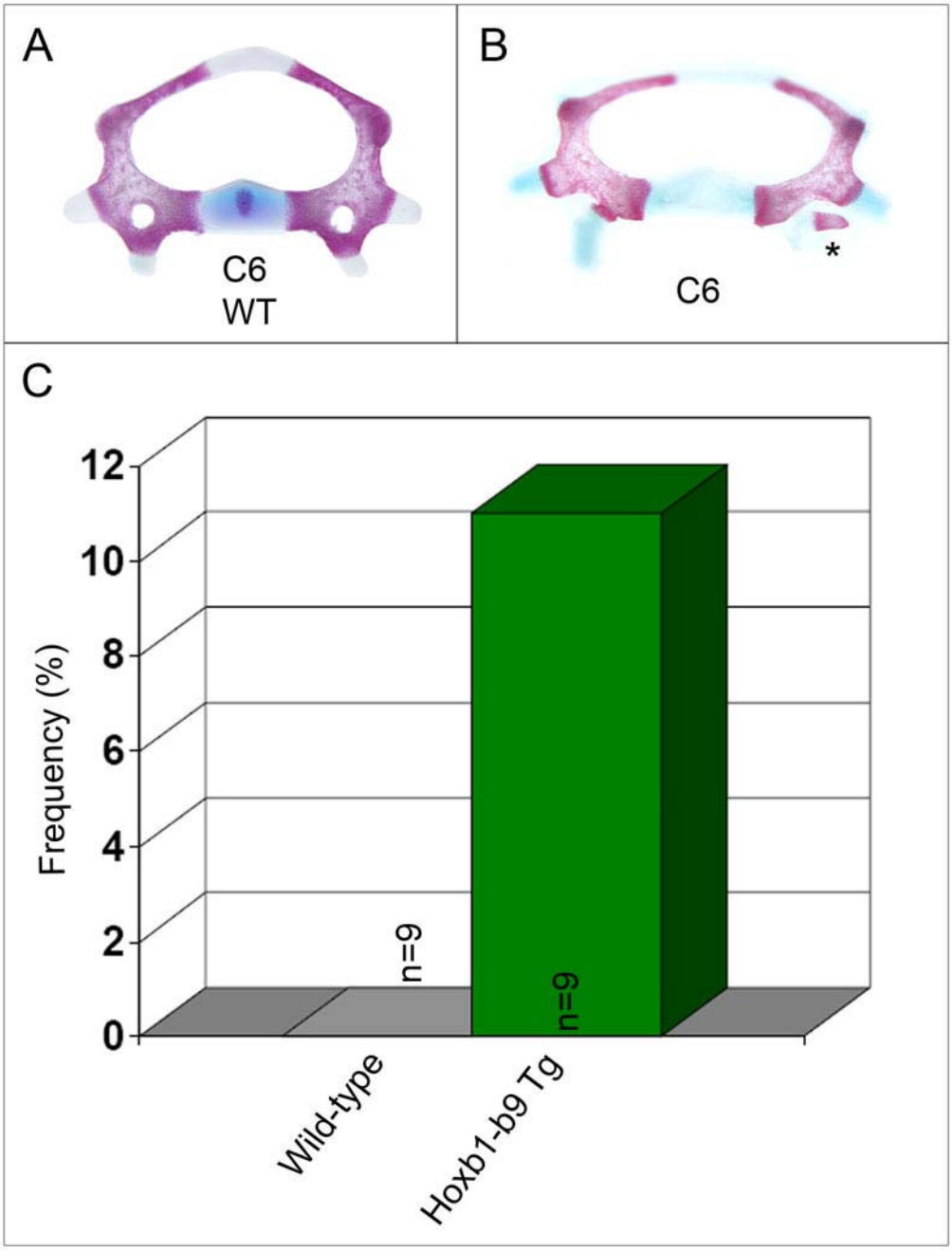
A
C6
WT
B
C6
*
C
Frequency (%)
12
10
8
6
4
2
0
n=9
n=9
Wild-type
Hoxb1-b9 Tg

Figure 40. Sternocostal junction of T8 ribs with the sternum in transgenic mice with increased *HoxB* gene dosage

(A) Ventral view of the sternum with its associated thoracic rib (R1-R7) sternocostal junctions as it is observed in the majority of wild-type mice at 18.5dpc.

(B) Ventral view of an additional junction of T8 ribs with the sternum (asterisks) in wild-type and *Hox* loss-of-function mutants. This variation was observed both unilaterally and bilaterally.

(C) Graph depicting the frequency of T8 rib sternocostal junctions in transgenic mice with increased *HoxB* gene dosage: the *Hoxb1-Hoxb9* Tg phenotype was not significant with respect to wild-type F1 mice.

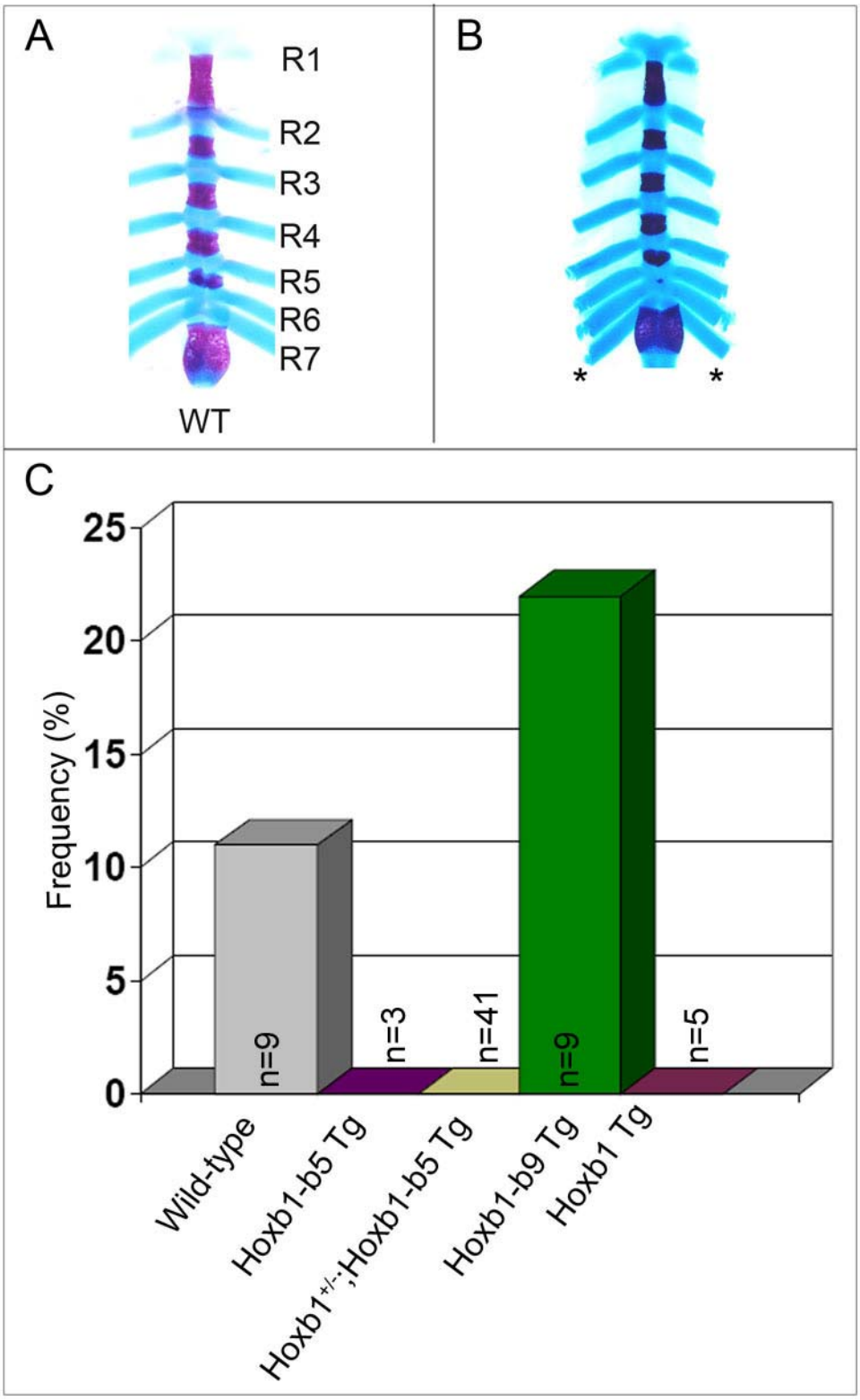
A
R1
R2
R3
R4
R5
R6
R7
WT
B
*
*
C
Frequency (%)
25
20
15
10
5
0
n=9
n=3
n=41
n=9
n=5
Wild-type
Hoxb1-b5 Tg
Hoxb1+/-;Hoxb1-b5 Tg
Hoxb1-b9 Tg
Hoxb1 Tg

Figure 41. The presence of ribs on the first lumbar vertebra in transgenic mice with increased *HoxB* gene dosage

(A) The first lumbar vertebra as it is observed in the majority of wild-type mice at 18.5dpc. L1 represents the first vertebra of the lumbar vertebral column and contains no ribs.

(B) L1 rib formations in wild-type and *HoxB* transgenic mice are present either unilaterally or bilaterally, as anlagen or fully-developed ribs.

(C) Graph depicting the frequency of L1 ribs in transgenic mice with increased *HoxB* gene dosage: the *Hoxb1-Hoxb9* Tg and *Hoxb1* Tg phenotypes were not significant with respect to wild-type F1 mice.

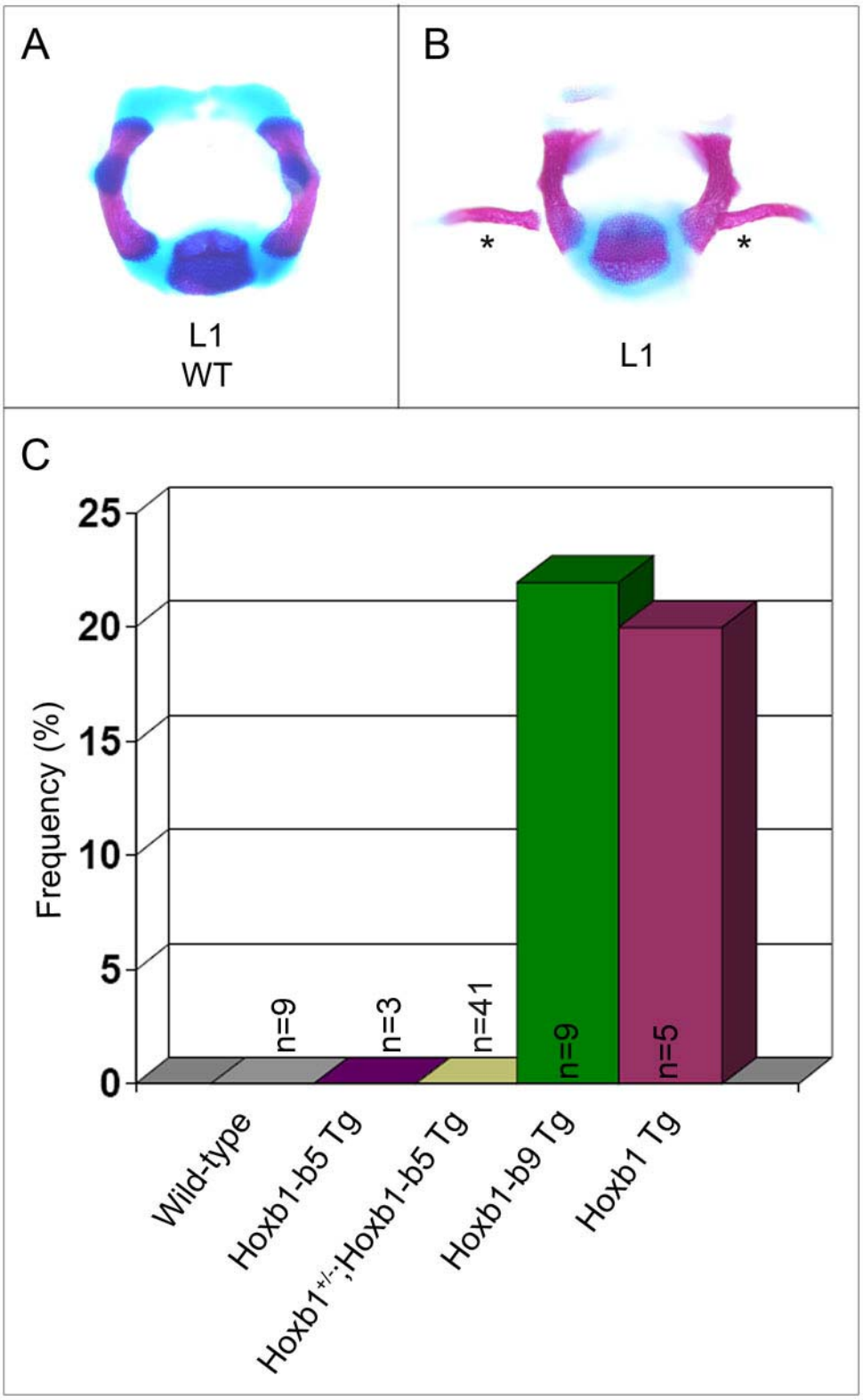
A
L1
WT
B
*
*
L1
C
Frequency (%)
25
20
15
10
5
0
n=9
n=3
n=41
n=9
n=5
Wild-type
Hoxb1-b5 Tg
Hoxb1+/-;Hoxb1-b5 Tg
Hoxb1-b9 Tg
Hoxb1 Tg

microinjection, plasmid transgenes are frequently integrated into the genome at higher copy numbers than are BAC transgenes, which are typically integrated as only one or two copies. Thus, the plasmid transgene would allow us to increase *Hoxb1* gene dosage to the greatest possible degree.

A plasmid-based transgene, containing 20kb of the endogenous *Hoxb1* locus, including all of the known *cis*-elements found in both the 5' and 3' regulatory regions, was microinjected into pronuclei of embryos harvested from CD1 superovulated donor females (Figure 30C). Two-cell stage embryos were transferred into F1 recipient females, who carried their litters to term. At weaning, the pups were genotyped by PCR with respect to the *Hoxb1* transgene. PCR-positive transgenic males and females were mated together, and litters were collected at birth (P0). PCR genotyping identified transgenic pups, whose skeletons were then prepared accordingly and analyzed for skeletal defects. To be consistent in comparisons with the previous *HoxB* transgenic mutants, phenotypes observed in the *Hoxb1* transgenic line were statistically analyzed with respect to F1 (CBA x C57bl/10) wild-type animals at 18.5dpc. While the P0 pups are slightly more developed than 18.5dpc embryos with respect to the skeleton, this did not interfere with our analysis of homeotic transformations and other skeletal malformations.

The most anterior transformation observed in *Hoxb1* transgenic mutants was a non-statistically significant unilateral fusion of C1 and C2 neural arches dorsally, similar to *Hoxb1*$^{+/-}$ mice with the *Hoxb1-Hoxb5* transgene (or extra copies of *Hoxb1* through *Hoxb5*; Figure 35). A C2→C1 transformation was the most penetrant

phenotype (80%) in these mutants and was determined to be statistically significant with respect to wild-type animals. C6→C5 and C7→C6 transformations were slightly less penetrant (60%) but were still significant compared to wild-type mice (Figures 36 and 37, respectively). Shortened T1 ribs (T1→C7) were observed in 2 (40%) of the transgenic mice, but were not significant (Figure 38). T2→T1 anterior transformations observed in transgenic mice were statistically significant and were characterized by both a fusion of T1 and T2 ribs and an ectopic T2 rib SCJ at the manubrium (Figure 33).

Taken together with the previous *HoxB* transgenic skeletal phenotypes, it is clear that increasing *HoxB* gene dosage both recapitulates several of the *HoxB* loss-of-function phenotypes and demonstrates new roles for *HoxB* genes in skeletal patterning by inducing novel phenotypes. One of the challenges of this transgenic mutant analysis has been in generating a sufficient number of embryos/pups for skeletal preparation. With small sample sizes, it is often difficult to determine whether the lack of certain phenotypes is due to sample number or actually reflects its absence in specific mutant lines. However, from the data generated, it is possible to draw some overall conclusions as to the impact of extra *HoxB* gene dosage on skeletal development. The penetrance of the ectopic EOB phenotype present in the *Hoxb1-Hoxb5* transgenic mice was increased in the same transgenic animals in the context of the *Hoxb1* loss-of-function mutation. A larger number of animals were collected from the latter group, supporting the idea that the low penetrance of this phenotype in *Hoxb1-Hoxb5* transgenic mice is due to small sample number (n=3). However, this

phenotype was never observed in the 9 *Hoxb1-Hoxb9* or 5 *Hoxb1* transgenic animals. A posterior prevalence phenomenon may explain the absence of this phenotype in *Hoxb1-Hoxb9* transgenic mice. This model postulates that the more posterior *Hox* gene products repress or antagonize anterior *Hox* gene products. Since *Hoxb1-Hoxb9* transgenic mice have increased functional copies of the more posterior *Hoxb6* and *Hoxb8* genes, it is possible that these genes' products are suppressing the ability of excess anterior *Hox* gene products (specifically, Hoxb1-Hoxb4) to influence the formation of an ectopic EOB. Unfortunately, this hypothesis does not explain why *Hoxb1* transgenic mice fail to produce ectopic EOBs, since there are not increased posterior *Hox* gene products present in these animals. Instead, the absence of this phenotype in *Hoxb1* transgenic mice suggests that ectopic EOB ossification may involve more than just Hoxb1 protein. There are two approaches that may be taken to distinguish between these two possibilities: 1) increase the sample size for each of the current transgenic lines; and 2) generate transgenic lines that singly increase *Hoxb2*, *Hoxb3*, and *Hoxb4* gene dosage. Together, both approaches should help to determine which gene(s) are responsible for patterning the transition between the occipital bone and cervical vertebrae.

3.5 Summary and Conclusions

Through the use of both loss- and gain-of-function approaches, we have been able to gain more meaningful insight into the roles of the anterior *Hox* genes, particularly, *Hoxa1*, *Hoxb1*, and *Hoxb2*, in patterning the axial skeleton. Interestingly, similar homeotic transformations were obtained whether gene copies

were increased or decreased, indicating that appropriate levels of gene dosage are critical to establish vertebral identity. From the data presented in this chapter, it is evident that an individual gene's dosage alone is important, as well as in the context of a neighboring gene (e.g., *Hoxb1* and *Hoxb2*).

With respect to *Hoxa1* mutants, there did not appear to be a significant impact on skeletal transformations. A single heterozygote possessed reciprocal transformations of C5→C6 and C6→C5 on the animal's left side. According to the gene dosage model, it would follow that these phenotypes would increase in penetrance as more copies of *Hoxa1* were eliminated. However, this was not the case, since defects of the axial skeleton were completely absent from *Hoxa1* single homozygotes. In the context of simultaneous *Hoxb1* mutations, the penetrance of vertebral anteriorizations increased significantly in $Hoxa1^{+/-}$;$Hoxb1^{-/-}$ compound mutants. Although statistical significance was assigned to phenotypes observed in *Hoxa1*/*Hoxb1* double homozygotes, the sample number (n=2) is simply too small to draw meaningful conclusions. The absence of significant phenotypes in $Hoxa1^{-/-}$;$Hoxb1^{+/-}$ mice further supports the conclusion that *Hoxa1* does not play a significant role in vertebral identity, since removing copies of this gene in the compound mutant condition fails to increase the severity or penetrance of vertebral homeotic transformations. Thus, the observation of skeletal transformations in *Hoxa1*/*Hoxb1* double mutants is likely due to the loss of *Hoxb1* gene function.

Hoxb1 and *Hoxb2* mutants, however, demonstrated several significant anterior transformations among cervical and thoracic vertebrae, particularly restricted to the

craniocervical and cervicothoracic boundaries (C2→C1, C6→C5, C7→C6, T1→C7, and T2→T1). Unlike *Hoxa1*/*Hoxb1* double mutants, the simultaneous heterozygous mutation of *Hoxb1* and *Hoxb2* (*Hoxb1*$^{+/-}$;*Hoxb2*$^{+/-}$ transheterozygotes) produced mutants whose cervical and thoracic vertebrae were similarly transformed. Except for the C2→C1 and T1→C7 transformations, the penetrance of all double mutant phenotypes were significantly increased over wild-type mice. Furthermore, increased statistical significance was also assigned for these phenotypes with respect to *Hoxb1* and *Hoxb2* single heterozygotes. In other words, an additive effect on phenotypic penetrance was observed in *Hoxb1*/*Hoxb2* double mutants, since phenotypes became increasingly penetrant in mice whose gene dosage of both *Hoxb1* and *Hoxb2* was reduced by one-half.

The results from single and double loss-of-function studies clearly indicated an important role for *Hox* gene dosage in the correct specification of elements within the axial skeleton. Through the use of three transgenic lines, we investigated the developmental impact of increasing *Hox* gene dosage on patterning vertebral identity. By simply increasing *Hoxb1* gene dosage alone, we were able to recapitulate all five of the *Hoxb1* loss-of-function homeotic transformations. The C2→C1, C6→C5, and T2→T1 anteriorizations showed increased penetrance over wild-type mice; though *Hoxb1* transgenic mice possessed C7→C6 and T1→C7 transformations, these phenotypes were found to be not significantly increased with respect to wild-type mice. However, the T1→C7 transformation was determined to be present at more significant levels than the same phenotype in *Hoxb1*$^{+/-}$;*Hoxb1-Hoxb5* transgenic

animals. Some of these transformations were also observed in mice containing transgenes carrying extra copies of either *Hoxb1-Hoxb5* or *Hoxb1-Hoxb9*, but statistical significance of these phenotypes could not be assigned.

Aside from cervical and thoracic transformations, increasing *Hoxb1-Hoxb5* gene dosage produced a novel and statistically significant phenotype that was not observed during *Hoxb1* single mutant analysis. The presence of an ectopic exoccipital bone in *Hoxb1-Hoxb5* transgenic animals alone or in the context of the *Hoxb1* loss-of-function mutation provided some insight into the role of anterior *HoxB* genes at the level of the developing occipital bone. Since this phenotype was not seen in *Hoxb1* mutants, it is possible that an ectopic EOB results from increased gene dosage of *HoxB* genes that lie more 5' to *Hoxb1* (i.e., *Hoxb2-Hoxb5*).

Until now, the comprehensive contributions of these anterior *Hox* genes during skeletal development were previously unknown. Taken together, these results help to establish a position for the anterior *HoxB* genes, specifically, *Hoxb1* and *Hoxb2*, in the hierarchy of factors that contribute to vertebral patterning.

Chapter 4

Discussion

The aim of this project was to address the roles that early anterior *Hox* genes, specifically, *Hoxa1*, *Hoxb1*, and *Hoxb2*, play in patterning various vertebral regions during skeletal development. To that end, I have characterized several skeletal malformations and one-segment anterior homeotic transformations among single *Hoxa1*, *Hoxb1*, and *Hoxb2* mutants, as well as *Hoxa1*/*Hoxb1* and *Hoxb1*/*Hoxb2* compound mutants. Through the use of transgenic mouse lines carrying extra copies of *HoxB* genes, generated by members of the Krumlauf lab, it became possible to investigate the functional consequences of increased HoxB protein on skeletal development. Interestingly, several key phenotypes were shared in common, whether *Hox* gene products were increased or decreased, through the use of transgenic or loss-of-function mouse lines, respectively. This result was surprising initially, since we suspected that increasing *HoxB* gene dosage would produce an effect that was opposite from that obtained through loss-of-function studies. For example, since *Hoxb1* homozygous mutants demonstrated anterior homeotic transformations, perhaps increasing *Hoxb1* gene dosage would cause the same vertebrae to take on more posterior identities. Instead, similar anterior transformations were retained in *Hoxb1* transgenic mice.

Furthermore, several of the transformations/skeletal defects identified during the course of this study overlap with those previously reported in mice harboring single and multiple mutations of the more posterior *Hox* genes. The split of the C1

neural arch that was observed in our *Hoxa1*/*Hoxb1* double homozygotes has been previously reported in *Hoxd4* heterozygotes and homozygotes (Barrow and Capecchi, 1996; Condie and Capecchi, 1993; Horan et al., 1995a; Manley et al., 2001; Manley and Capecchi, 1997; Medina-Martinez et al., 2000). The C2→C1 transformation observed in our *Hoxb1* and *Hoxb2* mutants was also detected separately in *Hoxb2*, *Hoxb3*, *Hoxb4*, *HoxBΔ1*, *Hoxd3*, and *Hoxd4* loss-of-function mutants (Horan et al., 1995b; Jeannotte et al., 1993; Medina-Martinez et al., 2000; Rancourt et al., 1995); the C6→C5 transformation in *Hoxa5*, *Hoxb5*, *Hoxb6* single mutants, *HoxBΔ1* mutants, and *Hoxa4*/*Hoxb4*, *Hoxa4*/*Hoxd4*, and *Hoxb4*/*Hoxd4* double mutants (Chen et al., 1998; van den Akker et al., 2001); the C7→C6 and T1→C7 transformations in many of the same mutants as the previous transformation, as well as *Hoxb7* single and *Hoxb8*/*Hoxc8* and *Hoxb8*/*Hoxd8* double mutants (Chen and Capecchi, 1997; Chen et al., 1998; Garcia-Gasca and Spyropoulos, 2000; Medina-Martinez et al., 2000; Medina-Martinez and Ramirez-Solis, 2003; Rancourt et al., 1995; van den Akker et al., 2001); and the T2→T1 transformation in *Hoxa11*, *Hoxb6*, *Hoxb7*, *Hoxb8*, *Hoxb9*, *Hoxc6* single mutants, *HoxBΔ1* mutants, and *Hoxb8*/*Hoxc8* and *Hoxb8*/*Hoxd8* double mutants (Lufkin et al., 1992). Interestingly, the occipital bone defects observed in our *Hoxa1*/*Hoxb1* double loss-of-function mutants and *Hoxb1-4* gain-of-function transgenic mice, specifically, fusion of the EOB to the BOB and an ectopic EOB (respectively), have been described in *Hoxd4* overexpression mutants. The *Hoxd4* gene was ectopically expressed under the *Hoxa1* promoter, driving its expression limit to a more rostral anterior boundary (Barrow and Capecchi, 1996;

Garcia-Gasca and Spyropoulos, 2000; Manley et al., 2001; Medina-Martinez and Ramirez-Solis, 2003; Ramirez-Solis et al., 1993; van den Akker et al., 1999). The resulting phenotype consisted of ectopic arches located between the endogenous EOBs and C1 vertebrae, as well as ventral fusions of the EOB and BOB. The authors classified these arches as C1 posterior transformations, since they claim that the ectopic formations more closely resemble the C1 vertebra. In our *Hoxb1-4* transgenic mice, however, the ectopic bone formations at 18.5dpc have not developed C1 vertebral characteristics, such as a wide neural arch, lateral foramina, and an aaa. Morphologically, they appear to more closely resemble the EOB. For these reasons, I propose that they represent duplications of the EOB that may be found fused anteriorly to the endogenous EOB, fused posteriorly to the endogenous C1, or completely unfused to either of these elements.

Sternal malformations, including reduction in the number of sternebrae and complete sternum bifurcation, were also previously reported in *Hoxb2*, *Hoxb4*, *Hoxb8*, and *Hoxc6* single mutants (McIntyre et al., 2007; Wellik, 2007). Special consideration must be given to this classification of skeletal phenotypes, since the origin of the sternum (lateral plate mesoderm) is different from the rest of the axial skeleton (somitic mesoderm). Previous studies have demonstrated that *Hox* patterning of each of these mesodermal tissues occurs independently. Specifically, the anterior boundary of gene expression for many of the *Hox* genes in the somitic mesoderm is significantly offset from expression limits in the lateral plate mesoderm (Nowicki and Burke, 2000). Furthermore, heterotopic transplantation of donor PSM

into a host embryo imparts the donor's *Hox* patterning information that is maintained in the host somitic tissue. The same does not hold true for the migration of the transplanted donor cells into the host lateral plate mesoderm; instead of retaining the donor *Hox* patterning information, these cells adopt the expression pattern of the host (Hassan et al., 2007). These observations strongly support the hypothesis that the influence of *Hox* genes in the somitic and lateral plate mesoderm occurs by independent mechanisms, just as *Hox* gene expression and patterning of neural and somitic mesoderm tissues are separate. However, with respect to sternal malformation, results from the present study demonstrate that *Hoxb1* and *Hoxb2* single homozygous mutants are similarly affected and that this phenotype is also partially-penetrant in compound *trans*-heterozygotes. Similar observations were made for cervical and thoracic homeotic vertebral transformations within *Hoxb1* and *Hoxb2* single and double mutant lines, suggesting that, with respect to these two *HoxB* genes, equivalent synergistic interactions may function in patterning both the paraxial and lateral plate mesoderm.

Finally, the remaining phenotypes observed in our *Hox* loss-of-function and transgenic mice (SOB perforation, increase in C1 neural arch width, and C5→C6 and C6→T1 posterior transformations) represent novel, yet significant, phenotypes that were previously unreported in *Hox* mutants.

Even though several of loss-of-function *Hox* mutants possess multiple anterior transformations, there is not a single mutant that contains all of the cervical and thoracic transformations that were identified in *Hoxb1* loss-of-function mutants

during the course of the present study. While clearly establishing a role for *Hoxb1* in vertebral patterning, these results also suggest that *Hoxb1* is responsible for imparting vertebral identity information to a wider range of cervical and thoracic vertebrae than other *Hox* genes. An explanation for this finding is addressed below.

Interestingly, the experiments reported in this dissertation revealed several anterior homeotic transformations that are shared in common among *Hoxb1* and *Hoxb2* single and compound loss-of-function mutant lines. One explanation for this result may be that a similar regulatory element is responsible for directing expression of both of these genes in the PSM. Previous unpublished work in the lab has shown that a mesodermal enhancer element located in the 3' control region of the *Hoxb1* locus is sufficient to recapitulate this gene's expression profile in mesoderm from 7.5dpc-10.5dpc. Since sharing of regulatory elements often comes as a consequence of *Hox* gene chromosomal clustering (Gérard et al., 1996), it is possible that the same mesodermal enhancer acts more globally on neighboring *HoxB* genes, namely, *Hoxb2*. Since this *cis*-acting element is located closer to *Hoxb1* than to *Hoxb2*, its effect on *Hoxb1* mesodermal expression is likely more pronounced. This hypothesis is consistent with the observation that the overall occurrence and penetrance of cervical and thoracic vertebral transformations are increased in *Hoxb1* single mutants, compared to *Hoxb2* single mutants. Additionally, the most anterior cervical transformation (C2→C1) was previously reported in *Hoxb3* and *Hoxb4* single loss-of-function mutants, and C6→C5 transformations were reported in *Hoxa4*/*Hoxb4* and

Hoxb4/*Hoxd4* double loss-of-function mutants. Thus, sharing of this mesodermal element may also extend to the more posterior *HoxB* genes.

Kristen Correia in the Krumlauf lab identified consensus Cdx and Lef/Tcf binding sites within the known *Hoxb1* mesodermal enhancer; thus, it is likely that this element is capable of integrating Wnt signals present as the PSM undergoes segmentation into somites. However, Hox/Pbx responsive sites have not been identified within this enhancer, and *Hoxb1* mesodermal expression is transient. If such sites were to be identified within this region (or in a second mesodermal enhancer that has yet to be identified), then it is possible that Hox proteins could be involved in auto- and cross-regulatory loops that maintain expression in the PSM, similar to the mechanism for maintaining expression in r4 of the hindbrain.

To explain the common phenotypes observed in both *HoxB* loss- and gain-of-function mice, the following two models are proposed that incorporate both *cis*- and *trans*- regulation (Figure 42). Under the *cis*-regulatory model (Figure 42A), the same enhancer is required to pattern the expression of each anterior *HoxB* gene in the mesoderm. This regulatory effect on *Hoxb1* would likely be the greatest, since it is the closest gene to the enhancer. Nevertheless, the mesodermal inputs are similarly affected through the same enhancer. Under the *trans*-regulatory model (Figure 42B), the enhancer influences *Hoxb1* mesodermal expression only. Hoxb1 protein may then regulate mesoderm expression through the *Hoxb2* locus; Hoxb2 protein then regulates the *Hoxb3* locus, and so on. Thus, in the *trans*-regulatory model, HoxB proteins themselves are major players in the cascade of factors that pattern vertebral

Figure 42. Models of *cis*- and *trans*-regulation for *HoxB* gene mesodermal patterning

(A) Schematic representation of the mesodermal enhancer's *cis*-effects on anterior *HoxB* genes, *Hoxb1-Hoxb4*. Sharing of this element among *HoxB* genes suggests that similar phenotypes arise in single mutants.

(B) Schematic representation of a *trans*-regulation model in which anterior Hox proteins regulate neighboring loci though a cascade effect. Changes within a single locus carry knock-on effects for downstream loci.

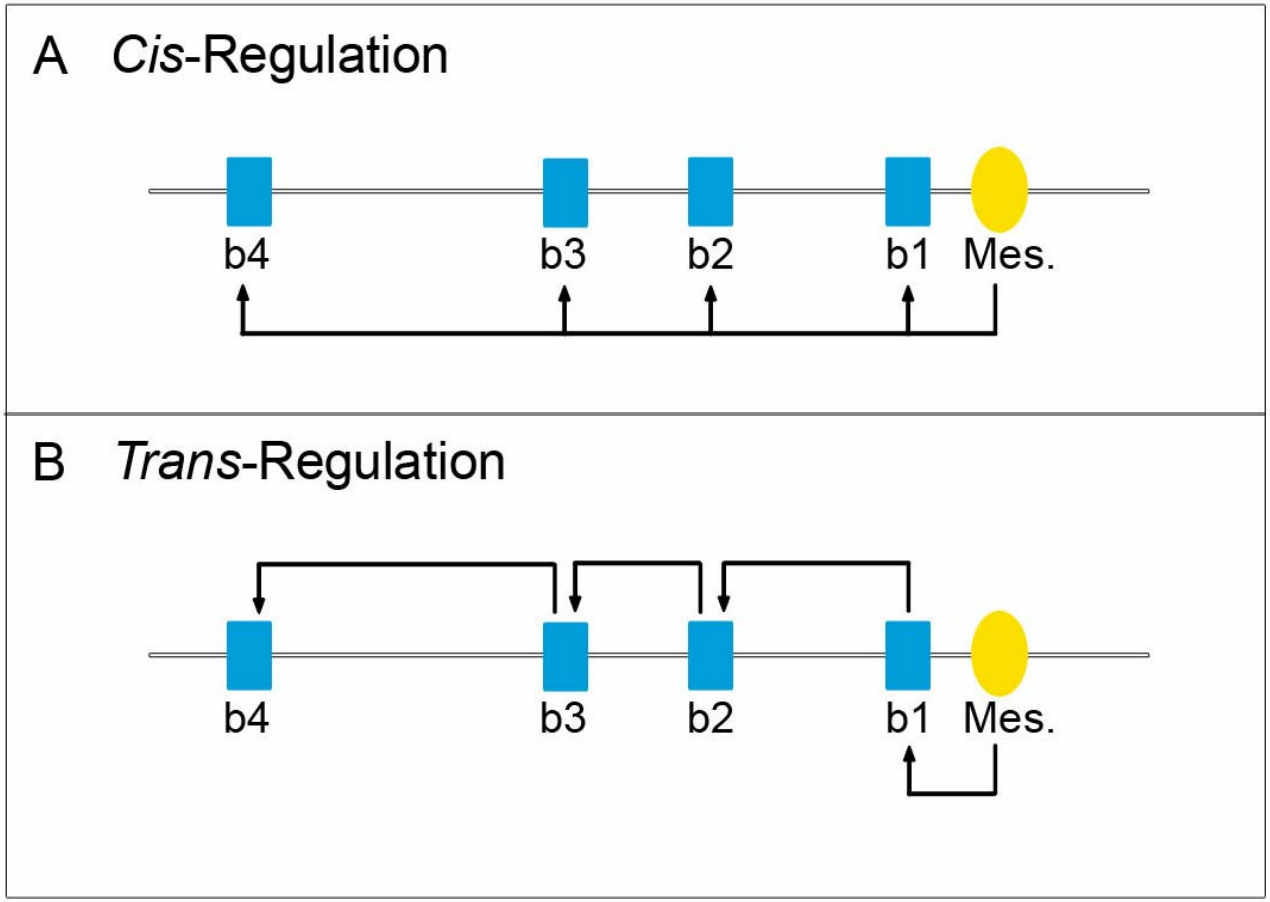
A *Cis*-Regulation
b4
b3
b2
b1
Mes.
B *Trans*-Regulation
b4
b3
b2
b1
Mes.

precursors. As individual copies of *HoxB* genes are either increased or decreased, there may be more deleterious consequences under this model. Altering the dosage of an upstream factor in the cascade (i.e., *Hoxb1*) would more significantly impact axial identity than would a shift in the dosage of a downstream factor (i.e., *Hoxb3*). In *Hoxb1* homozygous loss-of-function mutants, no functional Hoxb1 protein is produced. In the absence of Hoxb1 protein, the positive cross-regulatory input into downstream *HoxB* genes is lost, resulting in fewer *HoxB* transcripts available to impart axial information to the unsegmented mesoderm. When more Hoxb1 protein is produced through gain-of-function transgenesis, positive cross-regulation of downstream *HoxB* genes resumes, generating more *HoxB* transcripts than are normally sufficient to appropriately pattern vertebral precursors. In either case, loss or gain of HoxB function perturbs the overall levels of downstream *HoxB* genes' dosages. These results presented here, along with previously published reports, indicate that gene dosage plays an important role in specifying the unique identities of each vertebra. Thus, altering *HoxB* gene copy numbers in either direction generates similar skeletal phenotypes.

To test whether the above models of *HoxB cis*- and/or *trans*-regulation function in patterning vertebrae, one could conditionally eliminate the known *Hoxb1* mesodermal enhancer. If it functions as proposed above, then the resulting mice should contain the skeletal phenotypes described in the present survey of *HoxB* mutants. Additionally, whether the enhancer is shared or initiates the HoxB protein cascade effect, the penetrance of each phenotype should also increase, as a result of

the misregulation of each gene's expression profile in the mesoderm. To further investigate the underlying molecular mechanism, a two-fold approach could be taken. First, conditional mesodermal enhancer deletion mice are mated into a transgenic fluorescent reporter mouse line, in which each of the anterior *HoxB* (*Hoxb1-Hoxb4*) genes has been targeted with a unique fluorochrome. Deviations from endogenous *HoxB* gene expression patterns (i.e., shifts in anterior boundaries) would indicate that the enhancer regulates more than just *Hoxb1* mesoderm expression. Secondly, cervical and anterior thoracic somites are dissected out from early embryos (both wild-type and conditional mesodermal enhancer deletion mice), and RNA purified from these somites is hybridized to an Affymetrix microarray chip. The cervical and anterior thoracic somites are chosen since the *HoxB* mutant phenotypes were restricted to these regions. RNA from posterior thoracic somites may be included as an internal control. If the enhancer also regulates *Hoxb2*, *Hoxb3*, and *Hoxb4* mesodermal expression either in *cis* or *trans*, then the microarray data should reflect a relative decrease in each gene's mRNA expression, compared to wild-type. To show that this effect is mediated through cross-regulation involving *Hoxb1*, one would compare the relative mRNA levels of *Hoxb2-Hoxb4* among the same somites isolated from enhancer deletion mice and *Hoxb1* homozygous mice, which should reflect a similar decrease with respect to wild-type mice.

Of course, other *Hox* genes may not be the only genes involved in perpetuating the skeletal patterning information established by *Hoxb1* in the PSM. The genetic regulatory network downstream of *Hoxb1* that is responsible for

providing segmental identity to the vertebrae may involve non-*Hox* genes. The onset of *Hoxb1* gene expression is relatively early in development and transcripts are only detected for a short period of time (7.5dpc-9.5dpc) in the PSM, thus limiting the pool of candidate downstream effectors of *Hoxb1* expression. Such targets would have to be expressed during the same developmental window in the PSM, as well as later on in the somitic lineages that give rise to vertebral precursors. In this way, a target gene could facilitate the execution of the patterning program set up by *Hoxb1*. As an example, previous work has shown that *Hoxa10* targets *Runx2*, a transcription factor important for osteogenesis, in order to maintain the patterning information that this *Hox* gene imparts during early skeletal development to the precursors of the posterior vertebrae (Burgess et al., 1995). Furthermore, immunohistochemical analysis of both long bones and vertebrae showed colocalization of Hoxa10 and Runx2 proteins to the same cells of the osteogenic lineage.

The gene *Paraxis* may represent a potential downstream target for Hoxb1, since it has an important role in patterning the vertebral precursors and is expressed during the same developmental window as *Hoxb1* transcripts. Initially, *Paraxis* transcripts are expressed in the primitive mesoderm at 7.5dpc (Frohman et al., 1990), which overlaps with the initiation of *Hoxb1* gene expression . By 8.5dpc, *Paraxis* is strongly expressed in the newly-formed epithelial somites. As the somites begin to mature and undergo compartmentalization, *Paraxis* expression may be found in both the dermamyotome and sclerotome portions of the somite. Gradually, its expression declines in mature somites. However, a related gene, *Scleraxis*, is first expressed at

10.5dpc, and its expression profile overlaps with that of *Paraxis* initially in the sclerotome. As *Paraxis* expression decreases, *Scleraxis* expression increases and is maintained in the chondrogenic precursors that give rise to vertebrae. Thus, a possible mechanism for potentiating the patterning information imparted by *Hoxb1* in the PSM may involve both *Paraxis* and *Scleraxis* gene products. Together, these two genes meet the criteria proposed above for identifying potential downstream targets: 1) expression overlaps with *Hoxb1* in the appropriate tissue, and 2) target gene expression continues into cell lineages that will give rise to vertebral precursors. The above approach for discovering downstream targets is based solely upon a search of the published literature. The microarray approach described above will likely identify more meaningful candidates, upon comparison of genes that are either up- or down-regulated in somitic mesoderm isolated from *Hoxb1* loss-of-function mutants and wild-type mice.

Equally important to the genetic regulatory network are the factors that lie upstream of *Hoxb1* in the skeletal patterning hierarchy. Based upon the results obtained in this study from *Hoxa1*/*Hoxb1* double loss-of-function mutants, it is unlikely that Hoxa1 directly regulates *Hoxb1* in the paraxial mesoderm, as it does in r4 of the hindbrain. If such an interaction were to occur, we would have expected phenotypic penetrance to increase over single mutants, as copies of *Hoxa1* and *Hoxb1* were eliminated through simultaneous mutations. Thus, one may conclude that the synergistic relationship between these two genes that was illustrated in the hindbrain may not, in fact, play as prevalent a role in the paraxial mesoderm.

Another important input into Hoxb1 function in the hindbrain is retinoic acid (RA). With respect to skeletal patterning, though, RA exposure during late gastrulation stages (8.0dpc) resulted in anterior shifts in the identities of vertebrae within the mid-thoracic and more posterior regions, in addition to fusions of the EOB's to the BOB. Interestingly, RA exposure from 10.5dpc onward caused posterior transformations first in the anterior vertebrae, particularly, C5 through C7, and then in more caudal regions. The authors of this study also demonstrated a shift in the expression limits of the posterior *Hox* genes, correlating with the anterior homeotic transformations described (Kessel, 1992).

Similar vertebral elements were transformed in our *Hoxb1* and *Hoxb2* loss-of-function mutants, as well as in transgenic mouse lines carrying extra copies of *HoxB* genes. The overlap in phenotypes suggests that RA and specific codes of *Hox* genes share roles in establishing the early developmental programs for vertebral precursors. We know from previous work that RA lies upstream of *Hox* genes in regulatory networks that pattern neural and endodermal tissues. However, these studies have also shown that the 3' regulatory enhancer element responsible for *Hoxb1* expression in the paraxial mesoderm is unresponsive to retinoid signaling, in contrast to the neural and foregut enhancers (Marshall et al., 1994). Nevertheless, exposure of early gastrulation stage embryos to RA shifted the anterior limit of *Hoxb1* expression in the mesoderm, demonstrating that *Hoxb1* does, in fact, respond to retinoid signaling in this tissue. Thus, in order for the skeletal malformations observed in the present study to be induced through an RA pathway, it would likely require an additional

regulatory element, aside from the known 3' *Hoxb1* paraxial mesodermal enhancer. Since each vertebral region requires a unique code of *Hox* genes for its proper specification, it is likely that an upstream regulatory mechanism would be shared in a more global manner among a particular set of *Hox* genes. Such a mechanism has yet to be defined.

Vertebral transformations are found naturally in 1-5% of the human population, excluding those that occur as part of skeletal malformation syndromes. The Museum Vrolik in The Netherlands maintains a collection of human anatomical specimens and has recently identified both anterior and posterior homeotic vertebral transformations in cranial base and trunk preparations within a subset of this collection (Oostra et al., 2005). Furthermore, they find that vertebral homeosis and changes in the numbers of vertebrae are two independent phenomena, with respect to paraxial mesoderm patterning and segmentation. Clearly, a more complete understanding of how vertebral precursors are patterned during early development will allow us to better appreciate the etiological origins of homeotic transformations in both normal and pathological states. Results from the present study demonstrate that: 1) the amount of *HoxB* gene product, particularly, Hoxb1 and Hoxb2, contributes significantly to the incidence of cervical and thoracic vertebral transformations, and 2) both genes should be included into an overall model to explain how vertebral patterning in the presomitic mesoderm arises.

Appendix A

Assessing the role of *Hoxb1* in the pathogenesis of Chiari I Malformation

Type I Chiari malformation (CMI) is a congenital condition that is classically characterized by a herniation of ≥ 5mm of the cerebellar tonsils through the foramen magnum. CMI is often associated with a condition known as syringomyelia, or the formation of a cyst (syrinx) in the spinal cord; as a result, CMI patients often experience headache, difficulty swallowing, sleep apnea, and ocular disturbances. The embryological cause of CMI has been shown to originate from a fundamental defect during occipital somite development, resulting in an underdeveloped occipital bone, and, hence, a posterior fossa that is smaller in size than normal (Nishikawa, *et al*., 1997). Since the posterior cranial fossa is the intercranial cavity that houses the normally developed hindbrain, the cerebellar tonsils are herniated into the spinal cord.

Because CMI involves hindbrain abnormalities and *Hoxb1* is expressed in the developing hindbrain, it was hypothesized that *Hoxb1* could play a role in the pathogenesis of CMI. Moroni *et al.* originally identified three human *HOXB1* genetic variants within an Italian CMI patient population (n=49) by single stranded conformational polymorphism analysis. These three variants (Δ2, Δ3A, and Δ3B) diverged from wild-type sequence by at least three sites within exon 1 of *HOXB1*. The location of these polymorphic sites in exon 1 suggests that changes in the protein's predicted N-terminal domain may affect the ability of HOXB1 protein to activate transcription of downstream targets. Variant Δ2 was found to contain three silent mutations (G114A, C213T, and G246A) and one missense (C167T) change that

is predicted to replace the non-polar alanine found at codon 56 with a hydrophobic valine. The Δ2 allelic variant was identified in 3 unrelated patients (6%) and was found to be present only in a heterozygous condition. Additionally, this allele was completely absent from the control population. The Δ3A variant contained two silent transitions (C237T and G450A) in addition to a missense mutation (A309T), which changes the 103rd codon from a polar glutamine to a positively charged histidine. The Δ3B allele possessed these three mutations, as well as a 9 base pair random duplication (ACAGCGCCC) at nucleotide position 83, which inserts in-frame an additional three amino acids (histidine, serine, and alanine) at the 27th codon. Five patients (10.2%) were identified as Δ3A heterozygotes, compared to 24 (23.3%) individuals in the control group. While no patients were found to be Δ3A homozygotes, 6 control individuals (5.8%) possessed two Δ3A alleles. Thirteen patients (26.5%) contained the Δ3B allele in a heterozygous condition, compared to 10 control individuals (9.7%). The Δ3B homozygous condition was identified in 6 patients (12.2%) and 1 control individual (1%). This increase of the Δ3B allele in the patient population suggests a correlation between the Δ3B allele and the risk of CMI. While no patients were found to have both Δ3A and Δ3B alleles, one control individual was, in fact, genotyped as Δ3A/Δ3B (Figure 43, unpublished data).

Since HOXB1 protein is capable of affecting its own gene expression through a *Hoxb1* auto-regulatory enhancer (*B1-ARE*) located in the 5' regulatory region (Pöpperl et al., 1995), *in vitro* transient cell transfection assays were performed using the *B1-ARE* as a response element to investigate the effects of each of the above

Figure 43. Mutant *HOXB1* alleles identified in a Chiari I Malformation patient population.

The three human *HOXB1* allelic variants identified in control (n=103) and Chiari I Malformation patient (n=49) populations are shown on the left (Δ2, Δ3A, and Δ3B). The wild-type allele is listed as Δ1. Eight polymorphisms, including single nucleotide changes (G114A, C167T, C213T, C237T, G246A, A309T, and G450A) and a 9bp repeat insertion (ACAGCGCCC), were observed within the first *HOXB1* exon. Single nucleotide changes C167T and A309T (red) represent missense mutations, while the rest are silent mutations (black). Allele frequencies are listed as a percentage of either the patient or control population on the right.

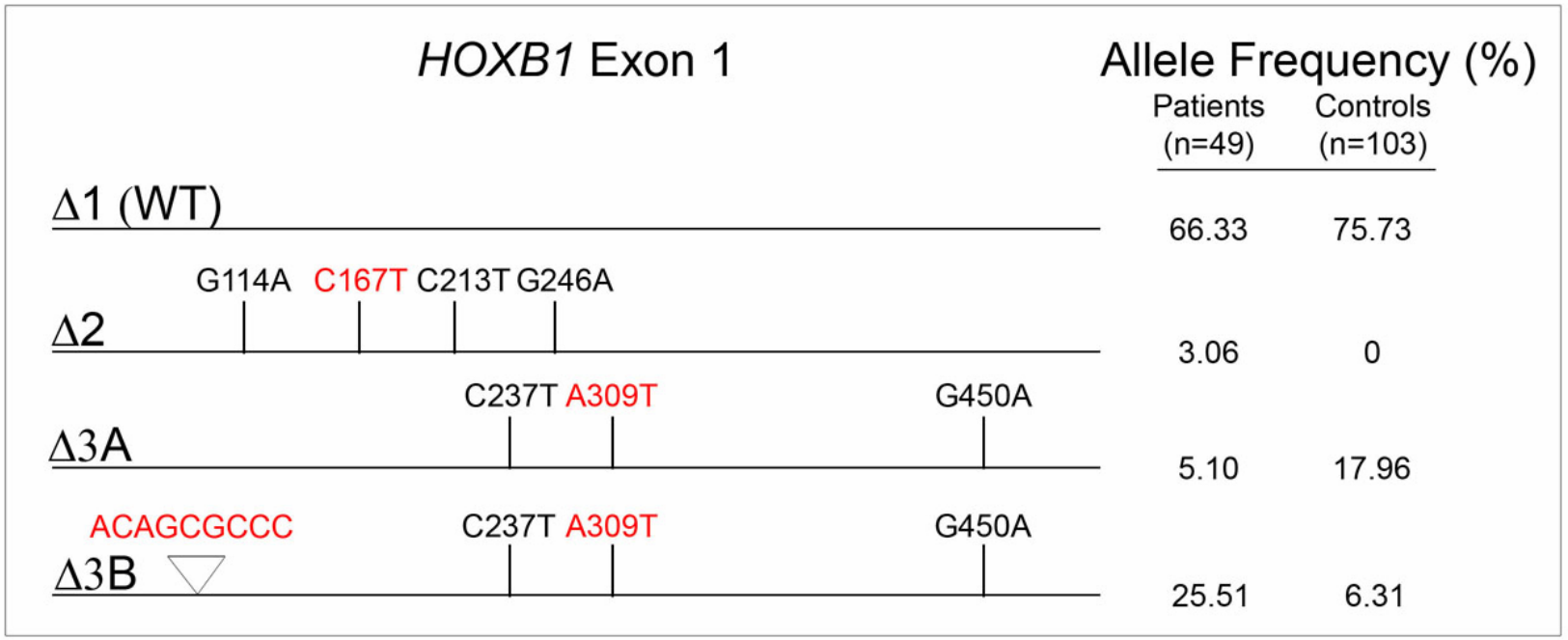
HOXB1 Exon 1
Allele Frequency (%)
Patients (n=49)
Controls (n=103)
Δ1 (WT)
66.33
75.73
G114A
C167T
C213T
G246A
Δ2
3.06
0
C237T
A309T
G450A
Δ3A
5.10
17.96
ACAGCGCCC
C237T
A309T
G450A
Δ3B
25.51
6.31

HOXB1 variants on *Hoxb1* transcription. Each of these variants was cloned into a eukaryotic expression vector (*pcDNA3.1*) and was transiently co-transfected with a luciferase reporter plasmid under the control of the B1-ARE and the adenovirus major late minimal promoter (*pAdML-ARE-Luc*) into COS cells (not shown). While the wild-type, Δ3A, and Δ3B expressed variants were able to transactivate the luciferase reporter 3-4 times over the basal level of activity, the effect of the Δ2 variant was weaker at 1.6 fold induction, suggesting that functional activity of this variant is reduced with respect to the Δ3A and Δ3B variants. When these experiments were repeated with co-transfection of an important HOXB1 cofactor (PBX), a much greater increase in luciferase levels over wild-type was observed with the Δ3A and Δ3B variants, suggesting that these variants synergize with PBX1 and cause a gain-of-function effect. However, when PBX1 was co-transfected with the Δ2 variant, no increase in induction over transfection of Δ2 alone was observed. This shows that Δ2 protein fails to synergize with PBX1 and may result in a loss-of-function of HOXB1 protein.

To further investigate the functionality of these variants, the Krumlauf lab performed *in ovo* chick co-electroporations of the *HOXB1-ARE-lacZ* reporter and each of the HOXB1 allelic variants into the right side of the developing chick hindbrain. Electroporation of the reporter alone produced expression that was specifically confined to r4 and r6/7 (Figure 44). Upon co-electroporation of the reporter with wild-type HOXB1 (Δ1) protein, reporter expression was transactivated

Figure 44. Testing the function of human *HOXB1* variants by reporter transactivation through the mouse *Hoxb1* r4 ARE.

(A)-(E) *In ovo* chicken co-electroporation of the mouse *Hoxb1* r4 ARE, each of the four human *HOXB1* alleles, and the *HOX* cofactor *PBX1*. Co-electroporation of the enhancer alone with *PBX1* produced strong *LacZ* reporter staining in r4 and weaker staining in r6 (A). Addition of the wild-type allele (Δ1) transactivated reporter expression anteriorly (asterisk) and extended the posterior expression limit into r7 (B). When the Δ2 variant was electroporated, reporter expression was limited to r4 (and migrating neural crest cells) and r6/7 (C). Reporter transactivation upon electroporation of the Δ3A and Δ3B variants (asterisks) was similar to that observed in the wild-type assay (compare D and E to B).

(F)-(J) The above co-electroporations were repeated without the addition of the *HOX* cofactor *PBX1*. There did not appear to be any difference in reporter transactivation with or without *PBX1*.

ncc=neural crest cells; ov=otic vesicle; r4=rhombomere 4; r6/7=rhombomeres 6 and 7

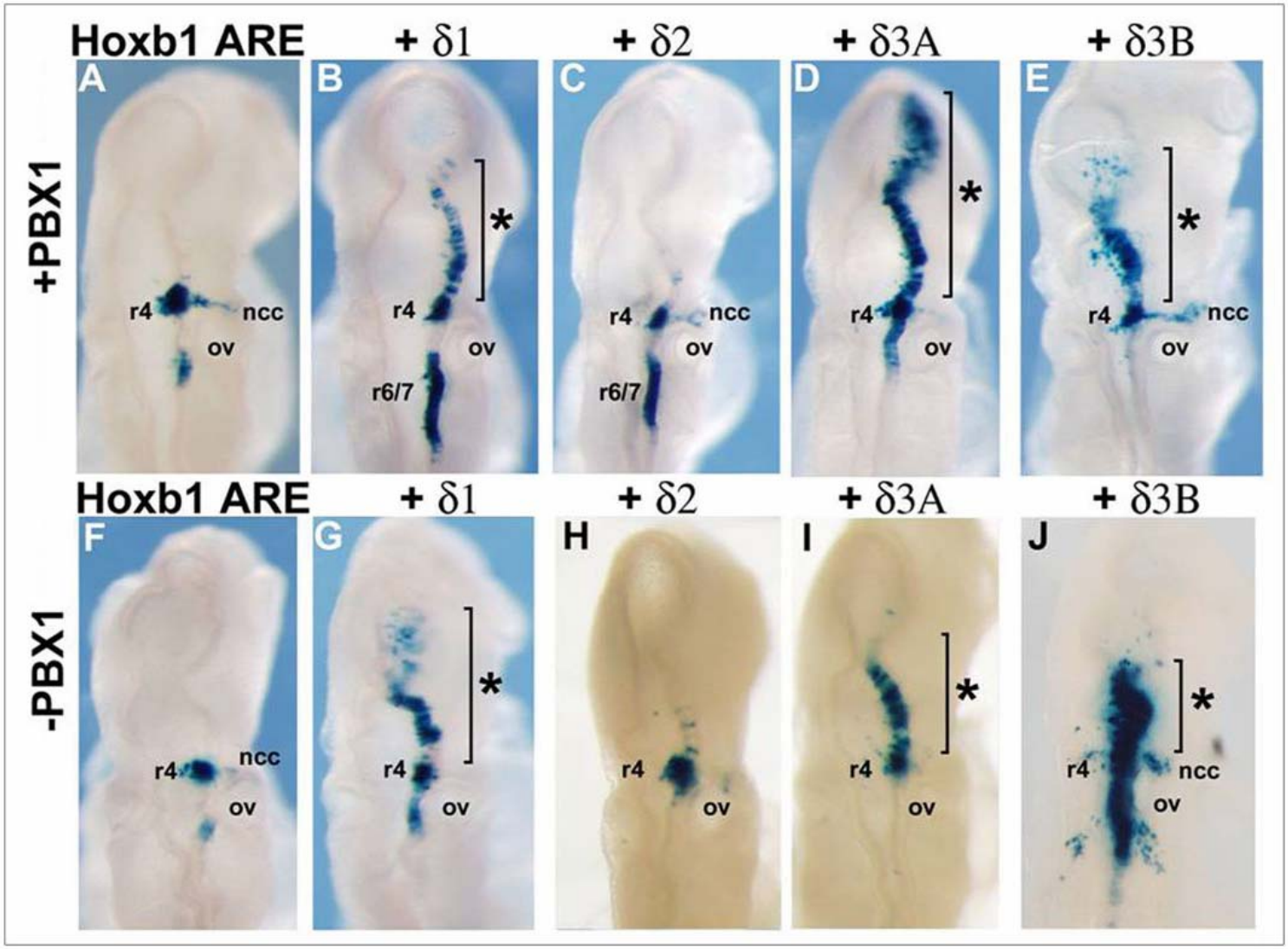
Hoxb1 ARE
+ δ1
+ δ2
+ δ3A
+ δ3B
+PBX1
A
B
C
D
E
r4
ncc
ov
r6/7
*
Hoxb1 ARE
+ δ1
+ δ2
+ δ3A
+ δ3B
-PBX1
F
G
H
I
J
r4
ncc
ov
*

and ectopically induced in more anterior brain regions. The results of reporter and HOXB1-Δ2 variant co-electroporations showed no transactivation of reporter expression; instead, expression was limited to r4 and r6/7, similar to electroporation of the reporter by itself. The Δ3A and Δ3B variant co-electroporations showed the same transactivation into more anterior brain regions that was seen in the wild-type electroporations. The results from the Δ2 electroporations are consistent with a loss-of-function associated with this variant. However, since the results from Δ3A and Δ3B electroporations were similar to that of wild-type and are not quantitative, it is unclear whether these variants perform an *in vivo* gain-of-function. For this reason, we decided to further pursue the *in ovo* electroporation system in an attempt to determine whether the Δ3B variant does, in fact, result in a gain-of-function, as was suggested by the *in vitro* cell transfection assays.

Taking advantage of the ability of HOXB1 protein to regulate the expression of other *Hox* genes, we performed *in ovo* chicken hindbrain co-electroporations of the human HOXB1 variants, along with wild-type HOXB1, with a number of auto-regulatory elements found in mouse *Hoxa2*, *Hoxa3*, and *Hoxb2* gene regulatory regions that were linked to either *lacZ* or GFP reporters. The above constructs were obtained from the Krumlauf lab's stock solutions, as they were created by previous lab members.

The first *in ovo* electroporations were performed with the mouse *Hoxa2* r2 ARE alone and in addition to wild-type HOXB1Δ1 and HOXB1Δ3B constructs (Figure 45). The *Hoxa2* r2 ARE was previously linked in two separate constructs to

Figure 45. Testing the function of human *HOXB1* variants by reporter transactivation through the mouse *Hoxa2* r2 ARE.

(A)-(E) *In ovo* chicken co-electroporation of the mouse *Hoxa2* r2 ARE (linked to a *LacZ* reporter), the human wild-type allele (Δ1), and the human Δ3B variant. Co-electroporation of the enhancer alone produced strong *LacZ* reporter staining in r4 and weaker staining in r6 (A). Addition of the wild-type allele (Δ1) produced either the same strong band restricted to r4 (B) or transactivated reporter expression (C). When the Δ3B variant was electroporated, reporter expression again was either limited to r4 (D) or transactivated anteriorly (E), similar to the results obtained for the wild-type allele.

(F)-(J) The above co-electroporations were repeated with the same *Hoxa2* r2 ARE linked to a GFP reporter. There did not appear to be any difference in reporter transactivation using this assay.

ov=otic vesicle

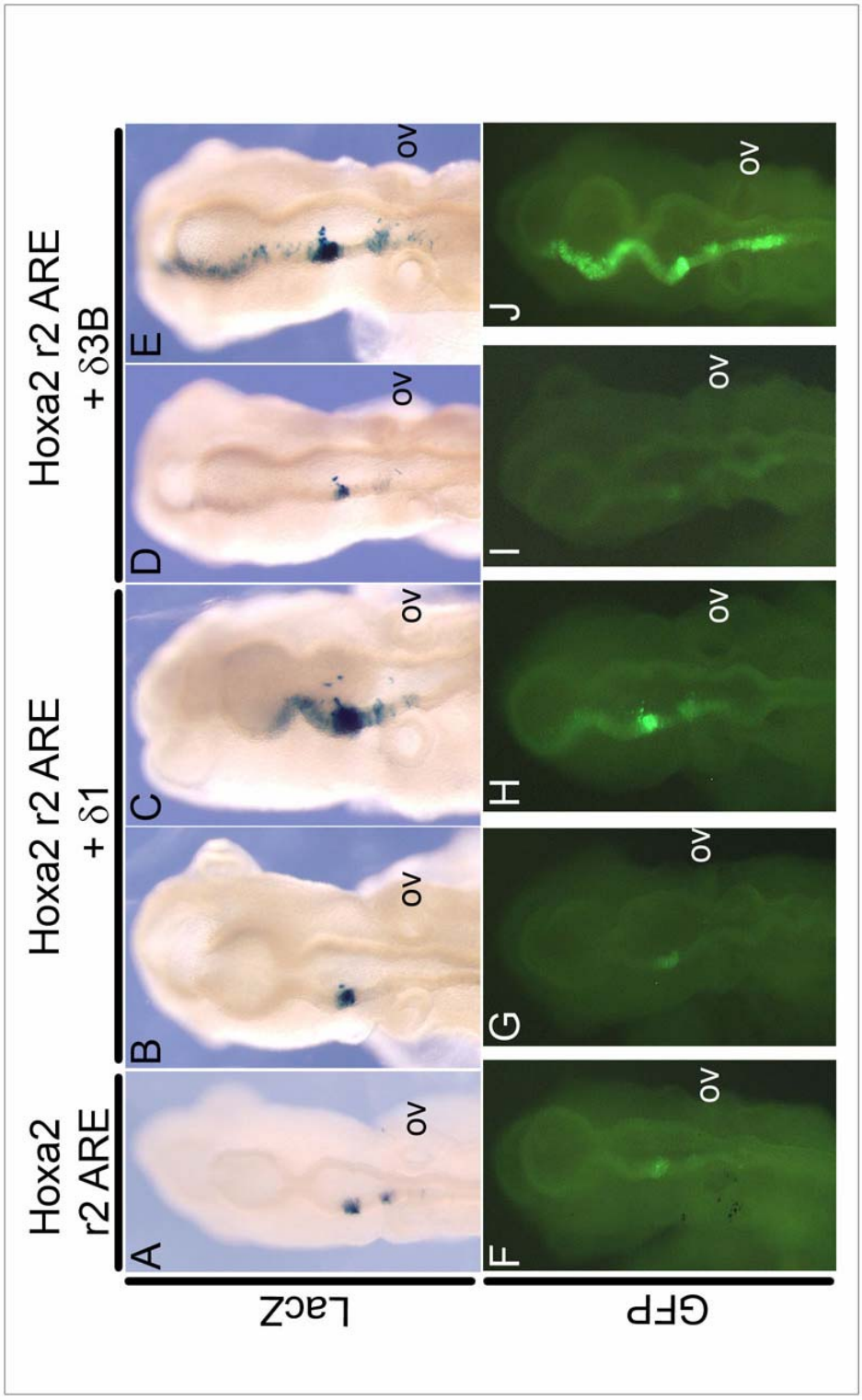
Hoxa2 r2 ARE
Hoxa2 r2 ARE + δ1
Hoxa2 r2 ARE + δ3B
LacZ
GFP
A
B
C
D
E
F
G
H
I
J
ov

LacZ and GFP reporters, both of which were used in this experiment (Figure 45A-E and F-J, respectively). Electroporation of the enhancer alone produced staining in r2 (Figure 45A and F). Co-electroporation of the enhancer with wild-type HOXB1Δ1 construct resulted in two separate responses: reporter expression was restricted to r2 (Figure 45B and G) or was strong in r2 and expanded anteriorly (Figure 45C and H). Similar results were obtained when the enhancer was co-electroporated with the HOXB1Δ3B construct (compare Figure 45D and I with Figure 45E and J).

When this experiment was repeated with the *Hoxa3* r5 enhancer, and again with the *Hoxb2* r4 enhancer, similar reporter expression was observed (not shown). Unfortunately, one of the drawbacks to the *in ovo* electroporation technique has been the high degree of variability among embryos injected with the same reporter constructs. From the data gathered from previous and present chicken electroporations, we were unable to conclusively demonstrate that the *HOXB1* variant identified in Chiari I Malformation patients is capable of enhancing HOXB1 activity in an *in vivo* functional assay.

Appendix B

The contribution of *Hoxb1* toward cranial suture development

Within the *Hoxb1* mutant line in a purebred 129s6/SVEV genetic background, there were two adult (4.5mo.) heterozygous animals that appeared to have severe non-closure defects in the cranial sutures, including the coronal, sagittal, and lambdoid sutures, compared to a wild-type animal at 3.5mo (Figure 46A, B, C, G, H, and I). By P45, closure of the sagittal suture is complete in wild-type mice. However, in these *Hoxb1* heterozygous mutants, the osteogenic fronts of the parietal bones (which normally meet to form the sagittal suture) remained widely separated. This led us to speculate that *Hoxb1* may have a role in cranial suture development. Sine this is a developmentally-regulated process, we began to look for the embryologic origins of this defect in 18.5dpc mutant embryos. Upon initial observation, it appeared that a non-closure phenotype could be seen at this stage. However, during the course of this investigation, we began to notice increasingly small litter sizes were being generated, making it even more difficult to obtain homozygous embryos for analysis. This problem is very often encountered in pure inbred strains, so we crossed the *Hoxb1* mutant line to a mixed F1 strain, consisting of CBA and C57Bl/6 genetic backgrounds. This resulted in the expected increased fecundity and the observation of homozygous mutants. The experiments that followed were performed in this mixed genetic background. When embryonic mutant skeletons were prepared and stained, there no longer appeared to be any difference between *Hoxb1* wild-type, heterozygous, or homozygous sutures at 18.5dpc (not shown). A number of *Hoxb1*

mutant animals seemed to have “open” sutures at this stage, but this occurrence was also noted in wild-type animals. What initially appeared to be a non-closure phenotype in the sagittal suture now seemed to reflect a delay in parietal bone osteogenesis/ossification by 18.5dpc. To further investigate the idea of developmental delay, we analyzed skulls from mice collected at P7, P14, and 6 months of age (Figure 46D, E, F, J, K, and L). These time points correlated to stages prior to (P7 and P14) and well after (6mo.) sagittal suture closure. Again, there were no appreciable differences in suture closure among *Hoxb1* wild-type, heterozygous, and homozygous postnatal animals. This led us to postulate that the delays in calvarial development could be due to genetic background. To investigate this possibility, we observed the degree of calvarial ossification by 18.5dpc from various inbred and outbred wild-type background strains, including 129s6/SVEV, CBA, C57bl/6, F1 (CBA, C57bl/10), and CD1. Upon staining of the skulls with Alizarin Red and Alcian Blue, a range of developmental stages could be observed (Figure 47). The relative amounts of Alizarin Red staining in the parietal bones from the above strains were used to evaluate developmental delays. Interestingly, the least amount of staining could be seen in 129s6/SVEV parietal bones (Figure 47E). The level of ossification was increased such that the F1 strain had slightly more staining (Figure 47D), C57bl/6 represented a mid-level of ossification (Figure 47C), CBA had even more (Figure 47B), and CD1 parietal bones had achieved the greatest amount of ossification by this stage (Figure 47A). This confirmed that genetic background does, in fact, have an impact on the development of the skull. Furthermore, the CD1

Figure 46. Adult mouse skull preparations with open and closed cranial sutures.

Adult mouse skulls were skinned and prepared with double Alizarin Red/Alcian Blue skeleton staining.

(A) Anterior view of the wild-type skull at 3.5 months, illustrating four major cranial sutures: metopic (M), coronal (C), sagittal (S), and lambdoid (L). The sagittal suture divides the paired parietal bones (P).

(B) - (C) *Hoxb1*$^{+/-}$ skulls at 4.5 months with an open sagittal sutures (asterisks).

(D) - (F) *Hoxb1*$^{+/-}$ skulls with normally-developing sagittal sutures at P7 (D) and P14 (E), as well as a fully closed sagittal suture at 6 months (F)

(G) - (L) Magnified images of the sagittal sutures depicted in (A)-(F).

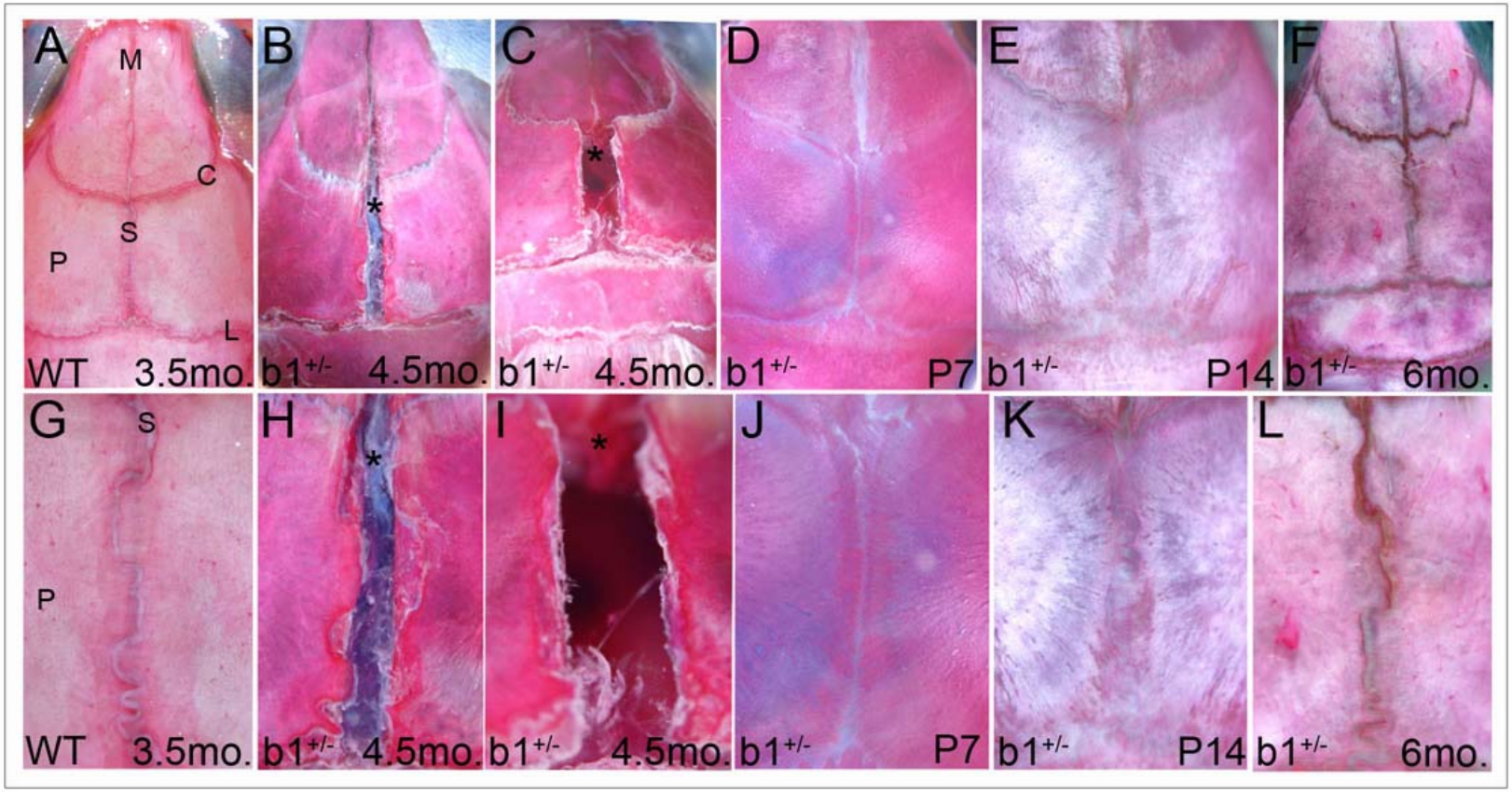
A
M
C
S
P
L
WT 3.5mo.
B
*
b1+/- 4.5mo.
C
*
b1+/- 4.5mo.
D
b1+/- P7
E
b1+/- P14
F
b1+/- 6mo.
G
S
P
WT 3.5mo.
H
*
b1+/- 4.5mo.
I
*
b1+/- 4.5mo.
J
b1+/- P7
K
b1+/- P14
L
b1+/- 6mo.

Figure 47. Developmental delay in wild-type parietal bone ossification is dependent upon genetic background.

Mouse skeletons were skinned at 18.5dpc and prepared with double Alizarin Red/Alcian Blue skeleton staining. Lateral views of wild-type skulls, illustrating the degree of parietal bone (P) ossification in CD1 (n=30; A), CBA (n=8; B), C57bl/6 (n=8; C), F1 (n=9; D), and 129s6/SVEV (n=6; E) background strains. Importantly, the skeletons obtained from the 129s6/SVEV background showed dramatic developmental delay with respect to calvarial ossification.

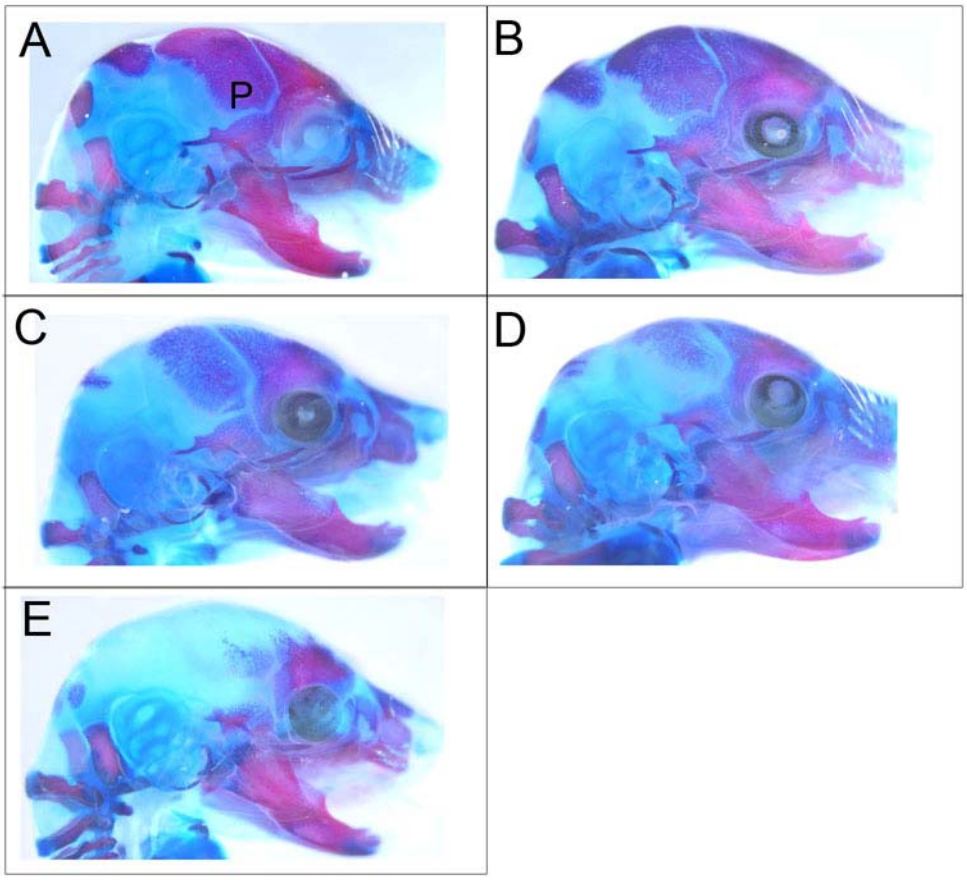
A
P
B
C
D
E

staining correlated the most to the widely-accepted amount of ossification that has taken place in the mouse skull by 18.5dpc. For this reason, the *Hoxb1* mutant line was rederived by using frozen mutant-derived sperm to fertilize 129s6/SVEV female eggs, generating inbred *Hoxb1* mutant pups. Heterozygous *Hoxb1* 129s6/SVEV males were mated to CD1 females to create a *Hoxb1* mixed background mutant line. The rationale for such a breeding strategy was that the CD1 background will likely "rescue" the developmental delay in skull ossification in the 129s6/SVEV background. Consequently, 18.5dpc embryo harvests from heterozygous matings of mice in this mixed background generated *Hoxb1* wild-type, heterozygous, and homozygous samples. The degree of Alizarin Red staining (i.e., amount of ossification) in all calvaria was constant among the three genotypes, and no further suture defects were observed (not shown). These results suggest two possibilities to explain the prior suture observations. First, the suture defects may exhibit extremely low penetrance, and perhaps they are most penetrant in the purebred 129s6/SVEV background. This would explain why the defects are lost upon crossing into other genetic backgrounds (e.g. CBA/C57b/10/ and CD1). Secondly, the phenotype observed initially in 18.5dpc embryos may not, in fact, be suture defects. Instead, there may be a developmental delay in the ossification of wild-type calvarial bones depending on the genetic background. In late embryonic stages, this gives the appearance that the osteogenic fronts are widely-separated, instead of nearing juxtaposition. However, we find that these fronts do overlap in early postnatal life and close to form a proper suture. This explains the embryonic findings, but does not

account for the two adult *Hoxb1* heterozygous mice whose coronal, sagittal, and lambdoid sutures appear open. During the process of suture formation, the osteogenic fronts of opposing skull bones will overlap in a zigzag-type fashion, resulting in a closed suture that resembles the fitting together of jigsaw puzzle pieces. Close inspection of the heterozygotes' sutures reveals the same jigsaw patterning found at the leading edges of the parietal, frontal, and interparietal bones, suggesting that the sutures did, in fact, undergo the process of suture closure and somehow separate later. Thus, it does not fit the nonclosure phenotype associated with human disorders such as Cleidocranial Dysplasia or its corresponding mouse model. Instead, it is possible that pressures from the underlying brain as it increased in volume could have forced open these sutures either during or after the process of suture closure.

In an attempt to further demonstrate that parietal bone ossification is not altered in *Hoxb1* mutants, osteogenic marker analysis and von Kossa staining were performed on slide-mounted sagittal sections through the sagittal suture (Figure 48). *In situ* hybridization of probes designed against the cDNAs of several osteogenic markers, including *BMP2*, *BMP4*, *Cbfa1*/*Runx2*, *Dlx5*, *Msx1*, *Msx2*, and *Spp1* (Figures 11 and 12), was performed on these sections. *Spp1* was specifically chosen for this study, since its expression marks differentiating osteoblasts located within the osteogenic fronts of the developing suture. The results obtained from the *Spp1* mRNA probe are shown at 15.5dpc (Figure 48A-C) and 16.5dpc (Figure 48D-F). Compared to wild-type, there does not appear to be a significant decrease in the amount of *Spp1* expression or a delay in the progression of its expression in the

Figure 48. Ossification of the parietal bone assayed by osteogenic marker *in situ* hybridization and von Kossa staining.

(A)-(C) *In situ* hybridization of the *Spp1* mRNA antisense probe to sagittal sections through the skull at the level of the sagittal sutures of 15.5dpc wild-type (A), *Hoxb1*$^{+/-}$ (B), and *Hoxb1*$^{-/-}$ (C) mice. The anterior boundaries of *Spp1*-expressing cells mark the developing parietal bones' osteogenic fronts (asterisks). Among wild-type and *Hoxb1* mutants, there does not appear to be any difference in the placement of these fronts at 15.5dpc.

(D)-(F) *In situ* hybridization of the *Spp1* mRNA antisense probe to sagittal sections through the skull at the level of the sagittal sutures of 16.5dpc wild-type (D), *Hoxb1*$^{+/-}$ (E), and *Hoxb1*$^{-/-}$ (F) mice. At first observation, the osteogenic fronts appear to be located more anteriorly in the wild-type suture compared to *Hoxb1* mutants. However, this difference may be due to the fact that the sections do not represent the same location through the suture.

(G)-(I) von Kossa staining on sections through the skull at the level of the sagittal sutures of 18.5dpc wild-type (G), *Hoxb1*$^{+/-}$ (H), and *Hoxb1*$^{-/-}$ (I) mice. The anterior limit of von Kossa staining (black) marks the osteogenic fronts, which are located slightly more anterior in the wild-type suture compared to *Hoxb1* mutants. Again, this difference may be due to non-matching sections.

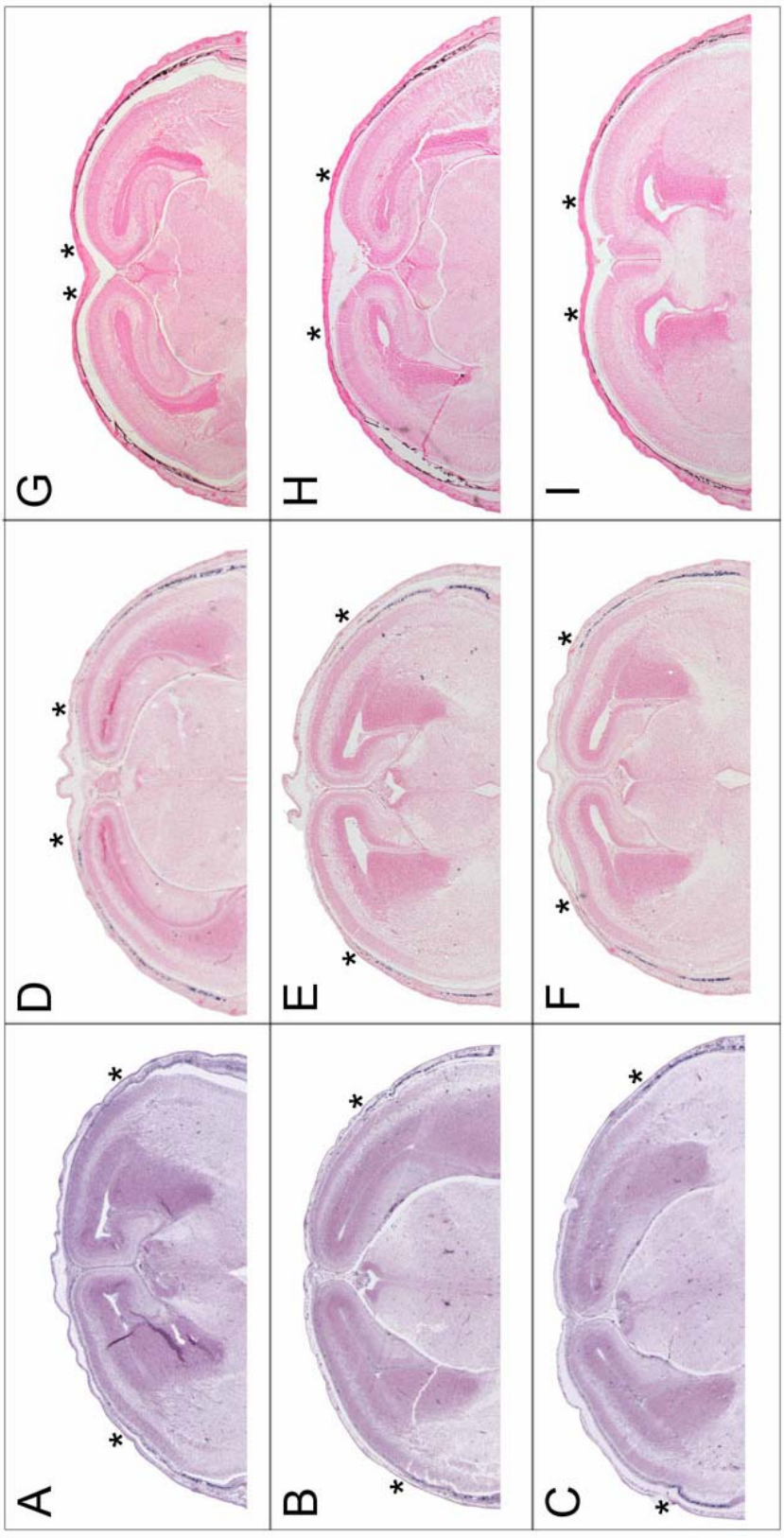
A
B
C
D
E
F
G
H
I

osteogenic fronts of the developing parietal bones (asterisks) at 15.5dpc in *Hoxb1* heterozygotes and homozygotes. By 16.5dpc, *Spp1* expression has extended anteriorly in the wild-type embryo skull (Figure 48D). Interestingly, it appears to remain laterally in both *Hoxb1* heterozygotes and homozygotes (Figure 48E and F, respectively). However, this difference may be due to the fact that the sections through the mutant sagittal sutures were not taken at the same position as those through the wild-type sutures, which is easily observed upon comparison of the sizes of the lateral ventricles within the underlying brain.

Finally, von Kossa staining was performed on sagittal sections through the sagittal sutures of 18.5dpc wild-type and *Hoxb1* mutant skulls (Figure 48G-I). This procedure is used as an indirect method for detecting calcium deposits within a given tissue sample. For the present study, this technique was used to determine ossification of the parietal bone. In wild-type skulls, von Kossa staining (black) extends almost to the midline of the head (Figure 48G), and the staining in *Hoxb1* heterozygous and homozygous skulls (Figure 48H and I, respectively) has nearly reached the same point. As with the *Spp1* mRNA expression results, the limitation to the von Kossa analysis is that the sections do not match exactly, with respect to their position within the sagittal suture.

The osteogenic marker analysis and von Kossa staining have not eliminated the possibility that there are differences between wild-type and *Hoxb1* mutant sagittal sutures. At best, these results were inconclusive. Based on the finding that *Hoxb1*

heterozygous cranial sutures at P7, P14, and 6 months have initiated and completed the closure process, it is likely that this process proceeded normally.

Appendix C

Tables of skeletal phenotypes identified in *Hox* individual and compound mutants and increased gene dosage transgenic mice

The following tables are intended to supplement the data presented in Chapter 3 pertaining to the skeletal defects observed in *Hoxa1* and *Hoxa1*/*Hoxb1* double mutants (Table 2), *Hoxb1*, *Hoxb2*, and *Hoxb1*/*Hoxb2* double mutants (Table 3), *HoxB* gain-of-function transgenic mice (Table 4), and wild-type animals (Table 5). For a full description of the phenotypes listed in these tables, please refer to Chapter 3.

Table 2. Skeletal phenotypes in single *Hoxa1* and double *Hoxa1*/*Hoxb1* loss-of-function mutants.

For each phenotype listed, the number and percentage (parentheses) of animals affected are noted for *Hoxa1* heterozygotes ($a1^{+/-}$:n=41), *Hoxa1* homozygotes ($a1^{-/-}$: n=18), and *Hoxa1*/*Hoxb1* double mutants ($a1^{+/-}/b1^{+/-}$:n=46; $a1^{-/-}/b1^{+/-}$:n=11; $a1^{+/-}/b1^{-/-}$: n=10; $a1^{-/-}/b1^{-/-}$:n=2). Natural skeletal variations are also included. Rows highlighted in yellow represent the homeotic transformations that are most significant for the genotypes listed.

aaa: anterior arch of the atlas; AT's: anterior tuberculi; (B): bilateral; BOB: basioccipital bone; EOB: exoccipital bone; NA: neural arch; SCJ: sternocostal junction ; SOB: supraoccipital bone; (U) unilateral.

Table 2. Skeletal phenotypes in single *Hoxa1* and double *Hoxa1*/*Hoxb1* loss-of-function mutants.

Phenotypes	**a1$^{+/-}$**	**a1$^{-/-}$**	**a1$^{+/-}$ b1$^{+/-}$**	**a1$^{-/-}$ b1$^{+/-}$**	**a1$^{+/-}$ b1$^{-/-}$**	**a1$^{-/-}$ b1$^{-/-}$**
EOB fused to BOB (B)	0	0	0	0	0	1 (50%)
SOB perforated 2x	0	0	0	0	0	1 (50%)
C1 NA's bifurcated (B)	0	0	0	0	0	2 (100%)
aaa fused to BOB	0	0	0	0	0	1 (50%)
C2->C1 full or partial	0	0	0	0	0	0
C2->C1 full	0	0	0	0	0	0
C2->C1 partial	0	0	0	0	0	0
C2 NA split	3 (7%)	4 (22%)	3 (7%)	0	1 (10%)	1 (50%)
C2 NA split (U)	1 (2%)	3 (17%)	3 (7%)	0	1 (10%)	0
C2 NA split (B)	2 (5%)	1 (6%)	0	0	0	1 (50%)
C5->C6 (U)	1 (2%)	0	0	0	0	0
C6->C5	1 (2%)	0	0	1 (9%)	3 (30%)	2 (100%)
C6->C5 (U)	1 (2%)	0	0	1 (9%)	2 (20%)	1 (50%)
C6->C5 (B)	0	0	0		1 (10%)	1 (50%)
C7->C6	0	0	0	1 (9%)	3 (30%)	2 (100%)
C7->C6 (U)	0	0	0	1 (9%)	2 (20%)	1 (50%)
C7->C6 (B)	0	0	0	0	1 (10%)	1 (50%)
C7->C6 partial	0	0	0	0	0	0
C7->C6 partial (U)	0	0	0	0	0	0
C7->C6 partial (B)	0	0	0	0	0	0
C6 and C7 AT's fused	0	0	0	0	0	0
C7 rib anlagen	35 (85%)	13 (72%)	5 (11%)	2 (18%)	0	0

Table 2. Skeletal phenotypes in single *Hoxa1* and double *Hoxa1*/*Hoxb1* loss-of-function mutants, continued…

Phenotypes	a1+/-	a1-/-	a1+/- b1+/-	a1-/- b1+/-	a1+/- b1-/-	a1-/- b1-/-
C7 rib anlagen (U)	13 (32%)	3 (17%)	3 (7%)	1 (9%)	0	0
C7 rib anlagen (B)	22 (54%)	10 (56%)	2 (4%)	1 (9%)	0	0
C7/T1 ribs fused (B)	1 (2%)	0	0	0	0	0
T1 rib shortened	0	0	0	0	0	0
T1 rib shortened (U)	0	0	0	0	0	0
T1 rib shortened (B)	0	0	0	0	0	0
T1/T2 ribs fused	0	0	1 (2%)	0	3 (30%)	2 (100%)
T1/T2 ribs fused (U)	0	0	1 (2%)	0	3 (30%)	1 (50%)
T1/T2 ribs fused (B)	0	0	0	0	0	1 (50%)
T2 rib SCJ at manubrium	0	0	0	0	0	0
T2 rib SCJ at manubrium (U)	0	0	0	0	0	0
T2 rib SCJ at manubrium (B)	0	0	0	0	0	0
T8 rib SCJ	0	1 (6%)	6 (13%)	2 (18%)	1 (10%)	2 (100%)
T8 rib SCJ (U)	0	1 (6%)	4 (9%)	1 (9%)	1 (10%)	2 (100%)
T8 rib SCJ (B)	0	0	2 (4%)	1 (9%)	0	0
3 sternal bands	0	0	0	0	0	0
5 sternal bands	0	0	1 (2%)	0	0	0
Crankshaft sternum	0	0	1 (2%)	0	0	0
Sternal bifurcation, partial or complete	0	0	2 (4%)	0	10 (100%)	1 (50%)
Bifurcated sternum	0	0	2 (4%)	0	10 (100%)	1 (50%)
Partially bifurcated sternum	0	0	0	0	0	0
L1 ribs	1 (2%)	0	1 (2%)	0	0	0
L1 ribs (U)	0	0	1 (2%)	0	0	0
L1 ribs (B)	1 (2%)	0	0	0	0	0

Table 3. Skeletal phenotypes in single *Hoxb1* and *Hoxb2* and double *Hoxb1*/*Hoxb2* loss-of-function mutants.

For each phenotype listed, the number and percentage (parentheses) of animals affected are noted for *Hoxb1* heterozygotes ($b1^{+/-}$; n=101), *Hoxb1* homozygotes ($b1^{-/-}$; n=29), *Hoxb2* heterozygotes ($b2^{+/-}$; n=70), *Hoxb2* homozygotes ($b2^{-/-}$; n=23), and *Hoxb1*/*Hoxb2* double mutants ($b1^{+/-}$/$b2^{+/-}$; n=22). Natural skeletal variations are also included. Rows highlighted in yellow represent the homeotic transformations that are most significant for the genotypes listed.

aaa: anterior arch of the atlas; AT's: anterior tuberculi; (B): bilateral; BOB: basioccipital bone; NA: neural arch; SCJ: sternocostal junction; (U) unilateral.

Table 3. Skeletal phenotypes in single *Hoxb1* and *Hoxb2* and double *Hoxb1*/*Hoxb2* loss-of-function mutants.

Phenotypes	b1 +/-	b1-/-	b2+/-	b2-/-	b1+/- b2+/-
C1 aaa fused to BOB	2 (2%)	2 (7%)	0	0	0
C2->C1 full or partial	3 (3%)	7 (24%)	1 (1%)	1 (4%)	1 (5%)
C2->C1 full	0	3 (10%)	0	1 (4%)	0
C2->C1 partial	3 (3%)	4 (14%)	1 (1%)	0	1 (5%)
C2 NA split	3 (3%)	1 (3%)	5 (7%)	0	0
C2 NA split (U)	2 (2%)	1 (3%)	5 (7%)	0	0
C2 NA split (B)	1 (1%)	0	0	0	0
C6->C5	6 (6%)	17 (59%)	4 (6%)	11 (48%)	12 (55%)
C6->C5 (U)	3 (3%)	10 (34%)	4 (6%)	5 (22%)	4 (18%)
C6->C5 (B)	3 (3%)	7 (24%)	0	6 (26%)	8 (36%)
C7->C6 full	6 (6%)	20 (69%)	4 (6%)	12 (52%)	12 (55%)
C7->C6 full (U)	6 (6%)	11 (38%)	4 (6%)	5 (22%)	3 (14%)
C7->C6 full (B)	0	9 (31%)	0	7 (30%)	9 (41%)
C7->C6 partial	3 (3%)	0	1 (1%)	0	1 (5%)
C7->C6 partial (U)	1 (1%)	0	1 (1%)	0	1 (5%)
C7->C6 partial (B)	2 (2%)	0	0	0	0
C6 and C7 AT's fused	1 (1%)	4 (14%)	0	1 (4%)	2 (9%)
C7 rib anlagen	10 (10%)	0	3 (4%)	0	0
C7 rib anlagen (U)	8 (8%)	0	3 (3%)	0	0
C7 rib anlagen (B)	2 (2%)	0	0	0	0
T1 rib shortened	1 (1%)	4 (14%)	0	0	1 (5%)
T1 rib shortened (U)	1 (1%)	2 (7%)	0	0	1 (5%)
T1 rib shortened (B)	0	2 (7%)	0	0	0
T1/T2 ribs fused	7 (7%)	16 (55%)	0	3 (13%)	7 (32%)
T1/T2 ribs fused (U)	5 (5%)	7 (24%)	0	2 (9%)	4 (18%)
T1/T2 ribs fused (B)	2 (2%)	9 (31%)	0	1 (4%)	3 (14%)
T2 rib SCJ at manubrium	1 (1%)	2 (7%)	0	0	1 (5%)
T2 rib SCJ at manubrium (U)	1 (1%)	1 (3%)	0	0	1 (5%)
T2 rib SCJ at manubrium (B)	0	1 (3%)	0	0	0
T8 rib SCJ	14 (14%)	9 (31%)	7 (10%)	5 (22%)	5 (23%)
T8 rib SCJ (U)	6 (6%)	5 (17%)	1 (1%)	3 (13%)	1 (5%)
T8 rib SCJ (B)	8 (8%)	4 (14%)	6 (9%)	2 (9%)	4 (18%)
Bifurcated sternum	0	10 (34%)	0	13 (57%)	6 (27%)
Bifurcated sternum, complete	0	6 (21%)	0	9 (39%)	2 (9%)
Bifurcated sternum, partial	0	4 (14%)	0	4 (17%)	4 (18%)
5 sternal bands	6 (6%)	0	4 (6%)	1 (4%)	0
3 sternal bands	0	2 (7%)	0	0	0
L1 ribs	2 (2%)	0	5 (7%)	0	1 (5%)
L1 ribs (U)	1 (1%)	0	1 (1%)	0	1 (5%)
L1 ribs (B)	1 (1%)	0	4 (6%)	0	0

Table 4. Skeletal phenotypes in *HoxB* gain-of-function transgenic mice.

For each phenotype listed, the number and percentage (parentheses) of animals affected are noted for transgenic mice containing the following transgenes: *Hoxb1-Hoxb5* (b1-b5; n=3), *Hoxb1*$^{+/-}$; *Hoxb1-Hoxb5* (b1$^{+/-}$;b1-b5; n=41), *Hoxb1-Hoxb9* (b1-b9; n=9), and *Hoxb1* (b1; n=5). Natural skeletal variations are also included. Rows highlighted in yellow represent the homeotic transformations that are most significant for the genotypes listed.

aaa: anterior arch of the atlas; AT's: anterior tuberculi; (B): bilateral; BOB: basioccipital bone; EOB: exoccipital bone; NA's: neural arches; SCJ: sternocostal junction; (U) unilateral.

Table 4. Skeletal phenotypes in *HoxB* gain-of-function mutants.

Phenotypes	b1-b5	b1+/-; b1-b5	b1-b9	b1
Ectopic EOB	1 (33%)	34 (83%)	0	0
Ectopic EOB (U)	0	24 (59%)	0	0
Ectopic EOB(B)	0	10 (24%)	0	0
Ectopic EOB fused to EOB	1 (33%)	10 (24%)	0	0
Ectopic EOB fused to EOB (U)	0	7 (17%)	0	0
Ectopic EOB fused to EOB (B)	1 (33%)	3 (7%)	0	0
Ectopic EOB fused to C1	0	15 (37%)	0	0
Ectopic EOB fused to C1 (U)	0	9 (22%)	0	0
Ectopic EOB fused to C1 (B)	0	6 (15%)	0	0
Ectopic EOB fused to EOB and C1 (B)	0	3 (7%)	0	0
Ectopic unfused EOB	0	9 (22%)	0	0
Ectopic unfused EOB (U)	0	8 (20%)	0	0
Ectopic unfused EOB (B)	0	1 (2%)	0	0
Thickened EOB	0	6 (15%)	0	0
Thickened EOB (U)	0	5 (12%)	0	0
Thickened EOB (B)	0	1 (2%)	0	0
C1 aaa fused to BOB	0	0	0	0
C1 NA increased	1 (33%)	2 (5%)	0	0
C1 NA increased (U)	1 (33%)	0	0	0
C1 NA increased (B)	0	2 (5%)	0	0
C1 NA split (U)	0	0	0	0
C1 and C2 NA's fused (U)	0	2 (5%)	0	1 (20%)
C2->C1 full or partial	0	0	0	4 (80%)
C2->C1 full	0	0	0	0
C2->C1 partial	0	0	0	4 (80%)
C2 NA expanded	0	0	0	5 (100%)
C2 NA expanded (U)	0	0	0	3 (60%)
C2 NA expanded (B)	0	0	0	2 (40%)
C2 NA split	0	0	0	1 (20%)
C2 NA split (U)	0	0	0	1 (20%)
C2 NA split (B)	0	0	0	0
C3 expanded (U)	0	0	0	0
C6->C5	0	5 (12%)	0	3 (60%)

Table 4. Skeletal phenotypes in *HoxB* gain-of-function mutants, continued...

Phenotypes	b1-b5	b1+/-; b1-b5	b1-b9	b1
C6->C5 (U)	0	4 (10%)	0	1 (20%)
C6->C5 (B)	0	1 (2%)	0	2 (40%)
C6 rib anlagen (U)	0	0	1 (11%)	0
C7->C6 full	0	3 (7%)	1 (11%)	2 (40%)
C7->C6 full (U)	0	2 (5%)	1 (11%)	0
C7->C6 full (B)	0	1 (2%)	0	2 (40%)
C7->C6 partial	0	0	3 (33%)	1 (20%)
C7->C6 partial (U)	0	0	3 (33%)	1 (20%)
C7->C6 partial (B)	0	0	0	0
C6 and C7 AT's fused	0	0	0	0
C7 rib anlagen	2 (67%)	0	7 (78%)	0
C7 rib anlagen (U)	0	0	0	0
C7 rib anlagen (B)	2 (67%)	0	7 (78%)	0
T1 rib shortened	0	1 (2%)	0	2 (40%)
T1 rib shortened (U)	0	1 (2%)	0	1 (20%)
T1 rib shortened (B)	0	0	0	1 (20%)
T1/T2 NA's fused (U)	1 (33%)	0	0	0
T1/T2 ribs fused	0	0	0	2 (40%)
T1/T2 ribs fused (U)	0	0	0	2 (40%)
T1/T2 ribs fused (B)	0	0	0	0
T2 rib bifurcated (U)	0	1 (2%)	0	0
T2 rib SCJ at manubrium	0	0	0	1 (20%)
T2 rib SCJ at manubrium (U)	0	0	0	0
T2 rib SCJ at manubrium (B)	0	0	0	1 (20%)
T8 rib SCJ	0	0	2 (22%)	0
T8 rib SCJ (U)	0	0	1 (11%)	0
T8 rib SCJ (B)	0	0	1 (11%)	0
T11 rib bifurcated (U)	1 (33%)	0	0	0
Bifurcated sternum	0	0	0	0
Bifurcated sternum, complete	0	0	0	0
Bifurcated sternum, partial	0	0	0	0
5 sternal bands	0	0	0	0
3 sternal bands	2 (67%)	0	0	0
L1 ribs	0	0	2 (22%)	1 (20%)
L1 ribs (U)	0	0	2 (22%)	1 (20%)
L1 ribs (B)	0	0	0	0

Table 5. Natural skeletal variation in wild-type genetic background mouse strains.

For each variation listed, the number and percentage (parentheses) of animals affected are noted for wild-type mice belonging to the following genetic backgrounds: 129s6/SVEV;CD1 (129/CD1; n=81), CD1 (n=30), F1 (n=9), 129s6/SVEV (129; n=6), CBA (n=8), and C57bl/6 (n=8).

aaa: anterior arch of the atlas; (B): bilateral; BOB: basioccipital bone; NA: neural arches; SCJ: sternocostal junction; (U) unilateral; VA: vertebrarterial canal.

Table 5. Natural skeletal variation in wild-type genetic background mouse. strains

Phenotypes	129 CD1	CD1	F1	129	CBA	C57bl/6
aaa fused to BOB	0	1 (3%)	0	0	0	0
C2 NA split (U)	6 (7%)	4 (13%)	0	0	0	0
C3 VA canal missing (U)	0	0	0	0	0	1 (13%)
C7 rib anlagen	40 (49%)	7 (23%)	2 (22%)	3 (50%)	1 (13%)	4 (50%)
C7 rib anlagen (U)	16 (20%)	7 (23%)	1 (11%)	3 (50%)	1 (13%)	2 (25%)
C7 rib anlagen (B)	24 (30%)	0	1 (11%)	0	0	2 (25%)
C7/T1 ribs fused (U)	1 (1%)	0	0	0	0	0
T8 rib SCJ	12 (15%)	12 (40%)	1 (11%)	0	0	0
T8 rib SCJ (U)	9 (11%)	5 (17%)	1 (11%)	0	0	0
T8 rib SCJ (B)	3 (4%)	7 (23%)	0	0	0	0
5 sternal bands	0	2 (7%)	0	0	0	0
L1 ribs	10 (12%)	12 (40%)	0	0	0	0
L1 rib (U)	4 (5%)	3 (10%)	0	0	0	0
L1 ribs (B)	6 (7%)	9 (30%)	0	0	0	0

Appendix D

Whole-mount *in situ* hybridization studies with *HoxB* genes in *Hoxb1* and *Hoxb2* mutant embryos

To further investigate a possible synergistic relationship between *Hoxb1* and *Hoxb2* in the patterning of vertebral precursors, whole-mount *in situ* hybridization was performed on 9.5dpc wild-type and *Hoxb1* and *Hoxb2* mutant embryos (Figure 49), using antisense RNA probes designed against the *Hoxb1*, *Hoxb2*, and *Hoxb4* genes (Figure 10). A standard *in situ* hybridization protocol for mouse embryos was followed (see Methods and Materials).

The *Hoxb1* mRNA probe revealed a very strong r4 band and strong staining in the presomitic mesoderm of the tail in wild-type embryos at 9.5dpc (Figure 49A). Specific staining was slightly decreased in both domains in *Hoxb2*$^{+/-}$ embryos (Figure 49B) and was nearly absent in *Hoxb2*$^{-/-}$ embryos (Figure 49C). The decrease in r4 and tail bud expression upon removal of functional Hoxb2 protein is consistent with previous results (Barrow and Capecchi, 1996).

Hybridization of the *Hoxb2* mRNA probe showed strong staining in the hindbrain at the level of r3-r5 and diffuse staining in the posterior half of the embryo, including the segmented and unsegmented mesoderm of the tail (Figure 49D). Both domains are drastically reduced in *Hoxb1* heterozygous (Figure 49E) and homozygous (Figure 49F) embryos. Taken together with the *Hoxb1 in situ* results, these data suggest that the interaction between *Hoxb1* and *Hoxb2* in the mesoderm resembles that of the hindbrain.

Figure 49. Whole-mount *in situ* hybridization of *Hoxb1, Hoxb2,* and *Hoxb4* antisense mRNA probes to wild-type and *Hoxb1* and *Hoxb2* mutant embryos at 9.5dpc.

(A)-(C) *Hoxb1* antisense mRNA probe hybridized to wild-type (A), *Hoxb2*$^{+/-}$ (B), and *Hoxb2*$^{-/-}$ (C) embryos. Neural (r4) and mesodermal (PSM) expression levels are decreased in *Hoxb2* mutants, compared to wild-type.

(D)-(F) *Hoxb2* antisense mRNA probe hybridized to wild-type (D), *Hoxb1*$^{+/-}$ (E), and *Hoxb1*$^{-/-}$ (F) embryos. Neural (r3-r5) and mesodermal (somitic and presomitic) expression levels are decreased in *Hoxb1* mutants, compared to wild-type.

(G)-(K) *Hoxb4* antisense mRNA probe hybridized to wild-type (G), *Hoxb1*$^{+/-}$ (H), *Hoxb1*$^{-/-}$ (I), *Hoxb2*$^{+/-}$ (J), and *Hoxb2*$^{-/-}$ (K). Overall expression was decreased in *Hoxb1* and *Hoxb2* mutants compared to wild-type. Without specific somitic expression in wild-type embryos, we were unable to determine if mutant expression was similarly affected.

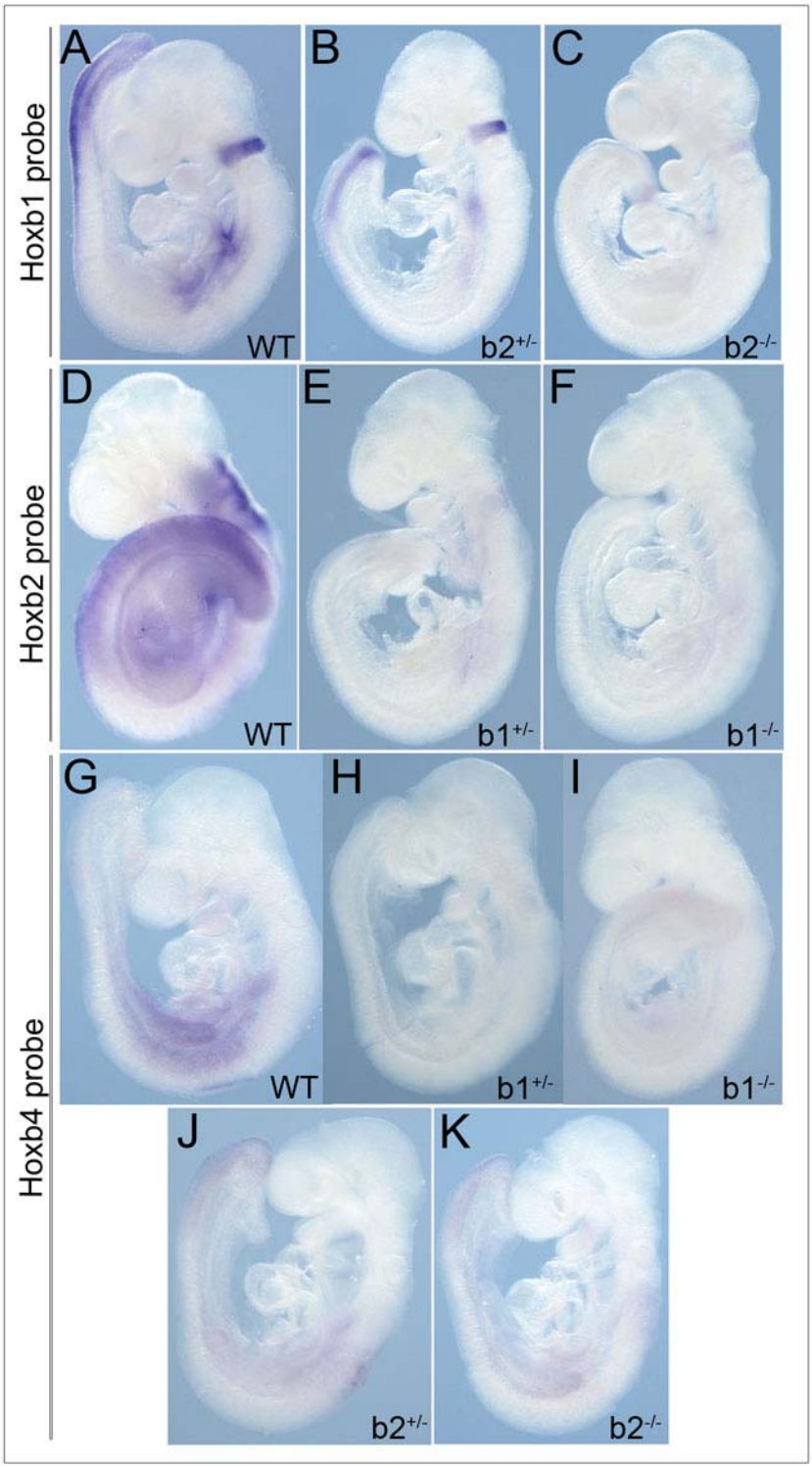
Hoxb1 probe
Hoxb2 probe
Hoxb4 probe
A
B
C
D
E
F
G
H
I
J
K
WT
b2+/-
b2-/-
WT
b1+/-
b1-/-
WT
b1+/-
b1-/-
b2+/-
b2-/-

The results generated upon hybridization of the *Hoxb4* mRNA probe to 9.5dpc embryos are less conclusive (Figure 49G-K). In wild-type embryos, *Hoxb4* mRNA expression (Figure 49G) did not appear to match the pattern of mesodermal expression previously reported (Gaunt et al., 1989). Thus, the evaluation of *Hoxb4* mRNA expression in *Hoxb1* (Figure 49H and I) and *Hoxb2* (Figure 49J and K) mutants with respect to wild-type embryos is difficult to determine at this point.

Overall, there was some variability among the expression profiles obtained for each probe within wild-type and mutant embryos. Unfortunately, this observation was anticipated, since variability in staining patterns is common to the technique. As a result, analysis of expression levels by *in situ* hybridization is only semi-quantitative. To more accurately determine a decrease in expression, a quantitative approach, such as RT-PCR, should be used.

Results from *in situ* hybridizations and loss-of-function skeletal analysis further support a genetic model involving these anterior *HoxB* genes in patterning vertebral precursors: as functional copies of *Hoxb1* and *Hoxb2* are eliminated, critical information specifying vertebral identity along the axis is lost from the presomitic mesoderm. As a result, the identities of individual vertebrae within the cervical and thoracic regions are shifted by a single segment anteriorly.

References

Akasaka, T., Kanno, M., Balling, R., Mieza, M.A., Taniguchi, M., Koseki, H., 1996. A role for mel-18, a Polycomb group-related vertebrate gene, during theanteroposterior specification of the axial skeleton. Development. 122**,** 1513-22.

Bachiller, D., Klingensmith, J., Kemp, C., Belo, J.A., Anderson, R.M., May, S.R., McMahon, J.A., McMahon, A.P., Harland, R.M., Rossant, J., De Robertis, E.M., 2000. The organizer factors Chordin and Noggin are required for mouse forebrain development. Nature. 403**,** 658-61.

Barrow, J., Capecchi, M., 1996. Targeted disruption of the *Hoxb2* locus in mice interferes with expression of *Hoxb1* and *Hoxb4*. Development. 122**,** 3817-3828.

Beddington, R., Robertson, E., 1999. Axis development and early asymmetry in mammals. Cell. 96**,** 195-209.

Benson, G.V., Nguyen, T.H., Maas, R.L., 1995. The expression pattern of the murine Hoxa-10 gene and the sequence recognition of its homeodomain reveal specific properties of Abdominal B-like genes. Mol. Cell. Biol. 15**,** 1591-601.

Boulet, A.M., Capecchi, M.R., 1996. Targeted disruption of *Hoxc4* causes esophageal defects and vertebral transformations. Dev. Biol. 177**,** 232-249.

Burgess, R., Cserjesi, P., Ligon, K.L., Olson, E.N., 1995. Paraxis: a basic helix-loop-helix protein expressed in paraxial mesoderm and developing somites. Dev. Biol. 168**,** 296-306.

Burke, A.C., Nelson, C.E., Morgan, B.A., Tabin, C., 1995. *Hox* genes and the evolution of vertebrate axial morphology. Development. 121**,** 333-346.

Carpenter, E.M., Goddard, J.M., Davis, A.P., Nguyen, T.P., Capecchi, M.R., 1997. Targeted disruption of Hoxd-10 affects mouse hindlimb development. Development. 124**,** 4505-14.

Chen, F., Capecchi, M.R., 1997. Targeted mutations in hoxa-9 and hoxb-9 reveal synergistic interactions. Dev. Biol. 181**,** 186-96.

Chen, F., Greer, J., Capecchi, M.R., 1998. Analysis of Hoxa7/Hoxb7 mutants suggests periodicity in the generation of the different sets of vertebrae. Mech Dev. 77**,** 49-57.

Chisaka, O., Capecchi, M.R., 1991. Regionally restricted developmental defects resulting from targeted disruption of the mouse homeobox gene *hox1.5*. Nature. 350**,** 473-479.

Chisaka, O., Musci, T.S., Capecchi, M.R., 1992. Developmental defects of the ear, cranial nerves and hindbrain resulting from targeted disruption of the mouse homeobox gene *Hox-1.6*. Nature. 355**,** 516-520.

Condie, B.G., Capecchi, M.R., 1993. Mice homozygous for a targeted disruption of *Hoxd-3(Hox-4.1)* exhibit anterior transformations of the first and second cervical vertebrae, the atlas and axis. Development. 119**,** 579-595.

Condie, B.G., Capecchi, M.R., 1994. Mice with targeted disruptions in the paralogous genes *Hoxa-3* and *Hoxd-3* reveal synergistic interactions. Nature. 370**,** 304-307.

Cordes, S.P., Barsh, G.S., 1994. The mouse segmentation gene *kr* encodes a novel basic domain-leucine zipper transcription factor. Cell. 79**,** 1025-1034.

Coré, N., Bel, S., Gaunt, S.J., Aurrand-Lions, M., Pearce, J., Fisher, A., Djabali, M., 1997. Altered cellular proliferation and mesoderm patterning in *Polycomb-M33*-deficient mice. Development. 124**,** 721-729.

Davenne, M., Maconochie, M.K., Neun, R., Pattyn, A., Chambon, P., Krumlauf, R., Rijli, F.M., 1999. *Hoxa2* and *Hoxb2* control dorsoventral patterns of neuronal development in the rostral hindbrain. Neuron. 22**,** 677-691.

Davis, A., Capecchi, M., 1994. Axial homeosis and appendicular skeleton defects in mice with a targeted disruption of *Hoxd-11*. Development. 120**,** 2187-2198.

de la Cruz, C.C., Der-Avakian, A., Spyropoulos, D.D., Tieu, D.D., Carpenter, E.M., 1999. Targeted disruption of Hoxd9 and Hoxd10 alters locomotor behavior, vertebral identity, and peripheral nervous system development. Dev. Biol. 216**,** 595-610.

Deschamps, J., Wijgerde, M., 1993. Two phases in the establishment of *Hox* expression domains. Dev. Biol. 156**,** 473-480.

Di Rocco, G., Gavalas, A., Popperl, H., Krumlauf, R., Mavilio, F., Zappavigna, V., 2001. The recruitment of SOX/OCT complexes and the differential activity of HOXA1 and HOXB1 modulate the Hoxb1 auto-regulatory enhancer function. J. Biol. Chem. 1**,** 1.

Dilworth, F.J., Fromental-Ramain, C., Remboutsika, E., Benecke, A., Chambon, P., 1999. Ligand-dependent activation of transcription in vitro by retinoic acid receptor alpha/retinoid X receptor alpha heterodimers that mimics transactivation by retinoids in vivo. Proc Natl Acad Sci U S A. 96**,** 1995-2000.

Dollé, P., Duboule, D., 1989. Two gene members of the murine *HOX 5* complex show regional and cell-type specific expression in developing limbs and gonads. EMBO J. 8**,** 1507-1515.

Duboule, D., Dollé, P., 1989. The structural and functional organization of the murine *HOX* gene family resembles that of *Drosophila* homeotic genes. EMBO J. 8**,** 1497-1505.

Dupé, V., Davenne, M., Brocard, J., Dollé, P., Mark, M., Dierich, A., Chambon, P., Rijli, F., 1997. *In vivo* functional analysis of the *Hoxa1* 3' retinoid response element (3' RARE). Development. 124**,** 399-410.

Favier, B., Le Meur, M., Chambon, P., Dollé, P., 1995. Axial skeleton homeosis and forelimb malformations in *Hoxd-11* mutant mice. Proc. Natl. Acad. Sci. USA. 92**,** 310-314.

Favier, B., Rijli, F.M., Fromental-Ramain, C., Fraulob, V., Chambon, P., Dollé, P., 1996. Functional cooperation between the non-paralogous genes Hoxa-10 and Hoxd-11 in the developing forelimb and axial skeleton. Development. 122**,** 449-460.

Frohman, M.A., Boyle, M., Martin, G.R., 1990. Isolation of the mouse *Hox-2.9* gene; analysis of embryonic expression suggests that positional information along the anterior-posterior axis is specified by mesoderm. Development. 110**,** 589-607.

Fromental-Ramain, C., Warot, X., Lakkaraju, S., Favier, B., Haack, H., Birling, C., Dierich, A., Dollé, P., Chambon, P., 1996. Specific and redundant functions of the paralogous Hoxa-9 and Hoxd-9 genes in forelimb and axial skeleton patterning. Development. 122**,** 461-472.

Garcia-Gasca, A., Spyropoulos, D.D., 2000. Differential mammary morphogenesis along the anteroposterior axis in Hoxc6 gene targeted mice. Dev Dyn. 219**,** 261-76.

Gaunt, S.J., Krumlauf, R., Duboule, D., 1989. Mouse homeo-genes within a subfamily, Hox-1.4, -2.6 and -5.1, display similar anteroposterior domains of expression in the embryo, but show stage- and tissue-dependent differences in their regulation. Development. 107**,** 131-141.

Gavalas, A., Ruhrberg, C., Livet, J., Henderson, C.E., Krumlauf, R., 2003. Neuronal defects in the hindbrain of Hoxa1, Hoxb1 and Hoxb2 mutants reflect regulatory interactions among these Hox genes. Development. 130**,** 5663-79.

Gavalas, A., Studer, M., Lumsden, A., Rijli, F.M., Krumlauf, R., Chambon, P., 1998. *Hoxa1* and *Hoxb1* synergize in patterning the hindbrain, cranial nerves and second pharyngeal arch. Development. 125**,** 1123-1136.

Geada, A.M.C., Gaunt, S.J., Azzawi, M., Shimeld, S.M., Pearce, J., Sharpe, P.T., 1992. Sequence and embryonic expression of the murine Hox-3.5 gene. Development. 116**,** 497-506.

Gendron-Maguire, M., Mallo, M., Zhang, M., Gridley, T., 1993. Hoxa-2 mutant mice exhibit homeotic transformation of skeletal elements derived from cranial neural crest. Cell. 75**,** 1317-1331.

Goddard, J., Rossel, M., Manley, N., Capecchi, M., 1996. Mice with targeted disruption of *Hoxb1* fail to form the motor nucleus of the VIIth nerve. Development. 122**,** 3217-3228.

Hassan, M.Q., Tare, R., Lee, S.H., Mandeville, M., Weiner, B., Montecino, M., van Wijnen, A.J., Stein, J.L., Stein, G.S., Lian, J.B., 2007. HOXA10 controls osteoblastogenesis by directly activating bone regulatory and phenotypic genes. Mol. Cell. Biol. 27**,** 3337-52.

Horan, G.S., Kovacs, E.N., Behringer, R.R., Featherstone, M.S., 1995a. Mutations in paralogous *Hox* genes result in overlapping homeotic transformations of the axial skeleton: Evidence for unique and redundant function. Dev. Biol. 169**,** 359-372.

Horan, G.S., Ramirez-Solis, R., Featherstone, M.S., Wolgemuth, D.J., Bradley, A., Behringer, R.R., 1995b. Compound mutants for the paralogous *Hoxa-4*, *Hoxb-4*, and *Hoxd-4* genes show more complete homeotic transformations and a dose-dependent increase in the number of vertebrae transformed. Genes Dev. 9**,** 1667-1677.

Horan, G.S., Wu, K., Wolgemuth, D.J., Behringer, R.R., 1994. Homeotic transformation of cervical vertebrae in *Hoxa-4* mutant mice. Proc. Natl. Acad. Sci. U S A. 91**,** 12644-12648.

Huang, D., Chen, S.W., Langston, A.W., Gudas, L.J., 1998. A conserved retinoic acid responsive element in the murine *Hoxb-1* gene is required for expression in the developing gut. Development. 125**,** 3235-3246.

Izpisua-Belmonte, J.-C., Dollé, P., Renucci, A., Zappavigna, V., Falkenstein, H., Duboule, D., 1990. Primary structure and embryonic expression pattern of the mouse *Hox-4.3* homeobox gene. Development. 110**,** 733-745.

Jeannotte, L., Lemieux, M., Charron, J., Poirier, F., Robertson, E.J., 1993. Specification of axial identity in the mouse: role of the Hoxa-5 (Hox1.3) gene. Genes Dev. 7**,** 2085-96.

Kessel, M., 1992. Respecification of vertebral identities by retinoic acid. Development. 115**,** 487-501.

Kostic, D., Capecchi, M.R., 1994. Targeted disruptions of the murine Hoxa-4 and Hoxa-6 genes result in homeotic transformations of components of the vertebral column. Mech. Dev. 46**,** 231-247.

Kulesa, P.M., Fraser, S.E., 1998. Segmentation of the vertebrate hindbrain: a time-lapse analysis. Int J Dev Biol. 42**,** 385-92.

Langston, A., Thompson, J., Gudas, L., 1997. Retinoic acid-responsive enhancers located 3' of the HoxA and the HoxB gene clusters. J. Biol. Chem. 272**,** 2167-2175.

Langston, A.W., Gudas, L.J., 1992. Identification of a retinoic acid responsive enhancer 3' of the murine homeobox gene *Hox-1.6*. Mech. Dev. 38**,** 217-228.

Le Mouellic, H., Lallemand, Y., Brulet, P., 1992. Homeosis in the mouse induced by a null mutation in the Hox-3.1 gene. Cell. 69**,** 251-64.

Lufkin, T., Dierich, A., LeMeur, M., Mark, M., Chambon, P., 1991. Disruption of the *Hox-1.6* homeobox gene results in defects in a region corresponding to its rostral domain of expression. Cell. 66**,** 1105-1119.

Lufkin, T., Mark, M., Hart, C., Dollé, P., LeMeur, M., Chambon, P., 1992. Homeotic transformation of the occipital bones of the skull by ectopic expression of a homeobox gene in transgenic mice. Nature. 359**,** 835-841.

Lumsden, A., Krumlauf, R., 1996. Patterning the vertebrate neuraxis. Science. 274**,** 1109-1115.

Maconochie, M., Nonchev, S., Morrison, A., Krumlauf, R., 1996. Paralogous *Hox* genes: function and regulation. Annu. Rev. Genet. 30**,** 529-556.

Maconochie, M.K., Nonchev, S., Studer, M., Chan, S.K., Popperl, H., Sham, M.H., Mann, R.S., Krumlauf, R., 1997. Cross-regulation in the mouse *HoxB* complex: the expression of *Hoxb2* in rhombomere 4 is regulated by *Hoxb1*. Genes and Development. 11**,** 1885-1896.

Manley, N.R., Barrow, J.R., Zhang, T., Capecchi, M.R., 2001. Hoxb2 and hoxb4 act together to specify ventral body wall formation. Dev. Biol. 237**,** 130-44.

Manley, N.R., Capecchi, M.R., 1997. *Hox* group 3 paralogous genes act synergistically in the formation of somitic and neural crest-derived structures. Dev. Biol. 192**,** 274-288.

Manzanares, M., Cordes, S., Ariza-McNaughton, L., Sadl, V., Maruthainar, K., Barsh, G., Krumlauf, R., 1999a. Conserved and distinct roles of *kreisler* in regulation of the paralogous *Hoxa3* and *Hoxb3* genes. Development. 126**,** 759-769.

Manzanares, M., Nardelli, J., Gilardi-Hebenstreit, P., Marshall, H., Giudicelli, F., Martinez-Pastor, M.T., Krumlauf, R., Charnay, P., 2002. Krox20 and kreisler co-operate in the transcriptional control of segmental expression of Hoxb3 in the developing hindbrain. EMBO J. 21**,** 365-376.

Manzanares, M., Trainor, P.A., Nonchev, S., Ariza-McNaughton, L., Brodie, J., Gould, A., Marshall, H., Morrison, A., Kwan, C.T., Sham, M.H., Wilkinson, D.G., Krumlauf, R., 1999b. The role of *kreisler* in segmentation during hindbrain development. Dev. Biol. 211**,** 220-237.

Marshall, H., Studer, M., Pöpperl, H., Aparicio, S., Kuroiwa, A., Brenner, S., Krumlauf, R., 1994. A conserved retinoic acid response element required for early expression of the homeobox gene *Hoxb-1*. Nature. 370**,** 567-571.

McIntyre, D.C., Rakshit, S., Yallowitz, A.R., Loken, L., Jeannotte, L., Capecchi, M.R., Wellik, D.M., 2007. Hox patterning of the vertebrate rib cage. Development. 134**,** 2981-9.

Medina-Martinez, O., Bradley, A., Ramirez-Solis, R., 2000. A large targeted deletion of Hoxb1-Hoxb9 produces a series of single-segment anterior homeotic transformations. Dev. Biol. 222**,** 71-83.

Medina-Martinez, O., Ramirez-Solis, R., 2003. In vivo mutagenesis of the Hoxb8 hexapeptide domain leads to dominant homeotic transformations that mimic the loss-of-function mutations in genes of the Hoxb cluster. Dev. Biol. 264**,** 77-90.

Melton, K.R., Iulianella, A., Trainor, P.A., 2004. Gene expression and regulation of hindbrain and spinal cord development. Front Biosci. 9**,** 117-38.

Morriss-Kay, G.M., Murphy, P., Hill, R.E., Davidson, D.R., 1991. Effects of retinoic acid excess on expression of Hox-2.9 and Krox-20 and on morphological segmentation in the hindbrain of mouse embryos. EMBO J. 10**,** 2985-2995.

Murphy, P., Hill, R.E., 1991. Expression of the mouse labial-like homeobox-containing genes, Hox 2.9 and Hox 1.6, during segmentation of the hindbrain. Development. 111**,** 61-74.

Nonchev, S., Maconochie, M., Vesque, C., Aparicio, S., Ariza-McNaughton, L., Manzanares, M., Maruthainar, K., Kuroiwa, A., Brenner, S., Charnay, P., Krumlauf, R., 1996. The conserved role of *Krox-20* in directing *Hox* gene expression during vertebrate hindbrain segmentation. Proc. Natl. Acad. Sci. USA. 93**,** 9339-9345.

Nowicki, J.L., Burke, A.C., 2000. Hox genes and morphological identity: axial versus lateral patterning in the vertebrate mesoderm. Development. 127**,** 4265-75.

Oostra, R.J., Hennekam, R.C., de Rooij, L., Moorman, A.F., 2005. Malformations of the axial skeleton in Museum Vrolik I: homeotic transformations and numerical anomalies. American journal of medical genetics. 134**,** 268-81.

Pöpperl, H., Bienz, M., Studer, M., Chan, S., Aparicio, S., Brenner, S., Mann, R., Krumlauf, R., 1995. Segmental expression of *Hoxb1* is controlled by a highly conserved autoregulatory loop dependent upon *exd/Pbx*. Cell. 81**,** 1031-1042.

Ramirez-Solis, R., Zheng, H., Whiting, J., Krumlauf, R., Bradley, A., 1993. Hoxb-4 (Hox-2.6) mutant mice show homeotic transformation of a cervical vertebra and defects in the closure of the sternal rudiments. Cell. 73**,** 279-294.

Rancourt, D.E., Tsuzuki, T., Capecchi, M.R., 1995. Genetic interaction between hoxb-5 and hoxb-6 is revealed by nonallelic noncomplementation. Genes & Development. 9**,** 108-122.

Rijli, F.M., Mark, M., Lakkaraju, S., Dierich, A., Dollé, P., Chambon, P., 1993. A homeotic transformation is generated in the rostral branchial region of the head by disruption of Hoxa-2, which acts as a selector gene. Cell. 75**,** 1333-1349.

Rijli, F.M., Matyas, R., Pellegrini, M., Diedrich, A., Gruss, P., Dollé, P., Chambon, P., 1995. Cryptorchidism and homeotic transformations of spinal nerves and vertebrae in *Hoxa-10* mutant mice. Proc. Natl. Acad. Sci. USA. 92**,** 8185-8189.

Saegusa, H., Takahashi, N., Noguchi, S., Suemori, H., 1996. Targeted disruption in the mouse Hoxc-4 locus results in axial skeleton homeosis and malformation of the xiphoid process. Dev. Biol. 174**,** 55-64.

Simeone, A., Acampora, D., Nigro, V., Faiella, A., D'Esposito, M., Stornaiuolo, A., Mavilio, F., Boncinelli, E., 1991. Differential regulation by retinoic acid of the homeobox genes of the four *HOX* loci in human embryonal carcinoma cells. Mech. Dev. 33**,** 215-227.

Small, K.S., Potter, S., 1993. Homeotic transformations and limb defects in Hoxa-11 mutant mice. Genes Dev. 7**,** 2318-2328.

Studer, M., Gavalas, A., Marshall, H., Ariza-McNaughton, L., Rijli, F., Chambon, P., Krumlauf, R., 1998. Genetic interaction between *Hoxa1* and *Hoxb1* reveal new roles in regulation of early hindbrain patterning. Development. 125**,** 1025-1036.

Studer, M., Lumsden, A., Ariza-McNaughton, L., Bradley, A., Krumlauf, R., 1996. Altered segmental identity and abnormal migration of motor neurons in mice lacking *Hoxb-1*. Nature. 384**,** 630-635.

Studer, M., Pöpperl, H., Marshall, H., Kuroiwa, A., Krumlauf, R., 1994. Role of a conserved retinoic acid response element in rhombomere restriction of *Hoxb-1*. Science. 265**,** 1728-1732.

Suemori, H., Takahashi, N., Noguchi, S., 1995. Hoxc-9 mutant mice show anterior transformation of the vertebrae and malformation of the sternum and ribs. Mech Dev. 51**,** 265-73.

Theil, T., Ariza-McNaughton, L., Manzanares, M., Brodie, J., Krumlauf, R., Wilkinson, D.G., 2002. Requirement for downregulation of kreisler during late patterning of the hindbrain. Development. 129**,** 1477-85.

Theil, T., Frain, M., Gilardi-Hebenstreit, P., Flenniken, A., Charnay, P., Wilkinson, D.G., 1998. Segmental expression of the EphA4 (Sek-1) receptor tyrosine kinase in the hindbrain is under direct transcriptional control of Krox-20. Development. 125**,** 443-52.

Tiret, L., Le Mouellic, H., Lallemand, Y., Maury, M., Brulet, P., 1993. Altering the spatial determinations in the mouse embryos by manipulating the Hox genes. Comptes rendus de l'Academie des sciences. 316**,** 1009-24.

Tümpel, S., Cambronero, F., Ferretti, E., Blasi, F., Wiedemann, L.M., Krumlauf, R., 2007. Expression of *Hoxa2* in rhombomere 4 is regulated by a conserved cross-regulatory mechanism dependent upon *Hoxb1*. Dev. Biol. 302**,** 646-60.

Tvrdik, P., Capecchi, M.R., 2006. Reversal of hox1 gene subfunctionalization in the mouse. Dev Cell. 11**,** 239-50.

van den Akker, E., Fromental-Ramain, C., de Graaff, W., Le Mouellic, H., Brulet, P., Chambon, P., Deschamps, J., 2001. Axial skeletal patterning in mice lacking all paralogous group 8 Hox genes. Development. 128**,** 1911-21.

van den Akker, E., Reijnen, M., Korving, J., Brouwer, A., Meijlink, F., Deschamps, J., 1999. Targeted inactivation of Hoxb8 affects survival of a spinal ganglion and causes aberrant limb reflexes. Mech Dev. 89**,** 103-14.

Vogels, R., De Graaff, W., Deschamps, J., 1990. Expression of the murine homeobox-containing gene Hox-2.3 suggests multiple time-dependent and tissue-specific roles during development. Development. 110**,** 1159-1168.

Wahba, G.M., Hostikka, S.L., Carpenter, E.M., 2001. The paralogous Hox genes Hoxa10 and Hoxd10 interact to pattern the mouse hindlimb peripheral nervous system and skeleton. Dev. Biol. 231**,** 87-102.

Wellik, D.M., 2007. Hox patterning of the vertebrate axial skeleton. Dev Dyn. 236**,** 2454-63.

Wellik, D.M., Capecchi, M.R., 2003. Hox10 and Hox11 genes are required to globally pattern the mammalian skeleton. Science. 301**,** 363-7.

Wilkinson, D.G., 2001. Multiple roles of EPH receptors and ephrins in neural development. Nat Rev Neurosci. 2**,** 155-64.

Xu, Q., Mellitzer, G., Robinson, V., Wilkinson, D.G., 1999. *In vivo* cell sorting in complementary segmental domains mediated by *Eph* receptors and *ephrins*. Nature. 399**,** 267-271.